



TECHNISCHE
UNIVERSITÄT
WIEN
Vienna University of Technology

DISSERTATION

Tissue-engineered strategies to repair chondrogenic and osteogenic defects.

ausgeführt zum Zwecke der Erlangung des akademischen Grades eines
Doktors der technischen Wissenschaften unter der Leitung von

a.o. Univ.Prof. Dipl.-Ing. Dr.techn. Heinz Redl
Institut für Verfahrenstechnik, Umwelttechnik und Technische Biowissenschaften
(E166)

eingereicht an der Technischen Universität Wien
Fakultät für Technische Chemie

von

Bernhard Rieder, MSc
01329280
Krummgasse 14/1
1030 Wien

Wien, am

.....

EIDESSTAATLICHE ERKLÄRUNG

Hiermit erkläre ich an Eides statt, dass ich die vorliegende Dissertation „*Tissue-engineered strategies to repair chondrogenic and osteogenic defects*“ selbstständig verfasst und keine anderen als die angegebenen Quellen und Hilfsmittel verwendet habe.

Wien, am

.....
Bernhard Rieder

Table of Contents

ACKNOWLEDGMENTS.....	4
KURZFASSUNG.....	5
ABSTRACT.....	7
GENERAL INTRODUCTION.....	9
1. Problem and Possible Solution.....	9
2. Bone and Cartilage – The Developmental Siblings.....	10
3. The Structure and Function of Articular Cartilage and Bone.....	11
3.1. Structure and Composition of Articular Cartilage.....	11
3.2. Mechanism of Articular Cartilage and Bone Development.....	16
3.3. Acute and Chronic Articular Cartilage Pathologies.....	21
3.4. Surgical Treatment Strategies in Clinics.....	21
4. Tissue Engineering.....	23
4.1. Cells.....	23
4.2. Growth Factors.....	24
4.3. Biomaterials and Scaffolds.....	25
4.4. Mechanical Stimulation.....	27
AIM OF THE THESIS.....	30
CHAPTER I.....	32
Tissue-engineered hypertrophic chondrocyte grafts enhanced long bone repair.....	33
Perfusion enhances hypertrophic chondrocyte matrix deposition, but not the bone formation.....	57
CHAPTER II.....	76
Repopulation of an auricular cartilage scaffold, <i>AuriScaff</i> , perforated with an enzyme combination.....	77
Chondroinductive properties of the decellularized auricular cartilage scaffold is further enhanced by mechanical loading.....	103
CHAPTER III.....	122
Hydrostatic pressure-generated reactive oxygen species induce osteoarthritic conditions in cartilage pellet cultures.....	123
REFERENCES.....	148
LIST OF ABBREVIATIONS.....	171
CURRICULUM VITAE.....	175

ACKNOWLEDGMENTS

First and foremost I want to thank my thesis supervisor Prof. Dr. Heinz Redl for giving me the opportunity to conduct this thesis, provide the necessary funding and embedding me in an environment with exceptional scientists. Furthermore, I want to thank FH-Prof. Mag. Dr. Dominik Rünzler and FH-Prof. DI Dr. Carina Huber-Gries for the opportunity to work and learn in their lab and the financial support aid, especially in the first years of the thesis.

Moreover, I want to thank Andi for his constant support. Without a doubt I can clearly state that without his guidance this thesis would be non-existent. He is not only a brilliant scientist but has also become a good friend over the years, who showed me what a passion for science and teaching can achieve.

In addition I would like to thank:

- Nane and Anna, for always being there for me since my early beginning in the lab. Their knowledge and common sense were impressive and refreshing.
- Raphael, for being one of my best friends during my studies and beyond. Casually talking about similar problems helped to dissuade from evil paths and get me back on track.
- Jon, for being a typical Yankee whose constant positive mood was infectious and brightened up my days. His passion for science and knowledge in his field of expertise were unmet.
- Babette, Daniel, Michi, Elias, Carina, Janine, Sabrina, Bettina, Safet, Sophie, Babsi, Eli, Dani, and all the other guys and girls in the lab for the great time and support.
- Conny, Marian, and Sylvia for being a part of the CartiScaff team.

My genuine thanks to my best friends Dora and Xavi, the infamous double. Seeing you evolve from curious students into scientists who outperform their former teachers not only with knowledge but also with enthusiasm warms my heart and encourages me to strive for my better self. I am sure that without the two of you, coming to the lab would have been less exciting and a lot tougher - I will miss every minute of it.

At last I would like to express my sincere gratitude to my parents and my siblings. To my older brother Franz, whose enthusiasm for biology brought me into science in the first place. To Waltraud, who shows that having a perfect relationship with (soon) two little kids is achievable. To Constanze, who constantly proves that being an awesome mother and a busy teacher with various side projects is manageable. To Antonia, who persistently follows her dreams without hesitation (although they regularly change). To Martin, who engaged in a relationship at a young age but shows enormous level of maturity ever since. To Viktoria, who balances party, student life, and relationship in an exceptional manner hardly seen before. To my father and my mother, for always supporting me financially and morally and never questioning the direction of my decisions.

KURZFASSUNG

Erkrankungen des Bewegungsapparates (MSD, engl. musculoskeletal disorders) betreffen hunderte Millionen Menschen auf der ganzen Welt, die an einer körperlichen Beeinträchtigung, welche mit starken langfristigen Schmerzen einhergeht, leiden. Die erhöhte Lebenserwartung in Kombination mit einem Wechsel von unverarbeiteten Lebensmitteln zu einer Ernährung mit hohem Glukose- und Fettgehalt sowie eingeschränkte körperliche Aktivität bei der Arbeit und zu Hause erhöht die weltweite Verbreitung von MSD kontinuierlich. Diese Krankheiten und Syndrome haben Dimensionen erreicht, die eine hohe wirtschaftliche Belastung für die Gesellschaft zur Folge haben. Schätzungen der Gesamtkosten reichen von 240 Mrd. EUR in der EU bis zu 213 Mrd. USD in den USA und erfordern daher ausgeklügelte Lösungen, um ein defektes Gesundheitssystem zu verhindern.

Daher bedarf es einer Überarbeitung der derzeitigen Behandlungsoptionen und den Ersatz dieser durch überlegene Ansätze, um Kosten zu reduzieren. Diese Behandlungsverfahren beinhalten immer noch die Transplantation von autologem oder allogenen Gewebe, die zu einer Morbidität an der Spenderstelle, sowie Immunreaktionen oder Erkrankungen bedingt durch Transfer führen kann. Das aufstrebende Gebiet „Tissue Engineering und Regenerative Medizin“ versucht daher, dem Mangel aktueller Therapien entgegenzuwirken. Dabei werden neue Technologien und Techniken entwickelt, um ein funktionelles Gewebe herzustellen, welches in den Patienten implantiert werden kann und sofort seine vorgesehene Aufgabe erfüllt.

In dieser Arbeit werden verschiedene Konzepte zur Knochen- und Knorpelreparatur untersucht. Obwohl Knochen eine angeborene Regenerationsfähigkeit besitzen, übertreffen große komplexe Frakturen oft die natürliche Heilkraft des Knochens und führen zu nicht zusammengewachsenen Knochenfrakturen. Für eine wirksame Behandlung erfordern diese Frakturen eine externe Intervention mit Hilfe von Autotransplantaten oder Allotransplantaten, welche jedoch die oben genannten Nachteile wie Morbidität an der Spenderstelle, Immunreaktionen oder Transfer-bedingten Erkrankungen bedingen können. In Kapitel I stellen wir eine Alternative zu dem derzeitigen klinischen Ansätzen vor, bei welchem ein dezellularisiertes Knochenransplantat von xenogenem Ursprung verwendet wird, welches ausgestattet mit aus Fettgewebe stammenden Stammzellen (ASC, engl. adipose-derived stem cells) in einem Perfusionsbioreaktorsystem stimuliert wurde. Wir konnten zeigen, dass hypertrophe Knorpelzellen, welche die endochondrale Ossifikation zeigen, 7 der 8 Defekte überbrücken konnten, während hingegen Osteoblasten nur 1 der 8 überbrücken konnten. Obwohl die Perfusion des Mediums die Bildung von Knochenmatrizen *in vitro* stimulierte, konnte die Knochenregeneration *in vivo* nicht gesteigert werden. Im Unterschied zu Knochen wird die Selbstheilungsfähigkeit des Knorpels durch ein insgesamt kaum metabolisch aktives Gewebe stark beeinträchtigt. Knorpelschäden, die durch ein Trauma oder degenerative Prozesse induziert werden, übertreffen somit das eingeschränkte Regenerationspotenzial und machen ein externes Eingreifen erforderlich. Ein wesentlicher Bestandteil der Funktionalität von Gelenkknorpel ist die spezialisierte Architektur und Struktur - dessen Zusammensetzung jedoch bisher

durch kein kommerziell erhältliches Biomaterial im klinischen Einsatz wiedergegeben werden konnte. In Kapitel II stellen wir *AuriScaff* als neuartiges Biomaterial xenogenen Ursprungs vor, welches *in vitro* erfolgreich mit ASC und Knorpelzellen besiedelt werden konnte. Wir konnten außerdem zeigen, dass es ein Alternativprodukt, welches derzeit klinisch verwendet wird, in Bezug auf mechanische Stabilität sowie die Herstellung von qualitativ hochwertigem hyalin-artigem Knorpel *in vivo* übertrifft. Mit einem biomimetischen Bioreaktor konnten wir zeigen, dass *AuriScaff* nicht nur schon von Anfang an dynamischen Belastungen standhält, sondern auch als Zellträger dient, welche in Folge reifen und die extrazelluläre Matrix reorganisieren. Während Knorpeldefekte bei Jugendlichen und jungen Menschen die Chance haben sich zu regenerieren, verringert Osteoarthritis (OA), eine degenerative Erkrankung des Gelenks, welche vermutlich durch ein akutes Trauma oder eine chronische Überlastung ausgelöst wird und einen großen Teil der erwachsenen Bevölkerung betrifft, dieses Potenzial erheblich. Historisch als einfache Abnutzungskrankheit eingestuft, identifizierten neuere Erkenntnisse reaktive Sauerstoffspezies (ROS) als einen maßgeblichen Faktor bei der Entwicklung von OA. Mit der Anwendung von hydrostatischem Druck mittels Druckluft konnten wir erhöhte Mengen an Superoxid und anderen ROS-Spezies produzieren, welche ein osteoarthritisches Knorpelmodell generierte. Dieses Modell wurde verwendet, um Signalwege zu untersuchen von denen bekannt ist, dass sie an OA beteiligt sind. Außerdem kann dieses System als vielseitiges Instrument für Tests von antioxidativen Arzneimitteln eingesetzt werden.

ABSTRACT

Disorders in the musculoskeletal (MSD) system affect hundreds of millions of people around the globe which suffer of physical disability accompanied with severe long-term pain. Increased life expectancy combined with a change of unprocessed food to a diet high on glucose and fat as well as limited physical activity at work and home continuously increases the prevalence of MSD worldwide. These diseases and syndromes have reached dimensions that result in a heavy economic burden for the society. Estimations of total cost range from €240 billion in the EU to \$213 billion in the US and thus demand sophisticated solutions to prevent a crippled health care system.

Therefore, current treatment options need to be revised and replaced with superior approaches to reduce costs. These procedures still involve transplantation of autologous or allogeneic tissue which can result in donor-site morbidity, trigger immune reactions, or transfer diseases. Thus, the emerging field of tissue engineering and regenerative medicine tries to address the shortcoming of current therapies. In doing so, new technologies and techniques are developed to produce a functional tissue able to be implanted into the patient and instantly perform its designated task.

In this thesis different concepts for bone and cartilage repair are investigated. Although bone has an innate ability to regenerate, large complex fractures often exceed the natural healing capacity of bone and will result in non-unions. For effective treatment, these non-unions require external intervention with the aid of autografts or allografts which cause aforementioned disadvantages such as donor site morbidity, immune reaction and transfer of diseases. In chapter I, we provide an alternative for the current clinical approach in using a decellularized bone graft of xenogenic origin which was seeded with adipose-derived stem cells (ASCs) and stimulated in a perfusion bioreactor system. We could show that hypertrophic chondrocytes that recapitulated endochondral ossification could bridge 7 out of 8 defects, while osteoblasts were able to bridge just 1 out of 8. However, although medium perfusion stimulated the formation of bone template *in vitro*, it failed to enhance bone regeneration *in vivo*. Contrary to bone, cartilage innate healing ability is heavily compromised by an overall hardly metabolic active tissue. Thus, cartilage damage induced via trauma or degenerative processes outperforms the limited regenerative potential and necessitates external intervention. An integral part in the functionality of articular cartilage plays the specialized architecture and structure – a composition which has not been met by any commercially available biomaterial in clinical use. In chapter II, we introduce *AuriScaff* as a novel biomaterial from xenogenic origin that could be successfully repopulated with ASC and chondrocytes *in vitro*. We further demonstrated that it could outperform a clinically used scaffold in mechanical stability as well as production of high-quality hyaline-like cartilage *in vivo*. Utilizing a biomimetic bioreactor, we could show that *AuriScaff* is able to not only withstand initial dynamic loading but also provides housing for cells to mature and reorganize the extracellular matrix. While cartilage defects in adolescent and young people have a chance to regenerate, osteoarthritis (OA), a degenerative disease of the joint presumably triggered by acute trauma or chronic overload, affecting a

vast portion of the adult population, heavily diminishes this potential. Historically classified as a simple wear-and-tear disease, recent findings identified reactive oxygen species (ROS) as a leading factor in the evolution of OA. With the application of hydrostatic pressure via compressed air, we could induce the production of elevated levels of superoxide and other ROS species that generated an osteoarthritic cartilage model. This model was used to investigate signaling pathways that are known to be involved in OA and could be further employed as a versatile tool for anti-oxidative drug testing.

GENERAL INTRODUCTION

1. Problem and Possible Solution

The musculoskeletal system is the backbone of the human body that is responsible for locomotion and stability as well as protection of internal organs against external physical forces. It unites different organs like bone, cartilage, tendons, ligaments and skeletal muscles into a complex moving apparatus that needs precise control to function seamlessly. Failure of this tight control, initiated either through acute or chronic conditions, results in musculoskeletal disorders (MSD) and severe restriction for the person. Besides having a detrimental impact on the person's life and wellbeing, it is also an immense socio-economic burden. Rough estimations of the total cost due to loss of productivity caused by work-related MSDs in the EU was in the range of €240 billion (around 2% of GDP) [1]. In the US, a nationwide survey consolidated healthcare reports of 102.5 million people (33.2% of the population) and calculated direct and indirect (earning losses) cost of MSDs to stress the budget for \$213 billion (around 5.73% of GDP) [2, p. 664]. To tackle these costs, healthcare systems across the globe are forced to increase fees while simultaneously reducing services [3].

A possibility to reduce cost might be to revise current treatment options which represent the golden standard and develop new approaches. The usual therapy, if not only palliative, involve surgical intervention that use autologous or allogenic grafts as well as replacements of synthetic origin. Based on the method employed various disadvantages arise like donor-site morbidity, immune reactions, transfer of diseases, or similar. Tissue engineering and regenerative medicine (TERM), a concept based back in the nineties [4], tries to find answers and provide alternatives. Tissue engineering (TE) was defined as *“an interdisciplinary field that applies the principles of engineering and the life sciences towards the development of biological substitutes that restore, maintain, or improve tissue function”* and utilizes *“isolated cells or cell substitutes“* combined with *“tissue-inducing substances“* that get *“placed on or within matrices“* [4]. In the latest years, the field of TE has grown rapidly and investigated uncountable options and ideas to provide solid solutions for health care problems. Therefore, the original triad of cells, growth factors, and matrix was even expanded with a functional component to prime the generated tissue [5].

With this interesting and potent tool, researchers are challenging the traditional concepts of musculoskeletal repair and regeneration. Although bone has an innate ability to regenerate following injury due to high vascularization, larger or more complex fractures exceed bone's natural repair capacity and result in non-union. Cartilage, on the other hand, is avascular and aneural and thus entirely depended on an overall less metabolic active tissue whose regenerative potential is rapidly exhausted. Both tissues are highly investigated with promising results [6]. Unfortunately, the translational nature of TE has to consider issues like biocompatibility, scaling up, and safety before preclinical and clinical trials can lead to sophisticated therapeutic products [7]. A future, everybody is striving for.

2. Bone and Cartilage – The Developmental Siblings

Although bone and cartilage are apparently different in their mature state, both tissue types share a common ancestor. Chondrogenesis, the underlying process that leads to skeletal development during endochondral ossification in long bones has a cartilage intermediate. In this process mesenchymal cells from 3 different sources differentiate and ultimately form the axial and appendicular skeleton (**Fig. 1A**). While cells for the axial skeleton arise from the neural ectoderm and the paraxial mesoderm to form the craniofacial bones as well as the rib cage and the vertebral column, the appendicular skeleton is a product of cells originating from the lateral plate mesoderm and gives rise to the limb skeleton [8]. Besides being an integral part of the locomotive system that provides an adequate load-bearing capacity, bone also acts as a protective barrier shielding internal organs and supports electrolyte homeostasis with storage buffers for calcium and phosphorus. In contrast to cartilage it is highly vascularized and dynamically remodels towards the needs of an individual throughout the whole lifetime [9]. Cartilage on the other hand is avascular, alymphatic and aneural by nature and thus its intrinsic self-repair capacity is extremely limited. It's a specialized tissue which plays an essential role in joint lubrication and impact absorption during motion [10]. Cartilage can be categorized into 3 different types – hyaline-, elastic-, and fibrocartilage – which vary in ECM composition and location in the body (**Fig. 1B**). Hyaline cartilage, the most abundant type, generally covers bones and is usually found in the nose, trachea, sternum and ventral segments of the ribs and is especially important in joints [11]. Its main matrix components are collagen type II and proteoglycans which attract water resulting in a moist and resilient environment that has excellent abilities to resist compressive forces at sites of articulated bones [12], [13]. Healthy hyaline cartilage has a smooth surface and appears white but becomes more yellowish when it gets thinner and dryer with age. Elastic cartilage, the most flexible type, is localized in the larynx, epiglottis and ear and lines the eustachian tube. Similar to hyaline cartilage, it comprises of collagen type II and proteoglycans which makes it resilient to pressure. In addition, it possesses elastic fibers which give extended flexibility to the tissue. Since these elastic fibers are not masked by other proteins, already juvenile and healthy elastic cartilage appears dull yellow. Fibrocartilage, the most resistant type, is commonly found in ligaments, tendons, intervertebral discs, and menisci but can also be found on articular surfaces of bones especially after trauma or injury [14]. In contrast to hyaline and elastic cartilage, it has significantly less proteoglycan content and comprises of collagen type I instead of type II. These alterations in matrix composition give fibrocartilage its resistance against high degrees of tension and compression [15]. Further fibrocartilage lacks perichondrium, the cartilage equivalent what is periosteum to bone. Perichondrium is a dense layer of connective tissue which covers the perimeter of elastic and hyaline cartilage, with the exception of articular (hyaline) cartilage. It is composed of 2 layers. The outer fibrous layer contains fibroblast which produce highly ordered collagenous fibers giving the perichondrium a similar appearance to a tendon [16]. The inner chondrogenic layer houses mesenchymal cells that can differentiate into chondrocytes or chondroblasts and thus contribute to production of new cartilage in a process call appositional growth, even in mature cartilage.

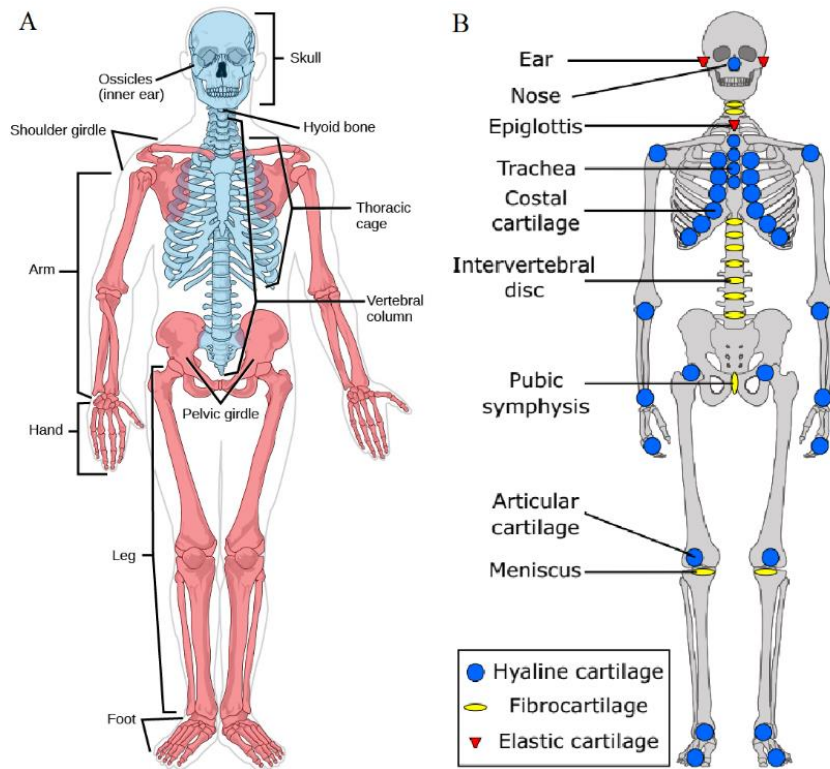


Fig. 1. Anatomical location of bones and cartilage in the human body. (A) The axial skeleton (blue) consists of the bones of the skull, ossicles of the middle ear, hyoid bone, vertebral column, and thoracic cage. The appendicular skeleton (red) consists of the bones of the pectoral limbs, pectoral girdle, pelvic limb, and pelvic girdle. (B) Hyaline cartilage (blue) covers nose, trachea, sternum, costal arch, and joints. Fibrocartilage (yellow) is found in ligaments, tendons, intervertebral disc, and menisci. Elastic cartilage (red) is localized in the larynx, epiglottis, ear, and the eustachian tub. A adapted from [17, p. 427]. B adapted from [18].

3. The Structure and Function of Articular Cartilage and Bone

3.1. Structure and Composition of Articular Cartilage

Articular cartilage (AC), a thin layer of 0.5 to 5 mm and specialized form of hyaline cartilage, covers the articulating ends of bones in joints and provides a lubricated and friction-reduced surface. It is wear-resistant but also slightly compressible and thus evenly distributes forces onto the bone [19]. AC is a biphasic tissue, meaning it constitutes out of a fluid and solid phase. In the fluid phase water is enriched with physiological concentrations of ionic and non-ionic solutes which account to about 75-80% of the wet weight of cartilage. The solid phase makes up for the remaining wet weight and consists of around 10% chondrocytes, the only cell type in AC, which are encapsulated in extra cellular matrix (ECM) which composes of 10-30% collagen, 3-10% proteoglycans, ~10% lipids, and minor amounts of glycoproteins [20].

Compared to other tissue, AC has a very scarce single cell population that only makes up 1-5% of the total tissue volume in AC [20], [21]. Since it lacks a perichondral layer and is avascular by nature, nutrient supply to and waste product removal from the chondrocyte, the singular cell type resident in AC, occurs mainly via diffusion from the synovial fluid or the subchondral [22]. Although compression

and relaxation during movement increases fluid flux in cartilage and hereby enhance diffusion, cartilage remains to be an anoxic environment ($<1-6\% \text{ O}_2$) [23]. Nevertheless, chondrocytes are a metabolic extremely active and constantly remodel the ECM in its immediate vicinity. Consequently, to support this high turnover rate, articular chondrocytes metabolism is highly glycolytic and carried out through anaerobic pathways [24] although negligible mitochondrial respiration could be shown *in vitro* [25], [26]. Especially unique and important for the homeostasis of the chondrocyte is articular cartilage's zonal structures.

AC is a zonal tissue which can be sectioned into an ultra- and a micro-structure. While the ultra-structure is divided into different zones in relation to the depth within the tissue, the micro-structure is dependent on the distance from the chondrocyte. Dependent on the zonal region, variations in cell morphology, collagen orientation and biochemical composition exist. The ultra-structure is divided into a superficial, middle, deep, and calcified zone from cartilage surface to bone (**Fig. 2**) [27]. The micro-structure is divided into a pericellular layer that encloses the chondrocyte and in turn is surrounded by the territorial and interterritorial matrices (**Fig. 3**).

Top down, the first region of the ultra-structure (**Fig. 2**) is the superficial (SZ) or tangential zone which is the thinnest layer with only 10-20% of the total tissue volume. Densely packed chondrocytes exhibit a flattened, discoidal shaped phenotype and are tangentially oriented towards neighboring collagen fibers. High concentration of parallel to the cartilage surface aligned small diameter collagen fibers and a low proteoglycan content generate a region with the highest water content in AC. On the joint surface, a thin film termed lamina splendens covers the SZ securing an almost frictionless joint [28]. The middle (MZ) or transitional zone is the largest layer with around 40-60% of cartilage thickness. Here, spherical shaped chondrocytes are less densely packed and synthesize the highest concentration of proteoglycans in AC [28]. Compared to SZ, collagen content is slightly decreased and fibers are randomly oriented in an arcade-like structure [27]. The deep (DZ) or radial zone is the second largest zone, making up about 20-50% of the total AC volume. It is also the last purely hyaline region before reaching subchondral bone and is characterized by slightly elongated chondrocytes that are clustered in a columnar organization [29]. Cells are oriented along large diameter collagen fibers that are anchored in the subchondral bone and perpendicular arranged to the AC surface [30]. Besides having a lower proteoglycan content than the MZ [31], cell count is also the overall lowest in this zone [32]. The calcified zone (CZ) is the last zone and marks transition from the flexible chondral region into the more rigid but less resilient subchondral bone [33], [34]. Hypertrophic chondrocytes are scarcely distributed in this calcified region and only moderately metabolically active. Between the MZ and CZ a distinct line called tidemark is easily visible due to its special affinity for basic dyes.

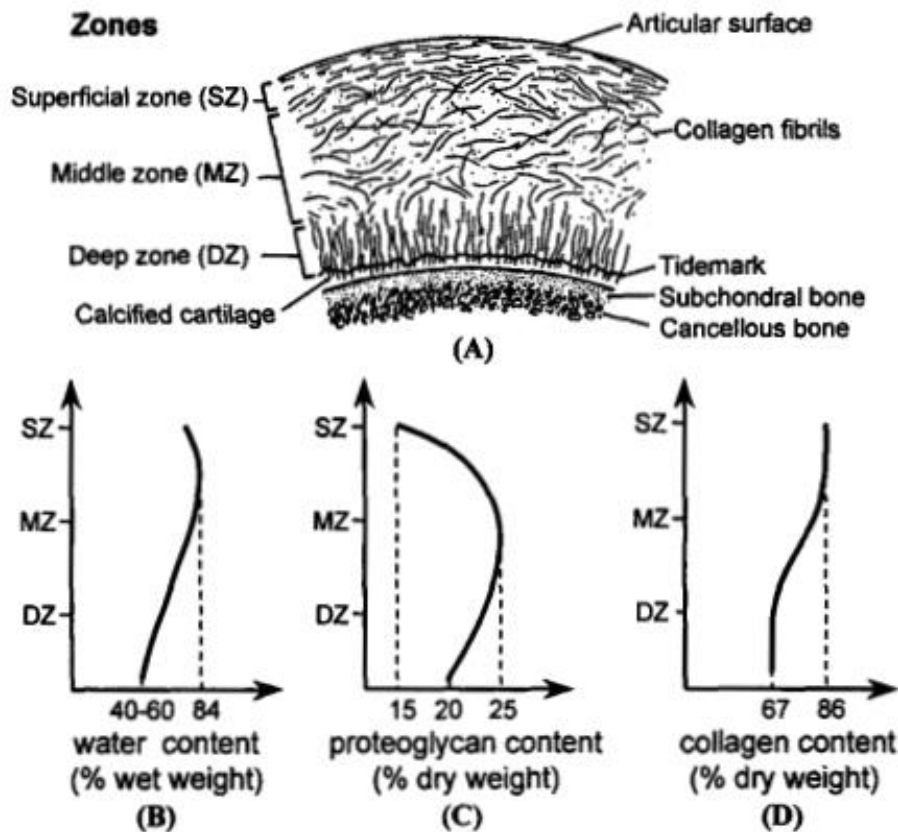


Fig. 2. Zonal arrangement of cartilage. In the superficial zone (SZ), flat cells and thin collagen fibrils are aligned in the direction of shear interspaced with the low proteoglycan content. The middle zone (MZ) is characterized by the highest proteoglycan content, with randomly organized spherical cells and thicker collagen fibrils. In the deep zone (DZ) cells are arranged in columns and align along radial oriented collagen fibrils. The tidemark separates the chondral layer from the calcified zone or osteochondral layer. Proteoglycan content is lowest in the SZ (15%), increases in the MZ (25%) and declines again in the DZ (20%). Collagen content steadily declines from a maximum in the SZ (87%) to a minimum in the DZ (67%). Water content is highest between SZ and MZ (84%) and steadily decreases to a ultimate low in the DZ (40-60%). Adapted from [35].

Inside out, the first region of the micro-structure (**Fig. 3**) is the pericellular matrix (PM), a roughly 2 μm thin region surrounding the individual chondrocyte that is described as fluid-filled bladder that provides a hydrodynamic micro environment which absorbs compressive loading and helps protecting the physical integrity of the chondrocyte [36], [37]. Together, the chondrocyte and the PM form the basic functional and metabolic unit defined as chondron [36]. The PM consists of membrane-associated proteins like fibronectin and decorin and is characterized by containing non-fibrillar collagen type VI and having a high proteoglycan concentration [38], [39]. The territorial matrix (TM) can either surround individual chondrocytes or a cluster of chondrocytes and their associated pericellular layers. Collagen type VI is still present in the region [40], although its matrix composition already mimics surrounding extracellular matrix with similar amounts of collagen type II but increased proteoglycan levels. Characteristic of this region are finer collagen structures which are organized in a criss-cross manner forming a fibrillar basket around a cluster of chondrocytes and thus protecting from mechanical impacts [27]. The remaining matrix that makes up for most of the volume in AC is termed interterritorial matrix (ITM). Dependent on the depth from the surface, concentrations of proteoglycans as well as orientation

of large collagen type II and type IV fibers vary constantly in the different ITM zones [41] giving the tissue its distinct mechanical properties. The ITM and the adjacent TM are collectively termed extracellular matrix (ECM) and responsible for force transmission to the chondrocytes but also assist in modulating experienced strain [42]. Thus, forces experienced by the individual cells can dramatically change when structural breakdown of the ECM occurs.

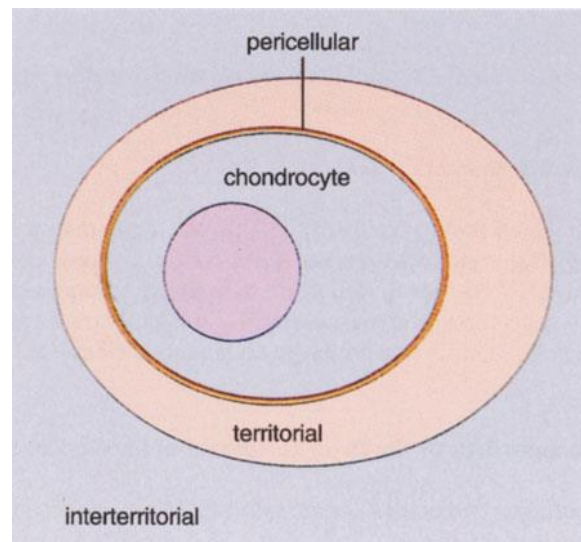


Fig. 3. Compartmentalization of the articular cartilage matrix. The chondrocyte is surrounded by a thin rim of pericellular matrix (PM, red) and further enclosed by the territorial matrix (TM, orange). Both form the metabolic active cell associated matrix, which is surrounded by the metabolic inert interterritorial matrix (ITM, violet) which accounts for more than 90% of the total volume in articular cartilage. The chondrocytes in combination with the PM form a functional unit called chondron. The TM and ITM form the extracellular matrix. Adapted from [21].

This structural breakdown is detrimental and likewise affects cells and extracellular matrix components. The most prominent matrix components in AC are collagen, proteoglycans, and other non-collagenous proteins [43] (**Fig. 5**).

Collagen, which makes up 65-85% of the dry weight in AC, is characterized by its repeating amino acid sequence (every 3rd residue is glycine) and triple helical structure. Procollagen, a roughly 1000 amino acid long protein, undergoes modification in the Golgi apparatus before it forms tropocollagen outside the cell. While the triple helix gets stabilized by hydroxyproline, hydroxylysine facilitates covalent binding of carbohydrates [44]. Collagen can be divided into fibril-forming (Collagen type II and XI) and non-fibril-forming (Collagen type VI, IX, and X). Collagen type II, with 90-95% the most abundant collagen type, is associated with collagen type XI to form a macro-fibril mesh which contributes to the tensile strength of AC [45]. Thus, dependent on the regional zone, collagen type XI can control the diameter of the macro-fibril while collagen type XI acts as interfibrillar (fibril to fibril) or intermolecular (fibril to aggrecan) bridge [46]. Collagen type VI, preferentially located in the PM, interacts with the cell surface via integrin and non-integrin mediated binding mechanisms [47]. Found close to hypertrophic chondrocytes in the calcified zone, collagen type X aids in cartilage mineralization and gives structural support [12].

The other major components, which make up 15-25% of the dry weight in AC, are **proteoglycans**. Due to its highly hydrophilic nature, proteoglycans are the major space-filling matrix macromolecule in AC which can be further divided into large aggregating proteoglycans like aggrecan (**Fig. 4**) or smaller proteoglycans including biglycan, decorin, or fibromodulin. Characterizing for both types are the covalently attached glycosaminoglycan (GAG) chains, making it one of the most complicated biological macromolecules. GAGs consist of long chains of non-branching polysaccharides which are usually sulfated (SO_4^{2-}) and, together with carboxylate groups (COO^-), account to an overall negative charge that attracts inorganic cations (Ca^{2+} , K^+ , Na^+) which increase osmolarity and ultimately hydrate cartilage via the Donnan effect [48]. The most abundant GAGs are the larger (~20 kDa) chondroitin sulfate (CS) and the smaller (~5-15 kDa) keratan sulfate (KS). Differences within these groups are dependent on the position of the sulfate group (e.g. chondroitin-6-sulfate, chondroitin-4-sulfate), disaccharide units, amino acid epimerization (chondroitin sulfate vs. dermatan sulfate) as well as linkage to the core protein (e.g. *N*- or *O*-linked keratan sulfate) [49]. Ratio and amount of both GAGs vary with age (increase of keratan sulfate, decrease of chondroitin-4-sulfate) [19] and depths in the tissue [50]. Aggrecan, the most abundant proteoglycan accounts for 4-7% of the wet weight in AC [43], is composed of a core protein that contains three globular (G1, G2, G3) and two extended interglobular domains (E1, E2). The major functional segment of aggrecan is the 260 nm long GAG carrying E2 domain that can be further divided into a KS and CS rich region. While the region closest to the G2 domain has high contents of proline, serine and threonine providing anchor points for KS, the region closest to the G3 domain is rich on serine and glycine which facilitates binding of all CS as well as half of all KS. After the aggrecan molecule is synthesized by the chondrocytes, it is secreted into the ECM. Here, up to 200 aggrecan molecules can form an aggregate with a single hyaluronic acid (HA) via highly specific non-covalent interactions at the G1 domain that are stabilized by a link protein [51]. Together, both collagen and the HA-aggrecan aggregate account for a pressurized ECM via the interaction of the swollen polyanionic aggrecans entrapped in the interstices of the highly tensile collagen network [52].

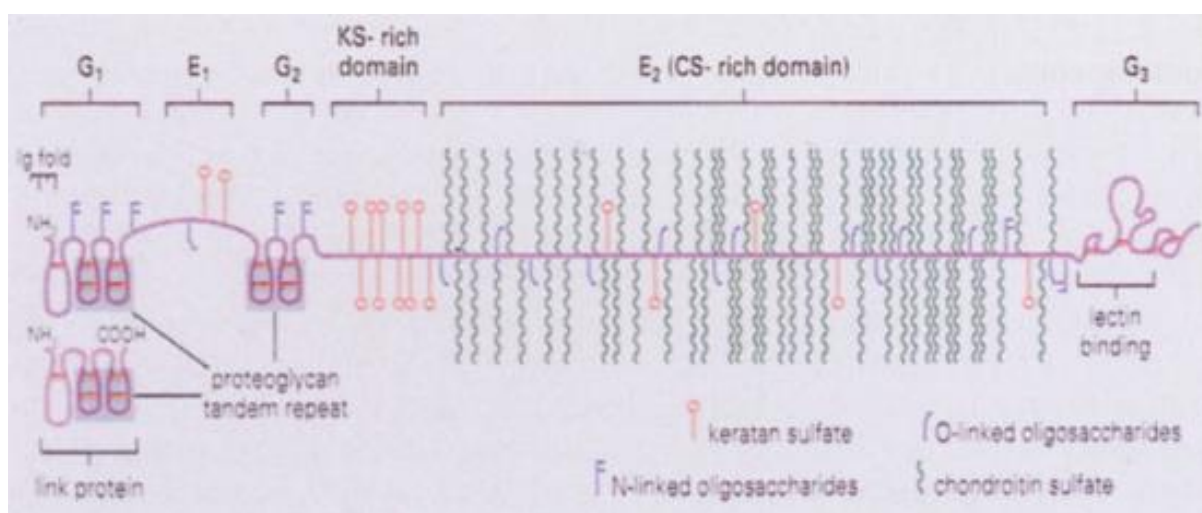


Fig. 4. Structure of aggrecan aggregate and link protein. Aggrecan is divided into three globular domains (G1, G2, G3) that are separated by two extended segments (E1, E2) that are rich on keratan and chondroitin sulfate. In between various N- and

O-linked oligosaccharides substituted the core protein. The G1 and link protein possess a loop structure that enables interaction with the hyaluronic acid chain forming a proteoglycan aggregate. Adapted from [14].

Special **non-collagenous proteins**, which neither belong to collagen nor proteoglycans, are abundantly present in AC: On the chondrocyte surface, anchorin acts as a mechanoreceptor and transmits altered stress to the cell [53]. Interacting with the cell membrane and different matrix constituents, fibronectin contributes to the matrix assembly [54]. Closely related and preferentially localized in the TM, the cartilage oligomeric matrix protein (COMP) further stabilizes collagen fibrils with multiple binding sites [55]. Together they participate in the formation of a cartilage spanning matrix molecule network and are essential for the stability and structure of AC.

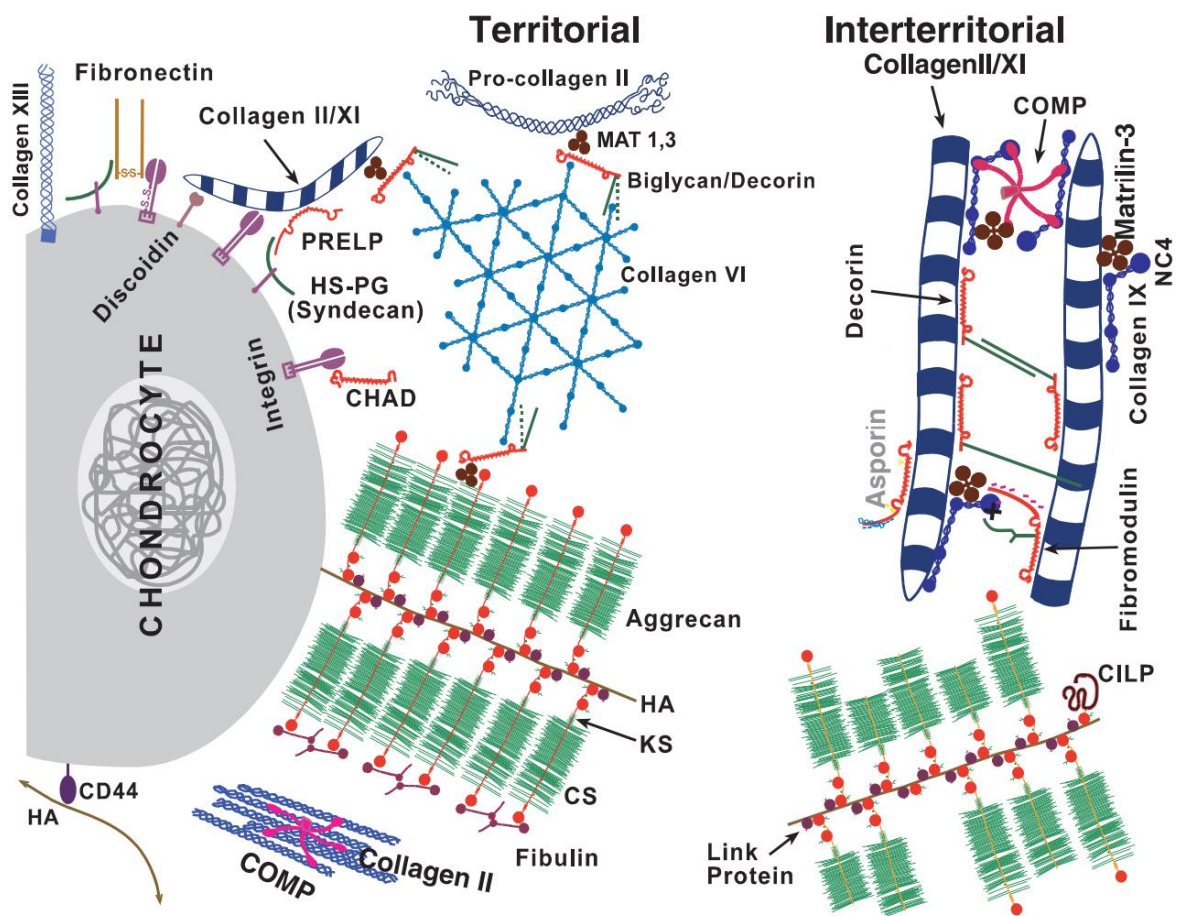


Fig. 5. Interactions of various macromolecules in the extracellular matrix of articular cartilage. Various aggrecan aggregates and link proteins attached to the hyaluronic chain and form a proteoglycan aggregate that is bound to the cell surface. Collagen type II is associated with collagen type XI forming cartilage typical collagen macro fibers. Collagen type IX is attached to a collagen macro fiber as well as to fibromodulin or decorin. Various other proteoglycans like biglycan (generally in the pericellular matrix) or anchorin (link between chondrocytes and collagen) are shown. Adapted from [56].

3.2. Mechanism of Articular Cartilage and Bone Development

During skeletal development, shape and size of bones is initially determined via a process called chondrogenesis. Chondrogenesis is involved in the formation of a cartilage template that results in a (i)

stable cartilage model or a (ii) transient cartilage model forming the growth plate and cartilage anlage. In time the transient cartilage model gets gradual replaced with bone tissue in a process called (1) endochondral ossification (ECO). The other process responsible for bone development is called (2) intramembranous ossification (IMO), which skips the cartilage intermediate step and directly ossifies the tissue. Generally, ECO is responsible for long bone (e.g. tibia, femur) growth while IMO happens during formation of flat bones (e.g. craniofacial skeleton). In the limb bud, mesenchymal cells condensate and trigger chondrogenesis which involves proliferation of chondroprogenitors that differentiate into chondroblasts and finally chondrocytes. This cell maturation is accompanied by a distinct change of extracellular matrix components from an undifferentiated type (Collagen type I, hyaluronan, tenascin and fibronectin [57]–[59]) into a cartilage specific type (collagen types II, IX and XI, aggrecan and link protein [60]–[63]). In distinct zones of the otherwise continuous cartilaginous anlage, rounded shaped cells become elongated and stop synthesizing collagen type II while regaining collagen type I production [64]. Interrupting and keeping developing bones apart, this nonchondrogenic region was termed interzone and marks the start of joint formation which finalizes in articular cartilage development. It involves several transcription factors and pathways like Sex-Determining Region Y-Box (SOX), Transforming Growth Factor β (TGF- β) superfamily and the Wingless-related Integration Site (WNT). Although the precise mechanisms are still not completely revealed, major steps are known. The downregulation of collagen type II and other cartilage specific markers [65] is accompanied by the SOX9 [66]. Further, the expression of different WNT signal molecules, especially WNT9A, are responsible for further progression in joint development. They are of particular importance, since inactivation of β -catenin, a downstream target of the WNT/ β -catenin pathway, resulted in bone fusion [67] as well as reduced expression of lubricin and deficiencies in the superficial zone [68]. The translocation of β -catenin into the nucleus resulted in regulation of TGF- β family proteins, especially of growth and differentiation factor 5 (GDF5) and bone morphogenetic protein 4 (BMP4). GDF5, one of the first markers identified in the developing joint (**Fig. 6**), is involved in initiation of chondrogenesis, promotes chondrocyte proliferation thus increasing final skeletal size, and maintains early joint formation [69], [70]. BMP4 on the other hand is tightly regulated by noggin since unbalanced BMP4 led to excess cartilage which resulted in failure to initiate joint formation [71]. Lineage tracing studies demonstrated that articular cartilage and other joint related structures originate from interzone cells first [68], but get continuously replenished by an influx of new population of cells [72] and thus support the theory of appositional growth [73]. However, it is still unclear and heavily discussed whether the unique structure of articular cartilage is adopted via proliferation [74] or rather owned to cellular rearrangement [75]. A fact, that seems solved for endochondral ossification [76]. As previously already mentioned, the process of ECO (**Fig. 7**) involves MCS undergoing condensation and formation of the cartilage anlage which grows both interstitial and appositional. Cells localized in the midsection undergo differentiation into a proliferative chondrocyte, mature and finally undergo hypertrophy. Instead of hypertrophy, cells close to the perichondrium undergo direct osteoblastic differentiation forming the bone collar which

subsequently becomes the cortical bone. Beside secretion of collagen type X and the calcification of surrounding tissue, hypertrophy is also indicated by cell enlargement (up to 5-fold) [77]. Counteracting this process, chondrocytes secrete matrix metalloproteinases (MMP) to degrade enclosing ECM. Since, hypertrophic chondrocytes also secrete pro-angiogenic factors like vascular endothelial growth factor (VEGF), blood vessels are attracted [78] which are of uttermost importance for further progression of bone formation [79]. Here, MMPs remove the transverse cartilage septae to permit longitudinal vessel ingrowth [80] and thus enable osteoclast as well as osteoprogenitor cells to migrate into the center of the bone, called diaphysis. There, cells (osteoblast as well as transdifferentiated chondrocytes [81]) remodel the partially calcified tissue and form the primary ossification center (POC). As bone growth advances, a medullary cavity is formed which subsequently stores yellow bone marrow (adipose-rich region) [82]. In the process of joint development, secondary ossification center (SOC) emerge at the periphery of the bones, at the epiphyseal ends. Between POC and SOC the growth plates develop with chondrocytes continuously undergoing hypertrophic differentiation and subsequent calcification. The growth plate is responsible for the continuous elongation of the bone until adulthood where it ceases to exist and gets remodeled into epiphyseal line.

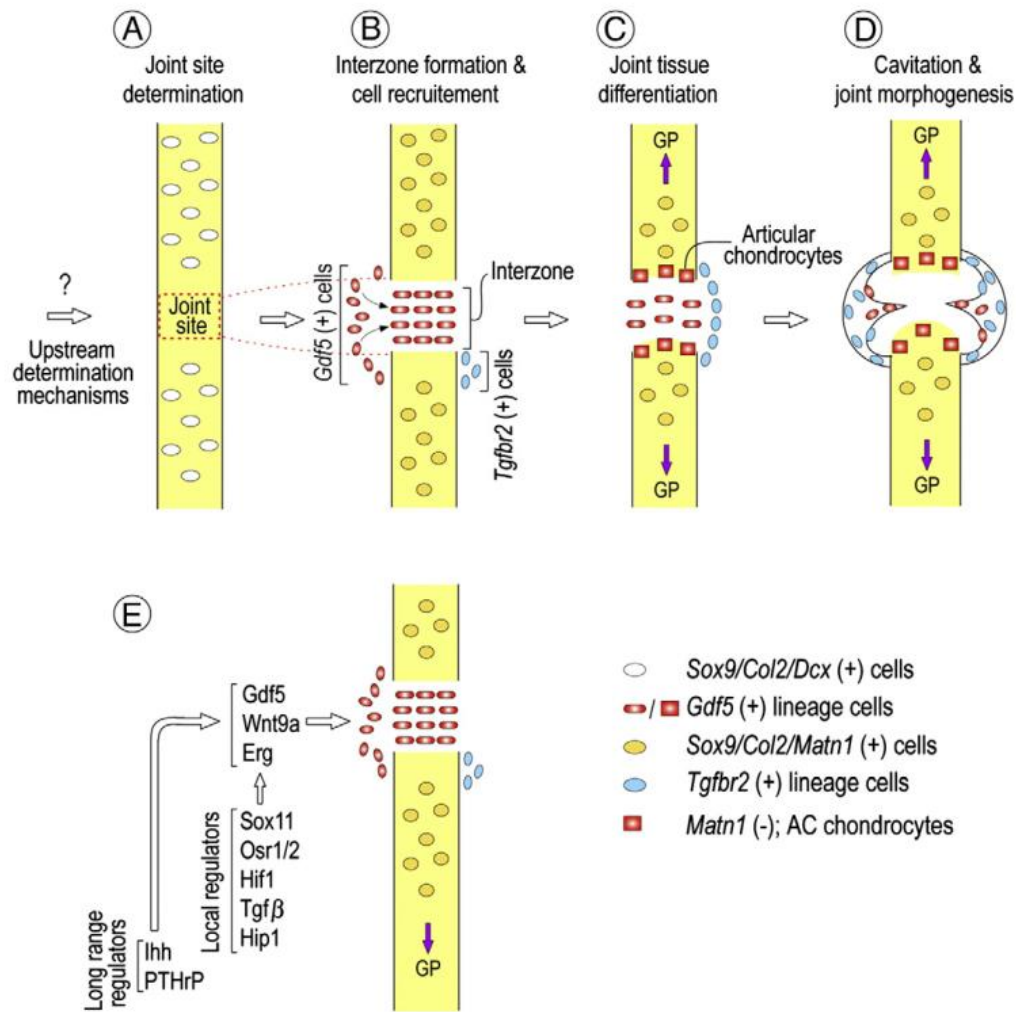


Fig. 6. Basic model of limb joint formation. (A) Unknown upstream determination mechanisms determine location of the joints along Sox9/Col2/Dcx-expressing anlagen. (B) Gdf5 expression is activated along with other interzone-specific genes (see E) and accompanied by Sox9/Col2/Matn1-positive cell influx from the flank. Cells located dorsally and ventrally of the interzone activate Tgfr2 expression. (C) Gdf5-positive cells adjacent their respective cartilaginous anlagen (Sox9/Col2 history but negative for matrilin-1) differentiate into articular chondrocytes. (D) Additional differentiation processes and mechanisms such as muscle movement would bring about cavitation and genesis of other joint tissues such as ligaments and other meniscus involving Gdf5- and Tgfr2-positive and -negative cell progenies. (adapted from [83])

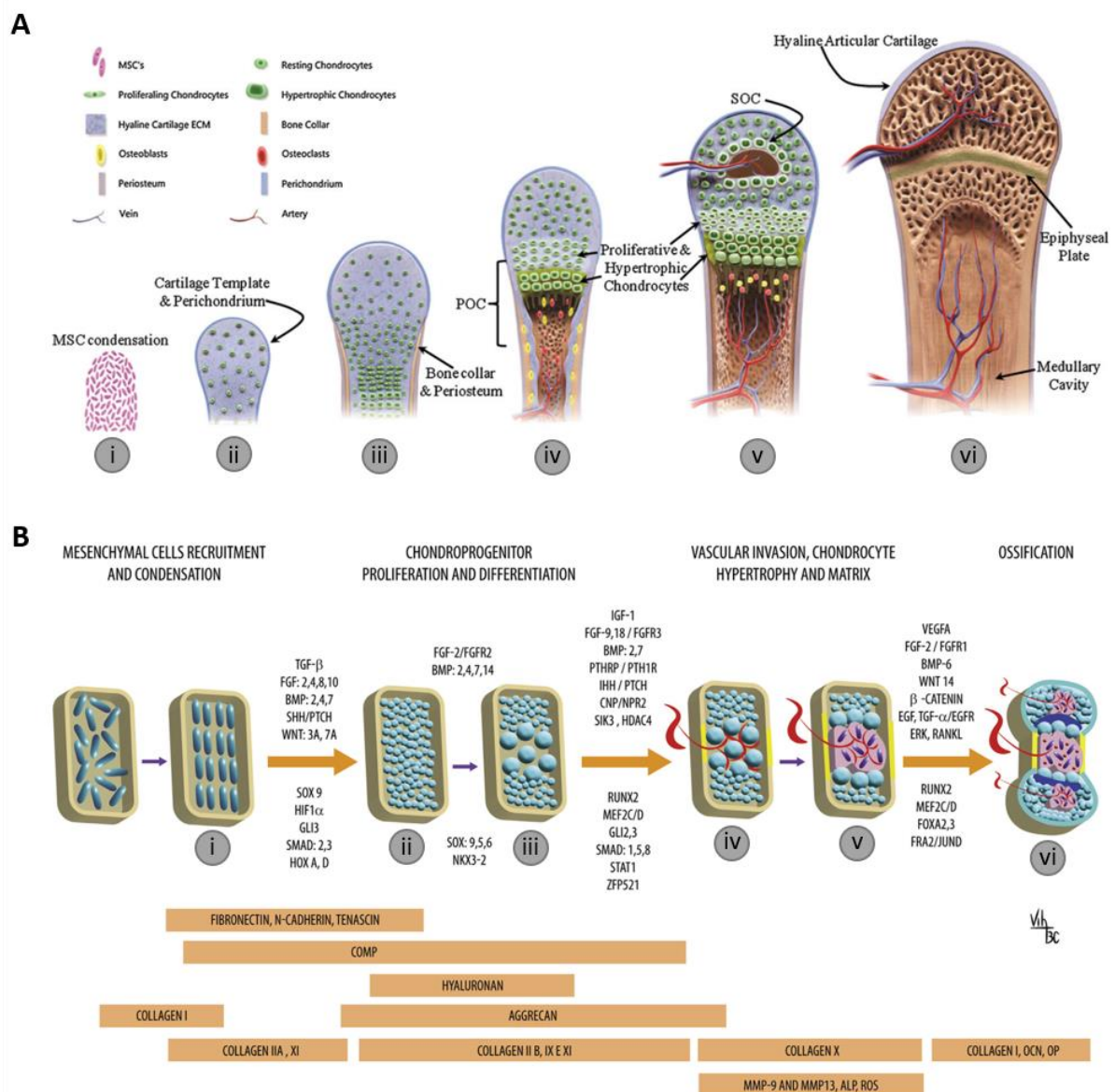


Fig. 7. Overview of chondrogenesis and endochondral bone development. (A) (i) Mesenchymal stem cells condense together and initiate bone formation. (ii) Subsequently MSC undergoing chondrogenic differentiation to form the hyaline cartilage template of future long bones. (iii) Cells in the center of the template undergo hypertrophic differentiation, while cells located on the periphery undergo direct osteoblastic differentiation and form an encircling bone collar. (iv) Hypertrophic cells initiate mineralization of the cartilage rudiment. The primary ossification center (POC) is formed in the diaphysis as blood vessel cells influx forming the ossification front. Osteoclasts remodel the calcified cartilage template, while osteoprogenitors develop into osteoblasts and form the osteoid of developing bone. (v, vi) In early postnatal life a secondary ossification center (SOC) is formed in the epiphyses triggered by invading blood vessels. Meanwhile the periphery maintains a stable cartilage phenotype resulting in hyaline articular surfaces seen within joints. Between the POC and SOC the epiphyseal growth plate persists and is responsible for longitudinal bone growth. In adulthood the growth plate gets ossified and replaced with an epiphyseal line. (B) Involved growth factors, differentiation factors, and some of their receptors are displayed above the arrows. Underneath each arrow, the relevant transcription factors involved are listed. Expressed extracellular matrix proteins at each step of this process are highlighted in orange. ALP, alkaline phosphatase; BMP, bone morphogenetic protein; CNP, C-type natriuretic peptide; COMP, cartilage oligomeric matrix protein; EGF, epidermal growth factor; ERK, extracellular signal-regulated kinase; FGF, fibroblast growth factor; FGFR, fibroblast growth factor receptor; FOXA, forkhead box A; FRA2, (FOS)-related antigen 2; HDAC4, histone deacetylase 4; HIF1 α , hypoxia-inducible transcription factor 1 alpha; HOX, homeobox transcription factor; IGF, insulin-like growth factor; IHH, Indian hedgehog; MEF2, myosin enhancer factor 2; MMP, matrix metalloproteinase; NKX3-2, NK3 homeobox 2; NPR2, natriuretic peptide receptor; OCN, osteocalcin; OP, osteopontin; PTCH, patched; PTHrP, parathyroid-hormone related protein; RANKL, RANK-Ligand; ROS, reactive oxygen species; Runx2, runt-related transcription factor 2; SHH, sonic hedgehog; SIK3, salt-inducible kinase 3; SOX9, sex-determining region Y-type high-mobility group box 9; STAT, signal transducer and activator of transcription 1; TGF, transforming growth factor; VEGFA, vascular endothelial growth factor A; Wnt, Drosophila segment polarity gene wingless and vertebrate homolog integrated int-1; ZFP521, zinc-finger protein 521 A adopted from [84]. B adopted from [85].

3.3. Acute and Chronic Articular Cartilage Pathologies

In tissue, the typical response to damage involves a cascade of necrosis, inflammation, repair and remodeling. Especially important for this response to trigger properly is access to the vascular network [86]. Being avascular in nature, articular cartilage lacks this vital connection thus repair is heavily hindered [20]. Prevalence of isolated cartilage defects is considerably low [87] and generally occur in combination with meniscus and/or ligament injuries [88], [89]. Dependent on the mode of **trauma**, two outcomes of cartilage repair exist [90]. If the trauma, considered as acute cartilage pathology, is direct mechanical and just imperceptible damages the matrix and does not exceed unharmed chondrocytes ability to regenerate destroyed matrix, the cartilage will be fully repaired. However, if blunt or penetrating trauma (common clinical situation) damages both matrix and cells, repair of cartilage depends on several different factors like depths, size and location of the defect as well as age of the patient [91], [92]. Dependent on the depth, injuries to the articular cartilage can be classified into chondral and osteochondral defects. Purely chondral defects can be further divided into a partial thickness or full thickness (extend to subchondral bone) and generally do not repair but increase in size and depth. On the other hand, osteochondral defects cross the tidemark and penetrate the subchondral bone enable migration of stem cells from the bone marrow into the site of the defect. Ultimately these cells produce fibrocartilage, which is mechanically less resilient than hyaline cartilage and can only support the tissue for a limited time until it breaks down with usage [93], [94]. When left untreated, this articular cartilage lesions can lead to the early onset of degenerative **osteoarthritis** (OA), a chronically developing cartilage pathology which is characterized by articular cartilage damage, osteophyte formation and inflammation of the synovial membrane [95]. Besides penetration into the depth of the tissue, the overall size of the defect is important. Defects smaller than 3 mm in diameter fully regenerated while large defects did not repair completely [91]. Fortunately, stress distribution on the subchondral bone is less likely for defects smaller than 1 cm² thus further progression is less likely. In terms of osteoarthritis (OA), age is a strong risk factor [96], [97]. With age, mitotic and synthetic activities of chondrocytes decline resulting in a smaller population which produce less extracellular matrix proteins responsible for cartilage hydration [98]. Studies conducted in rabbits showed increased regenerative potential for younger animals. This increased regenerative potential was also observed in patients during adolescent development and can partially be accounted to not yet fully developed and matured calcified zone. Thus, young patients suffering from osteochondritis dissecans (OCD), an osteochondral lesion, had smooth healing processes while the adult form generally remains severe [99].

3.4. Surgical Treatment Strategies in Clinics

Inadequate healing response of chondrocytes in partial thickness defects resulted in the development of treatment strategies that provide metabolically active cells to the site of the defect. These approaches are known as bone marrow stimulation techniques. It generally involves debridement of the joint and deepening of the defect to the subchondral bone. Originally the subchondral bone was penetrated via

drilling [100] to let bone marrow cells into the defect site. Further improvement of this method resulted in the development of **microfracture** [101] which involves an arthroscopic awl to create multiple fracture holes. Besides lower risk of over-heating or burning of the subchondral bone due to friction, the rougher surface facilitates adherence of newly formed tissue. Regardless of the applied method, proper distance between the holes is essential to maintain the integrity of the subchondral bone [102]. Being a minimally invasive arthroscopic approach resulting in reduced recovery time, microfracture is a popular treatment among athletes [103].

For full thickness defects, a technique called **mosaicplasty** can be applied. Usually spherical osteochondral plugs from low-weight bearing areas are harvested to fill the prepared (perpendicular vertical edges) defect site. Different sizes of plugs are used to reduce gaps between the plugs and increasing filling of the defect, thus creating a mosaic pattern. Although advocates claim that this technique provides a stable and firm weight-bearing surface, inter-plug space gets filled with mechanically inferior fibrocartilage [104], [105]. Thus, the ultimate goal is to reduce gap size. Nevertheless, outcomes of studies attempting to further reduce gap size by altering the plug shapes (e.g. honeycomb) remain inconclusive [106]. Reducing donor site morbidity to a minimum, treated defects should not exceed 4 cm² [104]]. Further issues of mosaicplasty involve lack of seamless lateral integration into the native cartilage caused by leaking of synovial fluid into the gaps [107] as well as difference in height of harvested plugs.

First described by Peterson *et al* [108], **autologous chondrocyte implantation** (ACI) involves a 2-step surgical procedure. First, chondrocytes are isolated from a biopsy from a low-weight bearing area and expanded in vitro until a sufficient cell number is reached. Second, the joint is opened, the lesion debrided and covered with a periosteal flap or collagen membrane. Finally, the patch is sutured or glued on the native cartilage establishing a water-tight seal before chondrocytes are injected into the defect. In succeeding generations, ACI was improved using a scaffold as filling matrix and provides anchor points for cells. However, studies comparing membrane covered ACI and matrix-assisted ACI (MACI) showed equivocal results with clinically equivalent groups [109], [110]. The latest improvement of ACI involves a chondroconductive/inductive matrix that is populated with allogenic tissue or autologous stem cells. Thus, elaborately and morbid cartilage harvest can be omitted and condensed in single minimally invasive surgical procedure [111], [112].

Besides the already mentioned techniques, several other approaches include but not limited to perichondral grafts [113], periosteal grafts [114] as well as osteotomy [115] are performed in clinics. Despite having so many different treatment options, current surgical procedures fail in producing neo-cartilage with a long-term functional stability of native cartilage. Thus, hopes in treating chondral and osteochondral defects are relayed to tissue engineering.

4. Tissue Engineering

Since the early 90s, tissue engineering (TE) remains to be an emerging interdisciplinary research field [4]. The ultimate goal is to develop biological substitutes by combining principles and methods of engineering, biology, chemistry, material science that will regenerate, maintain or even improve damaged tissue or organs. Originally, a triad consisting of the most important factors like cells, scaffolds and growth factors was defined and later extended by mechanical stimuli [5]. The following section will discuss TE in terms of articular cartilage in more detail.

4.1. Cells

Although not absolutely necessary, exogenous cells combined with a construct accelerates *in vitro* and *in vivo* tissue regeneration [116]. The logical cell source for articular cartilage TE would be **autologous chondrocytes**. Being native to regenerate tissue and expressing the desired phenotype, they already produce accurate cartilage matrix proteins while not triggering any immune response. However, the zonal organization of cartilage results in subpopulations with different morphology and synthetic activities [117], [118] and, thus, requires different mechanical stimulation protocols when creating functional tissue [119]. Besides being extremely scarce in native tissue which requires an extensive expansion endeavor, harvesting autologous chondrocytes from sites of extensive degradation or diseased tissue is not an option. An alternative would be chondrocytes from allogenic (same species, different individual) [120] or xenogenic (different species) [121] sources. However, potential immune response or transmission of diseases raise big concerns [122].

Other possible sources are **mesenchymal stem cells** (MSC), a progenitor cell type that is residing throughout the body and can be differentiated into various lineages [123]. Dependent on the harvesting position, minimal donor site morbidity and patient pain is to be expected. Generally, MSC exhibited a high proliferation rate thus reducing the amount of needed biopsy to a minimum. Beside their pluripotent nature, MSC have shown to have unique immunomodulatory properties [124] making them invaluable during tissue repair, especially when coping with chronic disorders. Although number of MSC decrease with age [125], [126], studies investigating proliferation and differentiation potential of MSC in patients suffering diseases found implications [127] or only marginal differences [128], [129].

Avoiding these limitations, researcher have laid focus on **embryonic stem cells** (ESC). Even during extensive expansion, no effect on proliferation rates, telomere shorting or the loss of multipotency was observed as was apparent in MSC cultures [130]–[133]. Since these cells are truly pluripotent, researchers struggling to develop effective differentiation protocols for every lineage. Nevertheless, defined media and environmental conditions (hypoxia) showed promising results for the chondrogenic differentiation [134]–[136]. However, the inherent risk of teratoma formation when using ESC as well as immunogenic problems when using allogenic sources raises concern. In addition, work with human ESC raises different ethical questions which must be considered in the greater scheme [137].

Although cases of teratoma formation are reported [138], [139], **induced pluripotent stem cells** (iPSC) do not have an ethical barrier. The origin of iPSC are somatic cells which are reprogrammed into a pluripotent state via the expression of certain transcription factors. Originally, these factors (Oct3/4, Sox2, Klf4, and c-Myc [140] or Oct3/4, Sox2, Nanog, and Lin28 [141]) were dependent on viral-mediated delivery, but also non-viral methods exist to date [142], [143]. Being in an infant state similar to ECS, iPSC are especially susceptible to an undefined environment, thus robust protocols to induce chondrogenesis are required [144]. Since iPSC can be harvested from any patient, even those suffering from degenerative disorders [145], immunogenicity related issues with allogenic sources are perfectly circumvented and thus allowing a wide clinical adoption.

4.2. Growth Factors

Dependent on the chosen cell type, use of different growth factors can result in various outcomes. Growth factors (GF) are biologically active polypeptides that influence cellular division, growth, and differentiation thus regulating development and homeostasis of articular cartilage. Throughout life, GFs play a vital role in healing and development, an aspect TE wants to use to accelerate tissue growth and promote rapid regeneration. Since varying amounts of GF are constantly present in the body, scientist typically use increased amounts to elicit dramatic and measurable effects. In vitro GFs are usually delivered as soluble components in the culture media. However, once implanted, deliver of GFs to the cells is more complicated. A solution might be the integration of carriers into biodegradable constructs which get release GF upon scaffold remodeling [144]. In articular cartilage engineering, various growth factors have reached significant relevance. This includes prominent members of the transforming growth factor beta (TGF- β) superfamily as well as insulin-like growth factor (IGF), basic fibroblast growth factor (bFGF), or platelet-derived growth factor (PDGF). Studies have shown that **IGF** increases collagen and proteoglycan deposition [146], [147], an effect that varies across cartilage zones [146]. Further, IGF is essential for articular cartilage integrity as loss results in AC lesions [148] and supports cartilage repair [149] and protects from chronic inflammation like OA [150]. On the other hand, **bFGF** has been reported to be heavily active after tissue damage [151] and thus is suspected to be involved in tissue remodeling [152]. Although it was shown that bFGF accelerates tissue regeneration [153], there is evidence suggesting that bFGF antagonizes IGF and reduces proteoglycan synthesis via upregulation matrix-metalloproteinases (MMPs) [154] making it a controversial tool [155]. **PDGF**, heavily concentration in platelet-rich plasma (PRP) [156], [157], has been shown to be a potent chemotactic (chondrocyte migration) [158] and mitogenic factor [159], [160]. Besides reducing the synthesis of proteoglycans, PDGF also changed the morphology of chondrocytes into a spindle shaped phenotype [161], contradicting the desired AC phenotype. Thus, studies investigated practicality of PDGF in meniscal repair showed good results [162], especially in combination with other GFs [163]. In articular cartilage repair the **TGF- β** superfamily is of particular interest. Members of this family are structurally related and active as homo- or heterodimer link via a disulfide bond [164]. Beside activins and inhibins, the two largest subfamilies are TGF-b [165] and bone morphogenetic proteins (BMP) [166] with

currently 3 and over 20 members, respectively. While TGF-bs are especially popular in cartilage engineering, BMPs play a crucial role in both chondrogenesis and osteogenesis. TGF-b1 has shown to enhance chondrocyte proliferation [167], promote synthetic activity [168], increase construct wet weight [169], increases in both aggregate and tensile modulus [170], and decreases the catabolic activity of IL-1 [171]. TGF-b3 significantly increased glycosaminoglycan and collagen content in MSC [172], [173] and chondrocytes [174]. Treatment with BMP-2 led to cartilaginous matrix production [175]–[177] and reduction in collagen type I expression [178] and robust aggregate production being the most effective factor from the BMP subfamily [172]. Being a critical signaling molecule, BMP-4 induces chondrogenic differentiation of MSC to chondrocytes [179] but also stimulates syntheses of chondrogenic (collagen type II and aggrecan) factors while suppressing osteogenic (collagen type I and type X) factors [180]. BMP-6, considered to regulate bone homeostasis via osteoclast generation, has also the potential to stimulate proteoglycan synthesis in chondrocytes from OA joints [181] as well as producing a strong cartilage phenotype in combination with other factors [182]. Similar to the already mentioned BMPs, BMP-7 plays a vital role in AC regeneration [183]. It has the potential of healing surface lesions via enhanced proliferation of chondrocytes [184] and protects cartilage against damage with strong pro-anabolic activity and exceptional anti-catabolic properties [185].

4.3. Biomaterials and Scaffolds

Biomaterials are the basic building blocks for scaffolds and can be of natural or synthetic origin. Based on their microstructure, biomaterials can be further classified into hydrogels, sponges, fibrous meshes, or nanofibers [174]. Regardless of the actual form, several essential criteria must be met: scaffolds must be (1) biocompatible/bioactive meaning sterile as well as non-toxic to the surrounding thus not triggering any immune response even when absorbed and remodeled by cells and allow a controlled release of GFs, be (2) biodegradable, ideally with an adjustable resorption rate, to provide initial structural support but gradually degrade with new tissue formation, have (3) suitable porosity and interconnectivity to permit and facilitate cell migration, adhesion and differentiation as well as efficient exchanges of nutrients and waste products but also allow for seamless integration into the host tissue, and possess enough (4) structural integrity to protect new tissue formation under native mechanical loads [186]–[188].

Natural biomaterials are based on polymers extracted from living organisms with prominent members like collagen, alginate, agarose, hyaluronic acid, chitosan, fibrin glue and silk fibroin to name a few. Due to their natural origin, natural biomaterials are believed to have reduced immunogenic activity and already provide anchor points for cell attachment and differentiation [189]. **Collagen**, being the most abundant protein [190], has always been in focus of researchers. To make it safe for clinical use, collagen is processed to remove its antigenicity either enzymatically via telopeptides removal or chemically via cross-linking [191]. Although collagen type II is the predominant collagen in native articular cartilage, most studies utilizing collagen type I due to its vast existence and ease of isolation. Nevertheless, studies

reported that chondrocytes cultured in collagen type I gels maintained their phenotype [192] or have been well integrated into the matrix following ACI [193] or microfracture treatment [194] as well as induced chondrogenic differentiation of MSC cultured in a hydrogel [195]. Comparison of both collagens showed that collagen type II retains a higher amount of chondrocytes in the spherical phenotype resulting in higher matrix production [196] but did not trigger different contractile behavior [197]. **Alginate or agarose**, both polysaccharides derived from algae or seaweed, can form gels via ionic bonding in the presence of calcium (Ca^{2+}) or change in temperature, respectively. The gels are generally used to encapsulate cells and provide a biocompatible three-dimensional (3D) environment, similarly experienced by chondrocytes in vivo [198]. Both materials do not rapidly degrade in vivo [199] and thus can interfere with new tissue growth. Since it is laborious to finetune the degradation properties and consequently the lifetime of the scaffold [200], [201], long-term implants facing the problem of undefined integrity loss since the material eventually gets removed or degraded. Nevertheless, it's a preferred option for scientist to mimic native cartilage environment [202], [203] in combination with mechanical stimulus [204], [205] and could show that it led to production of ECM proteins [206]. **Hyaluronic acid**, also known as hyaluronan, is a non-sulfated glycosaminoglycan that helps to lubricate the joint and serves as the backbone of the giant aggrecan aggregate. It can be used as an injectable to fill minor irregular shaped defects [188] or cross-linked to use as gel to support formation and maintenance of cartilage [207]–[209] or used as porous scaffold with increase mechanical stability to stimulate chondrogenesis and chondrogenic matrix production [210]–[212]. Besides its chondrogenic potential, hyaluronan has shown to be beneficial in treatment of early OA lesion because of downregulation of catabolic factors and apoptosis [213].

Synthetic biomaterials are obtained from various chemical processes with prominent members like polyglycolic acid (PGA), polylactic acid (PLA), polycaprolactone (PCL), or polyethylene glycol (PEG). Compared to natural biomaterials, properties of synthetic polymers can be easily adjusted and produced in bulk [214]. Dependent on the area of application, they can be modified to possess a specific degradation rate, provide a defined mechanical stability and can be equipped with bioactive substances [215]. **PGA** is the simplest thermoplastic aliphatic polyester [216] and usually produced via ring-opening polymerization or polycondensation and formed into a porous scaffold via salt-leaching. Total degradation time varies between 4 to 12 months, although mechanical stability is lost considerably earlier. Upon degradation, PGA gets naturally resorbed by the body, making it an attractive biocompatible material. Compared to collagen scaffolds, PGA could improve proteoglycan synthesis of chondrocytes [217]. **PLA**, another aliphatic polymer, matches many properties of PGA like body-resorbable degradation products as well as methods of fabrication. However, PLA has shown to have an increased reabsorption time (12 to 24 months) thus making it the preferential choice for applications needing longer matrix formation times [218]. Compared to PGA, chondrocytes had reduced affinity to PLA surfaces although the final cell count was not affected [219]. Thus, PLA and PGA are usually combined into a PLGA copolymer to have the prolonged stability of PLA and the increased affinity of

PGA. Dependent on the used ratio, this copolymer has equally high biocompatibility but more precisely controllable mechanical properties as the individual polymers. In addition, studies have shown that PLGA scaffolds are a better option than PLA alone to induce cartilage tissue formation in chondrocytes [220]. PLGA succeed in induce chondrogenesis in adipose-derived stem cells in combination with TGF- β 1 [221], hyaluronan [222] or fibrin [223]. Other synthetic polymers include PCL, which shows extensive resistance to hydrolytic scission and thus has prolonged degeneration time, or PEG, which is highly hydrophilic and thus prevents protein adsorption and cell attachment. Both polymers are generally used in combination with the previous mentioned ones to generate an optimal scaffold for the desired application.

Although natural and synthetic biomaterials could show to be chondroinductive on their own, combination of both into a **composite scaffold** might dissolve some drawbacks. While synthetic polymers can provide the structural backbone and control degradation time, natural polymers can increase cell affinity and reduce cytotoxicity. Following this proposal, several composite scaffolds have been developed with promising results [222], [224]–[226].

4.4. Mechanical Stimulation

Articular cartilage is heavily exposed to biomechanical stimulation, a stimulus that already plays an important part in cartilage development as well as in skeletal development via endochondral ossification. In mature cartilage, mechanical forces of relevant magnitudes control the phenotype, upregulate biosynthesis, and constantly reorganize the ECM and thus contribute to maintain cartilage homeostasis in a healthy joint. While relevant forces positively influence cartilage homeostasis, excessive loading like experienced in a trauma can contribute to develop degenerative joint disease such as OA. Usually, articular cartilage is exposed shear, direct compression, hydrostatic pressure, and tension (**Fig. 8**).

Although proteins on the cartilage surface as well as in the synovial fluid reduce friction to a minimum [19], **shear stress** is still experienced during normal physiological movement. Shear stress can be studied by exposing the AC construct to fluid flow [227] or direct shear stress [228], [229]. While direct shear stress involves sliding a solid sphere or platen along the surface of the construct, fluid flow generated shear generally involves a fluid. Unfortunately, it is almost impossible to decouple the effects of direct shear stress or fluid flow. While fluid flow can increase nutrient supply to the AC construct, direct shear stress adds a compressive factor to the equation. With this limitation in mind, researchers could show that dynamic direct shear stress results in enhanced proteoglycan and protein biosynthesis [230]–[232]. Mixed results were gained when investigate fluid-shear stress, with both collagen type I [233] or collagen type II [234] increased. However, shear stress has also shown to increase release of prostaglandin E2 [235], and increased levels of interleukin-6 [236] and nitric oxide [237].

Another prominent factor mediated in normal movement is **direct compression**. Force is transmitted directly onto the construct surface which results in deformation of the AC construct and enhanced salute

transport [238]. Both events are constantly triggered during dynamic compression, but solute transport is on hold or significantly reduced during static compression resulting in an decrease of intratissue pH and increase of osmotic pressure [239]. Thus, negative response on static compression are highly attributed towards this reduced mass transport [240] although no significant cell damage was verifiable [239]. Long-term dynamic loading has shown to increase gene expression of collagen type I and II but reduced aggrecan [241]. Others found contradicting results, with proteoglycans higher synthesized than collagens resulting in higher dynamic stiffness and higher equilibrium modulus [242]. A study comparing different frequencies (0.03-0.33 Hz) and load durations (12-120 min) resulted with highest GAG synthesis for 54 min at 33 Hz suggesting that cells may be sensitive cumulative (nonrecoverable) compressive strain [205]. Typically, dynamic compression at 1 Hz or lower and 10% or lower has shown to be beneficial [242], [243].

During motion, cells in native cartilage experience **hydrostatic pressure** triggered by compressive forces perpendicular to the complete cell surface. Hydrostatic pressure is caused by the dense matrix and Donnan osmotic pressure resulting in inhibition of fluid flow. Due to the intrinsically incompressible nature of fluid filled tissue, hydrostatic pressure is suspected to act on transmembrane proteins and induce conformation change triggered by void spaces inside the protein [244]. Generally, human chondrocytes are exposed to periodic HP in the range of 3-10 MPa [245], [246] with peak values of up to 18 MPa measured in the hip joint [247], [248]. Exposure of articular cartilage should not exceed 30 MPa because it alters chondrocyte proteoglycan synthesis [249], [250] and can induce expression of interleukin 6 (IL-6) and tumor necrosis factor α (TNF- α) [251]. However, when exposed to pressure magnitudes of physical range, dynamically cultured chondrocytes showed time-dependent effects of collagen type II and aggrecan mRNA [252], prevented GAG loss while simultaneously increasing collagen production [253], or enhanced both collagen and GAG deposition under presence of TGF- β 1 [254].

Contrary to expectations, native articular cartilage exhibits a lower compressive modulus (E_{-Y} ; 0.1-1 MPa) [255], [256] than tensile modulus (E_{+Y} ; 3-6 MPa) [257], [258]. However, upon axial compression the tensile modulus restricts lateral expansion of the tissue and thus, combination of both tensile modulus and interstitial fluid, results in an at least 6-times higher dynamic compression modulus (G^*) [259], [260]. This **tensile stress**, mainly actuated via collagen fibers in a uniaxial/biaxial manner, has shown to be an important stimulus for chondrocytes. Compared to other stresses present in AC, only very few studies tried to elucidate the effect of tensile stimulation [261]. A study using intermittent tensile strain on a self-assembled human neocartilage could reach tensile properties and collagen contents comparable to native tissue [262]. It is hypothesized that tension triggers cellular response via the ion channel transient receptor potential vanilloid-4 (TRPV4) [262]. A similar study found that uniaxial load promoted matrix alignment and increase collagen (27%) and glycosaminoglycan (67%) synthesis [263]. Since the tension-compression nonlinearity of particular importance for articular

cartilage, researchers developed a novel method to simultaneously measure compressive and tensile modulus via combined efforts of osmotic loading, video microscopy, and unconfined compression testing [264]. In a pilot study they could show that dynamic loading increased both tensile and compressive moduli [264].

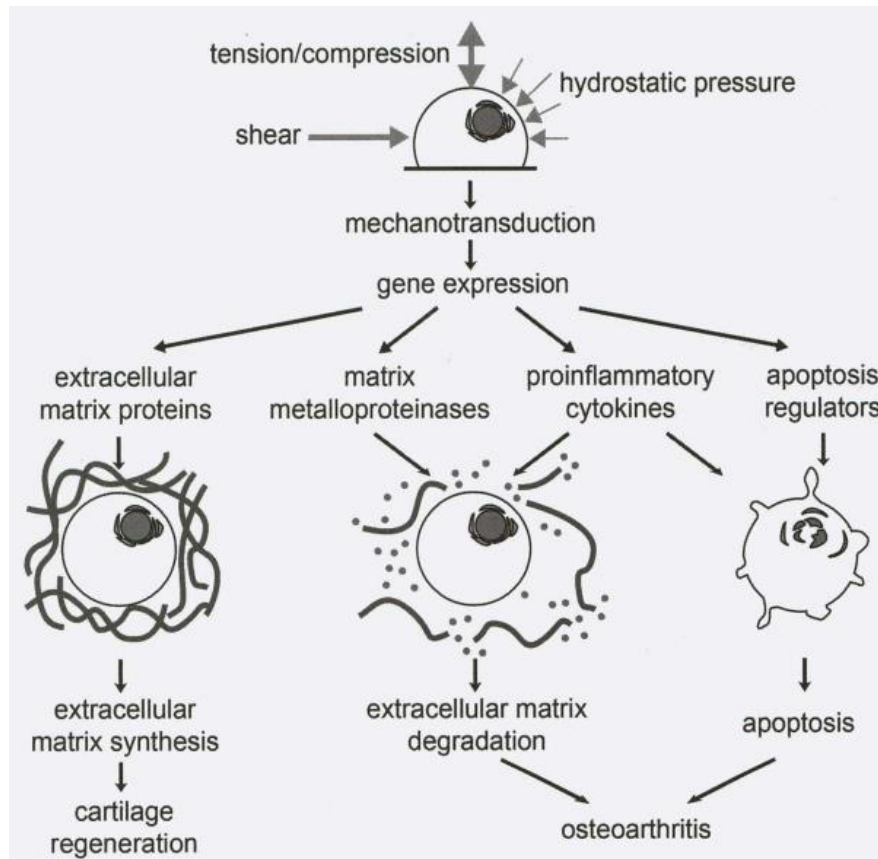


Fig. 8. Mechanotransduction pathway of a chondrocyte. Mechanical stimulation of a chondrocyte triggers a mechanotransduction pathways which results in different gene expression that either lead to cartilage regeneration or osteoarthritis. Adapted from [265].

AIM OF THE THESIS

This doctoral thesis focusses on tissues in musculoskeletal tissue apparatus closest related to each other. Bone and cartilage evolve from one precursor and provide stability to the human body like no other. Being an integral part, loss of function due to trauma or disease results in dramatic reduction in life quality. Thus, different options for bone and cartilage repair were investigated in an attempt to improve regenerative potential.

The thesis is divided into 3 major objectives:

i. Endochondral bone regeneration with a perfusion bioreactor system

Although bone has an innate ability to regenerate, large complex fractures exceed the natural healing capacity of bone and will result in non-unions. For effective treatment, these non-unions require external intervention which is generally accomplished with the aid of autografts or allografts. However, donor site morbidity and potential foreign body immune reaction are drawbacks accompanying this option. Thus, tissue engineering strives to offer bone grafting without the necessity of bone harvest from the patient. Hereby, osteogenic cells, osteoinductive scaffolds and external stimuli are combined to resemble an autologous graft. However, using these grafts to repair long bone non-unions produced mixed results. We hypothesized that mixed results are due to intramembranous ossification instead of endochondral ossification, which is the native process in long-bone development. Using a perfusion bioreactor to apply mechanical cues, we investigated the regeneration potential of adipose-derived stem cells (ASCs) seeded in a decellularized xenogenic graft for long-bone healing.

ii. Decellularized auricular cartilage as a new biomaterial for articular cartilage tissue engineering

Contrary to bone, cartilage innate healing ability is heavily compromised by an overall hardly metabolic active tissue. Thus, cartilage damage induced via trauma or degenerative processes outperforms the limited regenerative potential and necessitates external intervention. Dependent on the type of defect, current strategies for the treatment of large cartilage defects combine the use of scaffolds for structural support and cells to synthesize new functional matrix. Despite diverse options regarding surgical techniques, cell sources and biomaterials, the restoration of hyaline-like cartilage with its native characteristics remains unsatisfactory and often leads, after initial success, to treatment failure and need for reoperation. An integral part in the functionality of articular cartilage plays the specialized architecture and structure – a composition which has not been met by any commercially available biomaterial in clinical use. Therefore, we hypothesized that a biomaterial which mimics the native hyaline cartilage properties will improve the outcome of surgical interventions. An attractive candidate is elastic cartilage, which possesses characteristics comparable to articular cartilage. In addition, it features a traversing channel network of elastic fibers, which enables cell migration after removal. Here we investigated *AuriScaff* as potential chondrogenic graft when seeded with ASC and/or chondrocytes and functionally primed with a biomimetic bioreactor.

iii. Effect of hydrostatic pressure-generated reactive oxygen species on neo-cartilage formation

Osteoarthritis (OA), a degenerative disease of the joint presumably triggered by acute trauma or chronic overload, is a socio-economic burden affecting a vast portion of the adult population. Despite intensive research, the exact molecular mechanisms responsible for the initiation and progression of OA remains inconclusive. Historically classified as a simple wear-and-tear disease, recent findings draw a much more complex picture with extensive involvement of the immune system. In the last decade, a number of studies identified reactive oxygen species (ROS) as a leading factor in the evolution of OA. Different in vitro models were developed to investigate ROS impact on osteoarthritic tissue, which general base on the application of H₂O₂. However, in a real setting, osteoarthritic chondrocytes are exposed to a wide variety of ROS in addition to mechanical load. Thus, we hypothesized that with the application of hydrostatic pressure via compressed air, the production of elevated levels of superoxide and other ROS species will be induced. Then this model system will be utilized to investigate the influence of ROS on neo-cartilage formation of ASC in a pellet culture system.

CHAPTER I

**Endochondral bone regeneration
with a perfusion bioreactor system.**

Tissue-engineered hypertrophic chondrocyte grafts enhanced long bone repair

Jonathan Bernhard¹, James Ferguson², **Bernhard Rieder**³, Patrick Heimes^{2,4}, Thomas Nau²,
Stefan Tangl⁴, Heinz Redl², Gordana Vunjak-Novakovic^{1,5,*}

¹ Department of Biomedical Engineering, Columbia University, New York, NY 10032, USA

² Ludwig Boltzmann Institute of Experimental and Clinical Traumatology, Austrian Cluster for Tissue
Regeneration, Vienna A-1200, Austria

³ Department of Biochemical Engineering, University of Applied Sciences Technikum Wien, Austrian Cluster
for Tissue Regeneration, Vienna A-1200, Austria

⁴ Department of Oral Surgery, Medical University Vienna, Austrian Cluster for Tissue Regeneration, Vienna A-
1090, Austria

⁵ Department of Medicine, Columbia University, New York, NY 10032, USA

* corresponding author. gv2131@columbia.edu

Published in *Biomaterials* on May 31st, 2017

Abstract

Bone has innate ability to regenerate following injury. However, large and complex fractures exceed bone's natural repair capacity and result in non-unions, requiring external intervention to facilitate regeneration. One potential treatment solution, tissue-engineered bone grafts, has been dominated by recapitulating intramembranous ossification (bone formation by osteoblasts), although most serious bone injuries heal by endochondral ossification (bone formation by remodeling of hypertrophic cartilaginous anlage). The field has demonstrated that using endochondral ossification-based strategies can lead to bone deposition. However, stem cell differentiated hypertrophic chondrocytes, the key cell type in endochondral ossification, have not been studied for long bone defect repair. With translation in mind, we created tissue-engineered grafts using human adipose stem cells (ASC), a clinically relevant stem cell source, differentiated into hypertrophic chondrocytes in decellularized bone scaffolds, and implanted these grafts into critical-size femoral defects in athymic rats. Over 12 weeks of implantation, these grafts were compared to acellular scaffolds and grafts engineered using ASC-derived osteoblasts. Grafts engineered using hypertrophic chondrocytes recapitulated endochondral ossification, as evidenced by the expression of genes and proteins associated with bone formation. Markedly enhanced bone deposition was associated with extensive bone remodeling and the formation of bone marrow, and with the presence of pro-regenerative M2 macrophages within the hypertrophic grafts. As a result, hypertrophic chondrocyte grafts bridged 7/8 defects, as compared to only 1/8 for osteoblast grafts and 3/8 acellular scaffolds. These data suggest that ASC-derived hypertrophic chondrocytes in osteogenic scaffolds can improve long bone repair.

Keywords: Bone regeneration, Bone tissue engineering, Hypertrophic chondrocytes, Endochondral ossification

1 Introduction

An estimated 100,000 bone fractures per year exceed the regenerative ability of native bone and remain unhealed, with the clinical presentation of fracture non-unions [266]. To effectively treat non-unions, an external intervention is required. In situations requiring grafting material, autografts promote faster union formation and decrease the rate of surgical revisions compared to allografts [267]. Despite positive clinical outcomes, the use of autografts remains limited due to the scarcity of suitable autologous bone and the associated donor site morbidity [268]. As a possible treatment option, autologous bone grafts can be engineered *in vitro* from the patient's stem cells, to offer bone grafting without the necessity of harvesting bone from the patient [4], [269]. By combining osteogenic cells, osteoinductive scaffolds, and external stimuli, experimental bone grafts resembling autologous grafts have been engineered [270]. However, the use of these grafts to repair long bone non-unions have produced mixed results [270], [271].

In the case of long bone repair, the body utilizes endochondral ossification [272], [273]. During endochondral ossification, the initial fracture is stabilized by the formation of a cartilage anlage by mesenchymal stem cells [274], [275]. As the initial anlage-building chondrocytes mature into hypertrophic chondrocytes, they start controlling the turnover of the cartilage anlage into a bone template, and induce formation of vasculature and bone marrow [273]–[275]. Previous work has shown that initiating endochondral ossification [276]–[280] or including hypertrophic chondrocytes [281]–[285] *in vivo* will lead to bone formation. Due to the superior outcomes of autologous grafts [267] and the limitations associated with cell and factor therapies [271], we aimed to engineer clinically relevant, controllable, and reproducible tissue grafts for long bone repair. Based on these previous studies, we utilized differentiated hypertrophic chondrocytes within a suitable tissue engineered construct to facilitate bone formation and defect healing by mobilizing native-like processes.

To provide the stable environment necessary for effective long bone repair [286], and provide mechanical properties of the native skeleton, decellularized bone scaffolds were utilized. Adipose-derived stem cells (ASCs) were used, because they are multipotent with similar capability as bone marrow stromal cells, **Fig. S2** [287], easy to harvest, can be expanded to clinically relevant numbers to allow creation of autologous tissues [288], and were recently shown to have hypertrophic chondrocyte differentiation capability [289]. The protocols utilized for tissue engineering were based on previous studies that utilized embryonic [290] and bone marrow stem cells [282], [291]. With the creation of these unique hypertrophic chondrocyte bone tissue grafts, we studied their ability to repair orthotopic, critical-size defects in the rat femur, in a model of long bone fracture healing. To compare the performance of these constructs to the established tissue engineered grafts, we created complementary, osteoblast-based bone grafts optimized in a perfusion-controlled bioreactor [292], [293], and used acellular scaffolds as an additional control. Based on the previous studies highlighted above, and the natural path of bone repair, we hypothesized that the differentiation of hypertrophic chondrocytes would

result in more effective bone repair than traditional tissue engineered approaches. We found that the differentiated hypertrophic chondrocytes created robust, hypertrophic cartilage templates within the decellularized bone scaffolds. Upon implantation, the grafts mediated fast remodeling and integrated with the native bone to bridge critical size femoral defects, in contrast to either of the two groups that produced smaller amounts of new bone, and in most cases failed to bridge the defects. The results suggest the feasibility of hypertrophic chondrocyte-based tissue engineered grafts for long bone repair.

2 Materials and Methods

All materials were obtained from Sigma-Aldrich (St. Louis, MO, USA) unless otherwise noted.

2.1 Scaffold preparation

Trabecular bone was harvested from bovine juvenile wrists as in our previous studies [293], and cut into cylinders 4 mm diameter by 6 mm high. The initial material was sorted by bulk density (mass/volume) to provide consistent porosity and void volume among the scaffolds, and the bulk densities in the range 0.35-0.50 g/mL were used as in our previous studies [294]. Scaffolds were decellularized following published protocols [293]. Briefly, scaffolds were washed in a series of solutions: (1) 0.1% EDTA in PBS for 1 h, (2) hypotonic buffer consisting of 10 mM Tris and 0.1% EDTA in PBS for 12 h at 4 degrees Celsius, (3) detergent consisting of 10 mM Tris and 0.5% SDS in PBS for 24 h at room temperature on an orbital shaker at 300 revolutions per minute, (4) enzymatic solution of 100 units/mL DNase and 1 unit/mL of RNase with 10 mM Tris in PBS at 37 degrees Celsius for 6 h. After multiple washes in PBS, scaffolds were frozen and lyophilized.

2.2 Cell isolation, expansion, and seeding into decellularized bone scaffolds

Adipose tissue was obtained with informed consent from the patient and the ethical board of Upper Austria at the Rotes Kreuz facility in Linz, Austria, and adipose stem cells were isolated as previously described [288], [295]. The ability of the cells to give rise to chondrocytes, osteoblasts and adipocytes was verified by tri-differentiation testing and were positive for CD73, CD90, CD105, and negative for CD34 and CD14 by fluorescence-activated cell sorting (FACS) analysis (**Fig. S1**). The donor (Adipose Donor 1 in **Fig. S2**) was selected from three potential donors based on cell expansion numbers. Cells were expanded until passage 4 in expansion medium consisting of high glucose medium with L-glutamine, 10% fetal bovine serum, 1% penicillin/streptomycin, and 1 ng/mL basic fibroblast growth factor. In preparation for seeding, decellularized bone (DCB) scaffolds were incubated in 70% ethanol for 2 days and then in sterile culture medium for 1 day. P4 adipose derived stem cells were trypsinized, resuspended in culture medium, and infused into dried DCB scaffolds at a volume density of 30 million cells/mL of DCB scaffold volume. As the prepared scaffolds had an estimated volume of 75 μ L, 2.25 M cells were seeded.

2.3 Bone tissue engineering

Cell-seeded scaffolds were incubated in expansion medium for 2 days, to allow cell attachment, and divided into an experimental graft group, hypertrophic chondrocytes in static culture, and an engineered graft control, with osteoblasts in perfusion culture. The *hypertrophic chondrocyte* grafts, denoted here as H group, were formed by a two-step culture schematic, all under static conditions, using previously established methods [282], [291]. Grafts were first cultured for 2 weeks in chondrogenic medium (high glucose DMEM, ThermoFisher, Waltham, MA; 100 nM dexamethasone; 50 µg/mL ascorbic acid; 50 µg/mL proline; 100 µg/mL sodium pyruvate; 1% ITS+; 1% P/S; 10 ng/mL BMP6; 10 ng/mL TGF-β3). For the subsequent 3 weeks, the medium was changed to hypertrophic medium (high glucose DMEM, ThermoFisher, Waltham, MA; 1 nM dexamethasone; 50 µg/mL ascorbic acid; 50 µg/mL proline; 100 µg/mL sodium pyruvate; 1% ITS+; 1% P/S; 50 ng/mL of L-thyroxine; 5 mM of β-glycerophosphate).

The *osteoblast* grafts, denoted here as O group, were formed in osteogenic culture medium using a bioreactor system with perfusion. The perfusion rate was set to correspond to the interstitial flow velocity of 400 mm/s that was established in our previous study [292] as optimal for osteoblast differentiation. The bioreactor system and the methods used to culture osteoblast-based tissue engineered bone were identical to those that established the strong osteoblast differentiation and bone deposition of ASCs in our previous studies [296]. The cultivation was for 5 weeks, in osteogenic medium (low glucose DMEM, ThermoFisher, Waltham, MA; 100 nM dexamethasone; 50 µg/mL ascorbic acid; 10 mM HEPES buffer; 10% fetal bovine serum; 1% P/S; 5 mM β-glycerophosphate), culture medium was changed twice a week. At the end of 5 weeks of cultivation, tissue engineered grafts were evaluated and implanted into orthotopic defects created in the right femur of a nude rat.

The *control* grafts, denoted here as the Con group, were the acellular DCB scaffold sterilized in 70% ethanol for 2 days and then left in sterile phosphate buffered saline until surgery.

2.4 Critical-sized defect creation and graft implantation

Animal studies were conducted under an approved protocol and with the permit of the municipal government of Vienna, Austria. The experiments were consistent with the Guide for the Care and Use of Laboratory Animals of the National Institute of Health (revised 2011). Twenty-eight male, RNU nude rats were used. Animals were kept in housing cages with filter tops, in groups of two, and separate from other animals. At the time of surgery, the rats weighed between 260 and 392 g. Preoperatively, the animals were administered subcutaneously 0.05 mg/kg buprenorphine (Bupaq, Richterpharma AG, Austria) and 4 mg/kg carprofen (Rimadyl, Zoetis Osterreich Gesm.b.H, Austria). Anesthesia was induced with isoflurane (Forane, AbbVie Gesm.b.H, Austria) and maintained with 1.5-2.5% isoflurane/oxygen by way of mask inhalation.

Once the animal was under stable anesthesia, a lateral approach was used to expose the right femur. After fixation with a four-pin, POM fixator (modified from the method described in Ref. [297]), a defect of 5 mm was created with a Gigli wire saw. Grafts were placed into the defect and the muscle and skin were sutured around the graft and the fixator, respectively. For each experimental group (H, O, Con), eight rats underwent implantation, with four rats not receiving implants to confirm the non-healing in critical-size defects. 0.05 mg/kg buprenorphine and 4 mg/kg carprofen were given subcutaneously over the first four days post-implantation to manage pain and discontinued thereafter. The rats with an open defect and no implant experienced fixator failure between 6 and 9 weeks, and were euthanized, demonstrating a defect that had a non-healing non-union. Twelve weeks post-implantation, the rats were euthanized by an overdose injection of intracardially delivered thiopental sodium while under deep isoflurane anesthesia. The right femur of each animal was harvested for detailed characterization.

2.5 Micro-computed tomography (μ CT) and defect bridging determination

Animals were scanned at a 50 μ m resolution by μ CT at day 1, and at 3, 6, and 9 weeks post-implantation, using a vivaCT 75 (Scanco Medical, Bruttisellen, Switzerland) preclinical scanner. Rats were anesthetized with 2% isoflurane throughout the duration of the scan. The right femur was scanned at an isotropic resolution of 50 μ m. Scans were reconstructed to provide 3D representations of the defect area. After femur harvest at 12 weeks, μ CT scans were performed on a μ CT 50 (Scanco Medical, Bruttisellen, Switzerland) at an isotropic resolution of 10 μ m. Scans were reconstructed to provide 3D representations of the defect, and quantitative data for the bone volume and bone surface to volume ratio within the defect was calculated using the Scanco Medical morphometry software. Bridging was defined as the formation of a continuous segment of mineralized bone along a vertical plane that spanned the defect, and visualized through the μ CT image slices and 3D reconstruction. Two blinded researchers went through the slices and 3D reconstruction, and independently determined bridging. If both researchers agreed on bridging, the sample was considered bridged and given a 1, if the researchers disagreed on bridging, the sample was considered incomplete bridging, and given a 0.5.

2.6 Quantitative biochemical analysis

For pre-implantation analysis, grafts were cut in half and the wet weights were recorded. Graft halves were digested with papain (40 Units/mg) in digest buffer (0.1 M sodium acetate, 10 mM cysteine HCl and 50 mM EDTA, pH 6.0) at 60 °C overnight. DNA content was measured from the digest using Quant-iT PicoGreen assay kit and the supplied lambda DNA standard (ThermoFisher, Waltham, MA). Sulfated glycosaminoglycan (GAG) content was measured using the dimethylmethylene blue dye assay with chondroitin 6 sulfate as a control. Calcium quantitation was not performed due to the calcified nature of the decellularized scaffolds, and the confounding factor that played in the analysis. For each assay, n = 4 biological replicates were used per group and time point.

2.7 Real time RT-PCR

Pre-implantation, total RNA was extracted using the Trizol method (ThermoFisher, Waltham, MA). DNase I treatment was utilized for 10 min at 37 °C to remove any contaminating DNA. cDNA was transcribed using the High Capacity cDNA Reverse Transcription kit (ThermoFisher, Waltham, MA) according to the manufacturer's instructions. Quantitative RT-PCR was performed using Fast Sybr Green mix (ThermoFisher, Waltham, MA). Expression levels were quantified applying the ΔC_t method, with the C_t of GAPDH subtracted from the C_t of the gene of interest. Forward and reverse primers for each gene are presented in **Table 1**. Samples were evaluated using $n = 5$ biological replicates per experimental group and time point.

Table 1. Primers used in RT-PCR.

Gene	Forward	Reverse
RUNX2	CCGTCTTCACAAATCCTCCCC	CCCGAGGTCCATCTACTGTAAC
COL1A1	GATCTGCGTCTGCGACAAC	GGCAGTTCTTGGTCTCGTCA
MMP13	CCAGACTTCACGATGGCATTG	GGCATCTCCTCCATAATTTGGC
ALPL	GGGACTGGTACTCAGACAACG	GTAGGCGATGTCCTTACAGCC
IBSP	GAACCTCGTGGGGACAATTAC	CATCATAGCCATCGTAGCCTTG
COL10A1	CATAAAAGGCCCACTACCCAAC	ACCTTGCTCTCCTCTTACTGC
SOX9	AGCGAACGCACATCAAGAC	CTGTAGGCGATCTGTTGGGG
COL2A1	AGACTTGCGTCTACCCCAATC	GCAGGCGTAGGAAGGTCATC

2.8 Pre-implantation histology and immunohistochemistry

Grafts were fixed in 10% formalin, rinsed in PBS, and decalcified using a formic acid based solution (Immunocal Decalcifier, StatLab, McKinney, TX). After decalcification, grafts were washed multiple times with PBS, dehydrated, embedded in paraffin, and sectioned at 6 μm . Histological sections were stained with Alcian blue for GAG (Pre-Implantation) following standard protocols, and Movat's Pentachrome (Pre- and Implantation) following manufacturer's instructions. Antigen retrieval was conducted prior to immunohistochemistry. Slides were placed into a container filled with citrate buffer (1.8 mM citric acid, 8.2 mM sodium citrate, pH 6.0), and the container was submerged in boiling water for 20 min. Slides were blocked with 0.3% hydrogen peroxide in absolute methanol for 30 min before using the Vectastain Elite Universal staining kit (Vector Laboratories, Burlingame, CA). The primary antibodies for BSP (Pre-Implantation, EMD Millipore, 1/500 dilution, AB1854, Bilerica, MA), and OPN (Pre-Implantation, Abcam, 1/200 dilution, AB166709, San Francisco, CA) were incubated overnight at 4 °C. The slides were counterstained with Hematoxylin QS (Vector Laboratories, Burlingame, CA). Staining for collagen type X was conducted as previously described [298]. The primary antibody was obtained from Abcam (Pre-Implantation, 1/1000 dilution, AB49945, San Francisco, CA); Hematoxylin QS was used as a counterstain.

2.9 Hard bone histology

Femurs with the attached fixation devices were immersed in 4% neutral-buffered formaldehyde solution, then dehydrated in ascending grades of ethanol and imbedded in light curing resin (Technovit 7200 VLC; Kulzer & Co., Wehrheim, Germany). Thin ground sections along the longitudinal axis of the shaft oriented in a frontal plane were cut using a previously developed method [299] and stained with Levai-Laczko dye [300]. Histological specimens were digitized with the Olympus dotSlide 2.4, digital virtual microscopy system (Olympus, Japan, Tokyo) at a resolution of 0.32 μm . Semi-quantitative values for the amount of new bone deposited, the area of old bone, the area of fibrous tissue, the area of bone marrow, and the quantity and location of osteoclasts were determined in a blinded fashion on the stained samples within the defect area by two independent researchers using $n = 4$ femurs per staining. Levai-Laczko staining is a common stain used in calcified tissues that demonstrates the presence of several components related to bone and cartilage. Through the multiple staining components, it allows the identification of bone of different maturities, cartilage, calcified cartilage, bone marrow, and general fibrous tissue.

2.10 Post-implantation histology and immunohistochemistry

The femurs for immunostaining were submerged in 4% neutral-buffered formaldehyde solution for 24 h, followed by extensive washing in PBS. Femurs were decalcified using Immunocal (StatLab, McKinney, TX), followed by extensive washing in PBS and graded ethanol dehydration. Sections of the femur were made 6 μm thick, and histology was stained with Movat's Pentachrome following manufacturer's instructions. Immunohistochemistry was performed following the published citrate buffer antigen retrieval methods. Vectastain rabbit antibody kit (PK-4001, Vector Laboratories, Burlingame, CA), and AbCam's mouse on mouse kit (AB127055, San Francisco, CA) were utilized to stain for CD163 (Abcam, 1/500, AB182422). Semi-quantitation of the stainings was conducted in ImageJ, by first isolating the defect area, converting the images to 8-bit greyscale profile, and then indicating a threshold that allowed the isolation of positively-stained CD163 + cells, and finally using the ImageJ automatic particle analyzer with settings at 0.1-1.0 circularity and 10-200 microns² size. This process was completed on $n = 3$ biological replicates per group.

2.11 Statistics

Statistically significant differences between the two experimental groups during pre-implantation testing were evaluated using a Student's *t*-Test, $\alpha = 0.05$, with significance determined by $p < 0.05$ (Prism Software, GraphPad, La Jolla, CA, USA). Statistical significance of differences between the groups and time points was determined by using a one-way analysis of variance (ANOVA) followed by Tukey's post-test, $\alpha = 0.05$, with significance determined by $p < 0.05$.

3 Results

3.1 Bone formation in vitro by hypertrophic chondrocytes (endochondral ossification) and osteoblasts (intramembranous ossification)

Differentiation of ASCs into hypertrophic chondrocytes and osteoblasts was induced for cells cultured in decellularized bone (DCB) scaffolds, by adding appropriate molecular factors to culture medium, under either static conditions (hypertrophic chondrocytes) or interstitial flow (osteoblasts) (**Fig. 9**).

Static hypertrophic chondrocyte grafts (H group) were differentiated by inducing chondrogenesis and cartilage tissue formation for 2 weeks, and then inducing chondrocyte hypertrophy over the subsequent 3 weeks. After 5 weeks of culture, these grafts demonstrated endochondral-like characteristics, with upregulated gene expression of chondrocyte and hypertrophic chondrocyte markers, and deposition of collagen X and glycosaminoglycan around enlarged chondrocyte lacunae (**Fig. 9B**). Perfused osteoblast grafts (O group) were formed by osteogenic differentiation in a perfusion bioreactor for the entire 5-week culture period. These grafts demonstrated the cellularity and deposition profile of bone matrix similar to those in previous studies (**Fig. 10B-D**) [292], [293].

Expression of bone-related genes was highest in H grafts (**Fig. 10A**). A master regulator for bone production (RUNX2, expressed in both cell types [275], [301]–[303]), and the genes associated with matrix formation (COL1A1 and MMP13) and mineral deposition (ALPL and IBSP) were all upregulated in the H group. Movat's pentachrome staining (**Fig. 10B**, red deposition) revealed that H grafts had relatively little osteoid deposition, in stark contrast to the O grafts. Instead, hypertrophic chondrocytes deposited extensive cartilaginous matrix within the scaffold pores (green marks glycosaminoglycan, **Fig. 10C**). O grafts had high cellularity throughout the graft volume, with widespread and dense deposition of collagenous matrix (collagen fibers are shown in red). Deposition of bone sialoprotein (BSP), a key nucleator for bone mineral formation, correlated with the general matrix characteristics (**Fig. 10D**). In the H grafts, BSP was located near hypertrophic chondrocytes within the dense cartilage matrix. In the O grafts, BSP was present throughout the graft along the collagen fibers. Osteopontin (OPN), an important protein in bone formation and remodeling, was present throughout the cartilaginous matrix of the H grafts but was largely absent in the O grafts (**Fig. 10E**). At the time of implantation, H grafts had superior expression of bone-related genes and extensive deposition of bone forming and remodeling proteins.

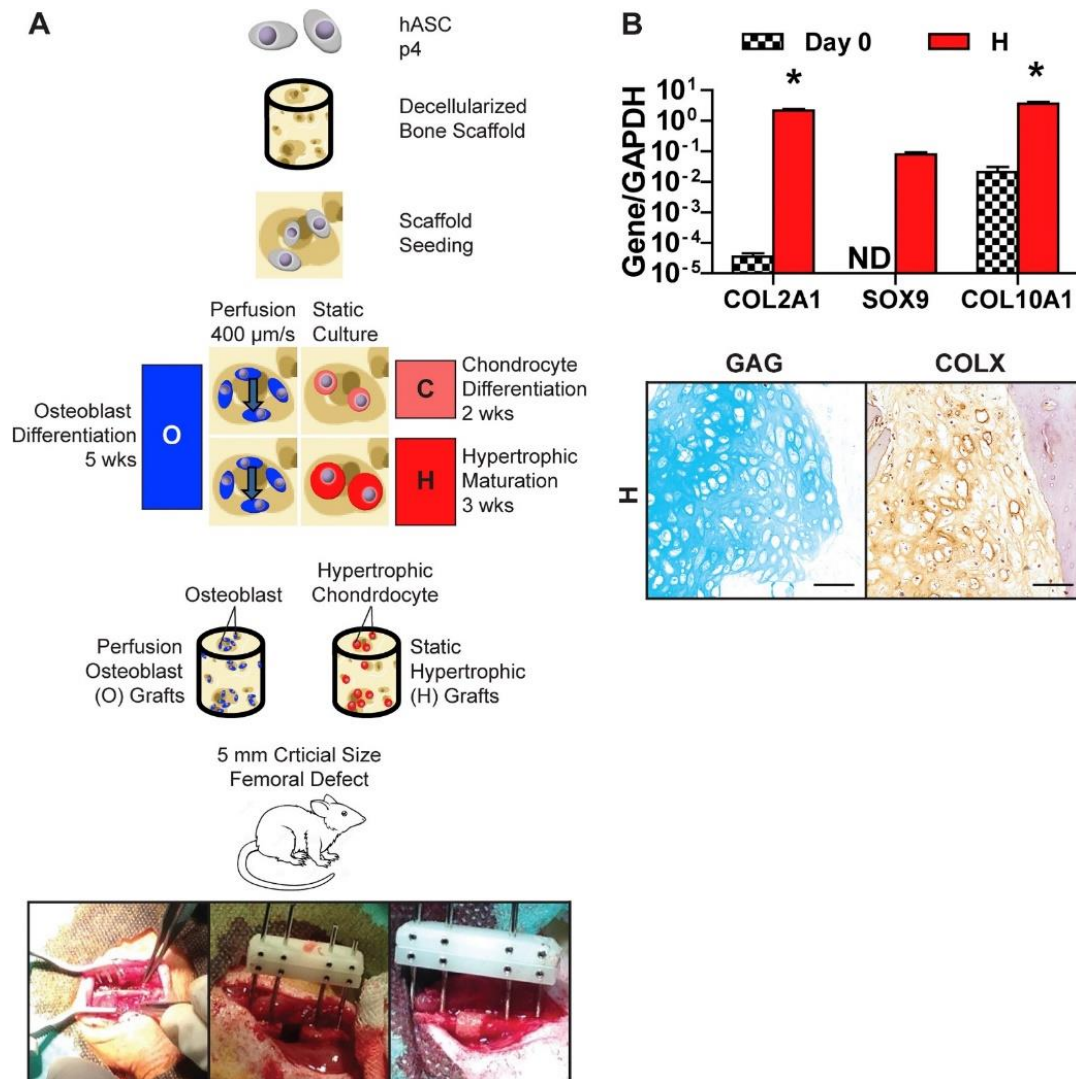


Fig. 9. (A) Experimental methodology and the creation of tissue engineered grafts. Tissue engineered grafts were constructed by seeding human adipose derived stem cells (ASCs), a clinically relevant source of mesenchymal stem cells, into decellularized bone scaffolds. Hypertrophic chondrocyte grafts (H) were cultured statically by differentiating ASCs for 2 weeks in chondrogenic medium and maturing the cells to hypertrophic chondrocytes for 3 weeks in hypertrophic medium. Osteoblast grafts (O) were generated from ASCs under perfusion of osteogenic medium for 5 weeks in bioreactors. Both groups of tissue engineered grafts, along with an acellular scaffold control, were implanted into an orthotopic, 5 mm critical-size defect created in the femur of athymic rats. The femur, but not the graft, was stabilized with an internal fixator. Bone deposition was monitored through micro computed tomography (μCT) at the time of implantation, and at 3, 6, and 9 weeks post-implantation. At the 12-week endpoint, femurs were harvested, and regeneration of the defect was evaluated in detail. **(B)** Verification of hypertrophic chondrocyte differentiation within tissue engineered grafts. Gene expression of key chondrogenic and hypertrophic genes were significantly increased, demonstrating chondrocyte differentiation and hypertrophic maturation of the resulting chondrocytes. Histological sections of cultured H grafts demonstrated glycosaminoglycan (GAG) deposition, indicating chondrocyte differentiation. Immunohistochemistry demonstrated collagen type X deposition, strongly present surrounding the enlarged lacunae of the hypertrophic chondrocytes, indicating hypertrophic maturation. Value \pm SD. Significant differences between the groups: $*p < 0.05$ ($n = 3$); Scale bars: 100 μm .

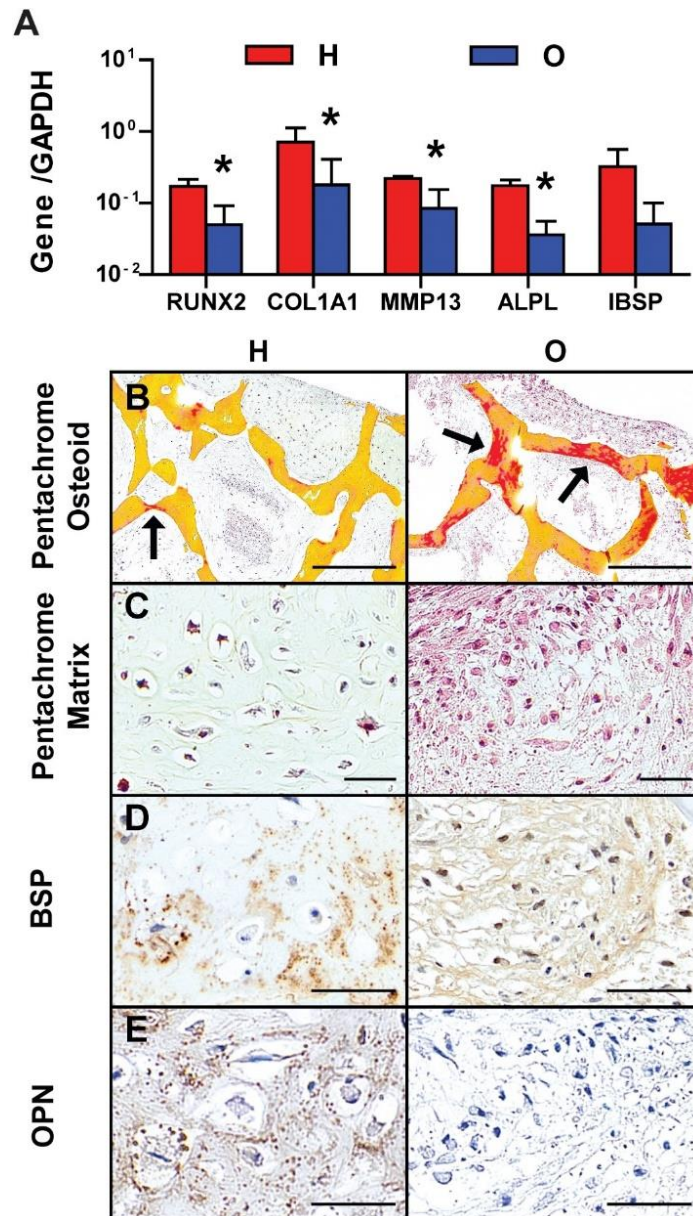


Fig. 10. Composition and behavior of engineered bone grafts *in vitro*. (A) Hypertrophic (H) grafts had significantly enhanced expression of bone development genes when compared to osteoblast (O) grafts. Histomorphology of hypertrophic (H, left) and osteoblast grafts (O, right). (B-C) osteoid and tissue matrix (by pentachrome) demonstrating increased osteoid formation (black arrows, red on yellow scaffold) in the O grafts and a difference in matrix deposition between H grafts (C cartilage, green GAG) and O grafts (F red fibrous tissue) within the DCB bone scaffold (yellow); (D-E) Bone sialoprotein and osteopontin (antibodies) demonstrating the differences in deposition with H grafts depositing around cellular lacunae and O grafts depositing along fibrous tissue. Scale bars: 500 μ m (2B), 50 μ m (2C, 2D, 2E). Value \pm SD. Significant differences between the groups * $p < 0.05$ (n = 4).

3.2 *In vivo* integration, matrix deposition, and bridging of the defects

H, O and Con grafts were implanted into critical-size 5-mm long defects in the femur of athymic nude rats, a standard orthotopic model for long bone fracture repair (Fig. 9). Live μ CT scans, at a resolution of 50 μ m, were taken throughout the time of implantation to monitor bone integration and matrix turnover (Fig. 11). At 3 weeks post-implantation, H grafts have already started to integrate into the native bone and had large mineral depositions along the medial exterior of the graft (Fig. 11B). The O

grafts had only minimal integration with the surrounding bone, without apparent mineral deposition. The Con grafts resembled the H grafts with respect to external mineral deposition.

By 6 weeks, the differences in regeneration between the groups became noticeable, as the H grafts had extensive integration along both ends, and a closing bridge along the medial side (**Fig. 11C**), while the O grafts had only partial integration along both ends. The Con had extensive mineral deposition along the medial side of the grafts, but very little remodeling of the scaffold. By 9 weeks, most H and some Con grafts have bridged the defect, in contrast to the O grafts that displayed large fissures (**Fig. 11D**). The H grafts underwent substantial remodeling, with deposition of the new matrix, and formation of bone bridges along the medial side of the graft. The O grafts showed integration with only minimal remodeling and appeared fragmented. The Con grafts had substantial deposition along the medial exterior; however, only minimal bone had been formed within the acellular scaffold and defect space.

High-resolution μ CT scans (10 μ m resolution) taken at the 12-week endpoint of implantation (**Fig. 11E and F**) revealed substantial differences in healing between the three groups. The exterior of the H grafts underwent extensive remodeling, integrated seamlessly into the femur, and contained large regions resembling native bone. Interior reconstruction demonstrated a thick, cortical-like bridge that formed along the medial segment of the graft. The O grafts lacked remodeling of the exterior zone and displayed severe lack of new bone matrix, fissures, and only minimal integration. In most cases, these grafts failed to facilitate defect bridging and regeneration. Con grafts facilitated some defect bridging and induced partial integration with the host bone. As determined through the post-harvest μ CT, 7/8 of H grafts, 1/8 of O grafts, and 3/8 of Con grafts bridged the defect (**Fig. 11G**). H grafts were associated with enhanced total mineral presence in the defect space, as shown by the greater total bone volume in the defect space (**Fig. 11H**).

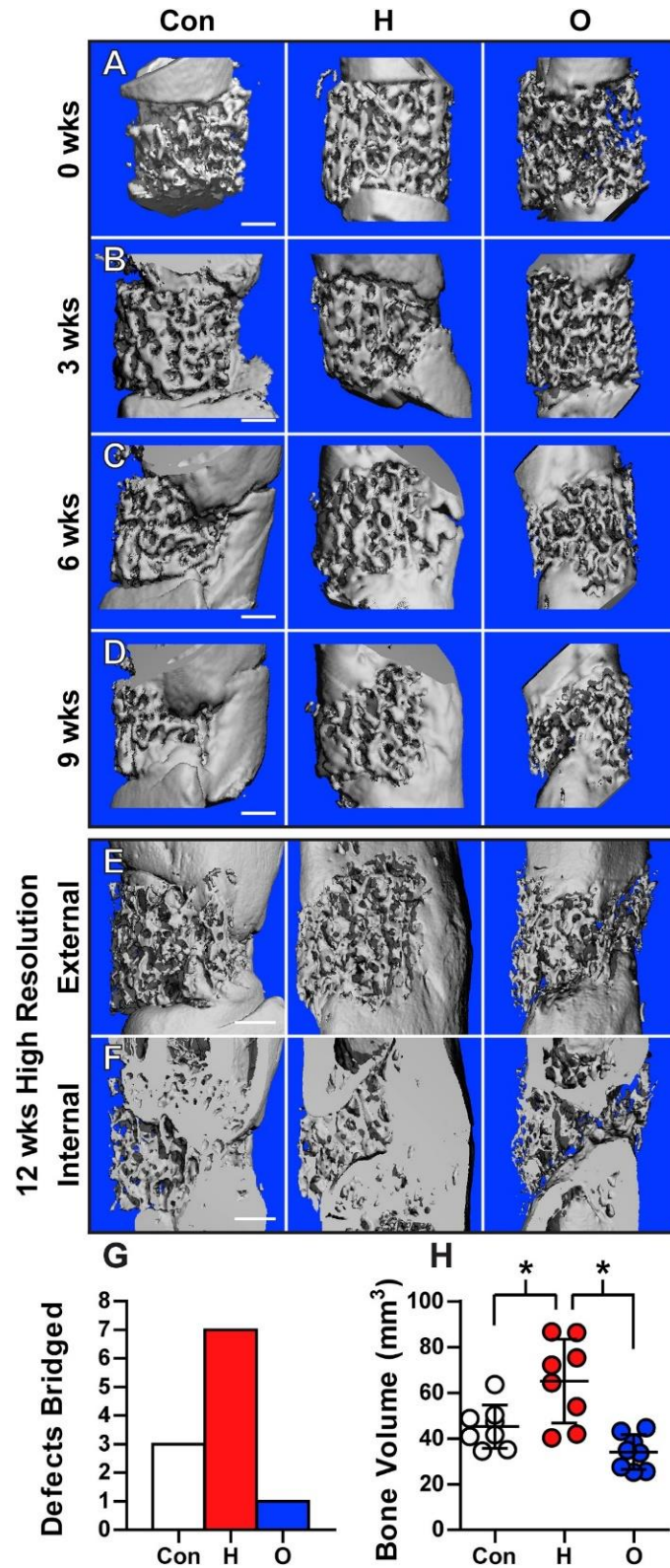


Fig. 11. Bridging of critically sized femoral defects. **A** Representative three-dimensional μ CT reconstructions of the rat femur at day 1, 3 weeks, 6 weeks, 9 weeks and 12 weeks post-implantation for all three groups: acellular scaffolds (Con), hypertrophic chondrocyte (H) and osteoblast (O) grafts. Internal and external regions are shown for 12 weeks (**E-F**). H grafts demonstrated the most complete femur regeneration demonstrated by defect bridging (**G**) and total bone volume deposited at 12 weeks (**H**). Scale bar: 1 cm. Value \pm SD. Significant differences: $*p < 0.05$ ($n = 8$).

3.3 Bone formation and regeneration

Hard bone histology was used to visualize the components of the regenerated defects. Newly deposited bone (NB, fuchsia), the implanted scaffold (DCB, light pink), and fibrous tissue (FT, pale yellow) could be identified (**Fig. 12A**). Magnified views revealed bone marrow (BM, blue) and calcified cartilage (CC, dark purple) regions (**Fig. 12B**). The presence of cartilage within the defect space indicates the use of endochondral ossification in the regeneration of the defect. Movat's pentachrome, in which cartilage is stained green, was utilized and demonstrated cartilage presence in all grafts, regardless of cellular differentiation (**Fig. 12C**). The enlarged, hypertrophic chondrocytes surrounded in cartilage matrix transitioning to the newly formed bone (yellow) indicated that endochondral ossification was involved in new bone formation in all grafts. Endochondral ossification was observed at the edges of the native femur within the Con and O grafts, and throughout the implant in H grafts.

New bone deposition histologically matched the mineral depositions visualized by μ CT. H grafts displayed strong deposition of new bone. In the O grafts, new bone was localized at the integration sites and in part in the defect space. In Con grafts, new bone deposition was localized at the integration sites and the medial side of the graft. The magnified views demonstrated that the new bone was formed around the scaffold, rather than replacing it. Semi-quantitation of the samples revealed similar amounts of the original scaffold present in all three groups (**Fig. 12D**). The extent of bone formation varied, with the H grafts containing significantly more new bone and bone marrow (**Fig. 12D**), and significantly less fibrous tissue (**Fig. 12D**) than either control, indicating advanced bone regeneration.

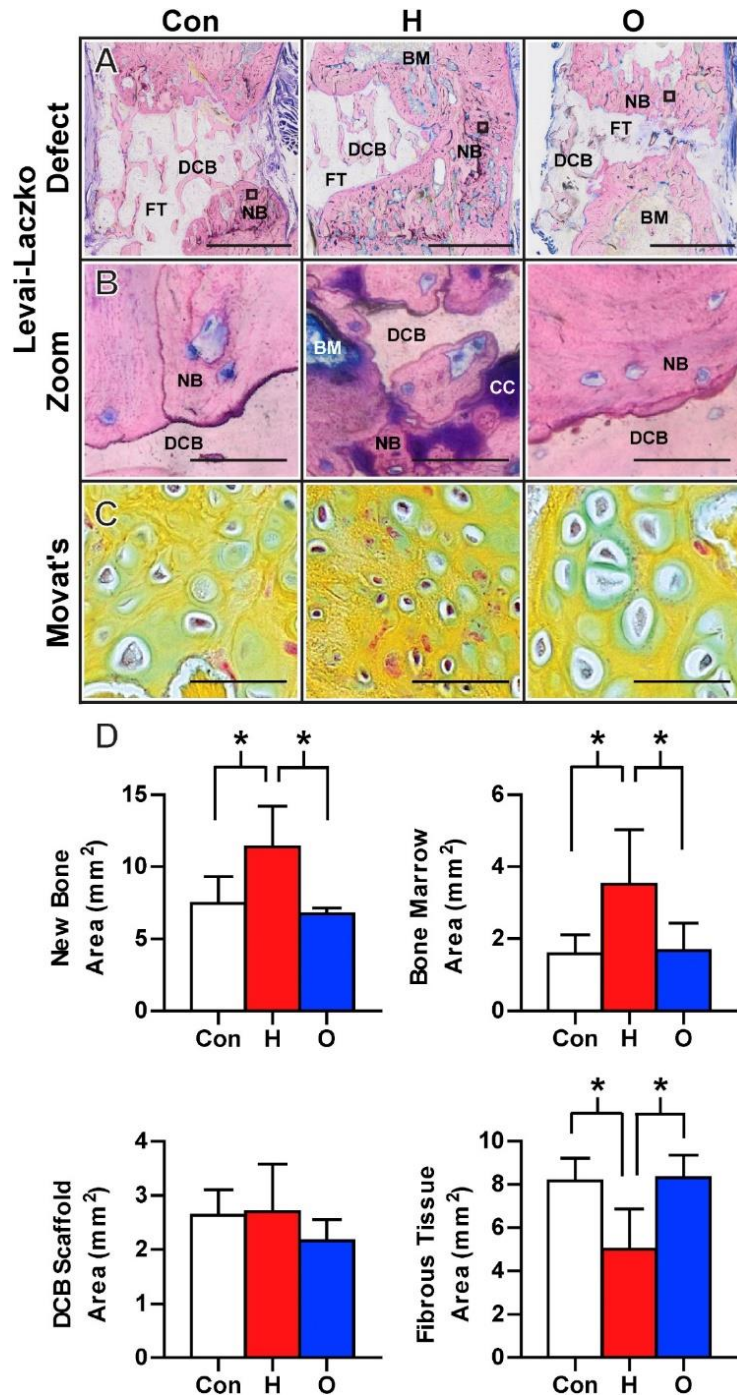


Fig. 12. Defect regeneration. Bone formation is shown at 12 weeks post-implantation. (A) Hard bone histology using the Levai-Laczko stain demonstrated the overall morphology of the defect region and differences between the scaffold material (DCB), newly deposited bone (NB), fibrous tissue (FT), and bone marrow (BM). In the Con graft, new bone deposition was largely constrained to the medial side at the integration sites. New bone deposition was widespread in the H graft, with some implanted scaffold material still present in the defect zone. In the O graft, new bone was located at the leading edge of the native skeleton, with minimal amounts of implanted scaffold scattered throughout the defect. (B) Magnified views allowed detection of calcified cartilage (CC), an important intermediate in endochondral ossification that was seen extensively in the H grafts, which also contained numerous bone marrow regions. (C) At the location of new bone formation, a cartilage anlage characteristic of endochondral ossification was present in all three groups (green staining in Movat's pentachrome sections). The images demonstrate turnover of cartilage (green) into newly deposited bone template (yellow). (D) There was a significantly higher presence of new bone and bone marrow within the H grafts. There was no significant difference in the amount of original DCB scaffold still remaining in the graft space, but there was significantly less fibrous tissue within the H grafts. Scale Bars: 2 mm (4A), 100 μ m (4B), 50 μ m (4C). Value \pm SD. Significant differences between the groups * $p < 0.05$ ($n = 4$).

M2 macrophages are integral to long bone regeneration, providing a pro-repair environment that aids in enhanced defect regeneration [304]. Immunohistochemistry staining of CD163 demonstrated the significantly increased presence of M2 macrophages within the H graft defect space (**Fig. 13**).

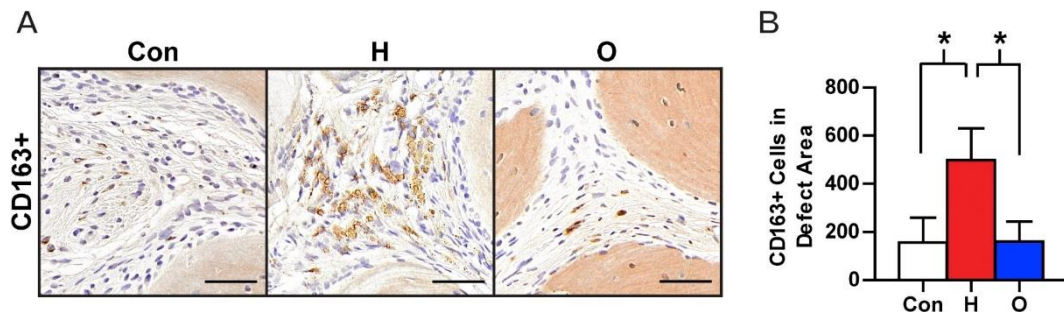


Fig. 13. M2 macrophages within the defect. (A) Histological sections of the defect were stained for M2 macrophages using a CD163 β antibody. (B) H grafts demonstrated significantly increased presence of M2 macrophages compared to the Con and O grafts (by CD163 + stain). Scale Bars: 50 μ m. Value \pm SD. Significant differences between the groups * $p < 0.05$ ($n = 3$).

Osteoclasts, a critical factor in bone regeneration, were identified by their multinucleation and Howship's lacunae, and were counted within the defect space of each graft. As seen in **Fig. 14A**, there was a tendency for osteoclasts to resorb DCB scaffolds located within the fibrous tissue of failed regeneration sites, with the H grafts containing significantly less osteoclasts overall (**Fig. 14B**). The ratio of osteoclasts digesting DCB matrix to the overall DCB area was calculated, and the H grafts once again had significantly less osteoclasts per area (**Fig. 14C**). Comparing the number of osteoclasts digesting DCB to new bone, the ratio for H grafts was significantly lower than in the other groups (**Fig. 14D**), indicating that the osteoclasts in H grafts were digesting newly deposited bone. The lower proportion of osteoclasts in H grafts, despite similar overall amounts of DCB, suggests a difference in repair environments amongst the graft types.

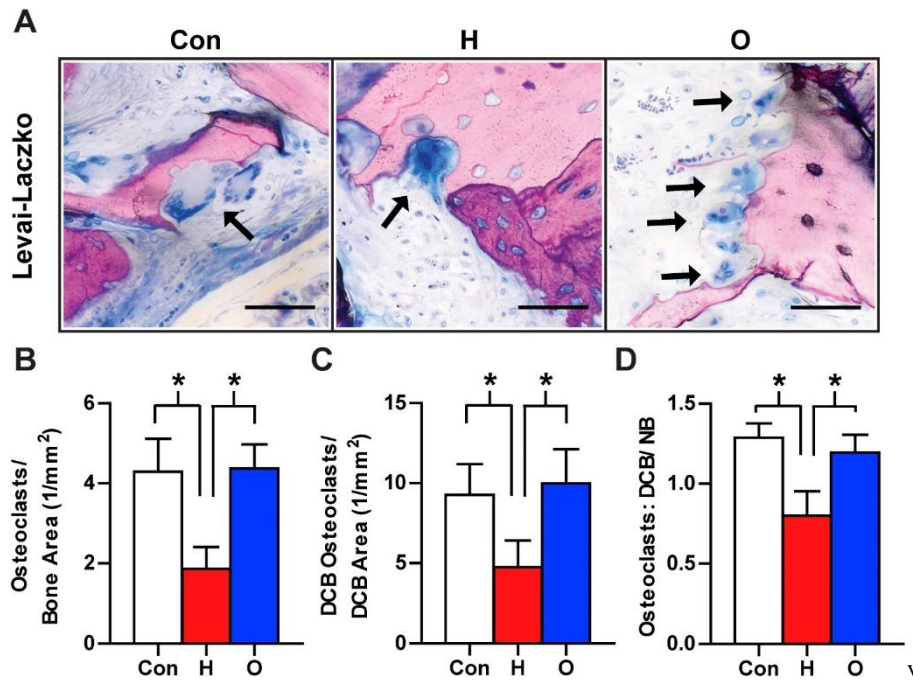


Fig. 14. Osteoclast presence and behavior within the defect. (A) Osteoclasts (black arrows) were determined by multinucleation and the formation of Howship's lacunae from the Levai-Laczko staining. Osteoclasts were located throughout all groups, on both the decellularized bone scaffold (light pink) and on newly deposited bone (fuchsia). (B) H grafts contained significantly less osteoclasts overall. (C) H grafts contained significantly lower amounts of osteoclasts resorbing the original DCB scaffold. (D) The ratio of osteoclasts found resorbing DCB scaffold to the osteoclasts found resorbing newly deposited bone was calculated and H grafts had a significantly lower ratio of DCB osteoclasts to new bone osteoclasts than the other two grafts. Scale Bars: 50 μ m. Value \pm SD. Significant differences between the groups * $p < 0.05$ (n = 4).

4 Discussion

Tissue engineering of autologous bone grafts has potential to provide effective repair of fracture non-unions, using methods customized to the patient and defect being treated [305]. Current efforts have proven to be insufficient for clinical translation due to various complications, including limited integration, incomplete regeneration, and poor mechanical properties of the grafts [271]. We hypothesized that these limitations could be overcome by using grafts based on differentiated hypertrophic chondrocytes engineered to withstand the challenging environment. We demonstrated the regenerative superiority of the hypertrophic chondrocyte grafts by (i) integration with adjacent native bone, (ii) more extensive bone deposition, (iii) more effective bridging of defects, and (iv) regenerative milieu established within the defect space.

Hypertrophic chondrocytes were differentiated from ASCs by modification of a previous protocol [282]. Rather than stopping after chondrocyte differentiation and cartilage anlage deposition, similar to previous studies [278], [279], [284], hypertrophic chondrocytes were matured, to markedly enhance mineral deposition and bone formation [282]. By maturing hypertrophic chondrocytes, chondrogenic and hypertrophic gene expression increased, and substantial hypertrophic cartilage-like matrix was deposited within the scaffold pores (Fig. 9B). These results agreed with recent reports on hypertrophic chondrocytes [285], [290].

Hypertrophic chondrocytes expressed bone-related genes [275], [301], [303] and when compared to the osteoblast-based grafts (**Fig. 10**), the differentiated hypertrophic chondrocytes showed elevated expression of these genes, consistent with expression values previously reported [306]. The differences in gene expression, though not correlated, are matched by differences in protein deposition, as the differentiated hypertrophic chondrocytes grafts had increased presence of BSP and OPN and deposited it in different locations within the graft (**Fig. 10**). The difference in behavior between the two cell types agrees with the putative roles of each cell type within the body. Hypertrophic chondrocytes are responsible for orchestrating large quantities of bone template deposition in a non-mineralized space [8], and the hypertrophic chondrocyte grafts showed similar behavior with deposition of the bone nucleating proteins of the bone template within the formed cartilage matrix located in the scaffold pore spaces (**Fig. 10**). Osteoblasts play a large role in modulating the existing bone [8], and the osteoblast grafts displayed similar behavior with osteoid deposition along the existing decellularized bone scaffold and only minimal matrix deposition within the scaffold pores (**Fig. 10**). The differences in expression and deposition experienced in this study might therefore be due to the natural scale of deposition each cell type is responsible for.

The orthotopic, critical-sized defect in the rat femur required considerable bone regeneration, and all three experimental groups demonstrated new bone formation through endochondral ossification. Similar to an earlier study in the rat calvaria [283] and the cell behavior pre-implantation, hypertrophic chondrocytes deposited significantly more bone than the osteoblasts in the long-bone fracture model (**Fig. 11**). Whereas hypertrophic chondrocyte-based grafts resulted in bridging 7/8 femoral defects, the osteoblast-based grafts caused bridging of only 1/8 femoral defects (**Fig. 11**).

Clearly, large long bone defects present a complex signaling environment with the biological, structural and mechanical cues instigating repair through endochondral ossification [272], [307]. The superior regeneration caused by the hypertrophic chondrocyte grafts is likely due to the progression of natural endochondral ossification, as was shown for femoral repair using pellets of chondrocytes implanted into the defect [279], [280]. Lower amounts of GAG-rich matrix in the H grafts, coupled with the smaller lacunae of the cells, are consistent with the progression of endochondral regeneration (**Fig. 12C**), and resemble the resorption behavior detailed in the subcutaneous implantation of differentiated hypertrophic chondrocytes [306]. Late stage hypertrophic chondrocytes also regulate local osteoblast activity [308] and differentiated hypertrophic chondrocytes have been shown to influence cortical and trabecular-like bone formation [306]. Where decellularized hypertrophic cartilage matrix has demonstrated potential for bone formation [309], it has been shown that the release of cytokines (partially contained in the matrix) by the hypertrophic chondrocytes are essential for this bone formation and remodeling [283], [310], [311], thereby suggesting that increased, remodeled bone in the H grafts was orchestrated by the implanted hypertrophic chondrocytes. Recent publications have shown that during the end stages of endochondral ossification, hypertrophic chondrocytes can transdifferentiate into

osteoblasts and osteocytes, cells that are smaller than hypertrophic chondrocytes [312]–[314] that can produce, remodel and maintain new bone matrix [313], [314]. These publications suggested that the hypertrophic chondrocytes, besides orchestrating host cell behavior, could also have played a direct role in increasing bone deposition.

Macrophages are essential for endochondral ossification [315]. When M2 macrophages were induced in the fracture defect at later stages of endochondral ossification, bone formation was enhanced [316]. The H grafts had a significantly higher presence of M2 macrophages (**Fig. 13**), indicating the benefits of hypertrophic chondrocyte grafts in influencing a bone-forming environment. One potential reason for the higher count of M2 macrophages could be the extensive osteopontin deposition in the H grafts (**Fig. 10**), as osteopontin has been shown to influence macrophage behavior and M2 polarization [317]. Reinforcing an anabolic environment, the H grafts contained significantly less osteoclasts within the graft defect and induced less overall resorption (**Fig. 14**), in agreement with recent studies [283]. A significant portion of the osteoclasts present within the defect were located within the deposited matrix, rather than in the original DCB scaffold (**Fig. 14**). The specific localization of osteoclasts and the enhanced remodeling, indicated by the seams within the H grafts, indicates the influence of the differentiated hypertrophic chondrocytes.

In addition to the regenerative environment, hypertrophic chondrocytes are integral to many other aspects of mature bone formation. Endochondral ossification is required for hematopoietic stem-cell niche formation, and studies have shown that suppressing hypertrophic progression inhibits niche formation [318]. Differentiated hypertrophic chondrocytes from MSCs facilitated bone marrow niche formation upon subcutaneous implantation [306], and it is the reversion of chondrocyte differentiation that supports the presence of stem cells within the niche [319]. When implanted orthotopically, hypertrophic chondrocyte grafts contained significantly more bone marrow compared to the other two groups (**Fig. 12D**).

Decellularized bone is an ideal biomaterial for bone regeneration, as it already contains the appropriate cell microenvironment, growth factors, and mechanical properties of bone [320]. Decellularized bone has shown ability to stimulate bone formation when implanted in calvarial defects, and to be osteogenic to the surrounding host cells [321]. This ability was readily apparent in this study in μ CT reconstructions (**Fig. 11**), as new bone formation occurred surrounding the scaffold, areas rich in stem and progenitor cells. The deposition was exaggerated by the lower resolution *in vivo* μ CT imaging (**Fig. 11A-D**), as the high resolution scans at 12 weeks demonstrated porous bone and quantifiably, significantly less total mineral than the H grafts.

Despite these known abilities of decellularized bone, it was surprising that the acellular control scaffolds performed better than the osteoblast-based scaffolds. We believe the poor performance was due to the characteristics of the defect, as previous osteoblast-based tissue engineered bone has shown successful results [305]. This cited study demonstrated methodical bone regeneration by differentiated osteoblasts,

with step-wise coordination of bone resorption and deposition at the graft-skeleton interface [305]. Within the defect, new bone deposition could be seen at the interfaces, and the new bone deposition lines could be determined in the section at 12 weeks (**Fig. 11F**). Interestingly, the O grafts didn't demonstrate heavy external, medial depositions like the H and Con grafts, potentially reinforcing the importance of graft-skeleton interface and the coordination of the osteoblasts. The mechanical loading exhibited on the defect appeared to overcome the mechanical stability of O grafts, as fissures formed in 7/8 of these grafts.

While significant bone was deposited in the H grafts, regeneration of the critical-sized defect remained incomplete. The bridging of only one side of the H grafts, and a clear bias towards one side in all grafts, is a typical phenomenon in long bone fracture repair that occurs in part to the mechanical stimulation gradient produced by the fixation [322]. The segment of the graft nearest to the internal fixator is stabilized and experiences only minimal forces, whereas the segments that are further away experience mechanical stimulation that is known to enhance bone regeneration [322]. As seen in μ CT reconstructions (**Fig. 10**), the lateral side of the H grafts, adjacent to the internal fixator, formed the least amount of new bone while the medial side underwent extensive bone regeneration. The high degree of regeneration in the medial segment suggests that hypertrophic chondrocytes might be directly affected by mechanical stimulation. The use of fixators allowing uniform mechanical environment, such as those used for cortical locking [323], would allow more complete defect regeneration.

One significant limitation of this study was the sole harvest time point at 12 weeks, leaving the exact contributions of the implanted and host cells to bone regeneration inconclusive. Future studies should elucidate the exact mechanisms initiated in the long bone defect by hypertrophic chondrocytes and the distinct roles of the implanted and host cells and determine if they match the preexisting work in other bone forming models [281], [306], [314]. Additional studies will also be needed to examine interactions between the implanted differentiated cells and the inflammatory milieu. While allogeneic cells have obvious commercial potential, better performance of autografts in long bone grafting [267] suggests that autologous cells present the preferred clinical option.

In summary, we found that hypertrophic chondrocytes enhance regeneration in critical-size, orthotopic long bone defects. The use of critical-size femoral defects in a rat model demonstrates the feasibility and promise of the differentiated hypertrophic chondrocyte grafts [324]. Because rats do not display haversian-type remodeling in the cortex [325], translation to the human bone model needs to be undertaken to extend the predictive power of the results of these studies. Large animal studies are certainly needed before translation to human trials; however, the positive repair environment with rapid bone deposition and integration into the native skeleton that was superior to the performance of both acellular scaffolds and the traditional, osteoblast-based tissue engineered grafts, warrants further study for long bone fracture repair.

5 Acknowledgments

We gratefully acknowledge the NIH funding support of this work (grants EB002520, DE016525, and AR061988). We thank Dr. Andrea Lindenmair, Dr. Eleni Priglinger, and Dr. Susanne Wolbank for the harvest, isolation, and characterization of adipose derived stem cells. We also thank Gabriele Leinfellner for *in vivo* computed tomography imaging of the rats, and Dominika Lidinsky and Dr. Sylvia Nuernberger for their help in preparation and staining of paraffin-embedded histological sections. We also thank Prof. Mag. Dr. Dominik Rünzler for the use of his laboratory space and facilities at the University of Applied Sciences Technikum Wien, Vienna.

6 Supplemental Information

6.1 Supplemental Figures

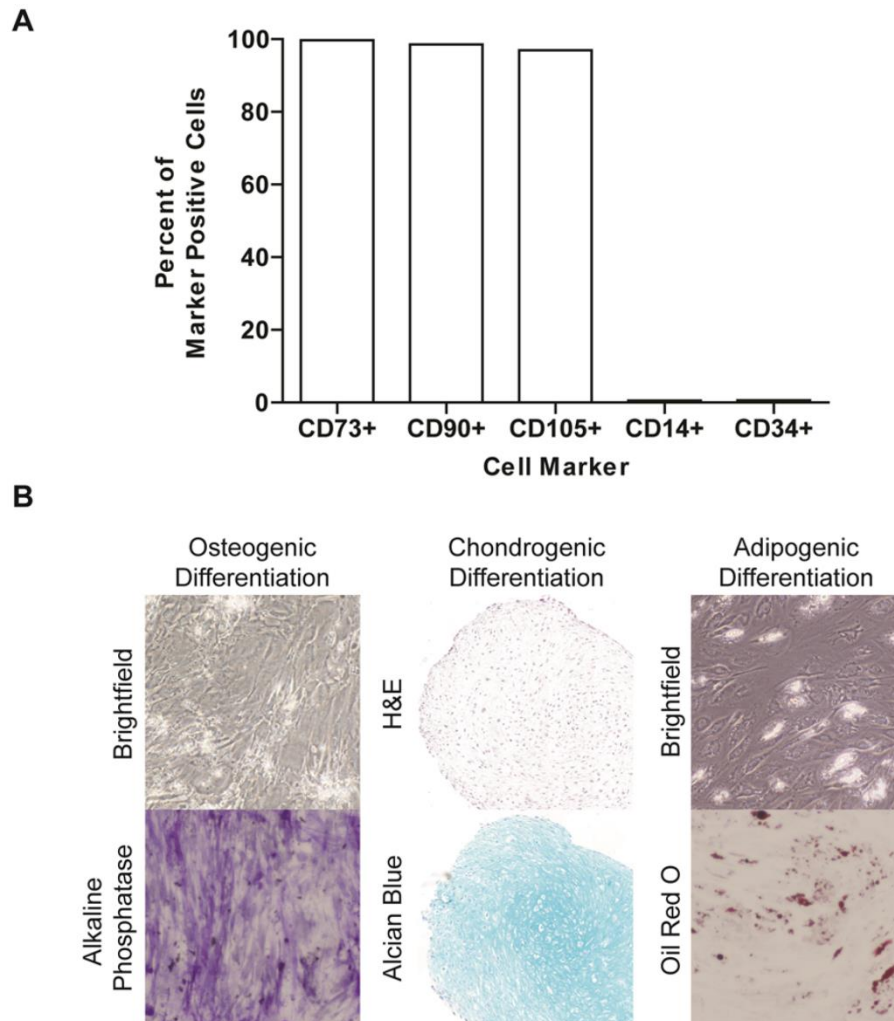


Fig. S1. Verification of ASC multipotency. **(A)** Percent of cells displaying stem cell surface markers, as analyzed by FACS. **(B)** Tri-differentiation potential of studied cell line.

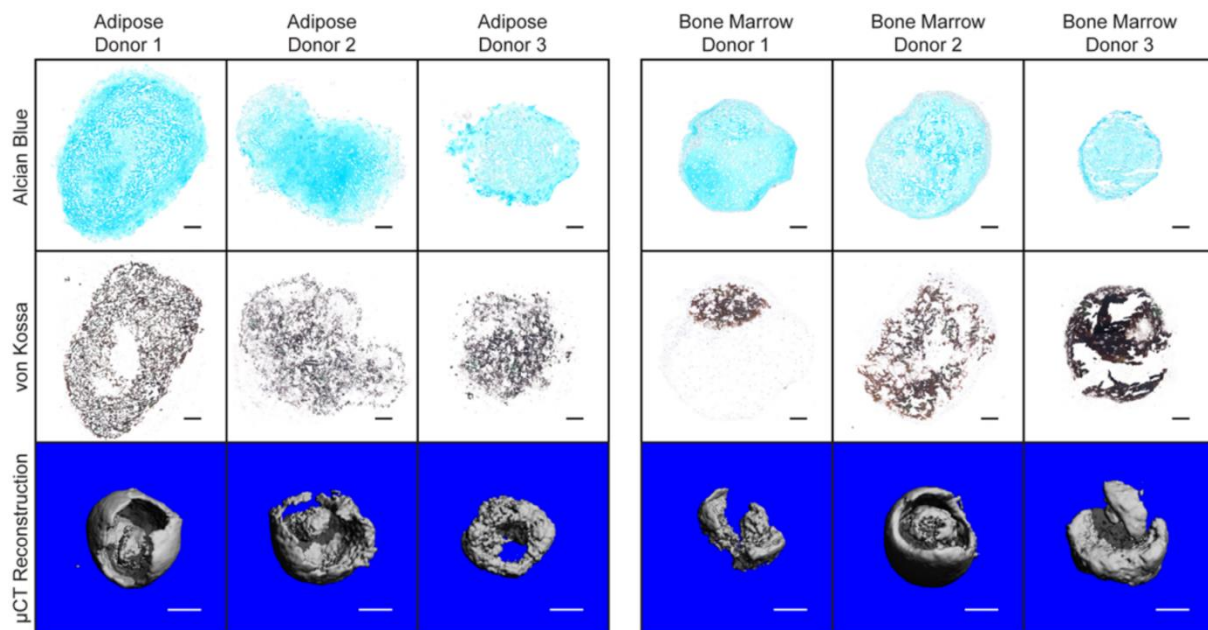


Fig. S2. Hypertrophic chondrocyte differentiation of adipose derived stem cells and bone marrow stem cells from various donors. After five weeks of differentiation following the hypertrophic chondrocyte protocol, harvested samples demonstrated GAG content (Alcian blue) and mineral deposition (von Kossa, μ CT reconstruction), both key matrix elements associated with hypertrophic chondrocytes. Scale Bars: Alcian blue and von kossa (100 μ m), μ CT (1 mm).

6.2 Supplemental Material and Methods

Materials were obtained from Sigma-Aldrich (St. Louis, MO) unless otherwise noted.

6.2.1 Flow cytometric analysis

The presence of stem cell surface markers was analyzed in the ASC line chosen for the primary studies. 125000 cells were incubated with each surface marker for 1 hour with antibodies for CD73, CD90, CD105, CD14, and CD34.

6.2.2 Tri-Differentiation Testing

ASC cells were expanded to passage 4 and then either plated on tissue culture plastic at a concentration of 5,000 cells/cm² (osteogenic and adipogenic differentiation) or pelleted at 250,000 cells/pellet (chondrogenic differentiation). Osteogenic and adipogenic cells were differentiated for 3 weeks. Osteogenic differentiation medium consisted of low glucose DMEM with L-glutamine, 100 nM dexamethasone, 50 μ g/mL ascorbic acid, 10 mM HEPES buffer, 10% fetal bovine serum, 1% P/S, and 5 mM β -glycerophosphate. Adipogenic differentiation medium occurred in high glucose DMEM with L-glutamine, with 1% P/S, 1 μ M dexamethasone, 1 μ M indomethacin, 500 μ M IBMX, and 10 μ g/mL insulin.

The cells were imaged at brightfield settings on the microscope to determine cell morphology.

Osteogenic cells were stained for alkaline phosphatase activity using the alkaline phosphatase staining kit purchased from EMD Millipore. Adipose cells were stained for lipid content with Oil Red O

following commonly available staining protocols. Chondrogenic differentiation was conducted in cell pellets for 2 weeks. The cells were harvested and stained with hematoxylin and eosin to evaluate cell morphology and Alcian blue to evaluate GAG distribution.

6.2.3 Cell Sourcing

Adipose tissue was obtained with informed consent under supervision of the ethical board of Upper Austria at the Rotes Kreuz facility in Linz, Austria, following the protocol described in the main text. Bone marrow stem cells were purchased from Lonza (Allendale, NJ). Adipose cells were obtained from one male and two females, with the average age of the donor being 35.3 years. Bone marrow cells were obtained from two males and one female, with the average age of the donor being 19.7 years. Cells were expanded until passage 4 in expansion medium consisting of high glucose medium with L-glutamine, 10% fetal bovine serum, 1% penicillin/ streptomycin, and 1 ng/mL basic fibroblast growth factor. Cells were pelleted at the fourth passage by aliquoting 250,000 cells into 96 U-bottom well plates (ThermoFisher, Waltham, MA), and centrifuging at 300 g for 5 minutes.

6.2.4 Hypertrophic Chondrocyte Differentiation

Pellets were first cultured for 2 weeks in chondrogenic medium (high glucose DMEM, ThermoFisher, Waltham, MA; 100 nM dexamethasone; 50 µg/mL ascorbic acid; 50 µg/mL proline; 100 µg/mL sodium pyruvate; 1% ITS+; 1% P/S; 10 ng/mL BMP6; 10 ng/mL TGF-β3). For an additional 3 weeks, the medium was changed to hypertrophic medium (high glucose DMEM, ThermoFisher, Waltham, MA; 1 nM dexamethasone; 50 µg/mL ascorbic acid; 50 µg/mL proline; 100 µg/mL sodium pyruvate; 1% ITS+; 1% P/S; 50 ng/mL of L-thyroxine; 5 mM of β-glycerophosphate).

6.2.5 Hypertrophic Chondrocyte Verification

Pellets were fixed in 10% formalin, rinsed in PBS, dehydrated, embedded in paraffin, and sectioned at 5 µm. Histological sections were stained for GAG (Alcian blue) and mineral (von Kossa) following standard protocols. Separate pellets were fixed in 10% formalin, rinsed in PBS, scanned and reconstructed using a Scanco VivaCT 40 micro-computed tomography system (Scanco Medical, Bassersdorf, Switzerland) to evaluate mineralization. Scans were performed using 55 kVp, 109 µA, and 200 ms integration time, and resulted in images with 21 µm isotropic voxel size. Reconstructed images were smoothed using a

Gaussian filter (Sigma 0.8, support 1), and segmented using a global threshold of 22% maximum grayscale value. Three-dimensional images were captured using the built in visualization software.

Perfusion enhances hypertrophic chondrocyte matrix deposition, but not the bone formation

Jonathan C. Bernhard, PhD^a, Elizabeth Hulphers, MS^a, **Bernhard Rieder**, MS^b, James Ferguson, DVM^c, Dominik Rünzler, PhD^b, Thomas Nau, MD^c, Heinz Redl, PhD^c, Gordana Vunjak-Novakovic, PhD^{a,d,*}

^a Department of Biomedical Engineering, Columbia University, New York, NY 10032

^b Department of Biochemical Engineering, University of Applied Sciences Technikum Wien, Austrian Cluster for Tissue Regeneration Vienna, Austria, A-1200

^c Ludwig Boltzmann Institute of Experimental and Clinical Traumatology, Austrian Cluster for Tissue Regeneration, Vienna, Austria, A-1200

^d Department of Medicine, Columbia University, New York, NY 10032

*corresponding author: gv2131@columbia.edu

Published in *Tissue Engineering: Part A* on March 1st, 2018

Abstract

Perfusion bioreactors have been an effective tool in bone tissue engineering. Improved nutrient delivery and the application of shear forces have stimulated osteoblast differentiation and matrix production, allowing for generation of large, clinically-sized constructs. Differentiation of hypertrophic chondrocytes has been considered as an alternative strategy for bone tissue engineering. We studied the effects of perfusion on hypertrophic chondrocyte differentiation, matrix production, and subsequent bone formation. Hypertrophic constructs were created by differentiation in chondrogenic medium (2 weeks), and maturation in hypertrophic medium (3 weeks). Bioreactors were customized to study a range of flow rates (0-1,200 $\mu\text{m/s}$). During chondrogenic differentiation, increased flow rates correlated with cartilage matrix deposition and the presence of collagen type X. During induced hypertrophic maturation, increased flow rates correlated with bone template deposition, and the increased secretion of chondroprotective cytokines. Following an 8-week implantation into the critical-size femoral defect in nude rats, non-perfused constructs displayed larger bone volume, more compact mineralized matrix, and better integration with the adjacent native bone. Therefore, although medium perfusion stimulated the formation of bone template *in vitro*, it failed to enhance bone regeneration *in vivo*. However, the promising results of the less developed template in the critical-sized defect warrants further investigation, beyond interstitial flow, into the specific environment needed to optimize hypertrophic chondrocyte-based constructs for bone repair.

Keywords: Perfusion flow, bioreactors, hypertrophic chondrocytes, bone tissue engineering

1 Introduction

Biomimetic approaches recapitulating some of the natural mechanisms of tissue formation [326] have gained increasing interest in engineering of functional bone grafts. One of the most promising directions is the study of endochondral ossification strategies in complex bone repair environments. In particular, utilization of cartilage anlage has resulted in the ability to form bone *in vivo* [276]–[280], [306]. Among these strategies, the use of hypertrophic chondrocytes, the cell that orchestrates endochondral ossification, appears particularly promising as the maturation from chondrocytes to hypertrophic chondrocytes resulted in significantly more bone formation [282]. The hypertrophic chondrocyte constructs have shown an ability to create maturing bone *in vitro*, that subsequently developed vasculature and bone marrow following subcutaneous implantation [285], [306], and facilitated healing of calvarial [281], [283] and long bone [327] defects. Robust performance of these constructs and their superiority over traditionally utilized osteoblast constructs [283], [327], suggested clinical potential for healing complex bone fractures.

Bioreactors provide an essential tool for the creation of tissue constructs, allowing control of numerous environmental factors that influence construct composition and behavior [328], [329]. In osteochondral tissue engineering, perfusion bioreactors have been applied to both osteoblasts and chondrocytes. Perfusion bioreactors increased nutrient delivery [330], [331] and provided shear stress [331], [332] that increased osteoblast cellularity, activity, matrix production and *in vivo* bone regeneration [292], [293], [305], [333]–[335], as well as chondrocyte differentiation and cartilage matrix production [336]–[338]. Through the application of perfusion flow, large, autologous, anatomically exact bone grafts were created that successfully repaired craniofacial defects [305]. The goal of our study was to investigate the effect of perfusion flow on hypertrophic chondrocyte-based bone constructs.

Though hypertrophic chondrocytes in perfusion bioreactors have not been directly studied, a recent study showed that chondrogenic culture of stem cell pellets in a perfusion bioreactor increased expression of hypertrophic markers, although without effects on cartilaginous matrix production [339]. Dynamic culture stimulated hypertrophic chondrocyte differentiation and resulted in increased bone production [340], [341]. We hypothesized that the perfusion flow will facilitate hypertrophic chondrocyte differentiation, deposition, and bone formation.

To test this hypothesis, we created hypertrophic chondrocyte-based constructs with clinical applicability in mind. Human bone marrow-derived stem cells (BMSCs), selected because of their extensive use in tissue engineering of bone and cartilage, were seeded into decellularized trabecular bone scaffolds, selected because of their osteogenic nature and mechanical properties, and cultured for 5 weeks. Perfusion flow was set to four different levels: 0 (static control), 100, 400, and 1200 $\mu\text{m/s}$, based on providing a broad range of flow rates to discern the impact of perfusion flow while also providing similar rates to our previous, impactful work with osteoblasts [342]. Tissue samples were harvested after chondrogenic differentiation at 2 weeks and after construct cultivation at 5 weeks and evaluated for

hypertrophic chondrocyte differentiation and bone matrix deposition. At the end of *in vitro* culture, tissue constructs grown without perfusion and at the perfusion rate of 400 $\mu\text{m/s}$ were implanted into an orthotopic, critical sized-femoral defect in athymic rats, and the bone regeneration was studied over an additional 8 weeks following implantation.

2 Materials and Methods

All materials were purchased from Sigma Aldrich (St. Louis, MO) unless otherwise noted.

2.1 Scaffold preparation

Trabecular bone cores were harvested from juvenile bovine wrists as in previous studies [293], [327]. Briefly, wrist joints were obtained from a local butcher and the metacarpal bone was isolated and cleaned from all other tissue. Diamond tip bores (Starlite Industries, Rosemont, PA), 4 mm in diameter, were utilized to remove trabecular bone. Scaffolds were trimmed to 5 mm height by 4 mm diameter. Trimmed cores were then washed of marrow and tissue by utilizing a high-powered water jet. Scaffolds were decellularized following our published protocols [293]. Briefly, scaffolds were washed in a series of solutions: (1) 0.1% ethylenediaminetetraacetic acid (EDTA) in phosphate-buffered saline (PBS) for 1 h, (2) hypotonic buffer consisting of 10 mM Tris and 0.1% EDTA in PBS for 12 h at 4 °C, (3) detergent consisting of 10 mM Tris and 0.5% sodium dodecyl sulfate in PBS for 24 h at room temperature on an orbital shaker at 300 revolutions/min, and (4) enzymatic solution of 100 U/mL DNase and 1 U/mL of RNase with 10 mM Tris in PBS for 6 h at 37 °C. After multiple washes in PBS, scaffolds were frozen and lyophilized. In an attempt to manage core variability, scaffolds were sorted based on their bulk density (mass/volume), with densities used for this study within the range of 0.35 to 0.50 g/mL. Scaffolds were disinfected by incubating in 70% ethanol for 2 days under ultraviolet light prior to cell seeding.

2.2 Cell expansion and seeding

Human bone marrow stem cells (BMSC) were obtained from Lonza (Basel, CH) and expanded until passage 5 in expansion medium consisting of high glucose medium with L-glutamine, 10% fetal bovine serum, 1% penicillin/streptomycin (P/S), and 1 ng/mL basic fibroblast growth factor. Before seeding, scaffolds were rinsed of 70% ethanol with sterile PBS, and incubated for 1 day in expansion medium. After passage 5, BMSC were trypsinized, resuspended in culture medium at a concentration of 30 million cells/mL, and integrated into the demineralized cancellous bone (DCB) scaffolds. As the scaffolds had an estimated volume of 75 μL , 2.25 million cells were seeded per scaffold.

2.3 Perfusion bioreactors and hypertrophic differentiation

The perfusion bioreactor utilized in the experiments had previously been developed and characterized for bone tissue engineering with osteoblasts [292], [296]. The bioreactor utilizes a central input that evenly divides the flow of medium into six individual culture wells. Polydimethylsiloxane (PDMS) rings were used to seal scaffolds in the culture wells, and to route perfusion flow into and through the scaffold.

Upon passage through the scaffolds, medium was collected in a reservoir above the constructs, where it was continuously equilibrated with oxygen and pH before recirculating through the exit port back into the wells. The bioreactor was powered by a multichannel peristaltic pump (Cole-Parmer, Vernon Hills, IL). Each six-well bioreactor was set to a specific flow rate, by adjusting the diameter of the tubing (Cole-Parmer, Vernon Hills, IL). It was determined that pump diameters of 0.51, 0.89, and 2.29 millimeters corresponded to flow rates of 136, 413, and 1144 $\mu\text{m/s}$, respectively at a pump rate of 225 revolutions/min (**Fig. 15**). Based on the analysis completed previously [342], these rates corresponded to shear stresses ranging from 1 to 15 MPa, with 100 and 1200 $\mu\text{m/s}$ providing an order of magnitude difference in both flow rate and shear stress, and the 400 $\mu\text{m/s}$ matching the optimal flow rate and shear stress for osteoblast cultivation. For simplicity, the groups corresponding to these flow rates were labeled 100, 400, and 1200 $\mu\text{m/s}$.

Seeded constructs were then placed within the bioreactor wells and perfusion flow was started. All experimental groups (0, 100, 400, 1200 $\mu\text{m/s}$) were cultured under the same 5-week long differentiation regime (**Fig. 15**). For the first 2 weeks, the constructs were cultured in chondrogenic medium consisting of high glucose DMEM (ThermoFisher, Waltham, MA), 100 nM dexamethasone, 50 $\mu\text{g/mL}$ ascorbic acid, 50 $\mu\text{g/mL}$ proline, 100 $\mu\text{g/mL}$ sodium pyruvate, 1% ITS+, 1% P/S, 10 ng/mL transforming growth factor- β 3 (TGF- β 3). The constructs were then matured to hypertrophic chondrocytes over the next 3 weeks in hypertrophic medium, consisting of high glucose DMEM (ThermoFisher) supplemented with 1 nM dexamethasone, 50 $\mu\text{g/mL}$ ascorbic acid, 50 $\mu\text{g/mL}$ proline, 100 $\mu\text{g/mL}$ sodium pyruvate, 1% ITS+, 1% P/S, 50 ng/mL L-thyroxine, and 5 mM of β -glycerophosphate. Constructs were harvested at 2 weeks, at the end of chondrogenic culture, and after 5 weeks, at the end of *in vitro* culture.

2.4 Biochemical Assays

Constructs from both harvest time points ($n = 4$) were weighed and digested with papain (40 U/mg) in digest buffer (0.1 M sodium acetate, 10 mM cysteine HCl, and 50 mM EDTA, pH 6.0) at 60 °C overnight. DNA content was measured by the Quant-IT PicoGreen assay kit (ThermoFisher) and normalized to the wet weight. The manufacturer's instructions were followed, and the supplied lambda DNA was used as the standard.

Sulfated glycosaminoglycan (GAG) content was measured from the papain digested constructs using the dimethylmethylene blue dye assay, normalized to wet weight, with chondroitin 6 sulfate utilized as control. The GAG content was normalized to the construct DNA.

2.5 Real Time PCR

RNA was extracted from the constructs using TRIzol (ThermoFisher). RNA content was measured using NanoDrop spectrophotometric quantitation (ThermoFisher) and contaminating DNA was removed through DNAase I treatment. cDNA was transcribed from the RNA through the use of the High-Capacity cDNA Reverse Transcription kit (ThermoFisher) according to the manufacturer's instructions.

Quantitative reverse transcriptase (RT) polymerase chain reaction (PCR) was performed using Fast Sybr Green master mix (ThermoFisher) with gene expression normalized using the ΔC_t , the C_t of GAPDH subtracted from the C_t of the gene of interest. Samples were run in technical duplicates, with $n = 4$ biological replicates for each experimental group. The genes examined were GAPDH (F: AAG GTG AAG GTC GGA GTC AAC, R: GGG GTC ATT GATG GCA ACA ATA), collagen type 10 (COL10A1, F: CAT AAA AGG CCC ACT ACC CAA C, R: ACC TTG CTC TCC TCT TAC TGC), RUNX2 (F: CCG TCT TCA CAA ATC CTC CCC, R: CCC GAG GTC CAT CTA CTG TAA C), bone sialoprotein (IBSP, F: GAA CCT CGT GGG GAC AAT TAC, R: CAT CAT AGC CAT CGT AGC CTT G), and alkaline phosphatase (ALPL, F: GGG ACT GGT ACT CAG ACA ACG, R: GTA GGC GAT GTC CTT ACA GCC).

2.6 Analysis of secreted cytokines

Conditioned medium (collected over 4 days of culture) was collected from each bioreactor. Commercially available quantitative ELISA kits were purchased for the following cytokines: VEGF-A (RayBiotech, Norcross, GA), BMP2 (RayBiotech, Norcross, GA), BMP7 (RayBiotech, Norcross, GA), β -catenin (LifeSpan BioSciences, Seattle, WA), DKK1 (RayBiotech, Norcross, GA), IHH (LifeSpan BioSciences, Seattle, WA). Assays were performed according to the manufacturer's instructions, with conditioned medium incubated overnight at 4 °C. Conditioned medium samples were pooled together for each experimental group and tested in triplicate.

2.7 Defect creation and graft implantation

Animal studies were conducted under an approved protocol and with the permit of the municipal government of Vienna, Austria. The experiments were consistent with the Guide for the Care and Use of Laboratory Animals of the National Institute of Health (revised 2011). Male Rowett Nude (RNU) rats, weighing 250 g at the time of surgery, were kept in housing cages with filter tops, in groups of two. Preoperatively, the animals were administered subcutaneously 0.05 mg/kg buprenorphine (Bupaq; Richterpharma AG, Austria) and 4 mg/kg carprofen (Rimadyl; Zoetis Österreich Gesm.b.H, Austria). Anesthesia was induced with isoflurane (Forane; AbbVie Gesm.b.H, Austria) and maintained with 1.5-2.5% isoflurane/oxygen by way of nose-cone inhalation.

Once the animal was under stable anesthesia, a lateral approach was used to expose the right femur. After fixation with a four-pin POM fixator (modified from the method described in Betz *et al.* [297]), a defect of 5 mm was created with a Gigli wire saw. Grafts were trimmed to fit, placed into the defect, and the muscle and skin were sutured around the graft and the fixator, respectively. For the two experimental groups (non-perfusion control; perfusion at 400 $\mu\text{m/s}$), four rats in each group underwent implantation, with an additional two rats not receiving implants to confirm the absence of spontaneous healing in critical-size defects. Pain management was completed with subcutaneous injections of 0.05 mg/kg buprenorphine and 4 mg/kg carprofen over the first four days post-implantation. The rats with an open defect and no implant demonstrated a non-healing non-union failure before study endpoint

and were euthanized. Eight weeks post-implantation, the rats were euthanized by an overdose injection of intracardially delivered thiopental sodium while under deep isoflurane anesthesia. The right femur of each animal was harvested for detailed characterization.

2.8 Histology and immunohistochemistry

Pre-implantation and post-implantation tissue samples (femurs with the implanted grafts) were preserved in 10% formalin for 24 h, rinsed excessively in PBS, decalcified using a formic acid-based solution (Immunocal Decalcifier, StatLab, McKinney, TX), and dehydrated in graded ethanol solutions. After dehydration, samples were embedded in paraffin and sectioned at 6 μm .

Samples of pre-implantation chondrogenic constructs were stained with Alcian blue for GAG following standard protocols. Immunohistochemistry was performed on sections of chondrogenic construct by first incubating the samples in 0.05% trypsin at 37 °C for 15 min. After rinsing in PBS, samples were incubated in 0.3% hydrogen peroxide in absolute methanol for 30 min with gentle shaking at room temperature. After washing in PBS, Vectastain Elite Universal staining kit (Vector Laboratories, Burlingame, CA) was utilized to prepare and detect the primary antibody. The collagen type II antibody was obtained from Abcam (San Francisco, CA) and applied at a dilution of 1/50. Samples were counterstained with Hematoxylin QS (Vector Laboratories, Burlingame, CA)

To demonstrate the progression of hypertrophic chondrocyte maturation, collagen type X immunohistochemistry was performed on both chondrogenic and hypertrophic samples from each group. Histological sections were first incubated with 2 mg/mL hyaluronidase (type IV from bovine testes) for 60 min at 37 °C, followed by PBS washing, and then incubated with 1 mg/mL Pronase E treatment for 60 min at 37 °C. After washing in PBS, Vectastain Elite Universal staining kit (Vector Laboratories) was utilized to prepare and detect the primary antibody. The collagen type X antibody was obtained from Abcam (San Francisco, CA) and applied at a dilution of 1/2000. Samples were counterstained with Hematoxylin QS (Vector Laboratories).

Immunohistochemistry was performed to visualize bone sialoprotein and osteopontin in the constructs. Antigen retrieval was done on histological slides placed in a container filled with citrate buffer and submerged into boiling water for 20 min. Slides were blocked by incubation of samples in 0.3% hydrogen peroxide for 30 min. Vectastain Elite Universal staining kit (Vector Laboratories) was utilized to prepare and detect the primary antibody. Primary antibodies for bone sialoprotein (EMD Millipore, 1/500 dilution, Bilerica, MA) and osteopontin (EMD Millipore, 1/500 dilution, Bilerica, MA) were incubated on the slides overnight at 4 °C. Samples were counterstained with Hematoxylin QS (Vector Laboratories, Burlingame, CA). Pre- and post-implantation samples were stained with Movat's Pentachrome (Cancer Diagnostics, Durham, NC) according to manufacturer's instructions

2.9 Microcomputed tomography (μ CT)

Explants were scanned on a μ CT 50 (Scanco Medical, Bruttisellen, Switzerland) using scanner settings as follows: voltage 70 kV, current 0.200 mA, and slice thickness 10 μ m. Scans had a 10 μ m isotropic resolution. Three-dimensional (3D) reconstructions and quantitation were performed by a global thresholding technique set at 282.9 mg hydroxyapatite (HA)/cm³. Bone volume and bone surface/bone volume (BS/BV) were calculated for the scanned samples (n = 4 biological replicates) utilizing software provided by Scanco Medical.

2.10 Statistics

All data are presented as mean \pm standard deviation. Statistical significance of biochemical quantitation and real time PCR data was evaluated using a one-way analysis of variance (ANOVA) followed by Tukey's post-test, $\alpha = 0.05$, with significance determined by $p < 0.05$ using statistical software (Prism Software, GraphPad, La Jolla, CA). Statistical significance of cytokine secretion and microcomputed tomography (μ CT) bone morphometry was determined using a Student's *t*-Test, $\alpha = 0.05$, with significance determined by $p < 0.05$.

3 Results

Perfusion (interstitial flow) at a set flow rate was applied to tissue engineered constructs to determine its effects on hypertrophic chondrocyte differentiation and matrix production. The effects of three different flow rates (100, 400 and 1200 μ m/s) were compared to non-perfused (0 μ m/s) controls (**Fig. 15**).

Tissues were harvested after 2 weeks, at the endpoint of chondrogenic differentiation, and evaluated for cartilage matrix production (**Fig. 16**). The DNA content, normalized to construct wet weight, was not significantly different between the 0, 100, and 400 μ m/s constructs, whereas the 1200 μ m/s constructs had significantly more DNA compared to all other three groups (**Fig. 16A**). Similarly, the GAG content was highest in the 1200 μ m/s group and was significantly higher than in the 0 μ m/s group (**Fig. 16B**). To determine matrix production per cell, the GAG content was normalized to the amount of DNA. All three perfusion flow groups (100, 400, and 1200 μ m/s) had significantly more GAG/DNA than the control group (**Fig. 16C**). The histological staining of GAG, by Alcian blue, was consistent with the GAG content (**Fig. 16D**), and the increased flow rate corresponded to increased Alcian blue staining. Of particular interest was the GAG staining located at the construct centers, as an increased flow rate resulted in increased GAG presence. Collagen type II staining matched Alcian blue, with the 0 μ m/s have relatively faint staining for collagen type II with a progression in staining intensity that corresponded with increased flow rate (**Fig. 16D**). Consistently, faster flow rates resulted in enhanced staining for cartilaginous matrix within the construct interior.

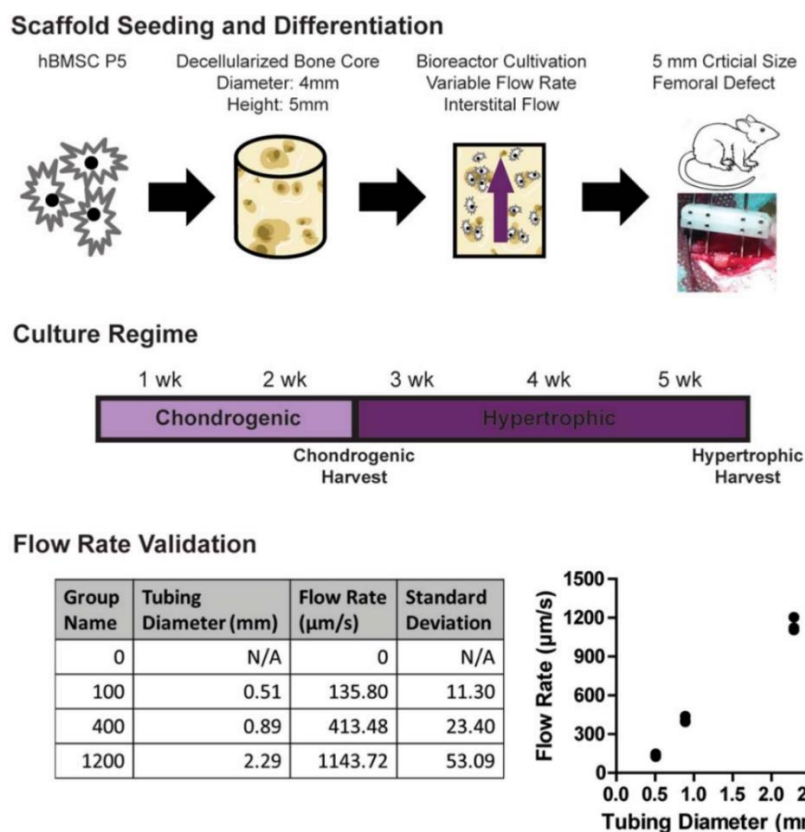


Fig. 15. Creation of hypertrophic chondrocyte constructs through application of variable flow rates. Bone cores were extracted from juvenile bovine wrists, decellularized, and sized to 4 mm diameter x 5 mm height. Human BMSC were expanded and seeded into the decellularized bone cores (2.25×10^6 cells/construct). Seeded constructs were then placed into previously validated perfusion bioreactors [292], [296] and differentiated for 2 weeks in chondrogenic medium, then matured to hypertrophic chondrocytes over an additional 3 weeks. Flow rates were determined by the tubing diameter, and flow rates approximating 0, 100, 400, and 1200 $\mu\text{m/s}$ were chosen for experimentation. At the end of 5 weeks of culture, constructs were implanted into a 5 mm, critical-size defect made in the right femur of RNU nude male rats. Construct regeneration occurred for 8 weeks *in vivo* before harvest and construct evaluation. BMSC, bone marrow-derived stem cell, RNU, Rowett Nude.

Collagen type X is a unique marker for chondrocyte hypertrophy [343], and the *in vitro* chondrogenic differentiation has been associated with cell hypertrophy and collagen type X deposition [344]. To evaluate the impact of perfusion on chondrocyte hypertrophy both during chondrogenic differentiation and induced hypertrophic maturation, tissue samples were immunohistochemically stained for collagen type X (**Fig. 17**). In general, collagen type X staining for both time points matched the GAG and collagen type II staining, with the faster flow rates corresponding to the higher presence of collagen type X within the center of the constructs. Interestingly, the localization of the collagen type X appeared to differ between the two time points. During chondrogenic culture, the collagen type X staining seemed to be only fibrillar and was dispersed throughout the construct volume; during hypertrophic maturation, pericellular localization of collagen type X was noticeable in all four groups.

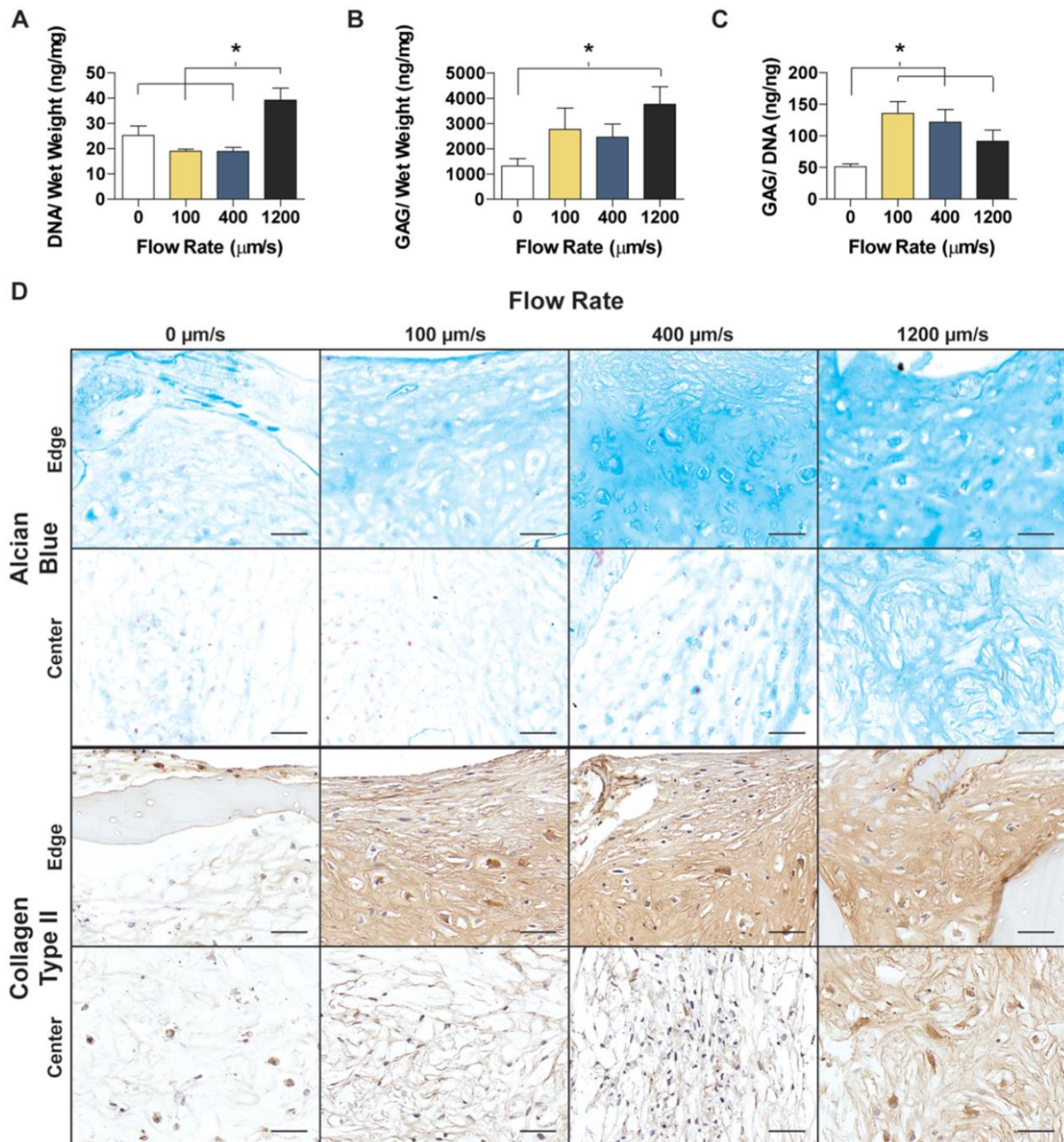


Fig. 16. Chondrogenic differentiation and cartilage matrix production. **(A)** DNA and **(B)** GAG content normalized to the tissue wet weight. **(C)** GAG normalized to DNA contents. **(D)** Histology and immunohistochemistry evidencing the distribution of GAG (Alcian blue staining) and collagen type II (antibody). Magnified images are shown for the edge and center of the construct. Data are shown as average \pm SD. * denotes significant differences between the groups, $p < 0.05$ ($n = 4$). **(D)** Scale bars: 50 μm . GAG, glycosaminoglycan.

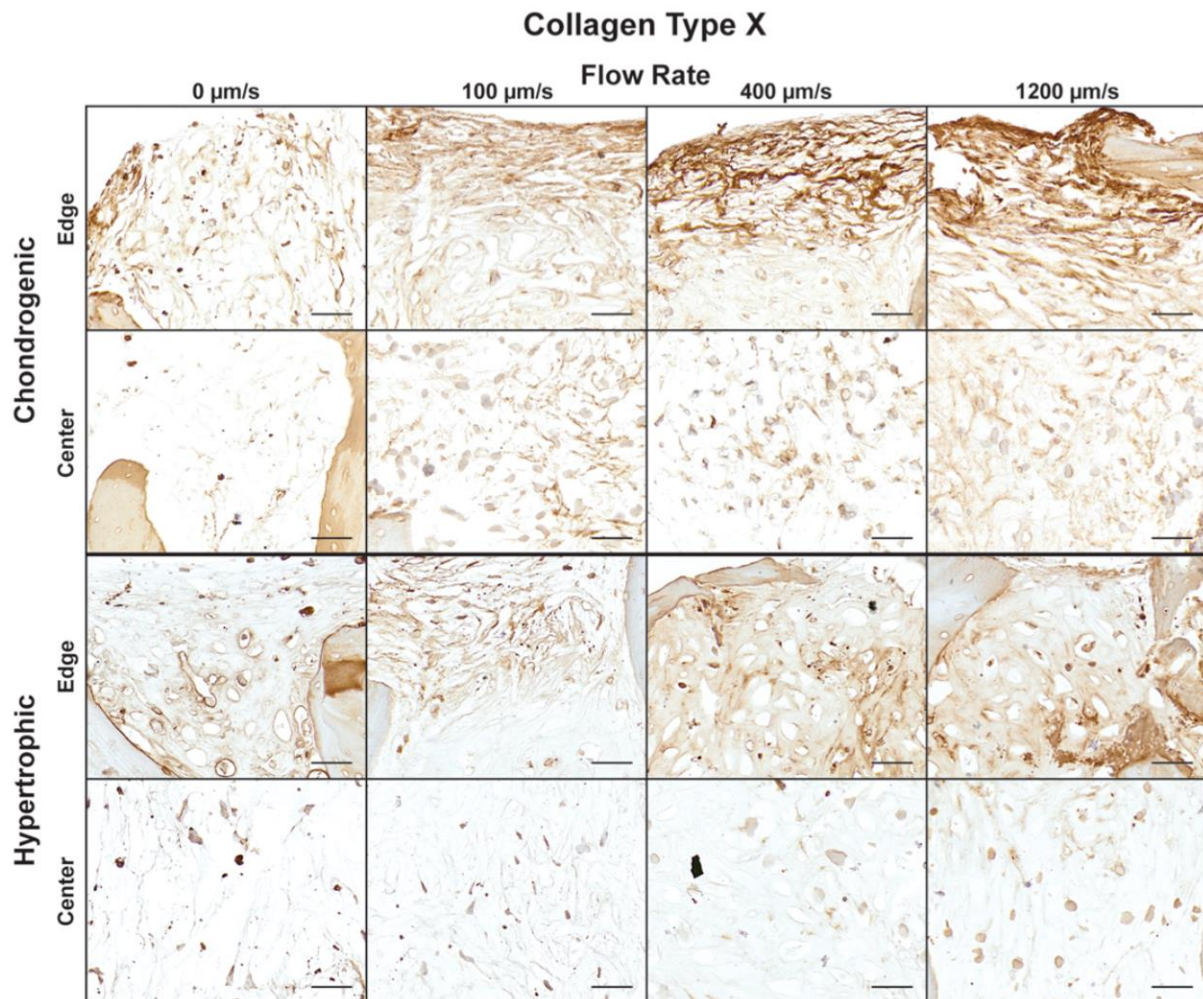


Fig. 17. Hypertrophic chondrocyte maturation. Immunohistochemistry for collagen type X at the end of chondrogenic and hypertrophic culture. Magnified images are shown for both the edge of the construct and the center of the construct. Scale bars: 50 μm .

The progression to hypertrophy changed the biochemical characteristics of the constructs (**Fig. 18**). The DNA content amongst the four groups was similar, with the 1200 $\mu\text{m/s}$ group having a 2-fold reduction in DNA content during the 3 weeks of hypertrophic culture (**Fig. 18A**). As expected with the turnover from a cartilage matrix to a hypertrophic bone template, the GAG content was reduced in all groups, with the maintenance of higher GAG and GAG/DNA contents at higher perfusion flow rates (**Fig. 18B**). In contrast to the chondrogenic analysis, the hypertrophic GAG/DNA content matched the GAG content trend, with the 1200 $\mu\text{m/s}$ containing significantly more GAG/DNA than the 0 and 100 $\mu\text{m/s}$ groups (**Fig. 18C**). Despite the differences in matrix content, the expression of advanced hypertrophic chondrocyte and bone production genes did not vary significantly among the groups (**Fig. 18D**).

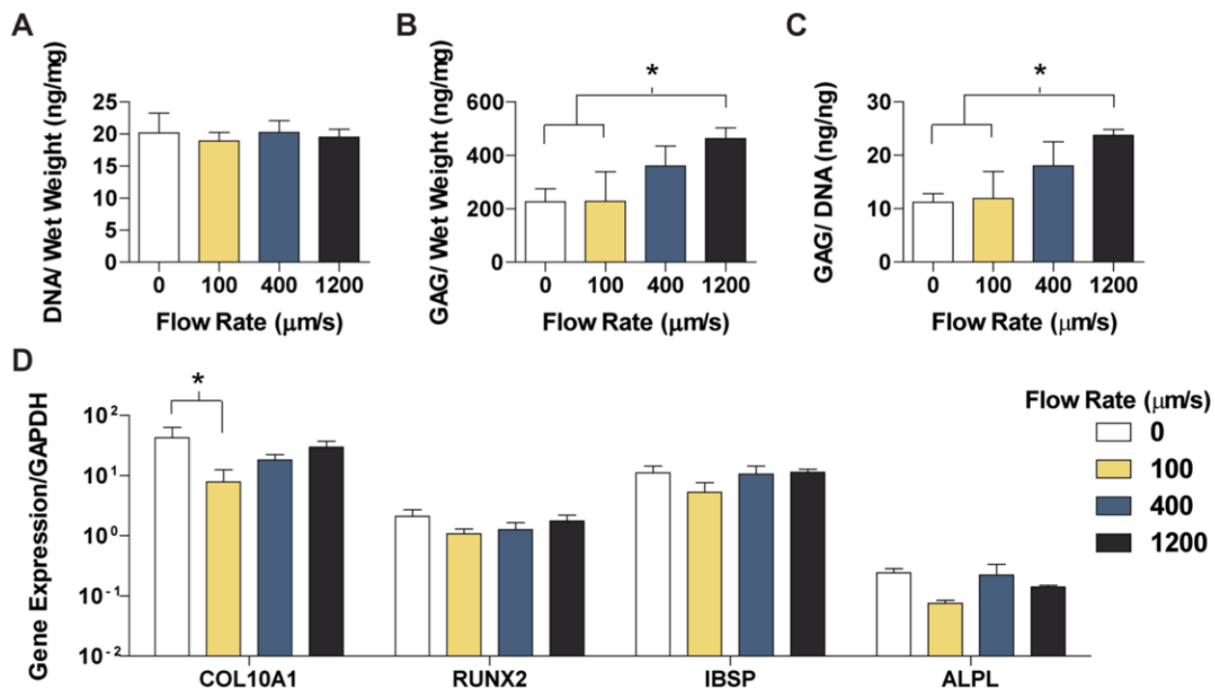


Fig. 18. Biochemical content and gene expression analysis of hypertrophic chondrocyte constructs. **(A)** DNA per unit wet weight. **(B)** GAG per unit wet weight. **(C)** GAG per unit DNA. **(D)** Expression of key genes related to chondrocyte hypertrophy and bone template formation. Data are shown as average \pm SD. * denotes significant differences between the groups, $p < 0.05$ ($n = 4$).

Histological and immunohistochemistry sections of the hypertrophic constructs confirmed the differences in matrix production quantified in **Fig. 18**. Movat's pentachrome staining was utilized to visualize the morphology of the constructs, with cell nuclei in dark red/black, GAG in green, and collagen in yellow (**Fig. 19**). The reduced flow rates (0 and 100 $\mu\text{m/s}$) had minimal matrix deposition, with very little GAG and collagen present in both the edge and center sections. The cell morphology in the 0 $\mu\text{m/s}$ group appeared round, while the application of 100 $\mu\text{m/s}$ flow appeared to flatten the cells at the exterior of the construct. Higher flow rates (400 and 1200 $\mu\text{m/s}$) resulted in clear presence of GAG matching the quantitated data, with GAG surrounding enlarged, rounded chondrocyte lacunae. Unlike any other group, the 1200 $\mu\text{m/s}$ contained both GAG and collagen within the center of the construct. Hypertrophic chondrocytes mediate the turnover of a cartilage matrix to a bone template [8], [272], with bone sialoprotein (BSP) and osteopontin being important bone matrix proteins secreted by hypertrophic chondrocytes [275], [303]. Similar to GAG deposition, both BSP and osteopontin presence increased with increased flow rate (**Fig. 19**). The edges accumulated more matrix with the 400 and 1200 $\mu\text{m/s}$ groups constructing a dense matrix with abundant GAG, BSP, and osteopontin.

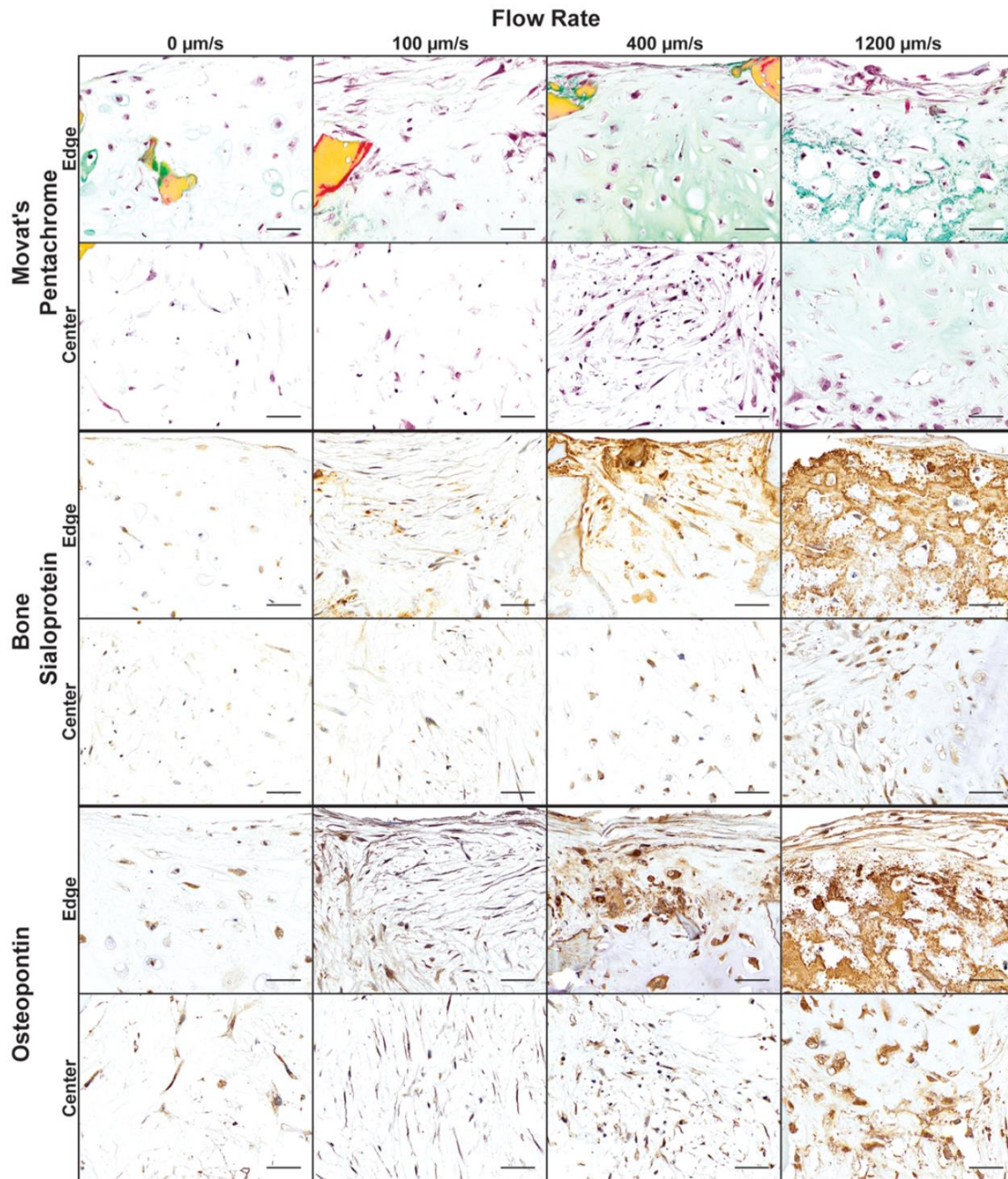


Fig. 19. Construct morphology and bone protein deposition. Histology and immunohistochemistry of constructs for general histomorphology and bone-specific proteins: Movat's pentachrome for GAG (*green*), collagen (*yellow*), decellularized scaffold (*dark yellow*), and cell nuclei (*red/black*). Immunohistochemistry for BSP and osteopontin. Magnified images are shown for both the edge and center of the construct. Scale bars: 50 μm . BSP, bone sialoprotein.

With clear differences in matrix deposition during cultivation, the ability of BMSC-derived hypertrophic chondrocyte constructs to facilitate bone regeneration was evaluated in an orthotopic, critical-size femoral defect. For comparison, the static culture group (0 $\mu\text{m/s}$) and a faster flow-rate group (400 $\mu\text{m/s}$) were implanted for 8 weeks within the critical-size femoral defect. The two grafts cultured at the faster interstitial flow rates (400 and 1200 $\mu\text{m/s}$) were not significantly different in biochemical composition or hypertrophic gene expression (Fig. 18) and contained similar matrix deposition by the differentiated

hypertrophic chondrocytes (Fig. 17, Fig. 19). Therefore, we selected the 400 $\mu\text{m/s}$ group for implantation, because of the more frequent and favorable use of this culture condition in previous studies of bone tissue engineering [292], [305], [342]. To assess the secreted cytokines at the time of implantation, a series of ELISA tests were conducted on conditioned medium (Fig. 20A). The concentrations of VEGF, BMP2, and BMP7 were not significantly different between the groups, β -catenin concentration was significantly higher in the 0 $\mu\text{m/s}$ group, while the concentrations of DKK1 and IHH were significantly higher in the 400 $\mu\text{m/s}$ group.

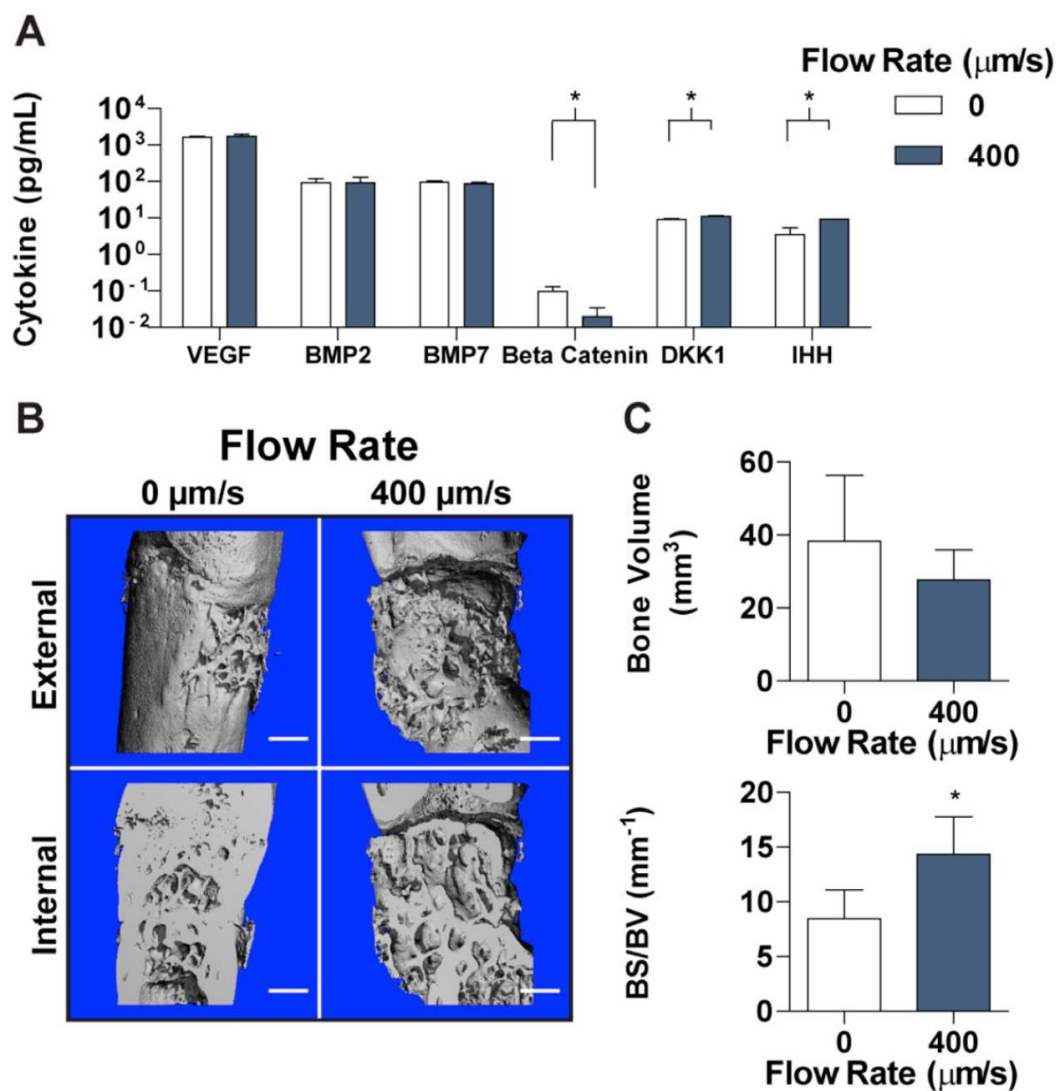


Fig. 20. Construct cytokine release and critical-size defect regeneration. (A) Secreted cytokines into culture medium were detected through ELISA. Cytokines investigated included bone generation cytokines (VEGF, BMP2, BMP7, β -catenin) and chondrocyte maintenance cytokines (DKK1, IHH). (B) μCT of the 0 and 400 $\mu\text{m/s}$ constructs following 8 weeks of implantation in a critically-sized femoral defect in nude rats. (C) The total bone volume and the BS/BV were calculated for each group and time point based on the μCT scans. Scale bars: 1 mm. Data are shown as average \pm SD. * denotes significant differences between the groups $p < 0.05$ (A: $n = 6$ constructs run in triplicate, C: $n = 4$). μCT , microcomputed tomography; BS/BV, bone surface/bone volume.

Upon harvest at 8 weeks, tissues were evaluated by high-resolution μ CT scans (10 μ m), to obtain 3D reconstructions and digital images of the graft exterior and interior (**Fig. 20B**). Bone deposition was evident in both groups, as demonstrated by the smooth, continuous sections seen within the porous trabecular bone. The internal reconstructions demonstrated noticeable differences between the internal bone architectures and the integration with the native femur. In the 0 μ m/s group, integration appeared seamless, with only a few areas of incongruity at the proximal interface. In contrast, the 400 μ m/s group had noticeable spacing between the femur and the construct at the distal interface. Quantitation of the bone volume in the defect space demonstrated slightly but not significantly more bone in the 0 μ m/s group (**Fig. 20C**). Calculation of the bone surface to bone volume (BS/BV), an indicator of deposition patterns, showed a significantly lower level for the 0 μ m/s group, indicating more compact, voluminous deposition, which matches the groupings seen in the interior 3D reconstructions.

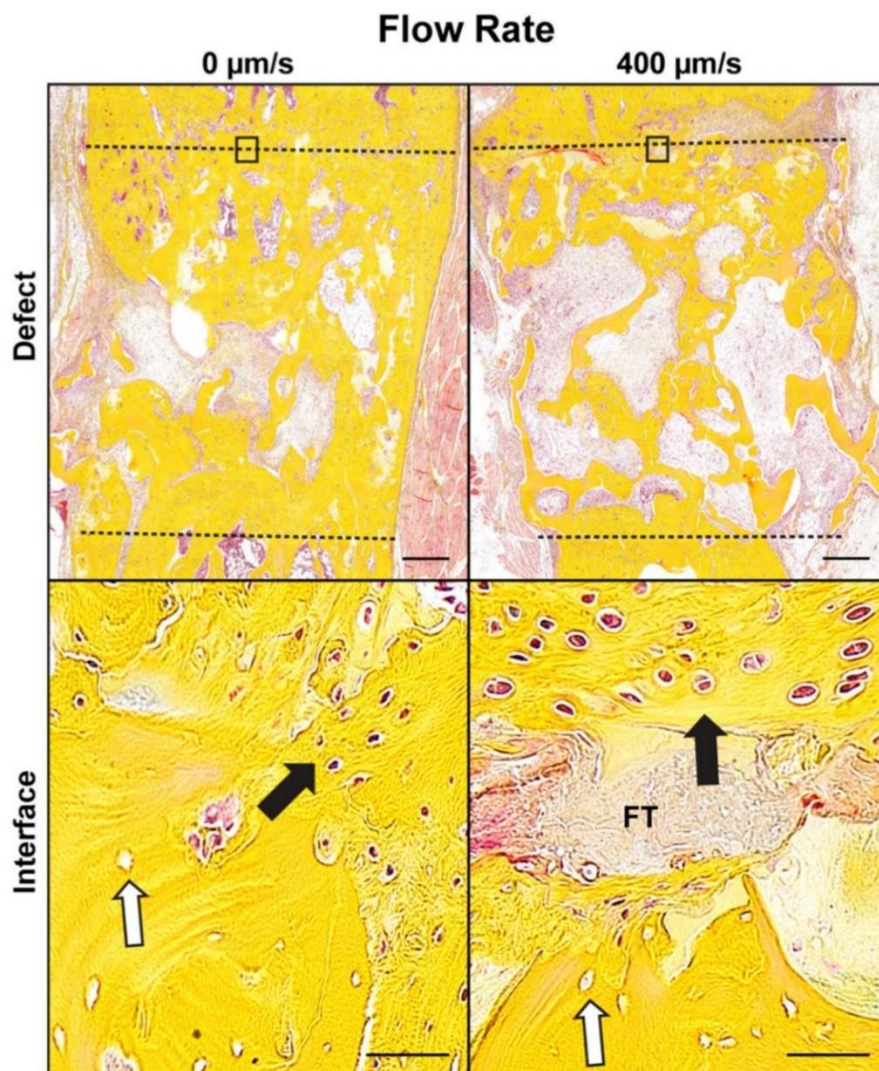


Fig. 21. Histology of critical-size defect regeneration. Movat's pentachrome staining after 8 weeks of 0 and 400 μ m/s construct implantation in the critical-size femoral defect. The defect is represented by the *dashed lines*, where *yellow* represents bone, and *light red* represents fibrous tissue. Magnified images of the construct-native bone interface were taken, with the *black rectangle* indicating the location of the interface within the defect. The *white arrows* represent the original decellularized bone, indicated by the empty cellular lacunae. *Black arrows* indicate formed bone, with FT indicating the fibrous tissue that is impeding integration. Scale bars: defect 500 μ m, interface 50 μ m

Tissue samples were then decalcified to investigate differences in bone regeneration (**Fig. 21**). Whereas neither group displayed complete defect regeneration, bone (yellow) appeared to be more densely deposited at the interface (dashed line) between the native femoral bone and the implanted tissue engineered construct, matching the μ CT reconstructions in **Fig. 20B**. Magnified images of the graft-bone interface demonstrated the bone containing empty cellular lacunae representing the decellularized bone scaffold (white arrows) and cellularized newly formed bone. Over the majority of the interface in the 0 μ m/s group, the newly formed bone was in direct contact with the adjacent host bone, whereas fibrous tissue (light red in both the defect and interface images) was present at the interface of the 400 μ m/s group.

4 Discussion

Hypertrophic chondrocytes derived from human BMSCs represent a promising option for bone tissue engineering [84], [271]. Perfusion bioreactors have demonstrated ability to enhance the properties of osteochondral constructs, and in this study our goal was to determine the effect of perfusion flow on hypertrophic chondrocyte differentiation and subsequent bone formation. As demonstrated, an increased perfusion flow facilitated enhanced hypertrophic chondrocyte differentiation and bone matrix deposition *in vitro*, but this did not correspond to improved bone formation when placed in an orthotopic, critical-sized defect.

As the rate of flow has major impact on osteoblast differentiation [342], flow rates along a broad range were investigated. With the hypertrophic chondrocyte differentiation regime first requiring the derivation of chondrocytes, constructs were harvested after chondrogenic differentiation to evaluate the impact of flow. In agreement with the published literature on perfusion cultures of chondrocytes, increased flow rates improved chondrocyte differentiation [336]–[338], as shown by the increased GAG deposition per cell (**Fig. 16C**). The enhanced presence of GAG and collagen type II in the construct interiors at higher flow rates indicated that the improved nutrient delivery dictated this behavior (**Fig. 16D**). In particular, the ability to deliver TGF- β further into the construct volume appeared to promote chondrogenic differentiation and matrix production [345].

Mathematical modeling of shear stress on chondrocytes suggests that the shear stress had negative impact on cartilage matrix production and instead facilitated early hypertrophic maturation [346], [347]. Staining for collagen type X, the unique collagen produced by hypertrophic chondrocytes, was intensified at higher flow rates, indicating an advanced state of maturation (**Fig. 17**). Despite increased staining, the constructs lacked enlarged lacunae and pericellular collagen type X staining indicative of hypertrophic chondrocytes [275], consistent with the existing literature on chondrogenic development of hypertrophy [344], [348]. Cultivation in hypertrophic differentiation medium promoted the hypertrophic phenotype, as enlarged chondrocyte lacunae and pericellular collagen type X became apparent in all groups, with increased flow rate corresponding to increased collagen type X staining (**Fig. 17**). Naturally, hypertrophic chondrocyte maturation leads into the remodeling of cartilage matrix

and deposition of a bone template [8], [274]. All groups displayed reduction in GAG content; however, the faster flow rates maintained significantly higher amounts of GAG at the end of culture (**Fig. 18B, C**).

In endochondral ossification, hypertrophic chondrocytes produce a calcified cartilage bone template in which the cartilage GAG influences mineral crystallinity and results in an immature mineral that is the basis of the initial bone [349], [350]. Movat's pentachrome stains supported the biochemical quantitation data, demonstrating that increased flow rates resulted in the increased presence of GAG co-localized with BSP and osteopontin, and indicating the formation of a bone template (**Fig. 19**). Whereas in the low flow rates the protein staining was present within the cells, the faster flow rates had more advanced bone template deposition with the deposited proteins in a denser pattern, with the extracellular matrix surrounding the enlarged hypertrophic lacunae and resembling hypertrophic cartilage (**Fig. 19**) [349], [351]. The increase perfusion flow rate dictated the deposition patterns of the hypertrophic chondrocytes, consistent with previous studies of osteoblasts and chondrocytes [333], [336]–[338], [342]. Interestingly, the more advanced deposition did not correspond to the expression of key hypertrophic genes (**Fig. 18D**).

We anticipated that the faster flow rate would result in improved bone regeneration upon implantation, based on the previous osteoblast-based work, which demonstrated that more mature tissue-engineered grafts resulted in enhanced bone regeneration [305]. However, *in vivo* the non-perfused (0 $\mu\text{m/s}$ control) group had more bone deposition and improved integration than the 400 $\mu\text{m/s}$ group (**Fig. 20** and **Fig. 21**). As has been shown previously for critical-sized femoral defects in rat [327], the bone tissue-engineered grafts regenerate through endochondral ossification, suggesting that the non-perfused grafts may facilitate enhanced endochondral ossification in this study. The progression of *in vivo* endochondral ossification is thought to be controlled by a number of cytokines, with BMPs, IHH/PTHrP, and Wnt/ β -catenin, providing key pathways to regulate bone formation [352]–[354]. In previous studies, cytokines produced by differentiated hypertrophic chondrocytes influenced bone formation and remodeling [310]. In this study, the flow rate did not affect the BMP concentration, indicating that the BMP pathways activated by the tissue-engineered grafts upon implantation did not play a significant role in bone regeneration. IHH is an essential cytokine released by hypertrophic chondrocytes to regulate the production of bone [354]. Increased levels of IHH have been shown to enhance PTHrP expression, stimulate chondrocyte proliferation, and delay further hypertrophic progression [354]–[356]. The elevated IHH concentration released by grafts cultured at 400 $\mu\text{m/s}$ suggests higher concentrations of cells in the hypertrophic chondrocyte state. In addition, the cytokines involved in the Wnt/ β -catenin pathway showed significantly different secretion patterns, indicating the different state of each graft (**Fig. 20A**). DKK1 inhibits hypertrophy by blocking the Wnt pathway, is heavily present in articular cartilage [357], and had a significantly higher concentration in the 400 $\mu\text{m/s}$ grafts (**Fig. 20A**). In addition, β -catenin, responsible for locally mediating osteoblast activity and the turnover of cartilage

matrix [308], had a significantly lower concentration in the 400 $\mu\text{m/s}$ group. The higher presence of DKK1 and lower presence of β -catenin suggest that the 400 $\mu\text{m/s}$ group was actively signaling to maintain its cartilage matrix, and that this signaling may have inhibited bone formation in the implanted graft.

As shown in **Fig. 18** and **Fig. 19**, the 400 $\mu\text{m/s}$ group had significantly more bone template and collagen matrix. However, after implantation, the grafts cultured at 400 $\mu\text{m/s}$ were resorbed along the graft/native bone interface and replaced with fibrous tissue, failing to heal the critical-size defects. This was in stark contrast to the grafts cultured without perfusion (0 $\mu\text{m/s}$), where only minimal deposition occurred *in vitro*, but extensive *in vivo* deposition led to integration with the native bone and regeneration of the femoral defects. Consistent with our data, the recent study of hypertrophic constructs by Thompson *et al.* showed that the grafts with a mineralized, more bone template-like scaffold produced inferior results in a calvarial defect model [283]. In their study, differing location and organization of host osteoblasts between the scaffolds suggested that bone template-like scaffold and implanted hypertrophic chondrocytes influenced cell infiltration and activity [283]. Coupled with the cytokine secretion data indicating an advanced graft state at 400 $\mu\text{m/s}$, the presence of fibrous tissue at the integration site suggests that the advanced matrix production during *in vitro* cultivation (**Fig. 19**) negatively impacted host cell infiltration and subsequent bone regeneration.

A limitation of our study was the single *in vivo* time point at 8 weeks. With a more comprehensive animal study, the progression of construct integration and bone regeneration could be modeled with more precision. The contribution of host and implanted cells could also be discerned, to determine the influence of the bone template on the regeneration. Better understanding of the differentiated hypertrophic state and how the cytokine secretion influence the various stages of endochondral ossification will be invaluable for optimizing the preparation of tissue constructs for bone repair.

In addition, the *in vivo* implantation of only two out of four experimental groups may also limit the impact of the study. While the experimental data clearly demonstrate that the perfusion flow during *in vitro* cultivation limits the regenerative ability of hypertrophic chondrocyte-based bone grafts, *in vivo* data from all experimental groups would provide further insights into the impact of the degree of perfusion *in vitro* on the performance of these grafts *in vivo*. The study of all experimental groups in the orthotopic animal model of bone healing would also help clarify future *in vitro* studies and help evaluate the *in vitro* markers that predict *in vivo* regeneration.

5 Conclusion

We documented the impact of perfusion flow on the hypertrophic chondrocyte differentiation and matrix production in tissue-engineered constructs, *in vitro* and in a rat model of long bone repair. Similar to differentiated osteoblasts and chondrocytes [292], [293], [305], [333]–[338], we demonstrated that engineering the environment experienced by the cells also impacted hypertrophic chondrocyte

differentiation and activity. In particular, the application of shear stress and enhanced nutrient delivery dictated the degree of hypertrophic differentiation and advanced bone template deposition *in vitro*. The responsive nature of hypertrophic chondrocytes to perfusion flow matched a previous study that showed their sensitivity to specific components in engineered scaffolds [283] and indicates the ability to engineer an ideal environment for hypertrophic chondrocyte-based bone graft creation. Unlike with osteoblast-based bone grafts, the results of our study suggest that the utilization of perfusion flow for the differentiation and stimulation of hypertrophic chondrocytes may not be appropriate for the construction of clinically relevant tissue-engineered bone grafts.

The positive regeneration facilitated by the control constructs, with a less developed template but enhanced cell signaling secretion, suggests that enacting an immature, developmental tissue engineering approach, rather than producing tissue-engineered grafts that resemble mature tissue, might be a better route for the future of bone tissue engineering and its application in the clinic [326]. To educate this opinion, further investigation into the specific activity of the differentiated hypertrophic chondrocytes, when implanted *in vivo*, is needed.

6 Acknowledgments

We gratefully acknowledge the NIH funding support of this work (grants EB002520, DE016525, and AR061988).

7 Disclosure Statement

No competing financial interests exist.

CHAPTER II

**Decellularized auricular cartilage
as a new biomaterial for
articular cartilage tissue engineering.**

Repopulation of an auricular cartilage scaffold, *AuriScaff*, perforated with an enzyme combination

S. Nürnberger^{a,b,c,*}, C. Schneider^{b,c}, G.V.M. van Osch^{d,e}, C. Keibl^{b,c}, **B. Rieder**^f, X. Monforte^f,
A.H. Teuschl^{f,c}, S. Mühleder^{b,c}, W. Holnthoner^{b,c}, B. Schädler^{b,c,g}, C. Gahleitner^a, H. Redl^{b,c}, S.
Wolbank^{b,c}

^a Department of Orthopedics and Trauma-Surgery, Division of Trauma-Surgery, Medical University of Vienna,
Vienna, Austria

^b Ludwig Boltzmann Institute for Experimental and Clinical Traumatology, Vienna, Austria

^c Austrian Cluster for Tissue Regeneration, Vienna, Austria

^d Department of Otorhinolaryngology, Erasmus MC, University Medical Center, Rotterdam, the Netherlands

^e Department of Orthopaedics, Erasmus MC, University Medical Center, Rotterdam, the Netherlands

^f Department Life Science Engineering, University of Applied Sciences Technikum Wien, Vienna, Austria

^g University Clinic of Dentistry, Medical University of Vienna, Vienna, Austria

* corresponding author: sylvia.nuernberger@meduniwien.ac.at

Published in *Acta Biomaterialia* on December 25th, 2018

Abstract

Biomaterials currently in use for articular cartilage regeneration do not mimic the composition or architecture of hyaline cartilage, leading to the formation of repair tissue with inferior characteristics. In this study we demonstrate the use of “*AuriScaff*”, an enzymatically perforated bovine auricular cartilage scaffold, as a novel biomaterial for repopulation with regenerative cells and for the formation of high-quality hyaline cartilage. *AuriScaff* features a traversing channel network, generated by selective depletion of elastic fibers, enabling uniform repopulation with therapeutic cells. The complex collagen type II matrix is left intact, as observed by immunohistochemistry, SEM and TEM. The compressive modulus is diminished, but three times higher than in the clinically used collagen type I/III scaffold that served as control. Seeding tests with human articular chondrocytes (hAC) alone and in co-culture with human adipose-derived stromal/stem cells (ASC) confirmed that the network enabled cell migration throughout the scaffold. It also guides collagen alignment along the channels and, due to the generally traverse channel alignment, newly deposited cartilage matrix corresponds with the orientation of collagen within articular cartilage. In an osteochondral plug model, *AuriScaff* filled the complete defect with compact collagen type II matrix and enabled chondrogenic differentiation inside the channels. Using adult articular chondrocytes from bovine origin (bAC), filling of even deep defects with high-quality hyaline-like cartilage was achieved after 6 weeks *in vivo*. With its composition and spatial organization, *AuriScaff* provides an optimal chondrogenic environment for therapeutic cells to treat cartilage defects and is expected to improve long-term outcome by channel-guided repopulation followed by matrix deposition and alignment.

Statement of Significance

After two decades of tissue engineering for cartilage regeneration, there is still no optimal strategy available to overcome problems such as inconsistent clinical outcome, early and late graft failures. Especially large defects are dependent on biomaterials and their scaffolding, guiding and protective function. Considering the currently used biomaterials, structure and mechanical properties appear to be insufficient to fulfill this task. The novel scaffold developed within this study is the first approach enabling the use of dense cartilage matrix, repopulate it via channels and provide the cells with a compact collagen type II environment. Due to its density, it also provides better mechanical properties than materials currently used in clinics. We therefore think, that the auricular cartilage scaffold (*AuriScaff*) has a high potential to improve future cartilage regeneration approaches.

Keywords: Decellularization, Auricular cartilage, Repopulation, Elastic fibers, Channels, Human chondrocytes, Human adipose derived stromal/stem cells, Cartilage regeneration, Tissue engineering

1 Introduction

Current strategies for the treatment of large cartilage defects combine the use of scaffolds for structural support and cells to synthesize new functional matrix. Despite diverse options regarding surgical techniques, cell sources and biomaterials, the restoration of hyaline-like cartilage with its native characteristics remains unsatisfactory [358]. After initial success there is often a late deterioration in clinical symptoms with treatment failure being reported in approximately ten to twenty percent of cases over a follow-up period of more than five years [359]–[363]. Debridement for hypertrophic repair tissue, lysis of lesions, joint arthroplasty and revision procedures are the most common causes for reoperation [364]. So far, the reason for this functional decline after initial improvement (secondary decline) is unknown. The rare biopsies available from successfully and unsuccessfully treated defects suggest that late term clinical outcome is related to matrix quality of the newly formed tissue, with only thirty percent of biopsies showing exclusively hyaline cartilage after matrix-associated chondrocyte implantation (MACI) [365]. Even in samples containing the hyaline cartilage specific collagen type II, the collagen architecture is frequently not resembling the complex alignment of the articular cartilage [366]–[368], which has a generally vertical alignment in deeper regions, bending towards the upper regions and being horizontally aligned at the surface, the only region containing collagen type I. Moreover, glycosaminoglycans (GAG) are less represented than in native cartilage and mask the collagen fibers incompletely.

The highly specialized fine structure and specific collagen architecture of articular cartilage play an integral part in its functionality [369]. The interplay between the specifically organized collagen type II and the swelling pressure of proteoglycans accounts for a dense matrix with high mechanical loading capacity, which is relevant during movement [370]. The architecture of newly formed cartilage after treatment is significantly influenced by the structure of the scaffold material. Yet commercially available scaffolds often have a random morphology and lack an architecture that guides accurately aligned matrix deposition [371]. Many of those commercially available scaffolds create a practically two-dimensional environment via large fibers or sheets of small fibers forming a fibrous but planar surface and thus encourage cell spreading. This cellular reaction is counterproductive to the chondrogenic phenotype of chondropotent cells, in both chondrocytes and stem cells. As a consequence, the dedifferentiated cells produce fibrous instead of hyaline cartilage matrix [358], [371].

As chondrocytes naturally occur tightly enclosed in a compact matrix, scaffold density plays an important part in the preservation or induction of the chondrogenic phenotype and formation of hyaline cartilage [372]. Hydrogels are a type of biomaterial that enclose the cells properly. However, they are prone to mechanical failure [358] due to their frequently loose and soft consistency, and need exact fine tuning regarding biodegradability [373], [374]. Furthermore, their often randomly aligned fibers do not mimic the cartilage composition or architecture.

In terms of a homologous environment cartilage itself represents the optimal defect filling material, preserving the phenotype of chondrocytes and guiding stem cells towards the desired lineage by providing biochemical and biomechanical cues [369], [375]. Several approaches have focused on engineering cartilage-like matrices *in vitro*, either using collagen type II extracted from native cartilage [376], [377] or decellularization of *in vitro* generated cartilage matrix [378]–[380], but failed to achieve the characteristic architecture of articular cartilage. Since the structure of articular cartilage could neither be induced *in vivo* nor engineered *in vitro*, decellularized native cartilage allografts pose the most promising option. Several studies with decellularized tissues including cartilage suggest that recellularized ECM scaffolds lead to superior results compared to a cell-free matrix [381]. Anyhow, repopulation of decellularized hyaline cartilage with cells has turned out to be challenging, as cellular ingrowth into the dense hyaline matrix is limited to outer regions [382], [383].

Within this study we propose cartilage of auricular origin as suitable scaffold for articular cartilage defect treatment. Decellularization of auricular cartilage for the use in cartilage tissue engineering has already been described in literature [384], but the repopulation has yet to be achieved. Like articular cartilage, auricular cartilage is composed of a dense collagen type II – GAG matrix with sparsely distributed cells. In contrast to articular cartilage, an elastic fiber network surrounds the cells and traverses the tissue. Its homogenous distribution, high abundance and diameter of up to 5 mm suggest that when selectively enzymatically removed, it will become a network of hollow channels enabling uniform repopulation. Being predominantly aligned orthogonally to the cartilage surface, these channels would enable uniform repopulation and promote the deposition of newly formed collagen in the direction which, when implanted, corresponds to the orientation of the collagen in articular cartilage.

The aim of this study was to generate a chondro-supportive scaffold from auricular cartilage, which is both dense yet easy to repopulate with regenerative cells. Hence, various *in vitro* experiments to demonstrate its potential to be repopulated and *in vivo* studies for its performance as a novel defect filling material in a chondral defect environment were conducted. Bovine and human articular chondrocytes (bAC and hAC) in monoculture or in cocultures with human adipose-derived stromal cells (ASC) were used to investigate the cellular behaviors and perform first experiments with clinically relevant strategies. The newly developed material with its favorable composition and geometry gives rise to the expectation of a fully revitalized, well-integrated graft providing a versatile temporal tissue replacement that supports cartilage tissue formation.

2 Materials and Methods

2.1 Sample harvest

Ears from adult cows (two-year-old Simmental cattle) were obtained from the local slaughterhouse and dissected within the first 12 h *post mortem*. To map the characteristics of auricular cartilage in relation to its position on the ear, full thickness biopsies of 8 mm in diameter were taken from different regions and subjected to histological examination. For pretreatment and reseeding experiments, cartilage was

isolated by skinning the respective area with a scalpel. Then the perichondrium plus the outermost cartilage layer were cut off using the Teixido cartilage cutter (MicroFrance, France), which was also used for thickness standardization in later experiments. Only the central part of the cartilage was used to punch biopsies of 8 mm in diameter (further referred to as cartilage discs). Samples were washed and stored in PBS (without $\text{Ca}^{2+}/\text{Mg}^{2+}$, Lonza, Switzerland) plus added Pen/Strep (Lonza, Switzerland).

2.2 Histological and immunohistochemical examination

Samples were fixed in 4% neutral buffered formalin overnight, washed in PBS and dehydrated with a graded series of alcohol. Osteochondral plugs were treated with USEDECALC decalcification reagent (Medite, United States) for five weeks for decalcification. Both, the cartilage discs and the osteochondral plugs were cut in half and embedded in paraffin via xylol (Roth, Switzerland). Sections of 3-4 μm thickness were cut with a rotary microtome (MICROM HM355S by Thermo Fisher Scientific, United States) and stained depending on the research question: Sections from the different ear regions were examined by Martius Scarlet Blue (MSB) staining, a trichrome staining with subsequent application of Martius yellow solution (0.5% Martius yellow and 2% phosphotungstic acid hydrate, both Sigma Aldrich, United States, in 96% ethanol) for 2 min, crystal scarlet solution (1% brilliant crystal scarlet, Sigma Aldrich, United States, and 2% acetic acid) for 10 min and methyl blue solution (0.5% methyl blue, Merck, Germany in 1% acetic acid) for 4 min (as described by Lendrum *et al.* 1962 [385]), to distinguish the perichondrium (blue) from the cartilage (whitish) and display the elastic fibers (red). For visualization of cell distribution in the seeded scaffolds, sections were subjected to Heidenhain's AZAN Trichrome (short "AZAN" for azocarmine and aniline blue) staining, consisting of 15 min in azocarmine G solution (1 g/L, Sigma Aldrich, United States), and 15 min in aniline blue (0.5%, Merck, Germany) plus orange G (0.2%, Roth, Switzerland) solution, displaying the collagen matrix in blue and the cells in intensive red. In order to examine the matrix composition, Alcian blue (0.1% in 3% acetic acid at pH 2.5) with sirius red counterstaining was used for GAG detection and immunostaining served to distinguish between collagen type I (Abcam, Great Britain) and collagen type II (Thermo Fisher Scientific, United States, clone 6B3 during scaffold development and clone 2B1.5 for reseeded samples). For the immunohistochemistry endogenous peroxidases and alkaline phosphatase were blocked with BLOXALL (Vector Labs, United States) and antigens retrieved with citrate buffer (pH 6) for collagen type I and pepsin (pH 2) for collagen type II staining. The primary antibodies were incubated 1:500 (collagen type I) or 1:100 (collagen type II) for 1 h at room temperature and as secondary antibody the polymer labelled system Bright vision poly HRP (VWR, United States) was incubated for 30 min at room temperature. A peroxidase substrate kit (NovaRED™, Vector Labs, United States) was used for development of the color reaction and hematoxylin for counterstaining.

2.3 Matrix treatment

To devitalize the cartilage discs four freeze/thaw cycles were performed. Therefore, samples were alternately kept at 20 °C and room temperature for 1 h respectively, twice frozen dryly and twice frozen

submerged in hypotonic buffer (10 mM Trisbase, Promega, United States, adjusted to pH 8.0 using HCl, Roth, Switzerland).

Afterwards samples were treated either only with elastase (0.03 U/mL, Sigma-Aldrich, United States, in 0.2 M Tris-base, pH 8.6) or, to enhance the efficiency and further loosen up the matrix, with a protocol combining pepsin and elastase: incubation in pepsin (0.1%, Sigma-Aldrich, United States, in 0.5 M acetic acid, Merck, Germany) for 24 h (renewing the pepsin solution after 6 h), washing with PBS for at least one hour and incubation in elastase overnight. Both treatments were concluded by two 30-minutes PBS wash steps and incubation in PBS overnight. All steps following the freeze/thaw cycles were performed under continuous shaking at 180 rpm and 37 °C.

Following the observations made concerning the enzyme penetration depth, scaffold thickness was reduced to 300 mm to ensure complete elastic fiber removal. This particular thickness could be successfully standardized with the Teixido cartilage cutter (MicroFrance, France), which was therefore used for sample preparation in all subsequent experiments.

2.4 Biochemical assays

Auricular cartilage discs, untreated, elastase treated, and pepsin-elastase treated, all of a standardized thickness of 300 mm, were digested with papain according to a protocol adapted from Kim *et al.* [386]. DNA content was quantified using the CyQUANT Cell Proliferation Kit (Life Technologies, United States) and GAG content using the dimethyl methylene blue (DMMB) assay described by Farndale *et al.* [387]. Samples were measured in duplicates and DNA and GAG content were calculated using linear regression to a standard curve (DNA sodium salt from calf thymus and chondroitin sulfate standard, both Sigma-Aldrich, United States).

2.5 Scanning and transmission electron microscopy

For scanning electron microscopy cartilage samples were fixed with 4% neutral buffered formalin overnight and washed in PBS buffer. To obtain a cross section for scanning, sample pieces were manually torn in two parts to obtain a surface without cutting artefacts from a razor blade. The pieces were further processed and dehydrated in a graded series of alcohol, chemically dried with hexamethyldisilazane (Sigma-Aldrich, United States) and sputter-coated with gold. Imaging was performed on a Zeiss MA10 scanning microscope (Carl Zeiss AG, Germany).

Samples for transmission electron microscopy were gained from freshly prepared cartilage samples. Small pieces were fixed with 2.5% glutaraldehyde in 0.1 M sodium cacodylate buffer overnight at 4 °C, rinsed in distilled water, post fixed in 0.5% osmium tetroxide in 1% potassium ferrocyanide and rinsed again, dehydrated in a graded series of alcohol and embedded in low viscosity resin via the intermedium acetonitrile (Merck, Germany). Sections were stained with gadolinium and lead citrate and imaging was performed on a Zeiss LIBA 120 transmission electron microscope (Carl Zeiss AG, Germany). Images were taken from the superficial region and the center of the sample.

2.6 Mechanical compression test

Cartilage discs were mechanically tested using a custom-made unrestrained compression set fitted on a Zwick BZ2.5/TN1S uniaxial testing machine (Zwick GmbH & Co. KG, Germany) equipped with a 50 N load cell. Prior to testing, all specimens were equilibrated in PBS for at least 24 h. After achieving a preload of 50 mN, data was recorded and the samples were compressed to 80% deformation with a constant speed of 100 $\mu\text{m}/\text{min}$. As controls human articular cartilage and the commercially available collagen type I/III scaffold Chondro-Gide[®] (Geistlich, Switzerland) were tested under the same conditions.

2.7 Cell culture

Human AC were gained from femoral heads of five donors (two female and three male) with a mean age of 55 years undergoing hip replacement, with patient's consent and the approval of the local ethical board. hAC were isolated via 1 h incubation in hyaluronidase solution (0.1%, Sigma-Aldrich, United States, in DMEM, Gibco, United States), 0.5 h in pronase solution (0.1%, Roche, Switzerland in DMEM) and overnight incubation in a collagenase/papain mix (200 U/mL collagenase, Gibco, United States and 1 U/mL papain, Sigma-Aldrich, United States, in DMEM), then cultivated in expansion medium (DMEM, Gibco, United States, supplemented with 10% FBS, PAN-Biotech, Germany, 50 $\mu\text{g}/\text{mL}$ ascorbate 2-phosphate, Sigma-Aldrich, United States, 10 mM HEPES, Gibco, United States, 5 $\mu\text{g}/\text{mL}$ insulin, Sigma-Aldrich, United States, 2 mM L-glutamine, Gibco, United States, 2 $\mu\text{g}/\text{mL}$ Amphotericin B, Gibco, United States, and 100 $\mu\text{g}/\text{mL}$ Gentamycin, Gibco, United States) until reaching sub-confluency. Cells were then cryopreserved in liquid nitrogen, thawed before the experiment and allowed to adapt to culture conditions for four days. For seeding the scaffolds, hAC were pooled to reduce the donor variability and restrict the number of animals, and used either in pure culture or in co-culture with ASC.

In order to avoid ASC donor variability, immortalized human ASC (ASC/TERT1, Evercyte GmbH, Austria) were used as ASC source and expanded in endothelial growth medium (EGM-2, Lonza, Switzerland), which has been shown to retain the chondrogenic potential (unpublished lab-internal standardization tests), and passaged at 70% confluency.

Bovine AC were harvested from the femoral condyles, dissected within 24 h *post mortem*, and isolated via overnight incubation in collagenase (0.15% in DMEM). They were plated and cultivated in expansion medium and used one day after isolation. All cells were incubated at 37 °C and 5% CO₂.

For dynamic cultivation during the reseeding tests, sample tubes were placed in the wells of a cylindrical cup (freezing container from "Mr. Frosty", Thermo Fisher Scientific, United States), which was rotated on a Stuart Roller Mixer SRT1 (Bibby Sterilin Ltd, United Kingdom) at 60 rpm, causing continuous rotation of the vials around an internal as well as an external axis.

2.8 Cell infiltration *in vitro*

Enzymatically perforated cartilage scaffolds, 8 mm in diameter, were transferred to 1.5 mL screwcap vials and preincubated in DMEM + 20% fetal bovine serum at 37 °C for 2 h. 0.5×10^6 cells, either hAC or mCherry-expressing ASC/TERT1 (retrovirally infected using Phoenix-Ampho cells as described previously by Knezevic *et al.* [388]), were seeded in 1 mL expansion medium (hAC) or EGM-2 (ASC/TERT1). Samples were incubated at 37 °C under continuous rotation of 60 rpm for the whole cultivation period and the medium was replaced two times during the week of cultivation. After one week the samples were fixed in 4% paraformaldehyde for 2 h and stored in PBS. ASC/TERT1 could be directly investigated with fluorescence microscopy while the hACs had to be labelled with the membrane binding Dil cell-labeling solution DOI (Vybrant, Great Britain).

2.9 Differentiation *in vitro*

Enzymatically perforated cartilage scaffolds, 4 mm in diameter (reflecting the diameter of the defect in subsequent experiments), were seeded with 0.25×10^6 cells, either hAC alone (in expansion medium) or in co-culture with ASC/TERT1 (25% hAC, 75% ASC/TERT1; in EGM-2). The relative number of cells was higher in this and all following experiments to ensure full recellularization and to supply enough cells to fill the spaces between scaffold and defect in later experiments. Scaffolds were cultivated under continuous rotation of 60 rpm for the whole cultivation period. After two days, medium was changed to Hennig's differentiation medium (DMEM-hg, Lonza, Switzerland, supplemented with 5 µg/ml insulin, 5 µg/mL transferrin and 5 ng/mL selenous acid via an ITS-premix, Gibco, United States, 0.1 µM dexamethasone, 0.17 mM ascorbic acid-2-phosphate, 1 mM sodium pyruvate, 0.35 mM proline, all Sigma Aldrich, United States, 2 mM L-glutamine, Gibco, United States and Pen/Strep, Lonza, Switzerland, as described by Hennig *et al.* [389]) with 10 ng/mL BMP6 (R&D Systems, United States) and TGF-β3 (Lonza, Switzerland) respectively and replaced three times per week. Chondro-Gide® was reseeded as control, applying the cell suspension onto the porous side of the bilayer membrane. Chondro-Gide® is a biphasic membrane with a porous side for cell seeding and a denser side covered by a tight sealing sheet (initially not penetrable for the cells) designed to be oriented towards the joint surface when implanted into the defect. In contrary, *AuriScaff* is symmetric and accessible by cells from both sides. Samples were subjected to histological examination 6 weeks after reseeded.

2.10 Osteochondral plug model with (aged) human chondrocytes in co-culture *in vitro*

To simulate the environment of deep cartilage defects [390], osteochondral plugs of 1 cm in diameter were harvested from bovine knee joints obtained from the local slaughterhouse. Full thickness defects were prepared in the cartilage down to the osteochondral interface using a 4 mm biopsy punch. Scaffolds were prepared and seeded with 0.25×10^6 hAC in coculture with ASC/TERT1 as in the *in vitro* differentiation experiment. Again, 4 mm biopsies of Chondro-Gide® were reseeded as control. Scaffolds were placed in the defect, fixed with a fibrin sealant (ARTISS, Baxter, USA) and covered with NeuroPatch (Aesculap, Germany) in accordance with the later *in vivo* experiment (where the

NeuroPatch serves to prevent infiltration of cells from the surrounding mouse tissues). If necessary, two scaffolds were stacked into the defect to match increased defect depth. Plugs were cultivated submerged in expansion medium at 37 °C and 5% CO₂ for two days. Afterwards the medium was changed to Hennig's differentiation medium [389] with 1 ng/mL BMP6 and TGF-β3 respectively to mimic the presence of growth factors inside the joint [181], [391] and replaced three times per week. Plugs were subjected to histological examination 6 weeks after reseeding.

2.11 Osteochondral plug model with (aged) human chondrocytes in co-culture *in vivo*

Osteochondral plugs and scaffolds were prepared and seeded as described in Section 2.10 . To test the performance of the scaffold *in vivo*, plugs were implanted subcutaneously in 10-weeks-old female NMRI nude mice (Charles River, Sulzfeld, Germany). The NMRI mouse (Naval Medical Research Institute) is an athymic breed allowing the implantation of non-autologous cells without rejection.

Prior to the study, the experimental protocols were approved by the City Government of Vienna (Animal Use Permit No: MA58/982788/2015/13) in accordance with the Austrian law and the Guide for the Care and Use of Laboratory Animals as defined by the National Institute of Health (revised 2011). Mice were anesthetized with isoflurane (2–3%, AbbVie, Austria) and two 1 cm incisions were made paramedian on the left and right side of the back. The osteochondral plugs were placed in subcutaneous skin bags, one on each side of the back and the incisions were closed by using 6-0 absorbable monofilament sutures (Monosyn, B Braun, Spain). All mice received 1 mg/kg meloxicam (Metacam®, Boehringer Ingelheim, Germany) orally two hours before surgical intervention and for 4 days (S.I.D.) after operation to alleviate pain and discomfort. After 6 weeks, the animals were sacrificed by using deep inhalation anesthesia with isoflurane followed by cervical dislocation. The osteochondral plugs were explanted and subjected to histological examination.

2.12 Bovine chondrocytes in an osteochondral plug model *in vivo*

Osteochondral plugs were prepared as previously described, focusing on regions with thick cartilage to test scaffold stacking. Defects were filled with the standardized 4 mm scaffolds seeded with $0.25 \cdot 10^6$ cells per scaffold, either bAC alone or in co-culture with ASC/TERT1. Bovine chondrocytes of young adult individuals were used to assess the performance of metabolically active chondrocytes, in contrary to elderly human donor cells (as in the previous experiment) that derive from joints afflicted with age-related changes. The bACs were applied freshly isolated, mimicking chondrogenic cells in a one-step procedure in combination with an alternative cell source, the ASC. The monoculture served to assess the performance of chondrocytes alone, in order to reveal their potential in participation to tissue formation in the co-culture setup. Two samples per defect were used to match the increased cartilage thickness. The plugs were implanted subcutaneously into nude mice as described previously. After 6 weeks the animals were humanly sacrificed and the osteochondral plugs were subjected to histological examination.

To comparatively quantify the homogeneity of collagen type II synthesis of the mono- and co-culture within the auricular matrix, the scaffolds on the collagen type II stained sections were divided in 16 zones per scaffold (amounting to 32 zones per defect), each zone spanning 500 mm of scaffold length and half the scaffold thickness. The presence of de novo collagen was evaluated for each zone.

2.13 Cell quantification

To evaluate how homogeneously the cells were distributed throughout the scaffold, the number of cells in different zones of the scaffold was assessed for *AuriScaff*, with the exception of the co-culture seeded *in vitro* samples (Section 2.9) which were highly contracted. Cell distribution in Chondro-Gide® was evaluated in the chondrocyte seeded *in vitro* samples, since in all other groups and experiments the scaffold was either deformed or already in an initial stage of disintegration, not allowing to clearly define the original scaffold area.

Regions of interest (ROI) were marked on scaffolds on AZAN stained sections, each region spanning 1 mm of scaffold length. Within the ROI the scaffold area was horizontally divided in three zones (two outer and one middle zone), each zone representing one third of the scaffold height. Cell counting was performed independently by two histologically trained individuals.

2.14 Statistical analysis

Quantitative data of DNA and GAG content as well as biomechanical data were evaluated using unpaired *t*-tests. In order to compare differences in the cellularity between the three zones statistically, variance analyses were performed. At first, the (metrical) data were tested for normal distribution with a Shapiro-Wilk-Test and variance homogeneity with the Levene-Test. Since both assumptions were fulfilled for all tested groups, one-way ANOVAs were performed. In case at least one significant difference was found, which happened in three out of six computations, many-to-one comparisons were performed using a Dunnett-Test to compare the middle region with the peripheral regions. The significance level for all tests was set at $p < 0.05$.

3 Results

In order to establish the channel-bearing auricular scaffold, the most suitable cartilage areas of the bovine ear were identified and treated for devitalization and elastic fiber removal. The created channel network was used for repopulation of the dense matrix with chondrocytes alone or in co-culture with ASC, and tested *in vitro* for its potential to guide cartilage-like matrix formation. Further, after insertion into an artificial defect in an osteochondral plug, integration was evaluated *in vitro* as well as *in vivo* in a subcutaneous nude mouse model.

3.1 Auricular areas

Eight different areas of the bovine ear were histologically analyzed and grouped regarding cartilage thickness and composition (**Fig. 9**). The thickness of the elastic fiber-bearing region, assessed with MSB staining, varied between 0.5 and 2 mm. Thin cartilage regions along the lateral border of the ear were

poor in elastic fibers (**Fig. 9**; region 1). Along the spine of the helix and in the inner ear regions cartilage was the thickest (**Fig. 9**; region 3), but featured a broad transition zone that was low in elastic fiber content. Furthermore, the fibers appeared to be less aligned. Cartilage from the center and medial border of the ear (**Fig. 9**; region 2), with a thickness ranging between 1 and 1.5 mm, turned out to be rich in elastic fibers with a higher tendency for parallel alignment orthogonally to the surface, and was therefore chosen for further experiments.

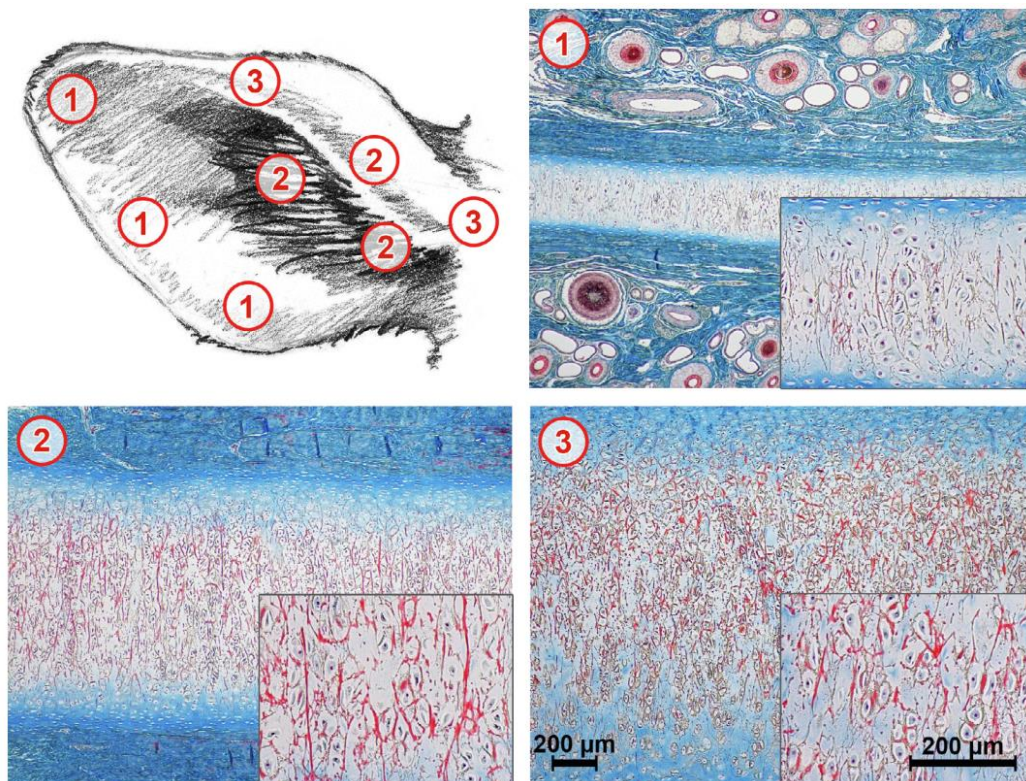


Fig. 22. Martius Scarlet Blue (MSB) staining of bovine auricular cartilage from different regions of the ear. MSB staining displays the elastic fibers in red; (1) along the lateral border of the ear the cartilage was found to be thin with low elastic fiber content; (2) towards the center and medial border the cartilage becomes thick and rich in elastic fibers which show a tendency to align in parallel; (3) in regions of exceptional thickness, along the spine of the helix and in the inner ear regions the cartilage is exceptionally thick, with an extended transition zone that is low in elastic fibers and with less regular fiber alignment.

3.2 Structural and bioanalytical scaffold characterization

Cartilage discs were devitalized via freeze/thaw cycles and treated with elastase (0.03 U/mL) alone or in combination with 1% pepsin. Elastase treatment alone following devitalization led to only partial depletion of the elastic fibers (**Fig. 23**). By adding pepsin treatment, elastic fibers were completely removed in the peripheral 150 μm leaving a hollow channel network in its place. Thickness standardization to 300 μm using the Teixido cartilage cutter resulted in samples devoid of elastic fibers, with the channel network homogeneously distributed throughout the tissue, defining the final scaffold. Channel diameters ranged between 5 and 10 μm , which is about half the diameter of cellular lacunae.

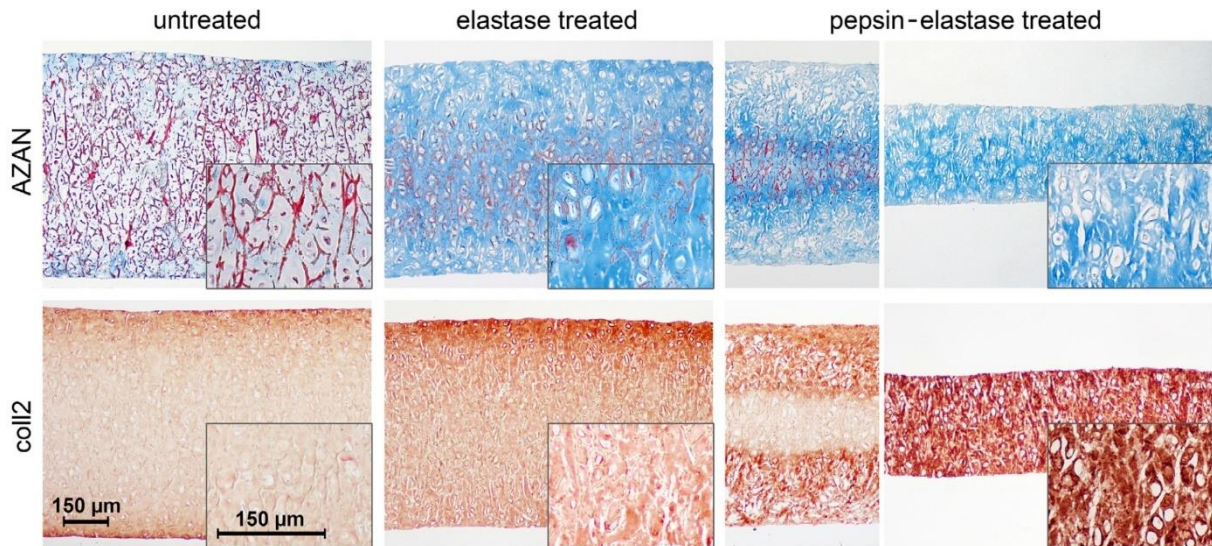


Fig. 23. Bovine auricular cartilage before and after enzymatic treatment. The elastic fiber network (red with AZAN) is not fully depleted after elastase treatment alone. Addition of pepsin leads to a full opening of the channels in the outer 200 μm while leaving the immunoreactivity to the MS-306-P1 collagen type II antibody intact (collagen type II fibers are more intensely stained in the treated matrix, due to the absence of glycosaminoglycans). After thickness reduction (standardization to 300 μm), the channel network is homogeneously distributed, traversing the entire scaffold; n = 6.

The matrix retained its immunoreactivity with the collagen type II antibody (**Fig. 23**), and the fibrillar nature of collagen appeared unchanged in SEM as well as TEM (**Fig. 24**), indicating that the collagen matrix remained intact. TEM sections showed the characteristic banding pattern of collagen and further revealed that some cell debris was present in the otherwise mainly empty lacunae of the treated cartilage. Quantitative analysis of cell remnants revealed that the DNA content was reduced by half from 1000 (± 340) to 520 (± 190) ng/mg (wet weight) after elastase treatment and by 75% to 210 (± 140) ng/mg (wet weight) after pepsin-elastase treatment. The GAG content was lowered by 40% from 25 (± 7.1) to 14 (± 1.8) $\mu\text{g}/\text{mg}$ after elastase treatment and by 70% to 7.6 (± 1.6) $\mu\text{g}/\text{mg}$ (wet weight) after pepsin-elastase treatment compared to untreated tissue (**Fig. 25**).

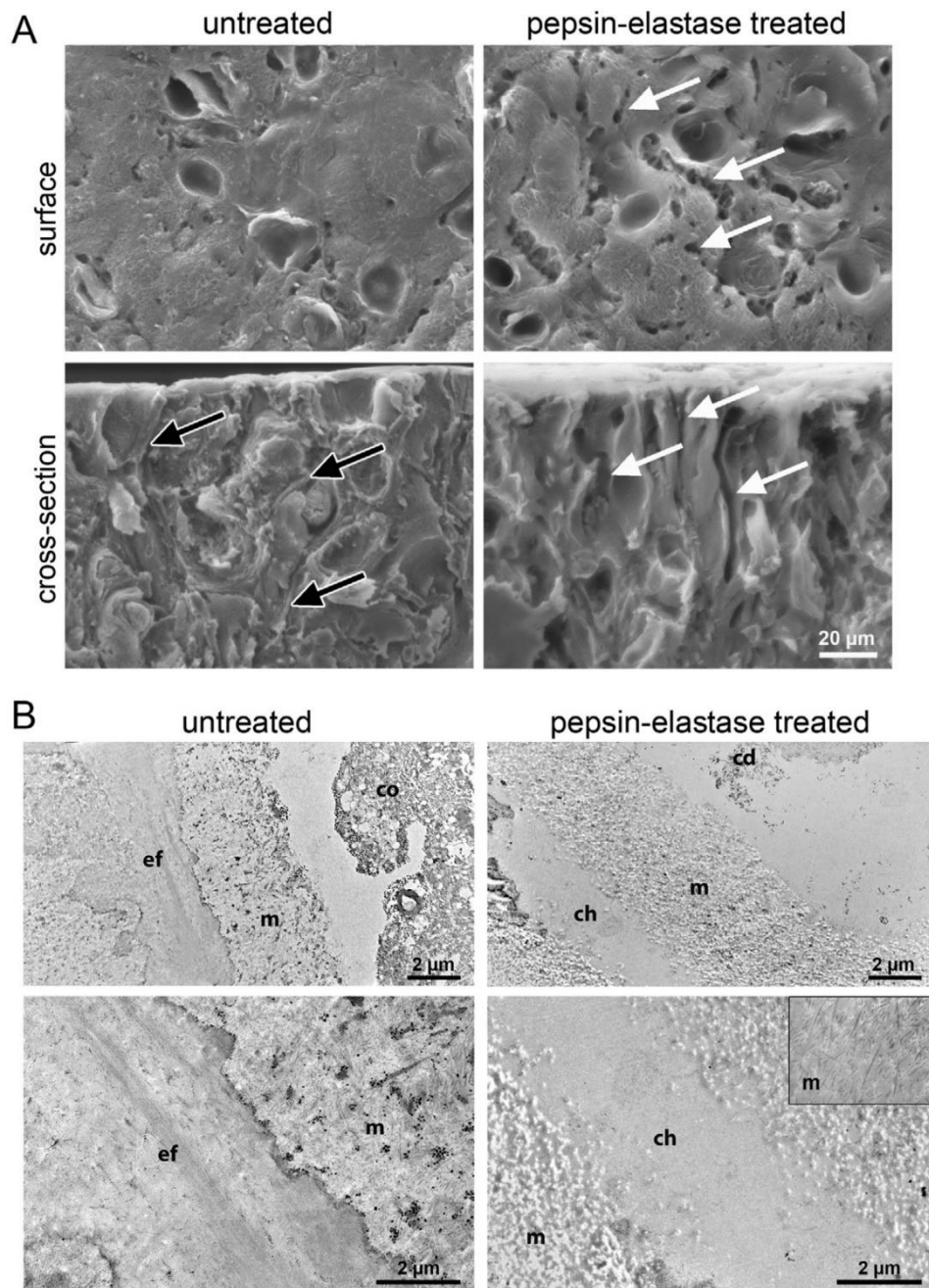


Fig. 24. SEM (A) and TEM (B) images of bovine auricular cartilage before and after enzymatic treatment. (A) Treatment with pepsin and elastase opened up channels (arrows) in place of the elastic fibers (black arrows) making the matrix accessible from the scaffold surface. (B) The collagen matrix (m, insert showing perpendicular cut, overview showing longitudinal cut) retained its fibrillary structure while channels (ch) opened up in place of the elastic fibers (ef). Chondrocytes (co) are depleted and washed out, in some places cellular debris (cd) is left; n = 3.

3.3 Mechanical compression test

In order to compare the mechanical properties of the created scaffold with native cartilage and commercial collagen type I/III scaffolds currently available for articular cartilage regeneration, mechanical compression tests were performed. The compressive modulus of 300 μm thin native auricular cartilage discs (500 ± 100 kPa) was shown to be in the same range as human articular cartilage of the same thickness (400 ± 70 kPa) (Fig. 25). Elastase treatment alone reduced the compressive

modulus of auricular cartilage to 180 (± 30) kPa and pepsin-elastase treatment to 90 (± 70) kPa. The compressive modulus of pepsin-elastase treated auricular cartilage is therefore one fifth of untreated cartilage, but still more than three times the modulus of the commercially available control scaffold (25 ± 6 kPa).

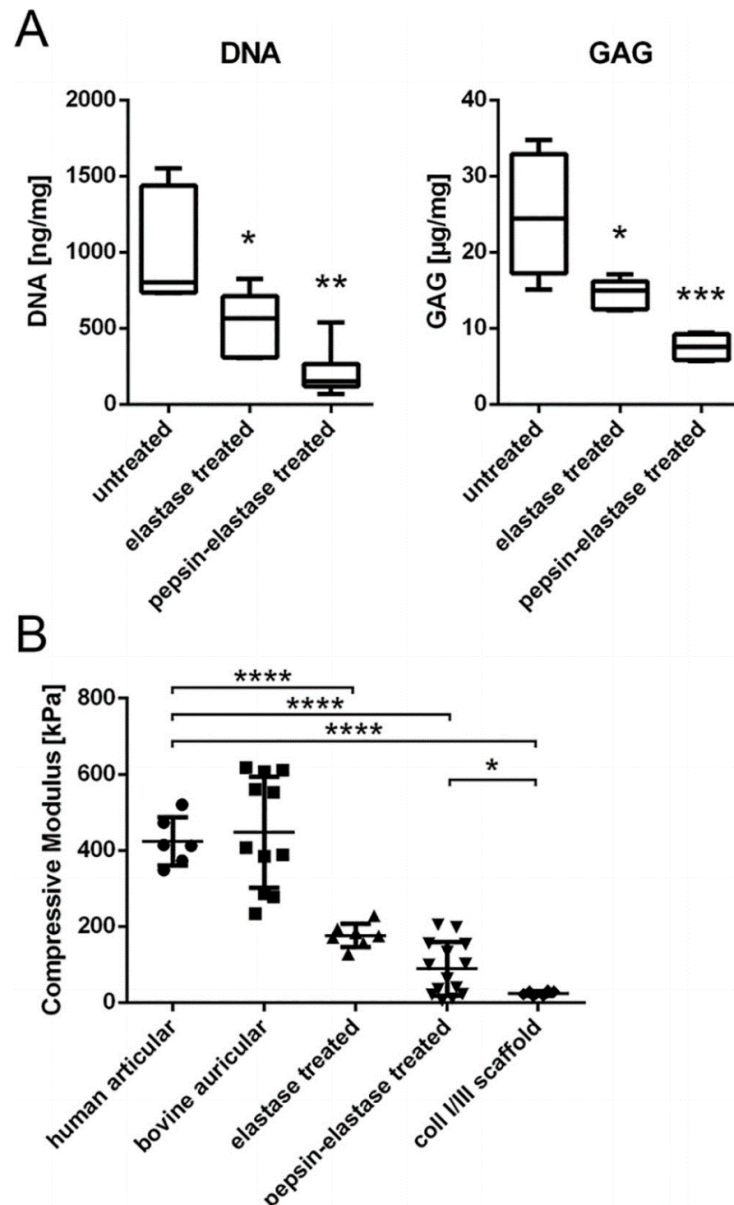


Fig. 25. DNA and GAG content and compressive modulus of auricular scaffolds before and after enzymatic perforation. **(A)** Pepsin-elastase treatment reduced the DNA content to 25% and GAG content to 30% compared to untreated tissue; $*p \leq 0.01$, $***p \leq 0.001$, while the effects were less pronounced when only elastase was used. $*p \leq 0.05$ ($n = 6$). **(B)** The compressive modulus of bovine auricular cartilage was shown to be in the same range as thin human auricular cartilage. Elastase treatment alone reduced the compressive modulus to less than 50%, pepsin-elastase treatment to one fifth. Compared to the commercial collagen type I/III scaffold, the pretreated auricular scaffold was still more than three times stronger. $*p \leq 0.05$, $****p \leq 0.0001$.

3.4 Cell infiltration *in vitro*

To evaluate each cell type's potential to infiltrate the scaffold, as well as to demonstrate the absence of cytotoxic effects, the enzymatically perforated scaffolds were seeded with hAC and ASC/TERT1. After

7 days ASC/TERT1, seeded on the enzymatically perforated scaffold, had already repopulated the entire scaffold spanning the whole thickness inside the channels. The slower migrating hAC had just begun infiltrating the surface of the scaffold by extending cell processes into the channel openings. At the surface ASC/TERT1 formed a multilayer of horizontally aligned cells while chondrocytes were predominantly round-shaped (**Fig. 26A**).

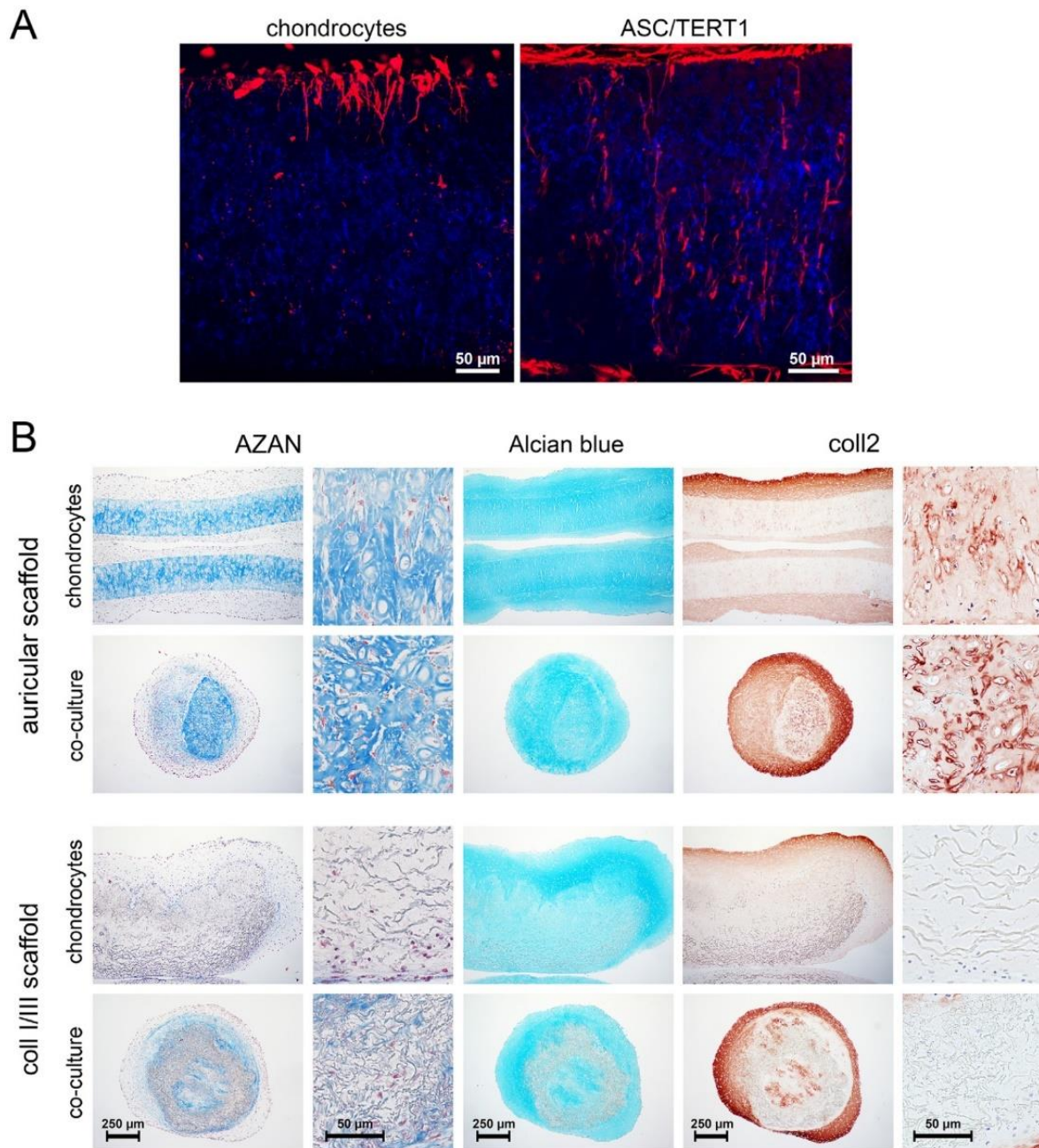


Fig. 26. *In vitro* seeding tests for cell invasion and differentiation. (A) Auricular cartilage scaffold seeded with fluorescently labelled hAC or ASC/TERT1. After one week chondrocytes are seen infiltrating the outer scaffold layer, while ASC/TERT1 have already repopulated the whole scaffold thickness. (B) Auricular cartilage scaffold and the collagen type I/III scaffold reseeded with hAC alone or in co-culture with ASC/TERT1. AZAN staining shows the cells (purple) repopulating the scaffolds. Alcian blue staining of glycosaminoglycans and immunostaining of collagen type II demonstrate the formation of cartilage-like matrix after 6 weeks in culture under chondrogenic conditions. In both scaffold types co-culture lead to contraction of the cell-scaffold construct. n = 3.

3.5 Differentiation *in vitro*

Enzymatically perforated cartilage scaffolds as well as commercially available collagen type I/III scaffolds were seeded with hAC alone or in co-culture with ASC/TERT1. The human cell source was chosen to be closest possible to the clinical situation, even though the age of the donors was higher (mean of 55 years) than the maximum age of patients undergoing cell-based cartilage regeneration (50 years). Both, mono- or co-cultures were cultivated in chondrogenic medium supplemented with growth factors to observe the performance of the cell-scaffold construct under differentiated conditions.

After 6 weeks in culture, histological evaluation (AZAN staining) revealed successful repopulation of auricular cartilage as well as the commercial controls. Cells were observed stretching inside the channels and inhabiting lacunae emptied by the pretreatment. Although hAC alone had invaded almost into the center of the scaffold, the innermost areas were not repopulated yet. In the commercial control scaffolds, hAC were abundant only in the outermost scaffold region and scarce in deep regions amounting to about half the scaffold thickness. In the co-culture groups, the cells were uniformly distributed throughout the full thickness of both scaffold types. In the co-culture groups both, the auricular and the control scaffolds were contracted and formed spherical-like structures (**Fig. 26B**).

Alcian blue staining of GAG and immunostaining of collagen type II indicated cell-associated formation of cartilage-like matrix. In both, the chondrocyte and the co-culture group, it was located within the enzymatically cleared channels and lacuna of the auricular scaffold and between the fibers of the commercial scaffold (**Fig. 26B**); furthermore, it was surrounding both scaffold types. On the collagen type I/III scaffolds deposition of cartilage-like matrix took place mostly on the surface rather than inside the scaffold.

3.6 Osteochondral plug model with (aged) human chondrocytes in coculture *in vitro*

Reseeded scaffolds were implanted into artificial defects created in the cartilage of osteochondral plugs. In accordance with a clinical one-step procedure averting the need to cultivate chondrocytes *in vitro*, co-cultures of hAC and ASC/TERT1 (as experimental ASC source) were used in the following osteochondral plug model experiments. Reseeded scaffolds in the artificial defects were cultivated for 6 weeks in a chondrogenic medium containing a reduced amount of growth factors to simulate a chondrogenic cartilage environment.

Histological characterization revealed that the scaffolds were well integrated in the artificially generated cartilage defect by the surrounding cells and filled out the defect space without contraction (**Fig. 27**). On the defect surface, a fibrous layer stretched from one defect edge to the other, covering the defect area and forming the surface layer of the repair tissue. Cells infiltrated the auricular channels and inhabited the empty lacunae over the whole scaffold diameter. The matrix produced by cells inside the scaffold was automatically oriented along the channels and therefore orthogonally to the cartilage surface, corresponding to the fiber alignment in native articular cartilage. However,

immunohistochemistry revealed that the *de novo* produced matrix was predominantly collagen type I instead of type II under the chosen cultivation conditions (**Fig. 27**). The majority of the defect site was filled by collagen type II matrix from the auricular cartilage scaffold that did not show any signs of degradation after six weeks of cultivation. In contrast, the control scaffold appeared loose and disintegrated, leading to gaps in the defect, especially in the deeper regions. Collagen deposition of the cells on the control scaffold had no specific orientation.

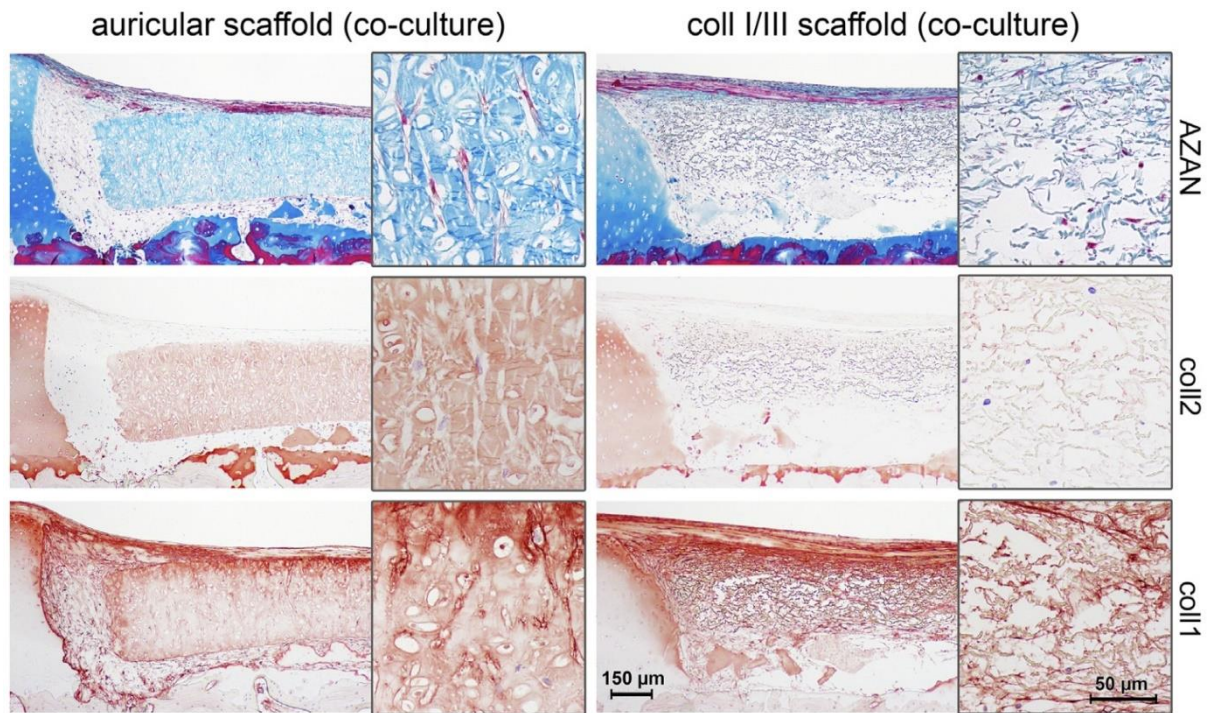


Fig. 27. Auricular cartilage and control scaffold reseeded with a co-culture of hAC and ASC/TERT1 in an osteochondral plug model *in vitro*. Scaffolds were well integrated into the defect and retained their flat shape. After 6 weeks of culture in light chondrogenic medium no collagen type II synthesis could be observed, instead cells produced collagen type I in both scaffold types. n = 3.

3.7 Osteochondral plug model with (aged) human chondrocytes in coculture *in vivo*

In order to test the performance of the scaffolds in a chondral environment *in vivo*, reseeded scaffolds were inserted into defects in osteochondral plugs and implanted subcutaneously into nude mice. This small animal model allows first investigations of how cells behave in response to a new biomaterial when implanted in a thick, human-like cartilage defect. Samples were explanted after 6 weeks, and macroscopic appearance of halved cylinders already gave a first impression of the defect, which was completely filled in the auricular scaffold group but had empty areas in the deep defect region in the control scaffold group (**Fig. 28**).

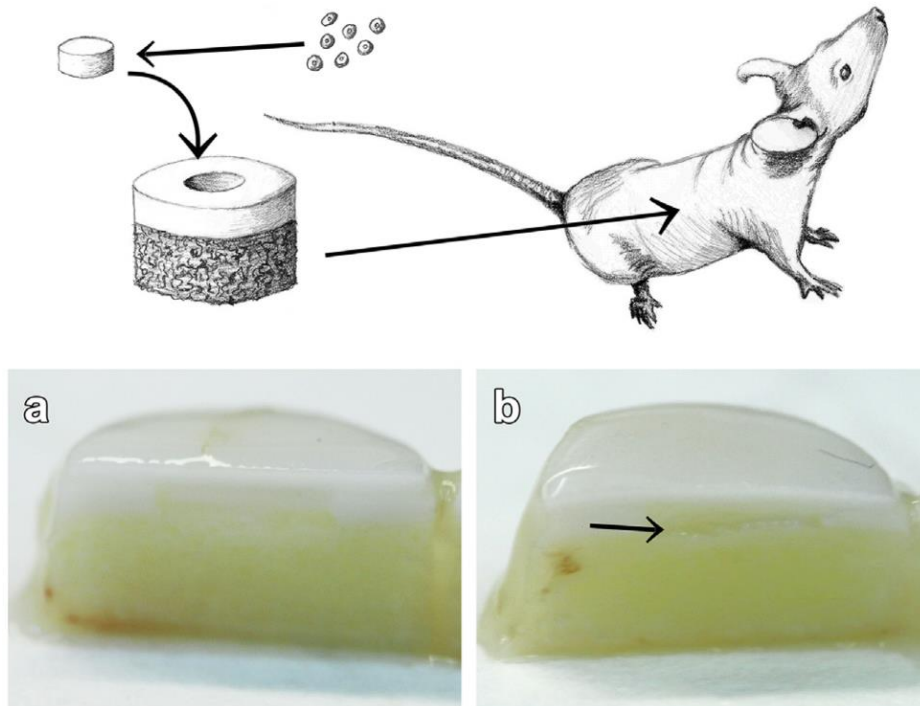


Fig. 28. Implantation into osteochondral plugs and cultivation in a nude mouse model. Defects were prepared into osteochondral plugs, filled with one or two reseeded scaffolds and implanted subcutaneously in a mouse model. Cross-section through the plugs reveals different degrees of filling: **(a)** auricular scaffolds filled the complete defect homogenously, **(b)** the commercial collagen type I/III scaffold formed a loose tissue with an empty space beneath (arrow). n = 6.

Histology revealed high numbers of cells present throughout the whole scaffolds and newly synthesized matrix in gaps between scaffold and defect edges. Collagen type II production was enhanced compared to the osteochondral plug model *in vitro*, with collagen type II formation clearly visible in channels and lacunae especially in deep regions of the auricular scaffolds (**Fig. 29**). However, a considerable amount of the newly synthesized matrix was collagen type I, produced along the scaffold edges. In the control collagen type I/III scaffolds cells were also uniformly distributed. As in the auricular scaffold some cells produced collagen type II in restricted areas, which was however deposited horizontally along the scaffold fibers (parallel to the bone or joint surface) which does not correspond to the natural orientation of native cartilage.

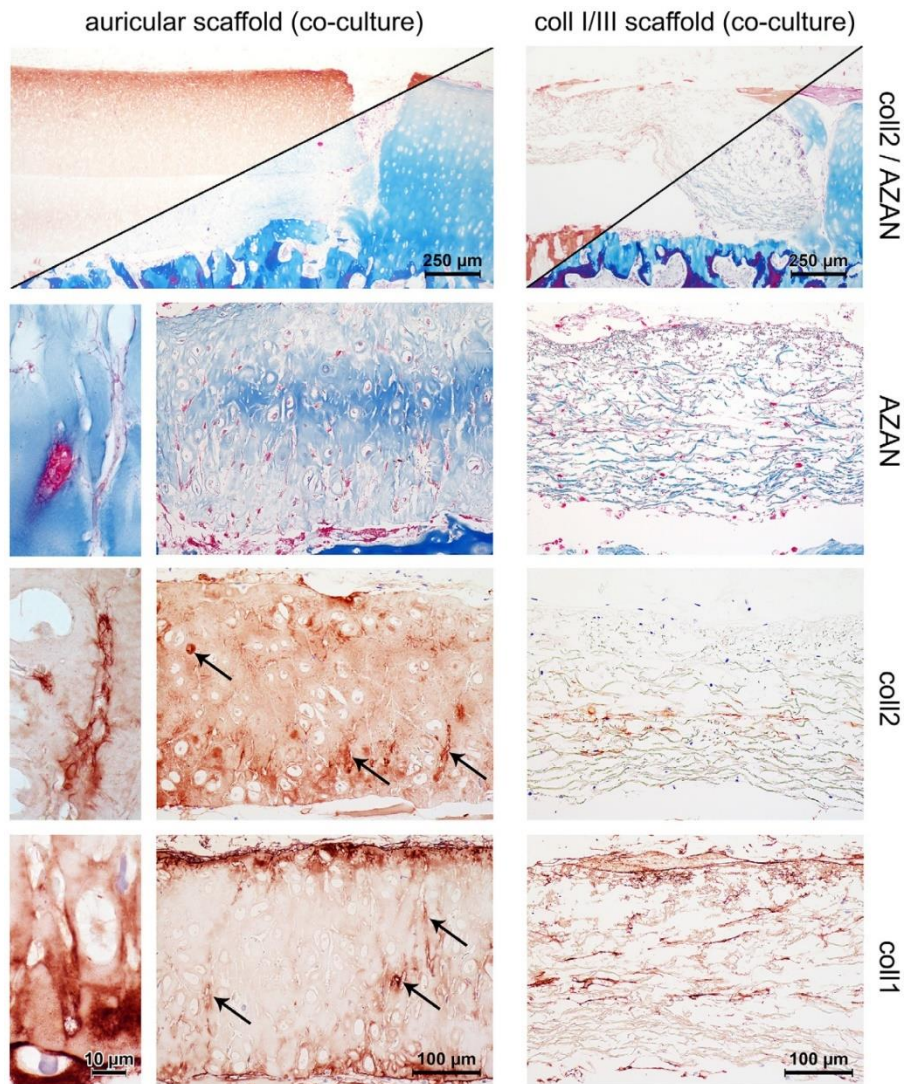


Fig. 29. Auricular cartilage and control scaffold reseeded with a co-culture of hAC and ASC/TERT1 in an osteochondral plug model *in vivo*. After 6 weeks in a nude mouse model collagen type II synthesis could be observed in channels and lacunae deep inside the scaffold (arrows), however in other channels collagen type I was still strongly expressed (arrows). n = 6.

3.8 Osteochondral plug model with bovine chondrocytes *in vivo*

Since the previous experiments demonstrated the regenerative potential, even of chondrocytes from donors of advanced age inside the scaffold, and cells of young human donors are rarely available, bovine chondrocytes (bAC) from adult cows were used instead to represent a metabolically active chondrocyte source.

After the *in vivo* period of 6 weeks the scaffolds were still firmly positioned straight and parallel in the defect, connected by *de novo* matrix formed in between the scaffolds as well as the surrounding tissues. Cells invaded the auricular channels throughout the whole thickness in both scaffold layers and filled channels and lacunae with matrix that stained positive for collagen type II (**Fig. 30**).

In the co-culture group, patches of matrix surrounding the scaffolds remained unstained for collagen type II in all three defects, indicating differentiation of ASC was not completed outside the scaffold.

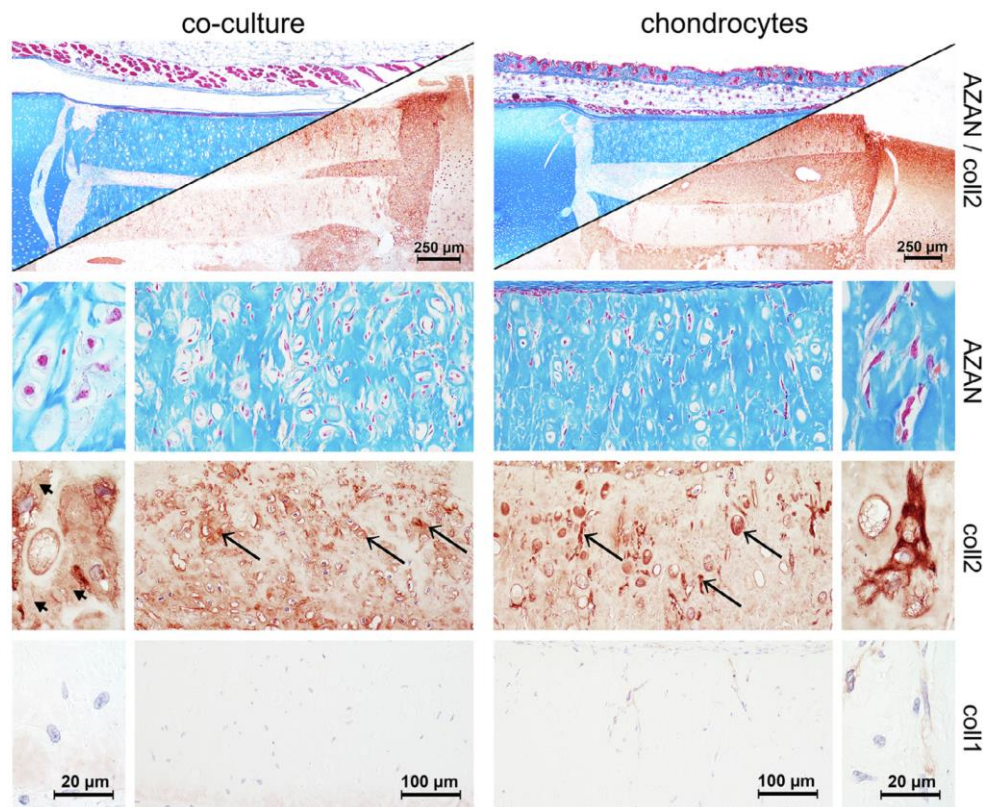


Fig. 30. Auricular cartilage reseeded with bovine chondrocytes alone or in co-culture in an osteochondral plug model *in vivo*. Cells invaded empty lacunae and channels created by elastic fiber depletion and synthesized new collagen type II inside the scaffold (arrows). Signs of beginning graft remodeling are visible (small arrows) in the coculture group. Collagen type I is weakly expressed by single cells in the chondrocyte group and completely absent in the co-culture group. n = 3

Inside the scaffold, *de novo* collagen type II formation was observed in 80% of the zones. Halos around the channels and lacunae of intermediate staining intensity indicated beginning tissue remodeling and replacement of scaffold matrix by endogenous collagen type II.

In the monoculture group, newly synthesized matrix surrounding the scaffolds stained highly positive for collagen type II in all defects, without any undifferentiated patches. Matrix deposited inside the scaffold was still restricted to the channels and the lacunae, with 90% of zones featuring *de novo* collagen type II. Inside the lacunae and broader channel areas, the collagen fibers were randomly aligned; however, inside narrow channels, there was a tendency of long fibrils to stretch alongside the channels (**Fig. 31**). Collagen type I was weakly expressed by single cells.

In conclusion, we were able to demonstrate that good outcomes can be achieved with both, repopulation with chondrocytes as well as the combination of chondrocytes and ASC, and that newly formed collagen type II matrix has a tendency to align along the channels.

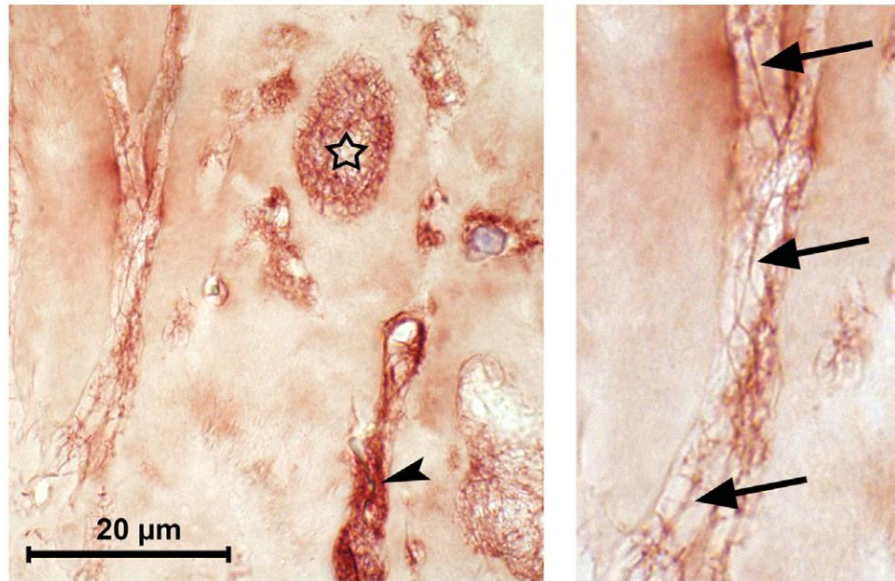


Fig. 31. Collagen type II deposited by bovine chondrocytes inside the scaffold. While the fibers in lacunae are randomly aligned (asterisk), long collagen type II fibers inside the narrow channels show a tendency to stretch along the channels (arrows). Once a space is fully filled, single fibers can no longer be distinguished (arrowhead). (The right image is a magnification of the left channel in the left image).

3.9 Cell quantification

The number of cells in the different zones, each representing one third of the scaffold thickness, varied from 20% to 45% of total cells identified in the respective ROI (**Fig. 32**). *AuriScaff* scaffolds which were cultivated without insertion into a plug *in vitro* showed especially homogenous repopulation (periphery $35 \pm 4\%$ and $35 \pm 6\%$ and middle zone $30 \pm 4\%$). In the commercial control scaffolds most cells were counted in the outer scaffold regions, even though with a high variation (both $40 \pm 20\%$) while the inner region featured only $16 \pm 3\%$ of the cells. In *AuriScaff* samples cultivated inside the defect *in vitro*, cell distribution was approximately 30–40% in all three regions (surface $30 \pm 10\%$, middle $39 \pm 8\%$, bottom $32 \pm 6\%$). Only in the *in vivo* samples significant difference between different zones were found with one-way ANOVA (human chondrocytes $p = 0.002$, bovine chondrocytes in monoculture $p = 0.003$ and bovine chondrocytes in co-culture with ASC $p = 0.033$), which was however only confirmed for the co-culture comparing the core to the surface zone (but not to the bottom) with the Dunnett-Test ($p = 0.043$).

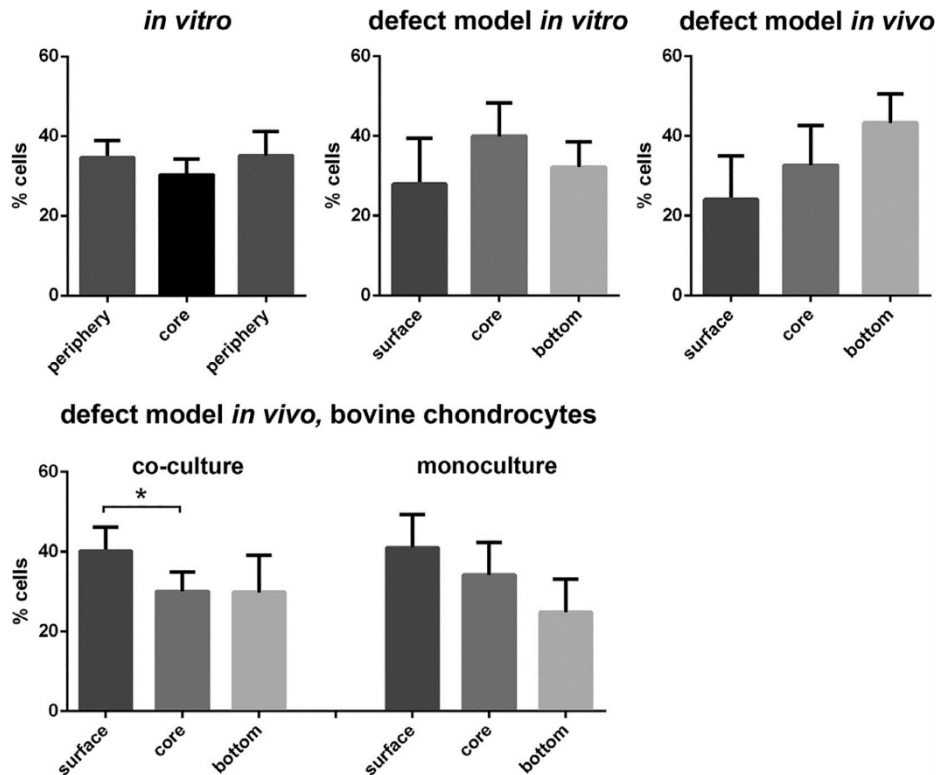


Fig. 32. Comparative cell quantification in histological sections of auricular cartilage scaffolds in different reseed setups. The proportion of cells in the different zones varied from 20% to 45% of total cells identified in the periphery versus the core (*in vitro*) and the surface, core and bottom region (in the artificial defects *in vitro* and *in vivo*). The three zones comprised a similar proportion of cells and a significant difference was assessed only in the co-culture group of ASC and bovine chondrocytes, where the cell number differed between the core and the surface zone (but not the core and the bottom zone). * $p \leq 0.05$.

4 Discussion

Uniform repopulation of articular cartilage allografts is an unsolved challenge due to the dense nature of hyaline cartilage. In this study we propose auricular cartilage as a graft alternative, similar to articular cartilage in its composition and abundantly available from xenogenic origin. We demonstrated that the elastic fibers in auricular cartilage can be selectively removed to create a traversing network of channels that enable cell migration into the matrix, leading to uniform repopulation of the scaffold. The thus generated channels tend to be aligned orthogonally to the scaffold surface, which forms the joint surface when implanted, promoting the deposition of new collagen in the same orientation found in the deeper layers of native articular cartilage.

Optimal regions on the bovine ear, defined by a high amount of well-aligned elastic fibers, were found in the center and medial border. Regular sample thickness is important for a standardized pretreatment with the lowest possible concentration of enzymes as well as future clinical application and was achieved using a cartilage cutter. The cartilage was devitalized using freeze/thaw cycles and further incubated in elastase to generate channels in place of the elastic fiber network. In order to enhance the effect of the elastase treatment a pepsin step was added to partially remove the GAG [392], thus making the elastic fibers more accessible to the elastase. Additionally, pepsin was found to be a suitable and cost-effective

reagent to facilitate complete opening of the channels also in deeper scaffold areas while keeping the elastase concentration low. The acetic acid, present in the pepsin solution to adjust the optimal pH for the enzyme, is also known as decellularization agent [393] and led to a DNA reduction of 75% with the current protocol. There is evidence in literature pointing towards a negative effect of acetic acid on collagens [393], [394]. However, immunostaining and electron microscopy showed that the pretreatment left the collagen matrix intact. In order to avoid the risk of immunological reactions, adding a designated decellularization step in the future is proposed to further reduce the DNA content to below 50 ng/mg dry ECM, a threshold defining a scaffold as “decellularized” [393]. In our previous decellularization study [392] we demonstrated the decellularization of even very dense articular cartilage with hydrochloric acid. Utomo *et al.* give an example of full decellularization of auricular cartilage matrix using sodium dodecyl sulfate [384].

Biomechanical parameters of the resulting *AuriScaff* featured better properties than scaffolds currently in clinical use. Its compressive modulus was more than three times higher than the tested collagen type I/III control scaffold and also higher than other commercially available scaffolds tested in previous experiments [392]. Altogether, its material properties closely mimic a native cartilage environment.

In vitro reseeding tests demonstrated successful repopulation of the elastin-depleted auricular cartilage, which was more efficient than in the commercial collagen type I/III control scaffold. The pore diameter of 5-10 μm , predefined by the former elastic fibers, appears to be optimal for the migration of cells into the dense auricular collagen type II matrix.

Chondrocytes are the desired cells for cartilage regeneration and cartilage matrix production, yet their use bears certain drawbacks such as limited availability, donor site morbidity and dedifferentiation during *in vitro* expansion [372], [395]. Therefore, we included ASC as therapeutically relevant mesenchymal stem cell type, already used in clinics in soft tissue reconstruction [396], [397] and recently achieving promising results in clinical studies regarding osteoarthritis [398]–[400]. The advantage of ASC over bone marrow-derived mesenchymal stem cells lies in their abundance: adipose tissue is available in large amounts and relatively easy to harvest, with higher yields of mesenchymal stromal/stem cells compared to bone marrow [401], [402]. They are known to be able to form functional cartilage *in vitro* and *in vivo* [403]–[406] which recommends them as potential chondrogenic cell alternative, either alone or in combination with chondrocytes, for future clinical application. Co-cultures of mesenchymal stem cells and chondrocytes have been shown to exceed chondrocytes in their capacity to form cartilage matrix [407]. Pleumeekers *et al.* demonstrated that 80% of chondrocytes could be replaced by mesenchymal stem cells without negatively influencing cartilage matrix production or stability [407]. No consensus on optimal co-culture ratios is yet available though, with chondrocyte ratios commonly ranging from 75% [408] to 20% [407], [409] in literature. Within this study, a low chondrocyte ratio (25% chondrocytes to 75% ASC) was chosen to make the approach feasible for

clinical application with a low yield of intraoperatively harvested chondrocytes, but enable a good potential for differentiation, as shown in several studies in literature [408], [410]–[412].

Cells were seeded on both sides of *AuriScaff* and only the porous side of the commercial control scaffold according to its architecture. The control scaffold is a bilayer membrane of porcine origin, consisting of a highly porous side and a dense side that is further covered by a tight sealing layer to shield the defect from the joint cavity. Cells can reach the dense side by migrating through the scaffold from the porous side where they have been applied, leading to an initial gradient until scaffold degradation allows ingrowth from both sides. The control scaffold's architecture also affected collagen type II deposition, which was, according to the scaffold fiber alignment, either random or in parallel to the joint surface.

When not implanted in the defect, both scaffolds experienced cell-mediated contraction in the co-culture group, forming spheroid-like structures with the scaffold at the center. Scaffold deformation is a well-known phenomenon observed in soft materials [413]–[417]. Responsible are not yet differentiated hACs and ASCs that bear a contractile cytoskeleton (actin stress fibers) which differentiated chondrocytes express to a much lower extent [418]–[420]. No scaffold deformation was observed when implanted in the defect. We hypothesize that this is due to the cells forming an integrating tissue to the defect borders on all sides, applying their contractile forces between scaffold and defect edge and thus stabilizing the implant in the defect. *AuriScaff* formed a compact filling of the whole defect depth, while the collagen type I/III matrix left an empty space between scaffold and subchondral bone, indicating insufficient initial integration or disintegration of deep collagen fibers.

Insertion of the scaffolds into chondral defects in our osteochondral plug model [390] served to mimic the cartilage environment. While cells did not differentiate when those plugs were cultivated *in vitro*, collagen type II was formed in some areas after subcutaneous *in vivo* implantation. These signs of differentiation, even in the ectopic non-loaded model, suggest good performance in a loaded, orthotopic *in vivo* environment, since mechanical stimulation further promotes the chondrogenic phenotype [421]–[424]. Moreover, the chondrocytes used in this experiment originated from donors above the common age limit for MACI (50 years [361], [425])). As chondrocytes are known to experience an age-related loss in proliferation and differentiation potential [358], the use of younger donors should allow for better differentiation and integration. However, since cartilage from younger donors is very rare and was not available, a non-human source was used to investigate young adult chondrocyte performance, although species differences may impact the outcome of tissue formation. Chondrocytes of bovine origin, alone or in co-culture with ASC, filled the channels and lacuna with collagen type II matrix. Additionally, the interspace between scaffold and defect edge was filled with differentiated tissue forming a continuum with the native and scaffold matrix. The use of the 300 μm thick materials in stacks in deeper defects showed the flexibility of the application of the auricular scaffold.

Within this study no cell tracking was performed in the defect scenarios, as none of the options for labelling was expected to be stable enough for long cultivation or subsequent plug decalcification.

However, in the all-over differentiated bovine chondrocyte experiment a thin collagen type II negative cell layer on top of the scaffolds (and plugs) might refer to murine fibroblasts. Otherwise, no cells from sources other than the seeded cells have been detected. Furthermore, results are different between the groups, with higher amount of collagen type II in monocultures of bovine chondrocytes than in co-cultures with ASC and the least differentiation in co-cultures of human chondrocytes with ASC.

A setup with cells from young human donors sufficient in number for individual use would have been preferable to closely represent the clinical situation in terms of patient age and species difference between seeded cells and scaffold material. However, articular chondrocytes from young patients are hardly available for research purposes. A potential alternative cell source for cartilage regeneration are chondrocytes from heterotopic origin such as nasal chondrocytes. They can be harvested from small biopsies of the nasal septum, propagated without losing their redifferentiation potential, form high quality cartilage and feature environmental plasticity [426]. These properties are related to their neuroectodermal origin, which is also the case for auricular cartilage. However, due to the tendency of auricular chondrocytes to regain their activity in elastic fiber production when implanted *in vivo* [426], nasal chondrocytes are the preferential choice. Promising outcomes for 24 months post-surgery in a first human trial examining nasal chondrocytes for articular cartilage repair [427] indicate them as favorable alternative cell source for upcoming approaches.

It is well documented that compact materials, mimicking the environment present in native cartilage, positively influence chondrogenic differentiation [358]. However, repopulation of dense matrices remains unsatisfactory, thus porous biomaterials are widely used in current MACI procedures. Hydrogels, where cells are encapsulated in the process of implantation, have unfavorable mechanical characteristics (soft collagen gels) and are challenged by the need for exactly fine-tuned biodegradability [358], [373], [374]. Auricular cartilage matrix consists of densely packed collagen type II, the type most prevalent and functionally important for articular cartilage. Potential low turn-over (though not expected) would not pose a problem, as the material is of a structure and composition very similar to articular cartilage. Its chondroinductive properties [375], [428] have been observed in course of our *in vivo* experiments. hAC inside the channels of *AuriScaff* locally produced collagen type II, indicating successful chondrogenic differentiation, which was generally not the case in the defect areas surrounding the scaffold. The channels promote a direct migration of the cells deeply into the scaffold as well as matrix deposition with a structural alignment that mimics the architecture of native articular cartilage.

Cartilage of xenogenic origin bears the advantage of abundant availability. Besides bovine also porcine donors are a viable option, as their auricular cartilage is similar in availability, thickness and composition [429]. As in all xenografts, the α -gal epitope (galactose- α -1,3-galactose glycosylation of glycoproteins) is expressed in bovine cartilage and may provoke an immune reaction in primates including humans [430]. It has been shown that the epitope can be successfully abolished by alpha galactosidase treatment, without any adverse effect on tissue structure or mechanical properties [431]–

[434]. Biomaterials from bovine origin are already used in the field of tissue engineering and reported to be safe in terms of viral contaminants such as Bovine spongiform encephalopathy due to stringent protocols enforced in sourcing and processing of the material [435], [436].

We have been able to develop a scaffold, *AuriScaff*, that is easily infiltrated by cells thus leading to uniform repopulation of the cartilage graft and differentiation of chondrogenic cells. The material is from a vastly available natural source and similar to articular cartilage. The intact native collagen of the enzymatically perforated auricular cartilage and its architecture provide an optimal environment regarding spatial organization and differentiation. It can be cut to any shape and stacked to fill defects of various sizes and depths. In combination with point of care cell harvest, *AuriScaff* could be applied in a one-step procedure in clinics. Our first *in vivo* experiments presented in this study, were performed for a relatively short period in a non-loaded model without synovial environment. The next step will be testing the scaffold in a long-term orthotopic *in vivo* model. Concluding, the herein presented exceptional characteristics of the auricular cartilage scaffold give reason to expect the formation of high quality hyaline-like cartilage, thus preventing graft failures due to inappropriate scaffold architecture and density.

5 Acknowledgments

Funding: This work was supported by the Austrian Research Promotion Agency FFG (project CartiScaff, grant number #842455) as well as the Lorenz Böhler Fonds (16/13) and the City of Vienna Competence Team Project Signaltissue (MA23, #18-08). The authors wish to acknowledge the Cell Imaging and Ultrastructure Research Unit from the Department of Life Science at the University of Vienna for providing their equipment, in particular the transmission electron microscope and further thank Sabine Novakovic´-Wagner for her illustrations used in **Fig. 22** and **Fig. 28** and Fritz Silmbroth and his team for their kind collaboration and Johannes Lehmann for valuable discussion regarding elastase treatment and cell seeding. The ASC/TERT1 cell line was kindly provided by Evercyte (Evercyte, Vienna, Austria, Cat# CHS-001-0005), Phoenix Ampho cells were a gift from Regina Grillari (University of Natural Resources and Life Sciences, Vienna, Austria).

6 Disclosures

All the authors declare they have no conflict of interest.

Chondroinductive properties of the decellularized auricular cartilage scaffold is further enhanced by mechanical loading

Bernhard Rieder^{1,8}, Cornelia Schneider^{2,8}, Niamh Fahy^{3,4,5}, Heinz Redl^{2,8}, Martin J. Stoddart³, Sylvia Nürnberger^{2,6,7,8,*}, Andreas H. Teuschl^{1,8}

¹Department Life Science Engineering, University of Applied Sciences Technikum Wien, 1200 Vienna, Austria

²Ludwig Boltzmann Institute for Experimental and Clinical Traumatology, AUVA Research Center, 1200 Vienna, Austria

³AO Research Institute Davos, 7270 Davos Platz, Switzerland

⁴Department of Orthopaedics, Erasmus MC, University Medical Center Rotterdam, 3015 Rotterdam, the Netherlands

⁵Department of Oral and Maxillofacial Surgery, Erasmus MC, University Medical Center Rotterdam, 3015 Rotterdam, the Netherlands

⁶Department of Orthopedics and Trauma-Surgery, Division of Trauma-Surgery, Medical University of Vienna, 1090 Vienna, Austria

⁷University Clinic of Dentistry, Medical University of Vienna, 1090 Vienna, Austria

⁸Austrian Cluster for Tissue Regeneration, 1200 Vienna, Austria

*corresponding author: sylvia.nuernberger@meduniwien.ac.at

To be submitted to *Journal of Tissue Engineering and Regenerative Medicine*

Abstract

Due to its avascular and aneural nature, articular cartilage intrinsic self-repair is extremely limited and thus relies on surgical interventions for regeneration. However, golden standards applied in clinics often incorporate autologous material which led to donor side morbidity – a detriment that result in the development of biomaterials to substitute for the patient’s own material. In this mindset, AuriScaff, a recently develop material originating from auricular cartilage showed promising results *in vivo* was tested in a biomimetic bioreactor setup simulating an orthotopic environment *in vitro*. We could show that human adipose-derived stromal cells were able to repopulate the decellularized biomaterial in the control groups as well in the stimulated groups. Immunohistochemical examination revealed no difference in collagen type II content between free swelling and dynamical loaded groups. However, cartilage specific markers (COL2, ACAN, SOX9) as well as dedifferentiation markers (COL1, VCAN) were significantly upregulated in dynamically loaded groups compared to control groups. Interestingly, cartilage differentiation index was highest in samples treated with 1 ng/ml of growth factors (BMP6, TGF- β 3) suggesting a masking effect due to physical stimulation. Although control samples had higher initial concentrations of total TGF- β 1 in the medium at week 3, stimulated samples could better harness occurring TGF- β 1 resulting in a higher ratio of active/total TGF- β 1. Utilizing the biomimetic bioreactor as orthotopic model, we could demonstrate that AuriScaff provides a platform that not only withstand initial dynamic loading but also provides housing for cells to mature and enables reorganization of the extracellular matrix.

Keywords: Tissue Engineering, Auricular Cartilage, Biomaterials, Bioreactors, Stem Cells, Mechanical Loading, Transforming Growth Factors

1 Introduction

Articular cartilage (AC), a specialized tissue lining the articulating surfaces of bones, plays an essential role in joint lubrication and impact absorption during motion. However, due to its avascular, alymphatic, and aneural nature and the lack of a perichondrium, the intrinsic self-repair capacity of articular cartilage is extremely limited [10]. Over the years different strategies for cartilage regeneration were developed and improved, spearheaded by treatment options like mosaicplasty, marrow-stimulating techniques, or autologous chondrocyte implantation (ACI). However, the majority of these procedures are associated with poor regeneration or donor site morbidity and, after initial success, failed to deliver satisfying long-term outcomes [437]–[439] or result in early transplant failure. Hence, unsatisfied by the result of the current clinical repair procedures [440]–[442], scientists strive to find an ultimate solution developing novel tissue engineering strategies focusing on biomaterials [443], [444] with or without the combination of therapeutically relevant cells [445]–[447]. While tissue engineering has no answer yet to joint spanning full sized lesions that require total joint replacement via arthroplasty, promising options for small to large sized defects are on the verge from the bench into clinics [448]–[450]. Although articular cartilage seems to be a “simple” tissue (no vasculature system, sparse population of a single cell type in a homogenous matrix) it features a highly complex architecture with different zones (prestressed matrix, hard to engineer structural and mechanical properties) in order to cope with the harsh biomechanical environment [451], [452]. Despite the continuous development of numerous natural and synthetic biomaterials as well as sophisticated scaffold fabrication techniques to engineer cartilage tissue grafts, the complex architecture of native cartilage remains to be uncopied. While natural biopolymers are generally used to create hydrogels that tightly enclose cells and thus mimic native chondrogenic conditions best, more rigid scaffold designs are traditionally composed of synthetic polymers in order to achieve mechanical properties closer to native hyaline cartilage. However, both biomaterial types are suboptimal. Due to high water content and commonly loose and soft structure, hydrogels are prone to mechanical failure [453] while rigid scaffolds tend to encourage cell spreading due to larger pore size [454], thus affecting and reducing cellular activities [455]. These obstacle can be overcome via combinations of synthetic and natural polymers that result in varying network density, degradation, and stiffness but could not improve the deficiency in their ability to integrate properly with the surrounding tissues [456]. Although several attempts have been made to engineer cartilage-like matrices, the distinctive architecture of articular cartilage has never been achieved [457], [458]. In terms of optimal homologous environment, cartilage itself serves as exceptionally regenerative material. Through biochemical and biomechanical cues it does not only support the chondrogenic phenotype of differentiated and redifferentiated chondrocytes but can also guide stem and progenitor cells towards the desired lineage [459], [460]. The use of autologous articular cartilage as defect filling material, however, bears drawbacks such as limited availability and donor site morbidity. Hence, the most promising option to overcome this obstacle is the decellularization of native cartilage allografts and the subsequent repopulation with the patient’s own cells. Although extraordinary advances have been made

in recent years in terms of developing an efficient decellularization protocol [461]–[464], reseeded attempts either remained limited to the cartilage surfaces [465] or were only achieved via needle generated artificial channels that facilitated cell migration [466], a process that is laborious and difficult to standardize. A solution to this problem was recently published by Nürnberger *et. al* [467]. Herein, cartilage of auricular origin is proposed as suitable scaffold, called AuriScaff, for articular cartilage defect treatment. While both share common characteristics of a dense collagen and proteoglycan matrix with sparsely distributed cells, auricular cartilage additionally possesses an elastic fiber network that surrounds the cells and traverses the tissue. Upon complete enzymatic removal of these elastic fibers, the opened channels enable cells to migrate into the scaffold. Feasible removal of these elastic fibers as well as uniform repopulation with human articular chondrocytes alone and in co-culture with human adipose-derived stromal cells (hASC) could be demonstrated [467]. AuriScaff's composition and spatial organization have already been shown to support the formation of matrix with cartilage-specific properties in an unloaded defect environment *in vivo*. However, native articular cartilage is exposed to physical stimulation and multiple studies have already shown that mechanical cues play a decisive role in chondrogenesis and preservation of the chondrogenic phenotype [468], [469]. Hence, the aim of this study was to investigate the effect of biomimetic mechanical loading on previously devitalized auricular cartilage which was repopulated with hASC to provide insights on AuriScaff's performance and behavior in an orthotopic environment.

2 Materials and methods

If not indicated otherwise, all chemicals and reagents were purchased from Sigma Aldrich (St. Louis, MO, USA) and were of analytical grade.

2.1 Harvest of cartilage discs

Auricular cartilage was harvested from ears of adult cows (2-year old Simmental cattle). Ears were obtained from a local slaughterhouse and processed within 12 hours following euthanasia. The cartilage was uncovered by skinning the respective area with a scalpel and the perichondrium as well as the outermost cartilage layer were cut off. Biopsies (8 mm in diameter) were punched out of the remaining central part and further cut into 300 μm thick slices with a Teixido Cartilage Cutter (MicroFrance, France); these slices ($\text{\O}8\text{ mm} \times 300\text{ }\mu\text{m}$) will be further referred to as cartilage discs. Cartilage discs were washed and stored in phosphate-buffered saline (PBS w/o $\text{Ca}^{2+}/\text{Mg}^{2+}$; Lonza, Basel, Switzerland) supplemented with 1% Penicillin-Streptomycin (P/S; Lonza, Basel, Switzerland) at 4 $^{\circ}\text{C}$.

2.2 Enzymatic treatment of cartilage discs

The cartilage discs were devitalized by means of four freeze/thaw cycles. Samples were alternately kept at -20 $^{\circ}\text{C}$ or room temperature (RT) for 1 hour each, twice dry frozen and twice frozen submerged in hypotonic buffer (10 mM Tris-base (Promega, Madison, WI, USA) adjusted to pH 8.0 using HCl (Roth, Karlsruhe, Germany)). Then samples were treated with pepsin and elastase to further open the dense cartilage matrix. Therefore, samples were incubated in pepsin solution (1 g/L pepsin in 0.5 M acetic acid

(Merck, Germany)) for 24 hours (pepsin solution renewed after 6 hours) followed by a 30 min washing step in PBS and concluded with 24 hours incubation in elastase solution (0.03 U/mL elastase in 0.2 M Tris-base (Promega, Madison, WI, USA) at pH 8.6). The procedure was completed by two 30 min washing steps in PBS and a final washing step in PBS overnight. All steps following the freeze/thaw cycles were performed under continuous shaking at 180 rpm and 37 °C (**Fig. 33A**).

2.3 Cell isolation and culture

Human adipose tissue derived stromal cells (hASCs) were kindly provided by the Ludwig Boltzmann Institute for Experimental and Clinical Traumatology in cooperation with the Red Cross Blood Transfer Service of Upper Austria. Cell isolation was performed in accordance with the relevant guidelines and regulations as described in Wolbank *et al.* [470] with authorization of the local ethics committee (Province of Upper Austria) and informed consent of the donor. Briefly, the stromal vascular fraction was obtained via several washing steps of lipoaspirate with PBS followed by enzymatic digestion of the tissue. Subsequently, the cellular fraction was seeded on plastic dishes, allowing for selection between plastic-adherent and non-adherent cells. The plastic-adherent hASCs were further cultivated and frozen, according to the laboratory-specific standard operating procedures (SOPs).

For expansion, hASCs were cultured in EGM-2 (Lonza, Basel, Switzerland) supplemented with 2 mM L-glutamine (Lonza, Basel, Switzerland), 1% Penicillin-Streptomycin (P/S; Lonza, Basel, Switzerland); this medium will be further referred to as expansion medium (EM). Cells were expanded in standard cell culture flasks in a humidified incubator at 37 °C and 5% CO₂. To avoid premature differentiation, cells were subcultured at 70% confluence. When hASCs reached desired cell concentration in passage 3, cells were dynamically seeded with a cell concentration of 1×10^6 cells per cartilage disc under continuous rotation of 60 rpm. After 3 days consumed medium was removed and discs were fed with fresh EM.

On day 4 the cartilage discs were attached to supportive scaffolds. Therefore, cylindrical polyurethane (PUR) scaffolds [471] (Ø8 mm x 4 mm, pore size 90-300 µm) were pre-wetted with plain DMEM and degassed for 1 hour under a vacuum bell. Afterwards, excessive medium was removed by squeezing the scaffold with tweezers under constant vacuum suction. Fibrin glue was used to attach the cartilage disc to the scaffolds. Therefore, the fibrin solution (17 mg/mL fibrinogen and 0.5 KIE/mL thrombin) was added on the simultaneously compressed PUR scaffold and got pulled into the pores after the scaffold went back into its original shape. The scaffold was repeatedly squeezed with tweezer to have an even distribution of the fibrin solution inside the scaffold. Fibrin solution was additionally put on top of the polyurethane scaffold to attach the cartilage to the supportive scaffolds. After 1 hour of incubation (37 °C, 5% CO₂, 80% relative humidity) to permit gel formation, the cartilage-polyurethane scaffolds were placed into the sample holder of the bioreactor and 2.5 mL medium were added according to the experimental groups. The basal formulation of the differentiation medium (DM) consisted of DMEM (Gibco, 52100-021) supplemented with 100 U/mL penicillin, 100 µg/mL streptomycin (1% P/S; Gibco,

15140122), 1 mM sodium pyruvate, 3.7 g/L sodium bicarbonate, 40 µg/mL proline, 6.25 µg/mL human recombinant insulin, 6.25 µg/mL human transferrin, 6.25 ng/mL selenous acid, 1.25 mg/mL BSA, and 5.35 µg/mL linoleic acid (ITS+ premix; Corning, 354352), 1% nonessential amino acid (NEAA; Gibco, 11140-35), 100 nM dexamethasone (DEX), 170 µM ascorbic acid (AA), and 5 mM ϵ -aminocaproic acid to inhibit fibrinolysis by plasmin. Dependent on the designated groups, differentiation medium was further supplemented with 0, 1, or 10 ng/mL transforming growth factor- β 3 (TGF- β 3; PeproTech, 100-36E) and bone morphogenetic protein 6 (BMP6; PeproTech, 120-06), respectively. Medium change was performed three times a week and medium of week one and three was pooled for further analysis. Cartilage-polyurethane constructs were divided either into free swelling (FS) or dynamic loading (DL). In combination with the three groups of differentiation medium with different growth factor (GF) concentrations (no \cong 0, low \cong 1, or high \cong 10 ng/mL GFs), this resulted in a total of 6 groups: FS0, FS1, FS10, DL0, DL1, DL10.

2.4 Mechanical stimulation and experimental plan

Mechanical loading of the cartilage-polyurethane constructs was performed using the already described biomimetic bioreactor system [472]–[476] (**Fig. 33C**). Briefly, a ceramic hip ball (\varnothing 32 mm) was used to apply compression strain as well as shear stress on the samples. Superimposed compressive strain along the cylindrical axis of the scaffold was applied by moving the hip ball up and down. Interface shear stress on the surface of the cartilage disc was generated by oscillating the hip ball about an axis perpendicular to the cylindrical axis of the scaffold (**Fig. 33B**). Loaded groups were subjected to a sinusoidal dynamic strain of 10% superimposed on a 10% static offset compression resulting in a cyclic displacement between 0.43 mm and 0.86 mm of the cartilage-polyurethane constructs surface. Simultaneously, shear stress was applied by a $\pm 25^\circ$ oscillation of the hip ball around the pin's axis. Both, compression and shear stress, were applied with a frequency of 1 Hz. Mechanical loading was performed for 1 hour a day on 5 days a week over a total of 5 weeks, summing up to a total of 25 hours of stimulation per construct (**Fig. 33E**). After 5 days in preculture (dynamic seeding on cartilage discs and attachment on supportive polyurethane scaffold) and 35 days of stimulation (**Fig. 33D**), constructs were vertically cut into two halves. One half was used for gene expression analysis and the other half was used for histological examination.

2.5 Immunohistochemical analysis

Cartilage-polyurethane construct halves were fixed in 10% formalin for 24 hours and dehydrated with a graded series of ethanol steps (50% to 100%). Samples were embedded in paraffin, sectioned (4 µm), and mounted on glass slides. Sections were deparaffinized with xylene (Roth, Karlsruhe, Germany) and rehydrated with a graded series of ethanol washes to distilled water. General matrix was visualized with AZAN trichrome stain. Therefore, rehydrated slides were stained with azocarmine G solution at 56 °C for 15 min and rinsed with distilled water before tissue slides were differentiated with aniline-ethanol. Differentiation was stopped with acetic acid-ethanol and rinsed again with distilled water and pickled

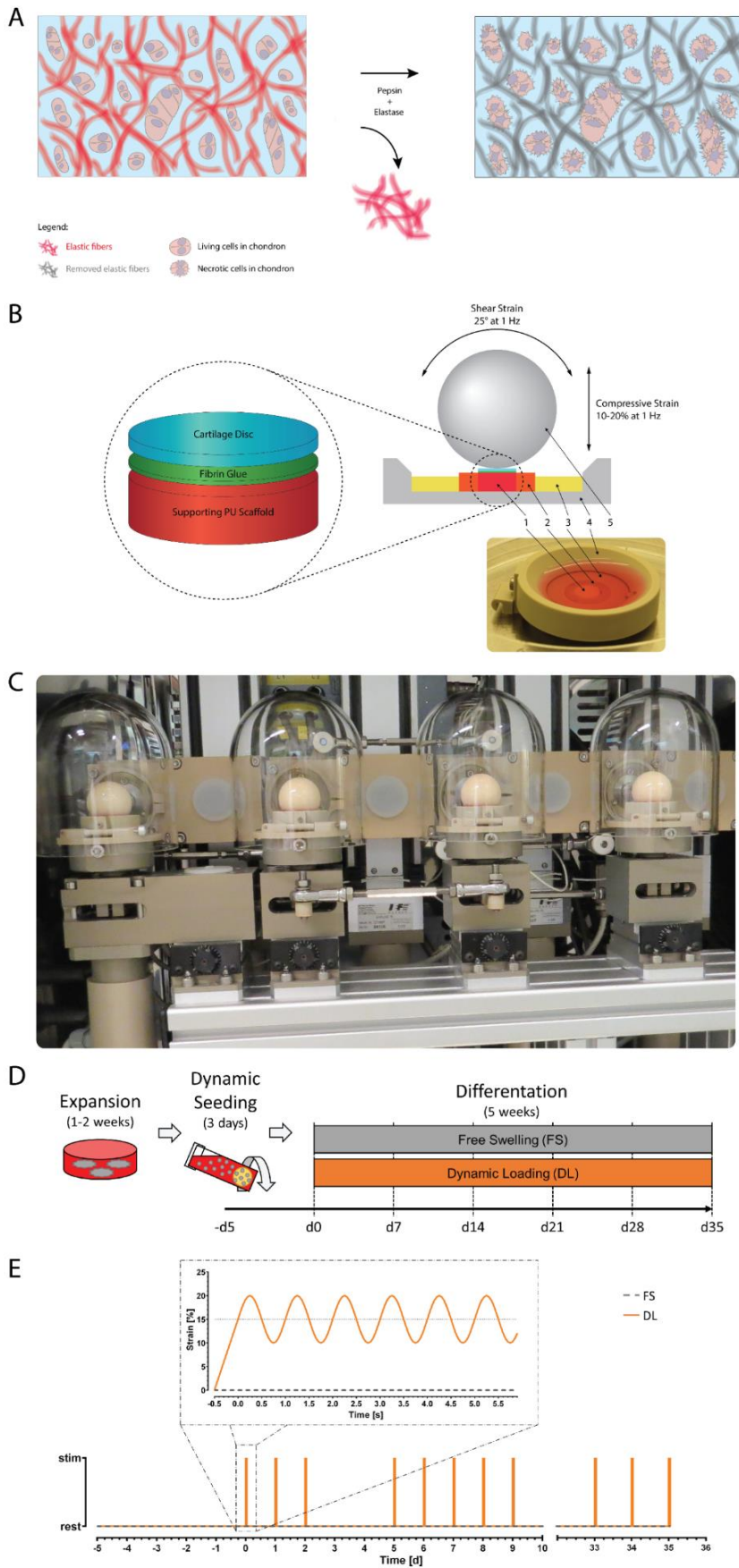


Fig. 33. Construct preparation and study design. (A) Cartilage discs harvested from ears of adult cows were devitalized killing existent cells and enzymatically treated to remove elastic fibers to open up corridors for new cells to invade the native cartilage. (B) The cartilage-polyurethane construct was assembled via layering the pre-seeded cartilage disc on top of a supportive polyurethane scaffold. The cartilage disc was held in place with fibrin glue administered on top of the polyurethane scaffold. The complete cartilage-polyurethane construct (1) was placed into the scaffold holder (4) and centered with a polyether ether ketone ring (3) as well as and polyurethane ring (2). A ceramic hip ball (5) applied the load according to a predefined stimulation program. (C) The assembled biomimetic bioreactor system. The custom-made bioreactor system was designed to fit in a standard incubator and enables the stimulation of up to four constructs simultaneously. The hip ball is used to transmit forces in the vertical axis and is further able to oscillate around the pin's axis. The scaffold holder is the designated place to house the stimulated construct and is further able to perform an oscillating movement around the vertical axis. Together with the hip ball, the scaffold holder allows for a complete stimulation of all possible motions of the human knee. (D) Timeline of the experimental study. Human ASC were expanded until passage 3 and dynamically seeded via rotation on the pre-treated cartilage discs. After cartilage discs were attached to the supportive polyurethane scaffold, the constructs were either culture statically (FS) or dynamically (DL) stimulated with the biomimetic bioreactor for 5 weeks. (E) Stimulation pattern performed by the bioreactor. After 5 days of cell seeding and construct assembling, the construct was stimulated with a sinusoidal dynamic strain of 10% superimposed on a 10% static offset compression as well as an $\pm 25^\circ$ oscillation of the hip ball with a frequency of 1 Hz for 1 hour on five consecutive days with 2 days of rest in-between. This pattern was repeated over a period of 5 weeks with just slight alterations on the first and the last week of the experiment.

in phosphotungstic acid for 20 min before rinsing again in distilled water. Finally, slides were stained in aniline blue-orange G solution for 15 min and rinsed in distilled water, quickly dehydrated and covered with a glass slide. Collagen type II was detected via immunohistochemical (IHC) staining to assess the distribution of collagen type II in the cartilage-polyurethane construct halves. Briefly, collagen type II staining was performed by drying paraffin sections for 30 min at 60 °C. Samples were deparaffinized and endogenous peroxidase was blocked with BLOXALL® solution (SP-6000, Vector Laboratories, Burlingame, CA, USA) for 10 min and rinsed with distilled water. Antigens were retrieved by treatment with pepsin solution (R2283) for 10 min at 37 °C followed by rinsing for 5 min with tris-buffered saline (TBS). Samples were incubated with normal horse serum (S-2012, Vector Laboratories, Burlingame, CA, USA) for 20 min to block non-specific binding, incubated with the primary antibody (mouse monoclonal anti-collagen II Ab-3 (MS-306-P0), Thermo Fisher, Waltham, MA, USA) for 1 hour at RT, rinsed with TBS for 5 min and incubated with the secondary antibody (BrightVision Poly-HRP-Anti Mouse (VWRKDPVM110HRP), VWR International, Radnor, PA, USA) for 30 min at RT, followed by rinsing with TBS for 5 min. For detection, sections were incubated for 6 min with 2-3 drops of ImmPACT™ NovaRED™ (SK-4805, Vector Laboratories, Burlingame, CA, USA) and the reaction was stopped by submerging in water for 10 min. Afterwards, sections were counterstained with Hemalum (Roth, Karlsruhe, Germany) for 1 min and blued for 10 min in tap water before embedding.

2.6 Quantitative reverse transcription polymerase chain reaction (RT-qPCR)

For each sample the associated other half of the cartilage-polyurethane constructs was mixed with peqGOLD TriFast (VWR International, Radnor, PA, USA) and minced using a TissueLyser (Qiagen, Hilden, Germany) followed by total mRNA extraction according to the manufacturer's protocol. RNA was measured using a NanoPhotometer (Implen GmbH, München, Germany) and 1 µg of mRNA was transcribed into cDNA using EasyScript™ cDNA Synthesis Kit (abm, Richmond, BC, Canada) using oligo(dT) primers. Quantitative PCR was performed using KAPA SYBR® FAST qPCR Kit (VWR International, Radnor, PA, USA) with a Stratagene© Mx3000P QPCR System (Agilent, Santa Clara, CA, USA) according to the manufacturer's instructions using 10 ng of cDNA per reaction. Thermal cycle conditions were 5 min at 95 °C followed by 40 cycles of 30 s at 95 °C and 1 min at 60 °C (B2M, COL1A1, COL2A1, SOX9) or 15 s at 95 °C and 30 s at 55 °C followed by 30 s at 60 °C (ACAN, VCAN). Target genes were normalized to the housekeeper β2-microglobulin (B2M) and compared to corresponding values of the not stimulated, non-growth-factor group (FS0) using the comparative CT ($\Delta\Delta CT$) method. Primer sequences and primer concentrations used are listed in **Table 2**.

2.7 TGF-β1 enzyme-linked immunosorbent assay

Pooled medium samples were analyzed for TGF-β1 concentrations for week 1 and week 3 with an enzyme-linked immunosorbent assay (ELISA; DY240; R&D Systems) according to the manufacturer's instruction. Briefly, capture antibody coated 96-well microplates were incubated for 2 hours at RT with standards and samples. Plates were washed and incubated for another 2 hours at RT with the added

detection antibody. Plates were washed again and a streptavidin-bound HRP enzyme was bound for 20 min to the detection antibody and after an additional washing procedure the substrate solution was added. TGF- β 1 concentration was read at 450 nm against 540 nm as reference wavelength using a plate reader.

Table 2: Primer sequences and concentrations used for qPCR.

Target	Primer forward	Primer reverse
B2M	GATGAGTATGCCTGCCGTGT	TGCGGCATCTTCAAACCTCC
COL1A1	GATCTGCGTCTGCGACAAC	GGCAGTTCTTGGTCTCGTCA
COL2A1	AGACTTGCGTCTACCCCAATC	GCAGGCGTAGGAAGGTCATC
ACAN	CCCCTGCTATTTTCATCGACCC	GACACACGGCTCCACTTGAT
VCAN	AGGTGGTCTACTTGGGGTGA	GATGGTTGTAGCCTCTTTAGGTTT
SOX9	AGCGAACGCACATCAAGAC	CTGTAGGCGATCTGTTGGGG

2.8 Statistical Analysis

Unless otherwise stated, all data are presented as mean + standard deviation (SD). All statistical calculations were performed using SPSS Statistics (IBM, Armonk, New York, USA) or GraphPad Prism software (GraphPad Software Inc., San Diego, CA, USA). Normal distribution of values was tested using Shapiro–Wilk test. Comparisons between two groups was calculated using unpaired *t* test or Mann–Whitney *U* test. *P*-values <0.05 were considered statistically significant.

3 Results

3.1 Removal of elastic fibers facilitates cell invasion

Prior to dynamic loading, auricular cartilage was harvested from bovine ears treated as described elsewhere [467]. Treatment with pepsin and elastase solutions removed elastic fibers and opened up hollow channels for repopulation of the scaffolds with therapeutic cells, which has been achieved within 7 days in a preliminary project (**Fig. S3**). After 5 weeks of culture, histology revealed that cells were able to invade the full thickness of the cartilage scaffold. Cross sections of both the free swelling control as well as the dynamic loading group displayed cells repopulating open spaces via channels of previously removed elastic fibers (**Fig. 34**).

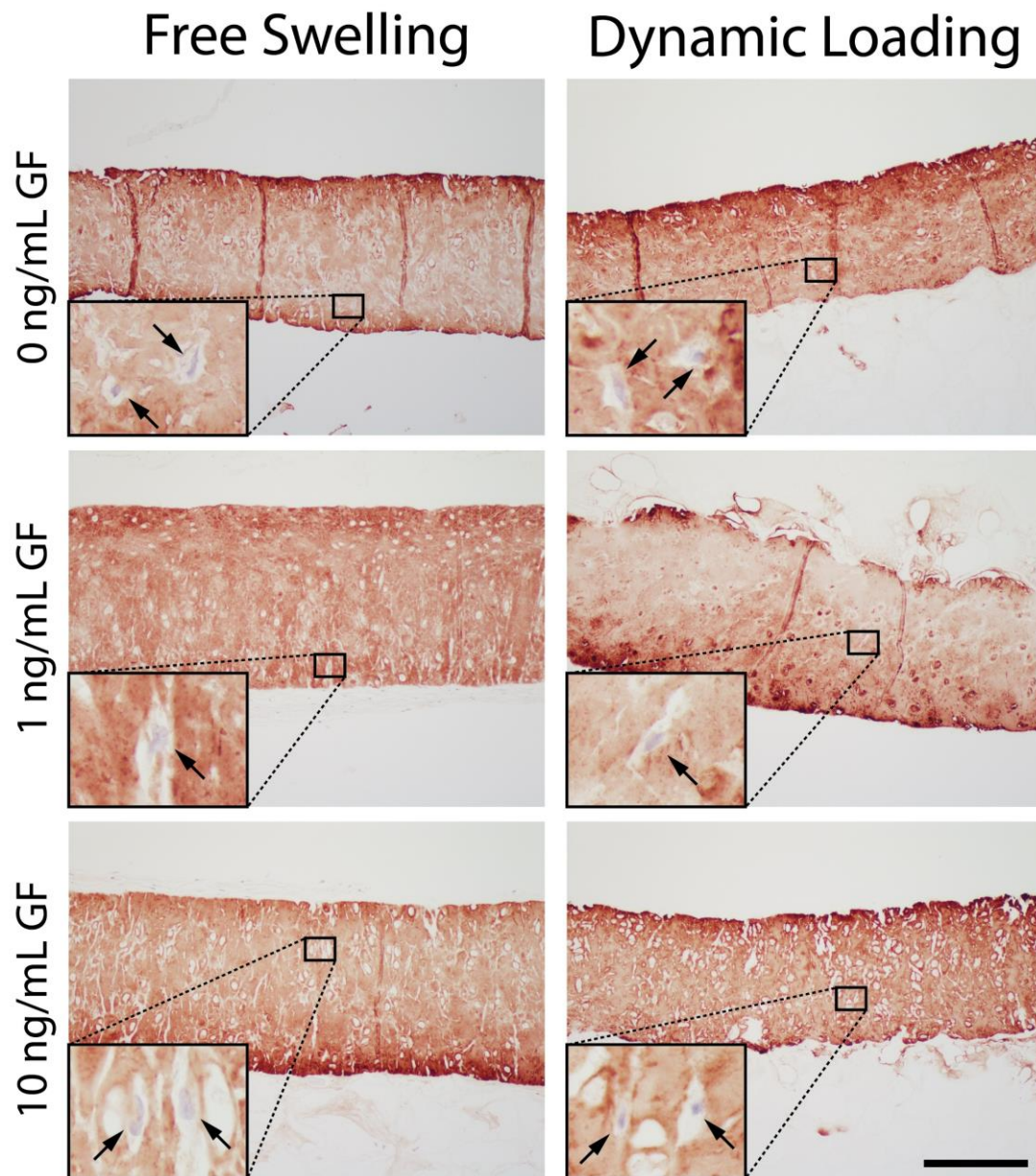


Fig. 34. Collagen II staining of reseeded bovine auricular cartilage discs after 5 weeks of cultivation. Cells repopulate enzymatically treated cartilage and reside in channels created by elastic fiber depletion as well as in empty lacunae in both the free swelling as well in the dynamically loaded group. Scale Bar = 200 μ m.

3.2 Dynamic loading showed no effects on collagen type II content

The influence of stimulation on reseeded cartilage discs was investigated by histological analysis after 5 weeks of culture. Therefore, one group of samples was stimulated according to the already described stimulation regime via the biomimetic bioreactor (dynamic loading) while the other group served as control and was statically cultured in an incubator (free swelling) (**Fig. 33E**). Collagen type II did not show extensive differences when comparing dynamically loaded samples with free swelling samples regardless of the used GF concentration (**Fig. 34**).

3.3 Dynamic loading enhances cartilage specific markers

Gene expression analysis of known cartilage specific markers was performed to gain deeper insight into the effects of stimulation on reseeded hASCs (**Fig. 35**). Here, dynamically loaded samples significantly upregulated collagen type II (COL2) in samples cultured with 1 or 10 ng/mL GFs compared to statically cultured samples. Similar to COL2, collagen type I (COL1) was significantly upregulated in dynamically cultured samples supplemented with 1 or 10 ng/mL GFs. Samples cultured without addition of GFs did not show significant differences between both groups, although a trend that loading increases expression of both COL2 and COL1 compared to statically cultured samples is visible. The ratio of collagen type II to collagen type I (COL2/COL1), generally described as cartilage differentiation index, was only significantly higher in samples cultured with 1 ng/mL GFs, while no apparent difference was visible for samples cultured with no or high GFs concentration. Aggrecan (ACAN), cardinal anchor for GAGs and thus an important core protein in cartilage, was significantly upregulated in all dynamically stimulated groups regardless of GFs concentration. Although supplemented with GFs, free swelling cultured samples expressed less ACAN mRNA than stimulated samples with no GFs added. In contrast, GF addition to dynamically loaded samples increased ACAN expression 10.7-fold and 5.4-fold compared to no GFs when supplementing 1 or 10 ng/mL GFs to the medium, respectively. This trend was also observed in versican (VCAN), which is predominantly expressed during tissue morphogenesis. While statically cultured samples had a similar gene expression level independent of added GFs concentration, low GFs concentration increased gene expression levels in dynamically cultured samples by 48.9-fold and by 11.4-fold when cultured with high GFs concentration compared to corresponding static cultures. When cultured without GFs, dynamic stimulation did not cause any differences in VCAN expression compared to static culture. The ratio of aggrecan to versican (ACAN/VCAN), generally assessed to evaluate the maturation of the investigated tissue, was increased in all dynamically cultured samples compared to statically cultured samples independent of applied GF concentrations. Although only the highest GFs concentration used lead to a significant difference between dynamically and statically cultured samples, a clear trend towards a more mature cartilage tissue is apparent. While ACAN/VCAN for the highest GF concentration was 10.3-times higher in dynamically cultured samples than in statically cultured samples, it was already increased 4.4-fold or 4.7-fold in cultures supplemented with low or no GFs, respectively. In order to substantiate the hypothesis that dynamic loading is favorable for repopulation of decellularized cartilage, SRY-Box 9 (SOX9), a major transcription factor essential for cartilage matrix formation was investigated. All dynamically loaded samples were significantly upregulated compared to their corresponding static controls. The highest difference was measured in samples supplemented with low GFs concentration resulting in a 146.8-fold upregulation, while samples with high GFs concentration have been upregulated 61.6-fold. Although no GFs were added, dynamic loading could increase the level of SOX9 in mechanically stimulated samples by a factor of 8 compared to free swelling cultures.

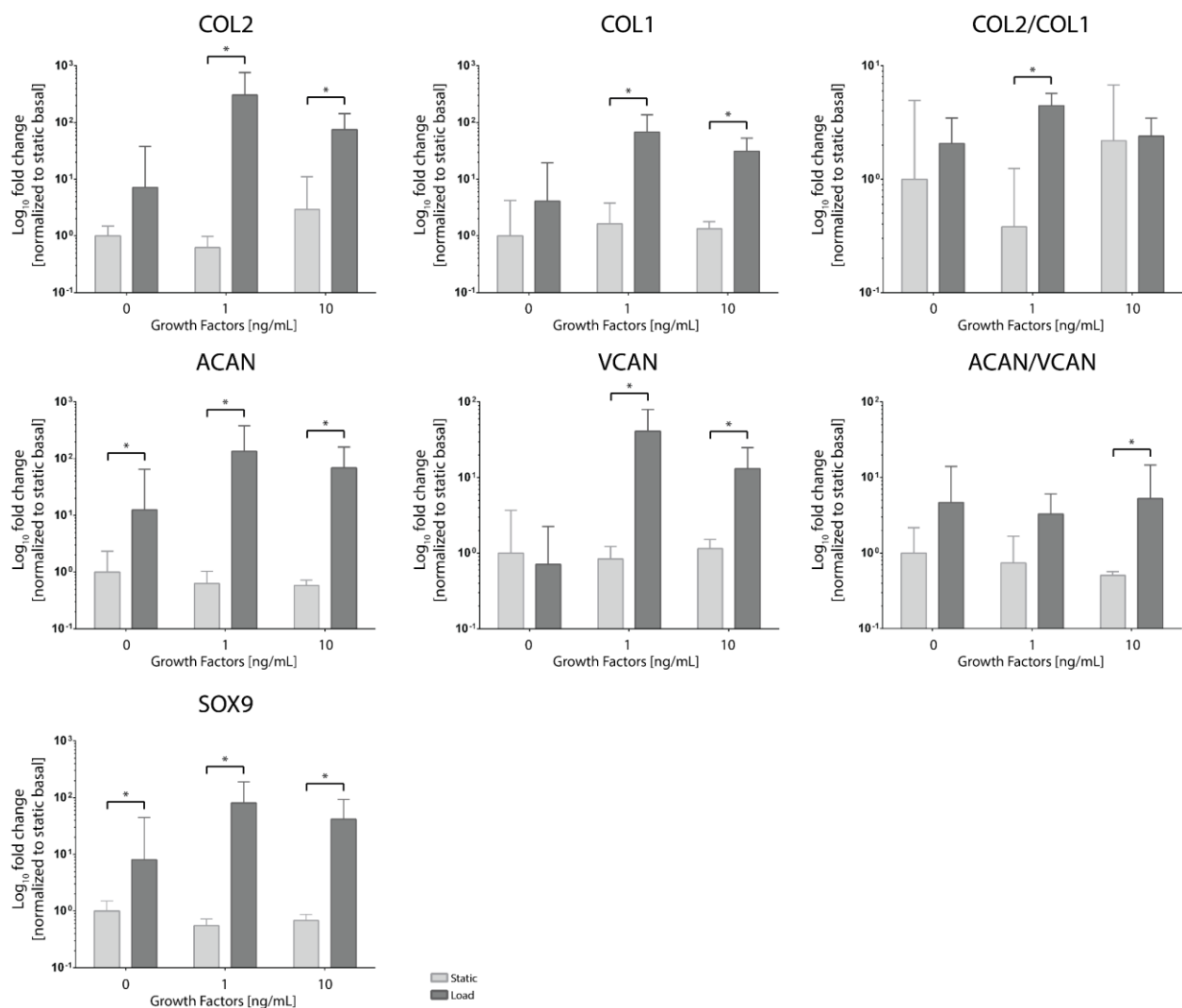


Fig. 35. Gene expression profile of cartilage specific markers. Collagen type II (COL2) as well as collagen type I (COL1) was significantly upregulated in samples cultured with 1 or 10 ng/mL growth factors (GFs) when mechanically loaded compared to statically cultured samples. COL2/COL1 ratio (cartilage differentiation index) was significantly higher for dynamically loaded samples supplemented with 1 ng/mL GFs than for samples cultured in 0 or 10 ng/mL GFs compared to free swelling control samples. Aggrecan (ACAN) was significantly upregulated in all dynamically loaded samples compared to statically cultured controls while versican (VCAN) was only upregulated in samples supplemented with 1 or 10 ng/mL GFs. The ratio of ACAN/VCAN (cartilage differentiation index) was significantly higher in the 10 ng/mL GFs supplemented dynamically loaded samples while it was just increased for 0 and 1 ng/mL GFs samples compared to the statically cultured group. SOX9 was upregulated in all dynamically cultured groups compared to free swelling groups regardless of GF concentrations. * $p < 0.05$

3.4 Dynamic loading increases TGF- β 1 activation

Observing increased expression of COL2 and COL1 due to dynamic loading, the focus was shifted towards GFs produced by the cells themselves and known to regulate the anabolic metabolism of articular cartilage. Beside the already medium supplemented TGF- β 3, we were interested in the amount of endogenously produced TGF- β 1 (Fig. 36). After the first week of culture, concentration of total as well as of active TGF- β 1 was generally higher in samples subjected to mechanical loading than in samples cultured statically, especially when supplemented with GFs. Specifically, total TGF- β 1 in loaded samples was significantly increased 3.1-fold or 2.5-fold compared to statically cultured samples when supplemented with 1 or 10 ng/mL GFs, respectively. Furthermore, the amount of active TGF- β 1 in loaded samples was 1.4-times, 2.3-times, or 1.7-times more than in the static samples when

supplemented with 0, 1, or 10 ng/mL GFs, respectively. Ratio of active to total TGF- β 1 steadily increased from 0.04 to 0.1 in statically cultured samples with increasing GF concentration but remained on an almost similar level of around 0.06 for dynamically cultured samples. In contrast to week 1, medium pooled on week 3 from stimulated samples had overall less total TGF- β 1 than medium of statically cultured samples. While dynamically stimulated samples had just 140 pg/mL total TGF- β 1, statically cultured samples produced 1.8-times or 3-times that amount when supplemented with 1 or 10 ng/mL GFs, respectively. In contrast to total TGF- β 1, active TGF- β 1 of statically cultured samples could not be acquired (n/a) when no GFs were added and was comparably low at 1 or 10 pg/mL when supplemented with 1 or 10 ng/mL GFs, respectively. Active TGF- β 1 in dynamically cultured samples was significantly higher than in static culture and peaked in values of 12.8 pg/mL for low and 22.6 pg/mL for high GFs concentration. Ratio of active to total TGF- β 1 was highest for dynamically loaded samples with 10 ng/mL GFs followed by dynamically loaded samples cultured with 1 ng/mL GFs. Compared to statically cultured samples, ratio of mechanically stimulated samples was 93-times higher when supplemented with 1 ng/mL GFs and 6-times higher when supplemented with 10 ng/mL GFs in the medium.

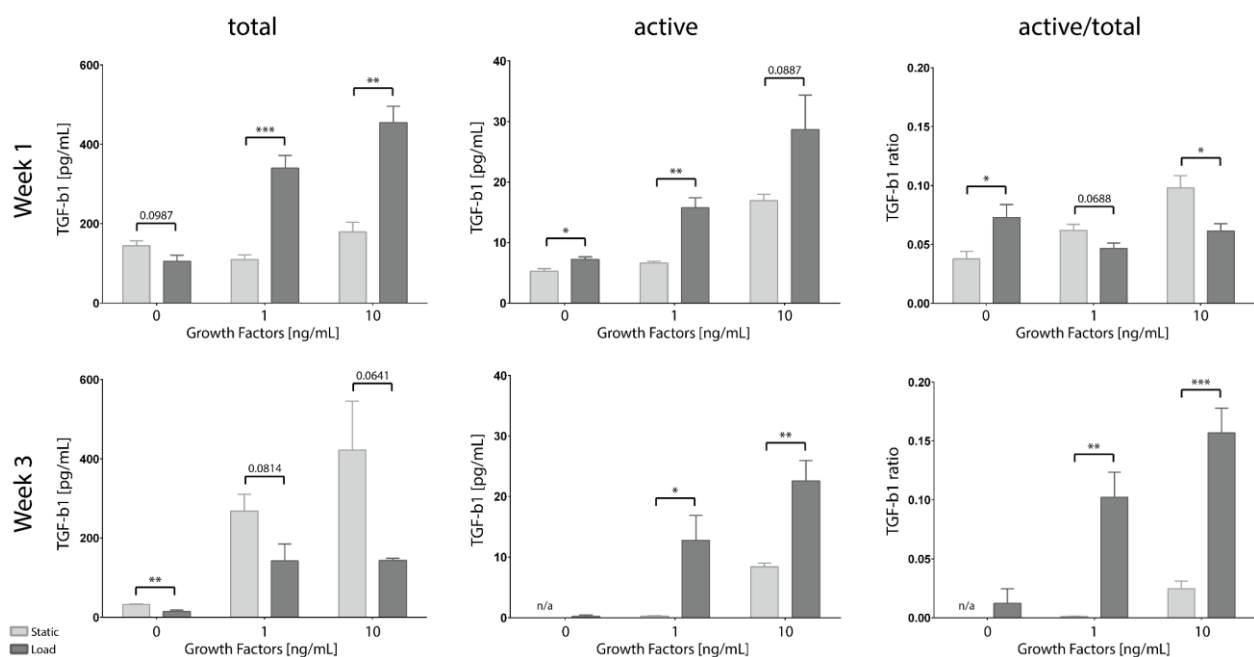


Fig. 36. TGF- β 1 concentration in the medium. Week 1: Concentration of total as well as of active TGF- β 1 was higher in samples subjected to mechanical loading than in samples cultured statically. Samples cultured in medium supplemented with growth factors (GFs) had an increased concentration of TGF- β 1 with ascending GF concentration. Ratio of active to total TGF- β 1 steadily increased in statically cultured samples with increasing GF concentration but remained on an almost similar level for dynamically cultured samples. **Week 3:** Concentration of total TGF- β 1 was higher in statically cultured samples versus dynamically cultured samples and steadily increased with ascending GF concentrations. Active TGF- β 1 was not acquirable (n/a) for samples without GFs and was generally higher for samples subjected to dynamical loading than for samples cultured statically when supplemented with GFs. Ratio of active to total TGF- β 1 was highest for dynamically loaded samples with 10 ng/mL GFs followed by dynamically loaded samples cultured with 1 ng/mL GFs. Statically cultured samples supplemented with 1 ng/mL GFs had a comparably low concentration of active TGF- β 1 as well as a low ratio of active/total TGF- β 1. Ratio of active/total TGF- β 1 was about 6-times and 93-times lower in statically cultured samples than in dynamically culture samples for 10 ng/mal GFs and 1 ng/mL GFs, respectively. *p < 0.05, **p < 0.01, ***p < 0.001

4 Discussion

Articular cartilage repair and regeneration procedures like microfracture, osteochondral autograft transfer (OAT), or autologous chondrocyte implantation (ACI) are the golden standards and routinely applied in clinics. However, despite constant refinement and improvement over the last decades, e.g. with ACI already being in its 3rd generation, these procedures often result in secondary decline of clinical parameters and are defect and patient dependent [437]. In a recent study by Frank *et al.* the number of patients that needed reoperation within two years after the first surgical interventions was almost 15% [477]. Hence, a universal and long-term solution is desperately needed to not only reduce medical costs but especially improve the patient's chance for a successful treatment and restore life quality permanently. The inherent problem of these repair or restoration procedures is that they fail to regenerate proper cartilage tissue due to production of fibrocartilage instead of hyaline cartilage. Fibrocartilage is unable to sustain the harsh environment and ultimately fails to support the load in the joint [478]. The herein used graft AuriScaff already meets the necessary articular cartilage composition while being available in unlimited quantities and consistent quality due to its xenogeneic origin. A recently developed protocol [467] permits removal of elastic fibers and opens up channels for the patient's own cell to migrate into the graft, further enhancing its regenerative potential. The presence of mechanical stimulation is expected to additionally contribute to its therapeutic potential by the stabilization of the chondrogenic phenotype and increasing the functionality of the generated tissue [479].

Hence, the aim of the present study was to investigate the effect of biomimetic stimulation on the pre-seeded graft to simulate the mechanical environment that the cartilage discs will be exposed to upon implantation into the patient's joint. The applied stimulation protocol mimics the normal walking cadence [245] and physiologic strain [480] experienced by chondrocytes of an active person and was already used with minor variations in several studies [472], [473], [475], [476], [481], [482] and demonstrated to be chondroinductive. Due to the limited height, the cartilage discs were attached to polyurethane support scaffolds to allow optimal force transmission from the ceramic hip ball onto the graft. Fibrin glue was used to stick both parts together and created a uniform cartilage-polyurethane construct (**Fig. 33B**). Although cells enzymatically digest fibrin over time [483], this bond was strong enough to endure mechanical stimulation over several weeks of cultivation. The fibrin network was stabilized by the addition of ϵ -aminocaproic acid, which inhibits fibrinolysis of plasmin. In this *in vitro* setup human adipose-derived stem cells (hASCs) were chosen due to certain advantages over generally desired chondrocytes. Chondrocytes are only available in limited quantity, cause donor site morbidity, and are known to dedifferentiate during *in vitro* expansion [484], while hASCs do not manifest these drawbacks. Furthermore, compared to bone marrow mesenchymal stem cells (BM-MSCs), hASCs are highly abundant and easy to harvest resulting in an overall higher cell yield [485]. Although the majority of stem cells used in cartilage tissue research are still of bone marrow origin and some studies claimed inferior chondrogenic potential of ASCs in comparison to BM-MSCs [486]–[488], others did not find any significant difference between the two cell types [489]–[491]. In fact, in several studies hASC could

demonstrate to form functional cartilage [492]–[494] and thus are a potent therapeutic cell type for future clinical application.

Besides a potent cell source, formation of proper functional cartilage tissue requires uniform cell distribution over the whole scaffold. Various studies utilize hydrogels as cell delivery vehicle as they offer equal distribution and tight enclosure of cells and thus resemble the cartilage micro-environment best. However, their commonly loose and soft structure is a major disadvantage [453] compared to native cartilage. Unfortunately, scaffolds with increased mechanical resilience are generally composed of synthetic materials which potentially release toxic substances during remodeling [495]. Further they encourage cell spreading [454] due to bigger pore sizes resulting the formation of unwanted cell phenotypes and generally lack anchor motifs for cells [455]. Although modifications and combinations with other materials reduced these drawbacks, an optimal solution is still pending. The scaffold presented in this study does not suffer these obstacles. Due to enzymatical removal of elastic fibers inherent to auricular cartilage [464] cells can easily travel via these generated channels. Thus, reseeded cells can either reside in the channels themselves or further migrate and invade empty lacunae of previously removed cells. Since these fibers span over the whole graft, cells did not only predominantly reside on the scaffold surface but also distributed inside the central zones of the scaffold (**Fig. 34**). Interestingly, repopulation was neither depending on concentration of used GFs nor on application of mechanical forces since all groups displayed cells inside the cartilage discs. Hence, we hypothesize that for initial cell migration no mechanical or biochemical cues are necessary to successfully repopulate the entire graft (**Fig. S3**).

Although mechanical stimulation seems negligible for uniform cell repopulation in our specific setup, there is a broad consensus that it supports chondrogenic differentiation [60] and maintains cellular viability in the generation of anisotropic and mechanically robust articular cartilage constructs [497]. Increased chondrogenic properties are generally associated with higher collagen type II production and reduced collagen type I production resulting in a higher cartilage differentiation index [498]–[501]. Comparing collagen type II (**Fig. 34**) amount, dynamically loaded samples exhibited only marginal differences when compared to free swelling samples, regardless of used GF concentrations. However, cartilage tissue only has a moderate matrix turnover rate and the used antibody visualized the entire amount of collagen type II residing in the constructs, even before initial cell reseeded and stimulation. Hence, it is plausible that a 5 weeks culture period was simply not long enough to not only ensure adequately differentiated hASCs, which is generally considered to take 3 to 4 weeks [502]–[505], but also give enough time to produce sufficient amounts of newly formed collagen type II to overcome the background from the initial collagen type II, making up the bulk in the graft. Another possible reason for insufficient production of collagen type II might be the overall cell number. Although cells migrated into the scaffold and repopulated AuriScaff's matrix, fewer cells were present in the cartilage disc than initially expected and tested in preliminary experiments (**Fig. S3**). A reason for this might be the

polyurethane support scaffold as well as joining fibrin glue necessary for the force transmission of the biomimetic bioreactor. While channel diameter in the cartilage disc range between 5 to 10 μm thus forcing the cells undergo extensive morphological changes during invasion, pores in the polyurethane support scaffold range from 90 to 300 μm thus facilitate easy migration. As a result, reseeded cells are likely to also populate the polyurethane scaffold. To overcome this limitation, higher cell seeding densities are necessary in future studies.

Beside histological investigation, gene expression analysis of known cartilage specific markers was performed to gain further insight into the effects of stimulation on the reseeded cartilage-polyurethane grafts. Cartilage specific markers (COL2, ACAN, SOX9) were generally significantly higher expressed in dynamically loaded groups than in free swelling controls (**Fig. 35**). This observation is in accordance with studies found in literature [472], [476], [481], [482], [506] that used comparable stimulation patterns. However, dedifferentiation markers (COL1 and VCAN) have been upregulated in loaded groups too, although to a lesser extent than the cartilage specific markers. COL1 gene expression pattern matches observations that have already been reported by groups using collagen hydrogels [507], [508]. Besides reports of upregulated COL1 in the loaded groups, a study suggested that VCAN is predominantly accumulated by cells in early stages of hyaline cartilage formation [509]. Although VCAN is generally expressed at low levels in mature articular cartilage [510] it has been shown to be expressed during chondrogenesis, particularly in differentiating cells undergoing pre-cartilage mesenchyme condensation, a precursor stage to chondrocyte differentiation [511]. Interestingly, we observed almost no difference for investigated genes in loaded groups cultured with 1 or 10 ng/mL GFs. Regarding the COL2/COL1 ratio, the loaded group supplemented with low GFs showed significant differences compared to the respective unloaded control, which was not apparent for groups with no or high GFs. This effect has already been described in different studies and reported as masking effect [475], [506], [512], where using higher concentrations of TGF- β in combination with mechanical load resulted in a lower change in gene expression to corresponding controls than using mechanical loading alone. This was also true for this study; while loaded groups cultured in medium with low GF concentrations had generally the highest gene expression of all investigated markers, groups cultured with higher GF concentrations were generally below these levels. An explanation for this effect can be found in literature. While mature articular cartilage contains a large pool of TGF- β , only a small proportion is readily accessible [513]. A study conducted by Albro *et al.* [514] discovered that even though around 68 ng/mL TGF- β 1 is present in articular cartilage less than 2% is in its active state. Thus, the physiological level of active TGF- β 1 is approximately 1 ng/mL.

Beside TGF- β 1, TGF- β 3 is an additional prominent member of the TGF- β family and important for cartilage engineering. Several reviews have outlined the significance of both TGF- β isoforms during condensation, proliferation, terminal differentiation and as well in maintenance of a chondrogenic phenotype [515]–[520]. Pre-chondrocyte condensation studies observed initiation of mesenchymal

condensation [521] as well as chondrogenesis [522] via TGF- β 1 while TGF- β 3 could simultaneously already accumulated twice as much glycosaminoglycan content [523] and was predominantly responsible for proteoglycan synthesis [524]. In postnatal/mature articular cartilage, TGF- β 3 inhibits terminal differentiation of chondrocytes [525] while TGF- β 1 already arrests differentiation at an early stage of hypertrophy [526]. In this study we used TGF- β 3 to induce chondrogenesis in hASCs and further differentiate them into mature chondrocytes previously shown in several studies [492], [527], [528]. However, addition of exogenously TGF- β 3 masks endogenously produced TGF- β 3. Hence, the chondroinductive environment generated via the combined effect of loading and GF addition was assessed via TGF- β 1 concentration in the medium. Interestingly, although higher TGF- β 3 concentrations seems to have no beneficial effect on gene expression of loaded groups due to the previously discussed masking effect, it did affect the amount of active TGF- β 1 in both assessed timepoints (**Fig. 36**). Higher GF concentrations in the medium led to increasing TGF- β 1 concentration in the active state as well as for total protein. This trend was clearly visible for dynamically loaded groups but also apparent in free swelling cultured control samples. However, after 3 weeks of culture, only cells subjected to mechanical loading converted latent TGF- β 1 into an active protein, while free swelling cultured cells had almost no active TGF- β 1, although a higher amount of latent TGF- β 1 was initially present. This loading dependent activation of latent TGF- β 1 has already been described by several groups either *in vitro* [529], [530] or *in vivo* [531], [532] thus contributing to the generally accepted opinion that mechanical stimulation is a necessary tool for healthy chondrogenesis and tissue maturation.

Originally, the here described AuriScaff was developed to perfectly mimic articular cartilage structure and provide an optimal environment regarding spatial organization and differentiation for repopulating cells. The initial driving force was to develop a scaffold that provides the possibility to be applied in a one-step surgical clinical procedure [533]–[535] but also possess the mechanical strength to instantaneously sustain the physical load in the joint thus resembling native hyaline cartilage best. Closing the gap between native hyaline cartilage and currently applied scaffolds would not only reduce the risk of graft failure but also shorten duration of post-surgery physiotherapy. In this notion we have shown that the reseeded AuriScaff is a promising candidate for cartilage regeneration. Besides being mechanical stable over the full time course of the experiment, chondrogenesis was not only triggered by biological factors as already reported in previous studies [475], [481] but was further enforced by the addition of mechanical stimuli. Especially in low GF concentrations mechanical load revealed to be a potent chondroinductive trigger. This is in accordance with the principle notion that mechanical stimulation has a positive effect on chondrogenesis in recent years [536].

However, for translational studies into clinics there is the need to prove whether the beneficial effects of a one-step surgical procedure with immediate loading outweighs an approach that is including an

unloaded pre-differentiation phase *in vitro* to increase functionality of the repopulated grafts [504] prior to implantation.

5 Conclusion/Outlook

In conclusion, a recently developed devitalized auricular cartilage scaffold was repopulated with hASCs and mechanically stimulated using a bioreactor system that mimics the loading environment of articular hyaline cartilage. So far, in previous experiments we showed that the enzymatically perforated cartilage matrix shows chondroinductive properties in *in vitro* and *in vivo* set-ups under unloaded conditions [464], [467]. For the first time we investigated the fate of repopulated mesenchymal stem cells under physiological loading of the grafts. We could demonstrate that stimulation comparable to the walking motion of a healthy person further enhanced the chondrogenic differentiation of the repopulated hASCs. The logical next step will be *in vivo* studies, where the cells are not only exposed to mechanical loading but additionally to the synovial knee environment.

6 Acknowledgments

Financial support by the Austrian Research Agency FFG (CartiScaff, #842445) as well as the Lorenz Böhler Fonds (16/13) and the City of Vienna Competence Team Project signalTissue (MA23, #18-08) is gratefully acknowledged. Human adipose tissue derived stromal cells (hASCs) were kindly provided by Gudrun Hager from the Ludwig Boltzmann Institute for Experimental and Clinical Traumatology in cooperation with Red Cross Blood Transfer Service of Upper Austria. Further we would like to thank Barbara Schädler from the University Clinic of Dentistry, Department of Histology for preparation of various histological stainings.

7 Competing interests

The authors declare no competing interests.

8 Supplemental Information

8.1 Supplemental Figures

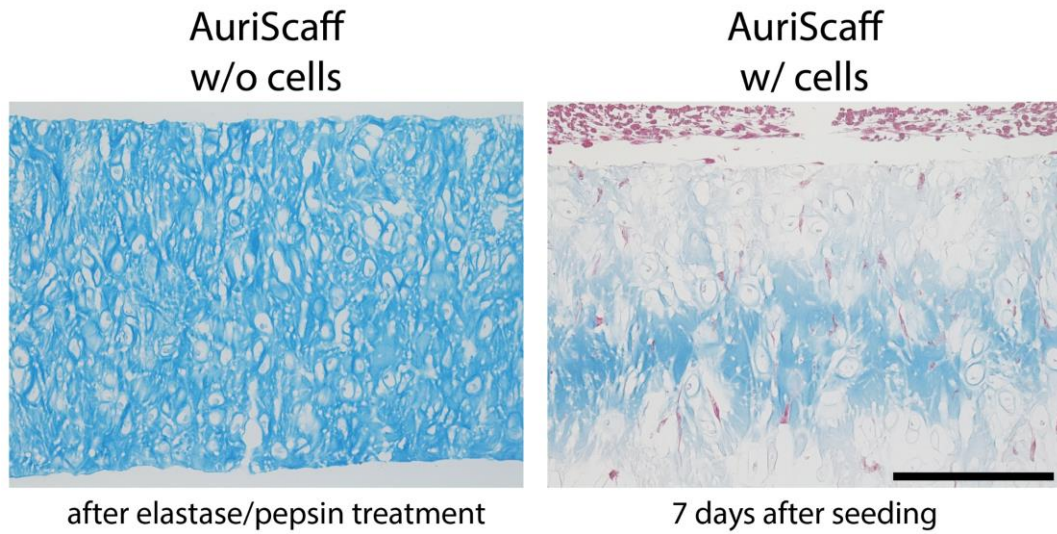


Fig. S3. Representative pictures of bovine auricular scaffold before and after repopulation with hASC stained with AZAN. Elastase/pepsin treatment: Bovine auricular cartilage was treated with a mixture of pepsin and elastase and devitalized with a series of freeze and thaw cycles. This treatment removed elastic fibers and glycosaminoglycans thus providing hollow channels for cells to invade. Reseeding: AuriScaff after a repopulation period of 7 days with hASCs. hASC successfully invaded the entire scaffold via created channels. Scale Bar = 100 μ m.

CHAPTER III

**Effect of hydrostatic pressure-generated
reactive oxygen species
on neo-cartilage formation.**

Hydrostatic pressure-generated reactive oxygen species induce osteoarthritic conditions in cartilage pellet cultures

Bernhard Rieder^{1,5}, Anna M. Weihs^{1,5}, Adelheid Weidinger^{2,5}, Dorota Szwarc^{1,5}, Sylvia Nürnberger^{2,3,4,5}, Heinz Redl^{2,5}, Dominik Rünzler^{1,5}, Carina Huber-Gries^{1,5}, Andreas H. Teuschl^{1,5,*}

¹ Department Life Science Engineering, University of Applied Sciences Technikum Wien, 1200 Vienna, Austria

² Ludwig Boltzmann Institute for Experimental and Clinical Traumatology, AUVA Research Center, 1200 Vienna, Austria

³ Department of Orthopedics and Trauma-Surgery, Division of Trauma-Surgery, Medical University of Vienna, 1090, Vienna, Austria

⁴ University Clinic of Dentistry, Medical University of Vienna, 1090, Vienna, Austria

⁵ Austrian Cluster for Tissue Regeneration, 1200, Vienna, Austria

* corresponding author: teuschl@technikum-wien.at

Published in *Scientific Reports* on November 19th, 2018

Abstract

Osteoarthritis (OA) is one of the most common causes of disability and represents a major socio-economic burden. Despite intensive research, the molecular mechanisms responsible for the initiation and progression of OA remain inconclusive. In recent years experimental findings revealed elevated levels of reactive oxygen species (ROS) as a major factor contributing to the onset and progression of OA. Hence, we designed a hydrostatic pressure bioreactor system that is capable of stimulating cartilage cell cultures with elevated ROS levels. Increased ROS levels in the media did not only lead to an inhibition of glycosaminoglycans and collagen II formation but also to a reduction of already formed glycosaminoglycans and collagen II in chondrogenic mesenchymal stem cell pellet cultures. These effects were associated with the elevated activity of matrix metalloproteinases as well as the increased expression of several inflammatory cytokines. ROS activated different signaling pathways including PI3K/Akt and MAPK/ERK which are known to be involved in OA initiation and progression. Utilizing the presented bioreactor system, an OA *in vitro* model based on the generation of ROS was developed that enables the further investigation of ROS effects on cartilage degradation but can also be used as a versatile tool for anti-oxidative drug testing.

1 Introduction

Osteoarthritis (OA) is the most common type of arthritis, affecting 25% of the adult population. It has been forecast that in the US alone, approximately 50 million people will suffer from OA by the year 2020 [537], [538]. This degenerative joint disease is predominantly observed in elderly people, which historically resulted in the hypothesis that OA is a simple “wear-and-tear” disease of articular cartilage [539], [540]. It was believed that the loss of articular cartilage subsequently results in altered biomechanics combined with cellular changes which over time lead to severe changes of the subchondral bone, synovium, menisci, ligaments, periarticular muscles and nerves [541]. This hypothesis is supported by results of *in vivo* models which induce mechanical instability of the knee joint, e.g. by transection of the anterior cruciate ligament [542], [543] to promote excessive wear of cartilage structures.

Lately, OA has increasingly become regarded as an inflammation process causing an imbalance in the homeostasis of articular chondrocytes, ultimately resulting in progressive loss and destruction of articular cartilage. Similar to rheumatoid arthritis (RA), OA is associated with synovial inflammation but generally to a lesser extent (lower number of synovial fluid leukocytes than in RA). In contrast, OA is characterized by high levels of a number of pro-inflammatory cytokines and chemokines which result in the production of extracellular matrix-degrading enzymes such as matrix metalloproteinases (MMPs) responsible for the loss of articular cartilage [541].

Despite over 20 years of research, the molecular mechanisms responsible for OA initiation and progression remain poorly understood. Nevertheless, it is now well accepted that the pathogenesis of OA is much more complex than just a wear and tear and that mechanical factors in the form of excessive and abnormal joint loading play a crucial role.

In this regard, different *in vivo* and *in vitro* OA models have been established to decipher the roles of specific factors contributing to the disease.

Most *in vitro* OA models use cartilage explants, primary (osteoarthritic) chondrocytes or mesenchymal stem cells (MSC) differentiated into the chondrogenic lineage and can be grouped according to the trigger utilized in the initiation of the catabolic process. The majority of studies involve the use of either cytokine treatment alone (such as the addition of pro-inflammatory cytokines IL-1 β or TNF- α) or in combination with physical stimulation, such as osmotic pressure, physical injury/deformation and mechanical loading regimes [544]–[546]. In this regard cyclic hydrostatic pressure has been shown to increase both the production of nitric oxide as well as proteoglycan synthesis [547] and to change the cellular ultrastructure [548], [549] of IL-1 β -treated osteoarthritic chondrocytes. These findings underline the importance of mechanical stimulation on the homeostasis of not only healthy but also osteoarthritic chondrocytes.

In the last decade a number of studies have demonstrated that reactive oxygen species (ROS) are involved in the initiation and progression of OA [550], [551]. So far only a few studies use adequate and physiological *in vitro* models to simulate elevated ROS-levels to generate an OA model. In select studies osteoarthritic chondrocytes are generated by application of H₂O₂ [552]–[556], which is based on *in vivo* production of H₂O₂ by neutrophils and macrophages or by chondrocytes themselves in inflamed knee joints. In this regard, chondrocytes have been shown to produce superoxide radicals by activation of NADPH oxidase (nicotinamide adenine dinucleotide phosphate oxidase) [557], which can subsequently dismutate into H₂O₂. Moreover, Regan *et al.* demonstrate that joint fluids of OA patients are characterized by significantly decreased extracellular superoxide dismutase (SOD) levels compared to samples from healthy patients [558], [559], indicating a crucial role of uncontrolled superoxide levels in the initiation of OA.

Here we demonstrate that the application of hydrostatic pressure (HP) by compressed air induced the production of elevated levels of superoxide and other ROS species (determined via electron paramagnetic resonance measurements), which subsequently hindered chondrogenic development of MSC pellet cultures by downregulating expression of cartilage specific proteins, such as collagen type II and glycosaminoglycans, and upregulating expression of collagen type I, matrix metalloproteinases and inflammatory cytokines. Moreover, the analysis of crucial signaling pathways revealed that applied hydrostatic pressure caused an enhanced activation of the OA-associated pathways MAPK/ERK and PI3K/Akt.

In this study, to the best of our knowledge, we are the first to show that acellular superoxide formation induced by a custom-made hydrostatic pressure system generates a degenerative OA-like environment for chondrogenic MSC pellets.

2 Materials and Methods

If not indicated otherwise, all chemicals and reagents were purchased from Sigma Aldrich (St. Louis, MO, USA) and were of analytical grade.

2.1 Cell isolation and culture

Human adipose tissue derived stromal cells (hASCs) were kindly provided by the Ludwig Boltzmann Institute for Experimental and Clinical Traumatology in cooperation with Red Cross Blood Transfer Service of Upper Austria. Cell isolation was performed in accordance with the relevant guidelines and regulations as described in Wolbank *et al.* [470] with authorization of the local ethics committee (Province of Upper Austria) and informed consent of the donor. Briefly, the stromal vascular fraction was obtained via several washing steps of lipoaspirate with phosphate-buffered saline (PBS) followed by enzymatic digestion of the tissue. Subsequently, the cellular fraction was seeded on plastic dishes, allowing for selection between plastic-adherent and non-adherent cells. The plastic-adherent hASCs

were further cultivated and frozen, according to the laboratory-specific standard operating procedures (SOPs).

For expansion, hASCs were cultured in DMEM:F12 (Lonza, Basel, Switzerland) supplemented with 10% foetal bovine serum (FBS; GE Healthcare, Little Chalfont, United Kingdom), 1% Penicillin-Streptomycin (P/S; Lonza, Basel, Switzerland) and 5 ng/mL basic fibroblast growth factor (bFGF; PeproTech, Rocky Hill, NJ, USA). This medium will be further referred to as expansion medium (EM). Cells were expanded on standard cell culture dishes (STARLAB, Hamburg, Germany) in a humidified incubator at 37 °C and 5% CO₂. To avoid premature differentiation, cells were subcultured at 80-85% confluence. When the desired cell concentration was reached, hASCs were transferred into round bottom 96-well plates (SPL Life Sciences, Korea) and spun down for 5 min at 300 xg to form cell pellets. Each well contained 2.5×10^5 cells and pellets were fully formed within 3 days after centrifugation. Pellets were differentiated with DMEM (Lonza, Basel, Switzerland) supplemented with 2 mM L-glutamine (Lonza, Basel, Switzerland), 1% P/S (Lonza, Basel, Switzerland), 1 mM sodium pyruvate, 10 mM HEPES, 50 µg/mL proline, 1x Insulin-transferrin-sodium selenite (ITS+3), 100 nM dexamethasone (DEX), 170 µM ascorbic acid (AA), 10 ng/mL transforming growth factor-β 3 (TGF-β3; PeproTech, Rocky Hill, NJ, USA) and 10 ng/mL bone morphogenetic protein 6 (BMP6; PeproTech, Rocky Hill, NJ, USA) for a total of 42 days. This medium will be further referred to as differentiation medium (DM). A partial medium change was performed on day 2 followed by a total medium changed every 3-4 days until the end of the experiment.

2.2 Custom-made hydrostatic pressure system

The pressure chamber (**Fig. 37A**) consists of a milled aluminium baseplate which fits any type of multi-well plate ranging from 6 to 96 wells. The pressure is flushed into the inner chamber via inlets inside the walls of this baseplate. For uniform air and equal pressure distribution, each side is equipped with 2 inlet ports, which sums up to 8 inlet ports in total. The pressure chamber is closed with an acrylonitrile butadiene styrene (ABS) cover plate (**Fig. 37B**). The cover plate has 6 outlet ports on the top side which are regularly distributed to allow for uniform air exhaust. To provide an airtight seal, the pressure chamber has an O-ring seal between the two components of the chamber. The ABS cover plate is fastened with 12 stainless steel screws.

The pressure is regulated via two solenoid valves (Bürkert, Ingelfingen, Germany), one before the inlet ports and one after the inlet ports of the chamber (**Fig. 37C**). The valves are controlled by a microcontroller (Microchip Technology Inc., Chandler, AZ, USA), running a customized program coded in C. The user accesses the microcontroller via a graphical user interface (GUI) coded in C# with Visual Studio (Microsoft, Redmond, WA, USA). The program was specifically designed to enable the user to define the critical experiment parameters like pressure, cycle time, and total stimulation period. Furthermore, the GUI displays the pressure in real-time, which is measured by a pressure transducer (RS Components, Corby, UK) attached to the pressure chamber.

The pressure is generated by a commercially available air-cooled gas compressor (Jun-Air, Redditch, UK) (**Fig. 37D**) that draws in air from the incubator and compresses it to a maximum pressure of 8 bars. The air is moisturized in a custom-made humidifier to prevent evaporation of the medium in the wells inside the pressure chamber. After passing the pressure chamber, the air gets transferred back into the incubator, closing the loop.

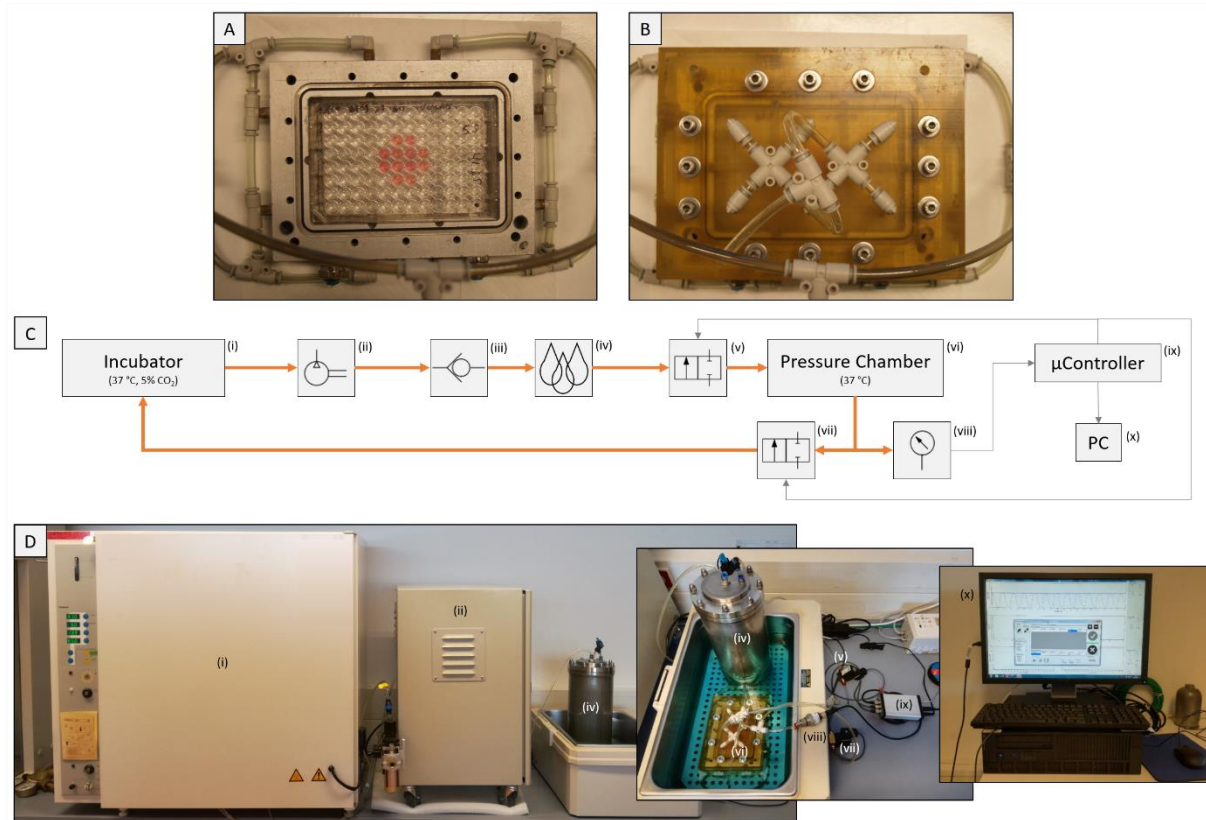


Fig. 37. The hydrostatic pressure bioreactor system. (A) Aluminum baseplate of the pressure chamber with a total of 8 inlet ports (2 inlet ports on each side) for uniform air and pressure distribution within the chamber. The baseplate is housing the pellet culture (1 pellet per well filled with 250 μ L of medium) in a 96 well plate. (B) The pressure chamber is closed with an ABS cover plate, which has a total of 6 outlet ports on top for fast and uniform air exhaustion. The cover plate is fastened with 12 stainless steel screws on the baseplate and an O-ring seal provides an airtight seal. (C) A schematic view of the custom-made bioreactor system: The incubator (i) provides CO₂ buffered air which can be pressurized up to 8 bars in the compressor (ii) and is forwarded to the humidifier (iv). A back-pressure valve (iii) was integrated to allow only unidirectional flow to the humidifier. Then the moistened air is introduced into the pressure chamber (vi) and the maximum pressure value as well as the planned regime is controlled via the inlet (v) and outlet (vii) solenoid valves. The pressure chamber, which contains the stimulated pellets, can house any standard well plate format (96- to 6-well plates). The pressure in the chamber is measured with a pressure transducer (viii) and measured values are processed in the μ Controller (ix) which controls the two solenoid valves according to the regime set by the user via the GUI/PC (x). (D) Assembled bioreactor system necessary to stimulate pellets. Humidifier and pressure chamber were placed in a waterbath to keep medium temperature constant at 37 $^{\circ}$ C.

2.3 Experimental plan and mechanical stimulation protocol

hASCs were cultured for 2-3 weeks until desired cell concentration was reached. Then, cells were harvested and spun down to form pellets. The day of harvesting and pelleting was defined as day 0 of the experiment. Pellets were divided into 3 experimental groups (no stimulation, HP stimulation, no stimulation for 21 days followed by 21 days of stimulation) (**Fig. 38A**) and cultured until day 42 with

sample harvest every seven days. All experimental groups were subjected to DM for the complete period of the experiment.

HP-stimulated pellets were subjected to 4 hours of intermitted stimulation in a 2 s on/off manner with a maximum and minimum pressure of 4 and 0 bars, respectively. Each stimulation phase was followed by a no pressure period of 20 hours. This regime was repeated on 5 consecutive days per week. This pattern was repeated until the end of the experiment on day 42 (**Fig. 38B**).

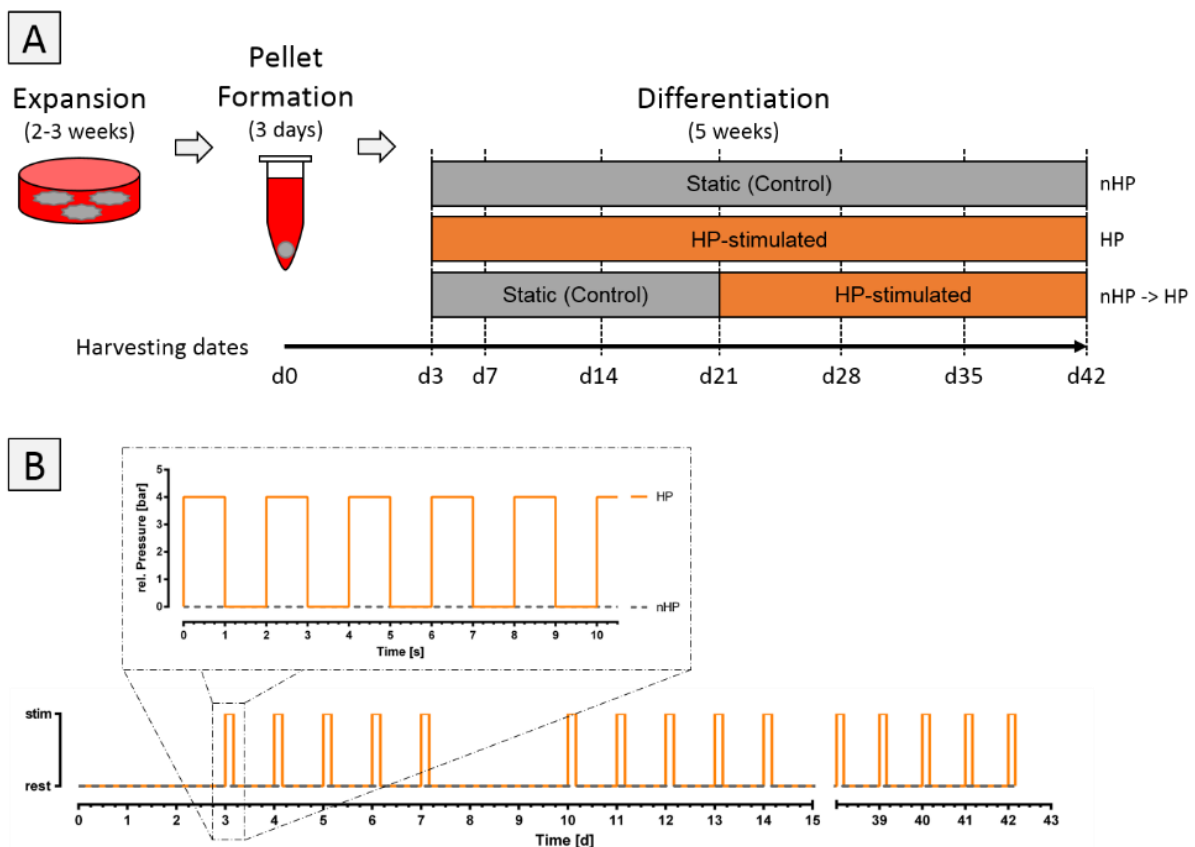


Fig. 38. Experimental study set-up. (A) Human ASCs were cultured for 2-3 weeks until desired cell concentration was reached. Then, 250,000 cells per pellet were spun down to induce pellet formation, which was completed within 3 days. Pellets were divided into 3 groups: unstimulated static control for 42 days (nHP), hydrostatic pressure stimulated (HP) for 42 days, no stimulation for 21 days followed by HP stimulation for 21 days (nHP→HP). Pellets were harvested on day 0 and day 3 and day 7 and from then on every 7th day for the total period of the experiment. (B) The hydrostatic pressure stimulation protocol. After 3 days of initial pellet formation, pellets were subjected to 4 hours of intermitted stimulation in a 2 s on/off manner with a maximum and minimum pressure of 4 and 0 bars, respectively. Each stimulation phase was followed by a no pressure period of 20 hours. This regime was repeated for 5 consecutive days per week. This pattern was repeated until the end of the experiment on day 42.

2.4 Histology and immunohistochemical (IHC) analysis

Harvested pellet cultures were fixed in 4% formaldehyde (Histofix®, Roth, Karlsruhe, Germany) for 24 hours at 4 °C and dehydrated with a graded series of ethanol steps (50% to 100%). Samples were embedded in paraffin, sectioned to 5 µm, and mounted on glass slides. To proceed with distinct

stainings, sections were deparaffinized with xylene (Roth, Karlsruhe, Germany) and rehydrated with a graded series of ethanol washes to distilled water. Glycosaminoglycans (GAGs) were detected by Alcian blue staining. Briefly, Alcian blue stain was performed by Alcian blue 8GX (Sigma, St. Louis, MO, USA) for 30 min followed by rinsing with distilled water till the sections were clean. Then, slides were counterstained with Mayers Hemalum (Roth, Karlsruhe, Germany) for 2 min and rinsed in running tap water for 10 min. Afterwards, sections were dehydrated with a graded series of ethanol washes, cleared with xylene (Roth, Karlsruhe, Germany) and covered with a glass slide.

Collagen types I and II were detected via IHC staining in order to assess the quality of cartilage tissue formation of the pellet cultures. Briefly, collagen type I staining was performed by drying paraffin coated samples at 40 °C overnight while collagen type II staining was dried for 30 min at 60 °C. Then samples were deparaffinized and endogenous peroxidase was blocked with 3% H₂O₂ (Thermo Fisher, Waltham, MA, USA) for 10 min and rinsed with distilled water. Slides were either steamed for 20 min in trisodium citrate buffer (pH 6.0) (ZUC028-500, Zytomed, Berlin, Germany) for collagen type I or treated with pepsin solution (Thermo Fisher, Waltham, MA, USA) for 10 min at 37 °C for collagen type II followed by rinsing for 5 min with tris-buffered saline (TBS). Samples were incubated in horse serum (S-2012, Vector Laboratories, Burlingame, CA, USA) for 20 min, incubated with the primary antibody (rabbit polyclonal anti-collagen 1 (Abcam, Cambridge, United Kingdom); mouse monoclonal anti-collagen 2 (MS-306-PO, Thermo Fisher, Waltham, MA, USA)) for 1 hour at room temperature (RT), rinsed with TBS for 5 min and incubated with the secondary antibody (collagen type I: goat anti-rabbit peroxidase labelled IG (Agilent Technologies, Santa Clara, CA, USA); collagen type II: goat anti-mouse peroxidase labelled IG (K4001, Agilent Technologies, Santa Clara, CA, USA)) for 30 min at RT, followed by rinsing with TBS for 5 min. For detection, slices were incubated for 3 min with 2-3 drops of VECTOR NovaRED (Vector Laboratories, Burlingame, CA, USA) and the reaction was stopped by submerging in water for 10 min. Afterwards, slides were counterstained with Hemalum (Roth, Karlsruhe, Germany) for 1 min and blueed for 10 min in tap water. Slides were dehydrated, cleared with xylene (Roth, Karlsruhe, Germany) and covered with a glass slide.

2.5 Determination of reactive oxygen species (ROS) via electron paramagnetic resonance (EPR) measurements

Differentiation medium was incubated with 500 µM of the spin probe cyclic hydroxylamine 1-hydroxy-3-carboxy-2,2,5,5-tetramethylpyrrolidine hydrochloride (CP-H; Noxygen, Elzach, Germany) for 4 hours under stimulated (4 bars, 2 s/2 s pattern) or under static condition. Additionally, to further clarify the underlying mechanisms, the iron chelator diethylenetriaminepentaacetic acid (DTPA), superoxide dismutase (SOD) or both DTPA and SOD were added to the medium. For analysis, medium was placed in 100 µL portions of 1 mL disposable pipettes (VWR International, Radnor, PA, USA) and snap frozen in liquid nitrogen. EPR spectra of frozen samples were recorded at 3359 ± 200 G using the Magnettech MiniScope MS 200 EPR spectrometer (Magnettech Ltd., Berlin, Germany)[560]. The general settings were as follows: modulation frequency 100 kHz, microwave frequency 9.425 GHz, microwave power

11 mW, modulation amplitude 7 G. The magnitude of oxidized CP-H (3-CP) signals was calculated and is expressed in arbitrary units (AU).

2.6 Quantitative reverse transcription polymerase chain reaction (RT-qPCR)

Cells were harvested on day 0, 21, and 42 by mincing the pellets with tissue grinding beads (Bertin corp., Rockville, MD, USA) in a tissue homogenizer (Precellys®24; Bertin corp., Rockville, MD, USA) followed by total mRNA extraction using the peqGOLD Total RNA Kit (VWR International, Radnor, PA, USA). RNA was measured using a NanoPhotometer (Implen GmbH, München, Germany) and 1 µg of mRNA was transcribed into cDNA using EasyScript™ cDNA Synthesis Kit (abm, Richmond, BC, Canada) using oligo(dT) primers. Quantitative PCR was performed using KAPA SYBR® FAST qPCR Kit (VWR International, Radnor, PA, USA) with a Stratagene© Mx3000P QPCR System (Agilent, Santa Clara, CA, USA) according to the manufacturer's instructions using 10 ng of cDNA per reaction. Thermal cycle conditions were 5 min at 95 °C followed by 40 cycles of 10 s at 95 °C and 30 s at 60 °C (B2M, MMP3, RUNX2, IL6) or 30 s at 95 °C and 1 min at 60 °C (ACAN, COL1A1, COL2A1, COL10A1, SOX9, MMP9, MMP13, IL-1β, IL-6, TNF-α). For time-dependent expression profiles, target genes were normalized to the housekeeper β2-microglobulin (B2M) and compared to corresponding values of day 0 using the comparative CT (ΔΔCT) method. Primer sequences and primer concentrations used are listed in **Table 3**.

Table 3: Primer sequences and concentrations used for qPCR.

Target	Primer forward	Primer reverse
B2M	GATGAGTATGCCTGCCGTGT	TGCGGCATCTTCAAACCTCC
ACAN	CCCCTGCTATTTTCATCGACCC	GACACACGGCTCCACTTGAT
COL1A1	GATCTGCGTCTGCGACAAC	GGCAGTTCTTGGTCTCGTCA
COL2A1	AGACTTGCGTCTACCCCAATC	GCAGGCGTAGGAAGGTCATC
COL10A1	CATAAAAGGCCCACTACCCAAC	ACCTTGCTCTCCTCTTACTGC
SOX9	AGCGAACGCACATCAAGAC	CTGTAGGCGATCTGTTGGGG
MMP3	ATGCCCACTTTGATGATGATGAAC	CCACGCCTGAAGGAAGAGATG
MMP9	GTACTCGACCTGTACCAGCG	TTCAGGGCGAGGACCATAGA
MMP13	CCAGACTTCACGATGGCATTG	GGCATCTCCTCCATAATTTGG C
RUNX2	CCGTCTTCACAAATCCTCCCC	CCCGAGGTCCATCTACTGTAA C
IL-1β	CAACAGGCTGCTCTGGGATT	GTCCTGGAAGGAGCACTTCAT
IL-6	AGTTCCTGCAGAAAAGGCAAAG	CATTTGCCGAAGAGCCCTCA
TNF-α	TCTCCTTCTGATCGTGGCA	GGGTTTGCTACAACATGGGCT

2.7 Quantification of matrix components

Biochemical assays were performed to quantify GAG and DNA content. Therefore, pellets were flash frozen in liquid nitrogen and digested with ≥30 units/mL proteinase K buffered in 50 mM TRIS, 1 mM EDTA, 1 mM iodoacetamide and 10 µg/mL pepstatin A at 56 °C overnight.

2.7.1 GAG quantification

GAG content of pellet cultures was determined using a dimethylmethylene blue (DMMB)-based staining assay. Briefly, 5 μL of the proteinase K-digested sample were diluted with 95 μL phosphate buffered EDTA (100 mM Na_2HPO_4 and 10 mM EDTA in PBS) in a flat bottom 96-well plate and a dilution series with chondroitin-4-sulfate in 1.75 mg/mL cysteine was made as standard. Both, 100 μL of diluted sample and standards were mixed with 200 μL DMMB solution (38.5 μM DMMB, 1% EtOH, 40.5 mM NaCl, 40.5 mM Glycine, and 9.5 mM Acetic Acid in ddH₂O) and absorbance of samples was measured at 540 nm against 595 nm as reference wavelength using a plate reader (Sunrise Basic; Tecan Trading AG, Männedorf, Switzerland).

2.7.2 DNA quantification

DNA present in the pellets was quantified using the QuantiFluor® dsDNA kit (E2670; Promega, Madison, WI, USA). Briefly, 5 μL of proteinase K digested sample were diluted with 95 μL 1X tris-EDTA (TE) buffer in a black flat bottom 96-well plate and a standard curve was generated using provided Lambda DNA Standard. Sample and standards were mixed with 100 μL of 1X QuantiFluor® dsDNA dye and incubated for 5 min at room temperature (RT) in the dark before fluorescence measurements (Blue Fluorescence Optical Kit; 490 nm_{Ex}/510–570 nm_{Em}) using the GloMax®-Multi+ Detection Systems (Promega, Madison, WI, USA) were performed.

2.7.3 Viability assessment

Cell viability in pellets was assessed with a colorimetric assay using the standard Methylthiazolyldiphenyl-tetrazolium bromide (MTT) method. Therefore, pellets were stimulated for 4 hours (4 bars, 2 s/2 s pattern) or cultured under static conditions. Pellets were transferred into a 48 well plate and incubated for 2 hours with 500 μL of MTT working solution (650 mg/mL MTT in ddH₂O). MTT working solution was discarded and generated formazan was dissolved in 500 μl DMSO for 1 hour. Absorbance was measured at 540 nm wavelength using a plate reader.

2.8 Western Blot

PBS-washed pellets were flash frozen in liquid nitrogen and crushed into powder with tweezers. The powder was reconstituted in Nonidet P-40 buffer containing 40 mM HEPES (pH 7.9), 120 mM NaCl, 1 mM EDTA (pH 8.0), 10 mM 2-glycerolphosphate, 50 mM NaF, 0.5 mM Na_3VSO_4 , 1% Nonidet P-40 substitute, and 1 mM Phenyl-Methyl-Sulfonyl Fluoride (PMSF) supplemented with 2 $\mu\text{g}/\text{mL}$ aprotinin, 2 $\mu\text{g}/\text{mL}$ leupeptin, 0.3 $\mu\text{g}/\text{mL}$ benzamidine chloride, and 10 $\mu\text{g}/\text{mL}$ trypsin inhibitor and lysed. Total protein of pellets was extracted by several freeze and thaw cycles. The protein extract was incubated on ice for 1 hour and centrifuged at 22,000 $\times g$ for 20 min at 4 °C. The supernatant of each sample was collected, transferred into a new vial and protein concentration was determined on a NanoPhotometer (Implen GmbH, Munich, Germany) using Bradford assay (Protein Assay Dye Reagent Concentrate; Bio-Rad, Hercules, CA, USA) according to manufacturer's instructions. Equal amounts of protein (10 $\mu\text{g}/\text{lane}$) were applied to each lane on a SDS-polyacrylamide gel (10% running gel and 5% stacking

gel) and run at increasing voltages (60, 80, 100 V). Then, the protein was transferred onto a nitrocellulose membrane (GE Healthcare, Little Chalfont, United Kingdom) and blocked with 5% milk powder in TBS buffer with 0.1% Tween (TBS/T). Primary antibodies were incubated at 4 °C overnight in 5% BSA in TBS/T and secondary antibodies were incubated at RT for 1 hour in 5% milk in TBS/T. Signals were detected using the Odyssey® Fc Imaging System (LI-COR, Lincoln, NE, USA) and assessed with Image Studio Lite (LI-COR, Lincoln, NE, USA) to generate ratios of phosphorylated protein to the total protein or housekeeper. Antibodies for phospho-AKT (Ser-473), total AKT, phospho-p44/42 MAPK (Thr-202/Tyr-204) (phospho-Erk1/2), total p44/42 MAPK (total ERK1/2), phospho-p38 MAPK (Thr-180/Tyr-182), total p38 MAPK, phospho-S6 ribosomal protein (Ser-240/244), total S6 ribosomal protein, β -Catenin, and GAPDH were obtained from Cell Signaling Technology (Danvers, MA, USA).

2.9 Statistical Analysis

Unless otherwise noted, all data are presented as mean + standard deviation (SD). All statistical calculations were performed using GraphPad Prism software (GraphPad Software Inc., San Diego, CA, USA). Normal distribution of values was tested using D'Agostino-Pearson omnibus test. Comparisons between two or multiple groups were calculated using Mann–Whitney *U* test or either one-way analysis of variance (ANOVA) with Tukey's multiple comparison test or Kruskal–Wallis test with Dunn's multiple comparison test, respectively. *P*-values < 0.05 were considered statistically significant.

3 Results

3.1 Generation of reactive oxygen species (ROS) via hydrostatic pressure (HP)

In a series of EPR-experiments, ROS-formation as a result of HP stimulation was verified and the involved reactive oxygen species and mechanisms were elucidated. Stimulation of DM resulted in approximately five times higher levels of ROS compared to unstimulated control medium (**Fig. 39A**). DTPA was added to show the involvement of iron ions in the radical generation process. The addition of the iron-chelator led to significantly lower ROS generation, whereas the addition of SOD resulted in high levels of ROS. SOD converted superoxide to hydrogen peroxide (H₂O₂), which is then further converted to hydroxyl radicals (HO[•]). The conversion of SOD was driving the main reaction of Fe²⁺ and O₂ to Fe³⁺ and superoxide, which resulted in high ROS levels (**Fig. 39B**). SOD and DTPA simultaneously added to the differentiation medium, hindered the accumulation of ROS, as the detected levels were similar to DTPA addition alone.

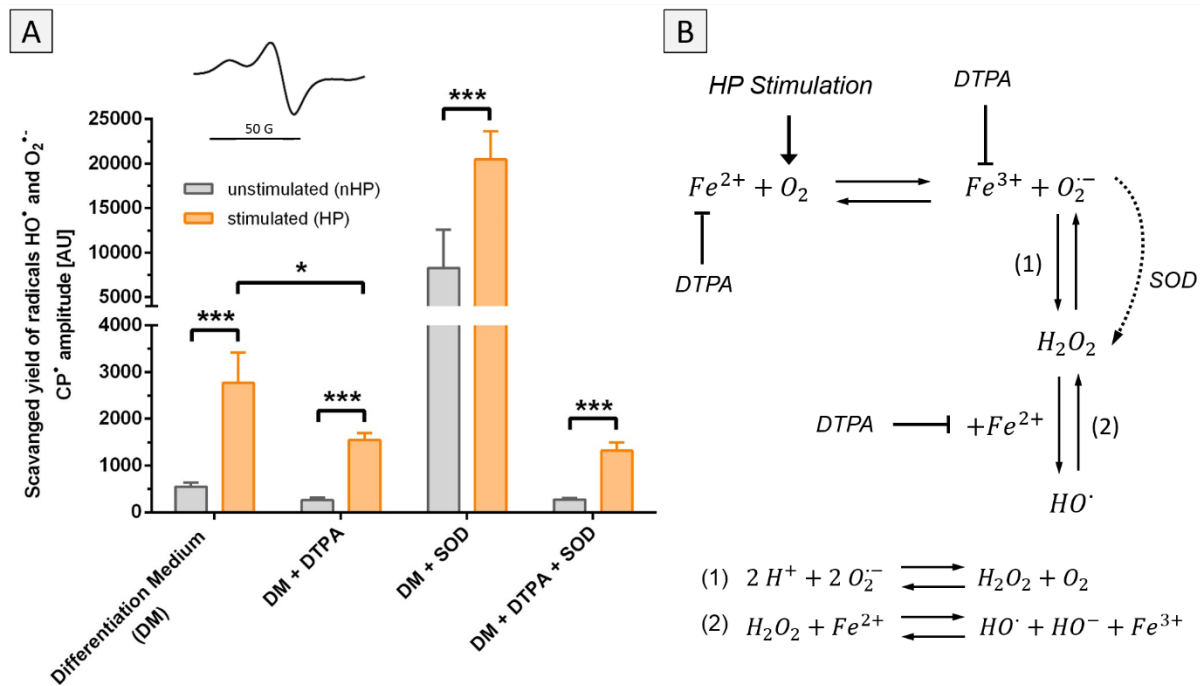


Fig. 39. Acellular ROS formation by hydrostatic pressure stimulation. (A) DM without cells was stimulated according to the described pressure regime and generated reactive oxygen species (ROS) were measured using the spin probe CPH. Pressurized DM showed a five times higher amount of ROS than unpressurized medium. Adding DTPA into the medium to capture free iron (Fe^{2+}/Fe^{3+}) led to a substantial reduction of ROS (DM+DTPA). In contrast, the addition of SOD led to an enhanced accumulation of ROS (DM+SOD). The pressurized group showed almost twice the amount of ROS in the stimulated medium compared to unstimulated medium. Adding both SOD and DTPA simultaneously (DM+DTPA+SOD) hindered the accumulation of ROS and resulted in ROS levels comparable to the group where just DTPA was added. Inset: EPR signal of 3-CP. (B) Hydrostatic pressure stimulation increases partial oxygen pressure in the medium. In combination with free iron (Fe^{2+}), superoxide ($O_2^{\cdot-}$) is generated which is further converted via SOD into hydrogen peroxide (H_2O_2). H_2O_2 can then interact with free iron (Fe^{2+}) to generate hydroxyl radicals (HO^{\cdot}). Using DTPA to bind free iron reduces production of superoxide and therefore also generation of other ROS. *p < 0.05, ***p < 0.001

3.2 HP stimulation prevents cartilage matrix formation

The influence of elevated ROS levels on cartilage matrix formation in pellet cultures was investigated by histological analysis of pellets cultured for up to 42 days. Six days after pellet formation, one group of pellets was stimulated with HP according to the described pressure regime (Fig. 38B), whereas an unstimulated group of pellets served as control. These unstimulated pellets showed increased positive stainings for both cartilage-specific extracellular matrix (ECM) components collagen II and GAGs, stained via immunohistochemistry and Alcian blue staining, respectively (Fig. 40). In contrast to unstimulated pellets, HP-treated pellets showed nearly no formation of collagen II and only low expression of GAGs. In both groups, collagen I was substantially expressed; in the stimulated group generally throughout the whole pellet, whereas in the unstimulated control group the staining was limited to the outer region of the pellet.

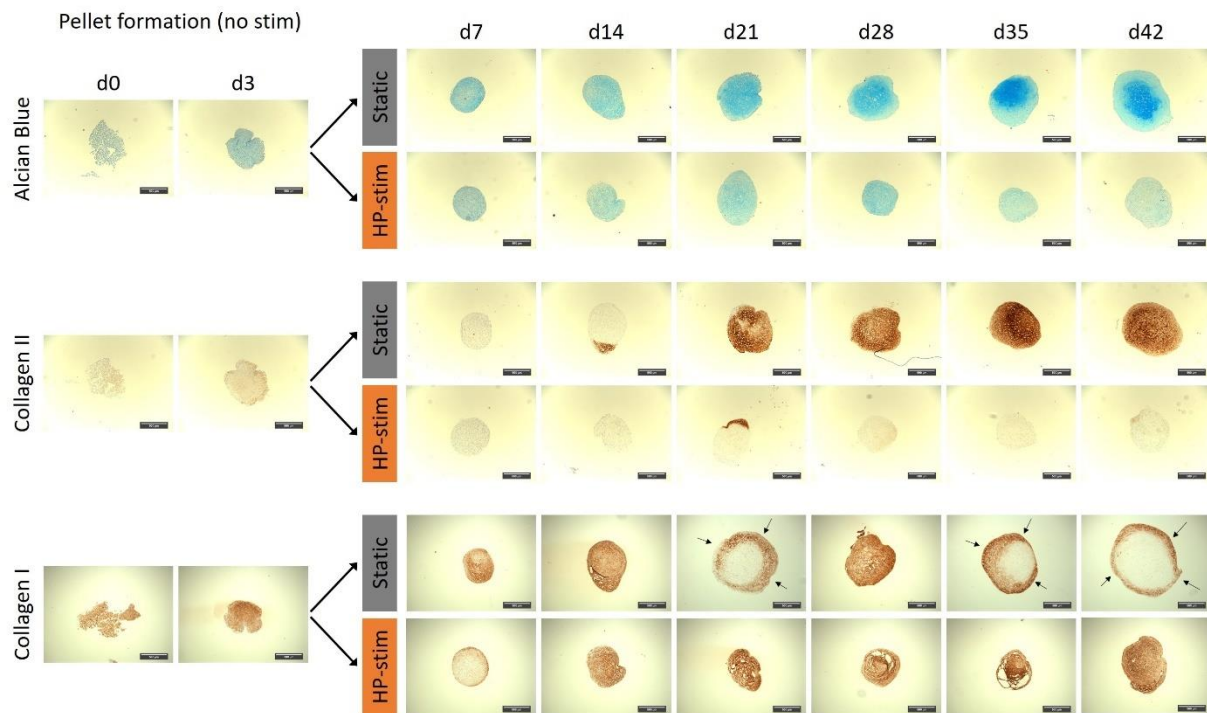


Fig. 40. Histological analysis of chondrogenic ASC-pellet cultures under static and hydrostatic pressure stimulated (HP-stim) conditions. Static chondrogenic cultured pellets show an increasing amount of glycosaminoglycan (determined via Alcian blue staining) and collagen II (determined via immunohistochemical staining) over time. In contrast, HP-stimulated pellets are negative for these markers but show uniform distribution of collagen I during the full culture time of 42 days. Static pellets also express collagen I, especially at earlier time points, but generally at the outer region of the pellets (indicated by black arrows). Scale bar: 100 μ m

3.3 HP stimulation degrades preformed cartilage matrix

After observing the inhibitory effect of HP stimulation on cartilage formation in pellet cultures, the focus was to determine whether the HP stimulation also leads to degradation of cartilage matrix. Therefore, unstimulated static pellet cultures were cultured for 21 days in which a significant amount of GAGs and collagen II was formed. Pellets then received HP stimulation for another 21 days (**Fig. 38A**). As a control, pellets were cultured for a total of 42 days without stimulation under static conditions. After 21 days of static culture, positive staining for GAGs and collagen II was observed (**Fig. 41**), which further increased under static conditions but decreased in stimulated groups over time. HP stimulation led to a uniform collagen I expression throughout the pellets, whereas in static controls only the margins of the pellets were positively stained.

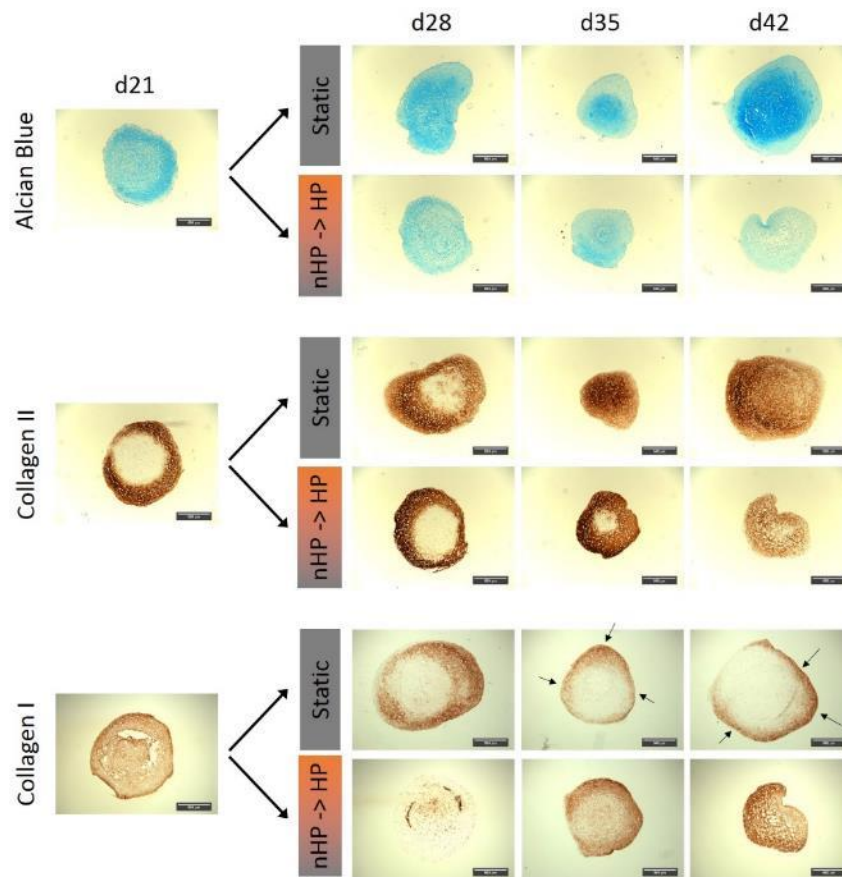


Fig. 41. Histological analysis of chondrogenic ASC-pellet cultures under static and switched hydrostatic pressure (nHP→HP) stimulated conditions. Until day 21, pellets of both groups were cultured under static conditions and formed substantial amounts of GAGs (determined via Alcian blue staining) and collagen types I and II (determined via immunohistochemistry stainings). Afterwards, static pellet cultures gradually increased GAG content as well as collagen II content whereas collagen I content decreased gradually and was only locally expressed in the outer shell of the pellet structures (indicated by black arrows). Pellets cultured under switched conditions steadily lost pro-chondrogenic markers (Alcian blue, collagen II) after day 21 but showed an increased collagen I content throughout the whole pellet. Scale bar: 100 μ m

Quantitative GAG to DNA content measurements confirmed the histological staining analysis that HP stimulation affects GAG content in a dual manner: (1) pellets stimulated from day 3 on showed inhibited GAG deposition compared to unstimulated static controls and (2) pellets under switched conditions showed a decreasing amount of GAG content indicating degradation of already formed ECM matrix (**Fig. 42, Fig. S4A**). Although the GAG/DNA amount of pellets stimulated after day 21 increased marginally from day 28 to day 35, the final ratio (3.2 μ g GAG/ μ g DNA) on day 42 was below the original value (5.4 μ g GAG/ μ g DNA) of static cultured pellets on day 21. Pellets stimulated continuously for 42 days showed a significant difference of produced GAG already on day 21 compared to unstimulated pellets, gradually increasing to a 10-fold difference on day 42. Similar to continuously stimulated pellets, pellets that were stimulated after day 21 (after a pre-chondrogenic differentiation phase) showed a significant 7-fold difference on day 42 compared to static culture pellets.

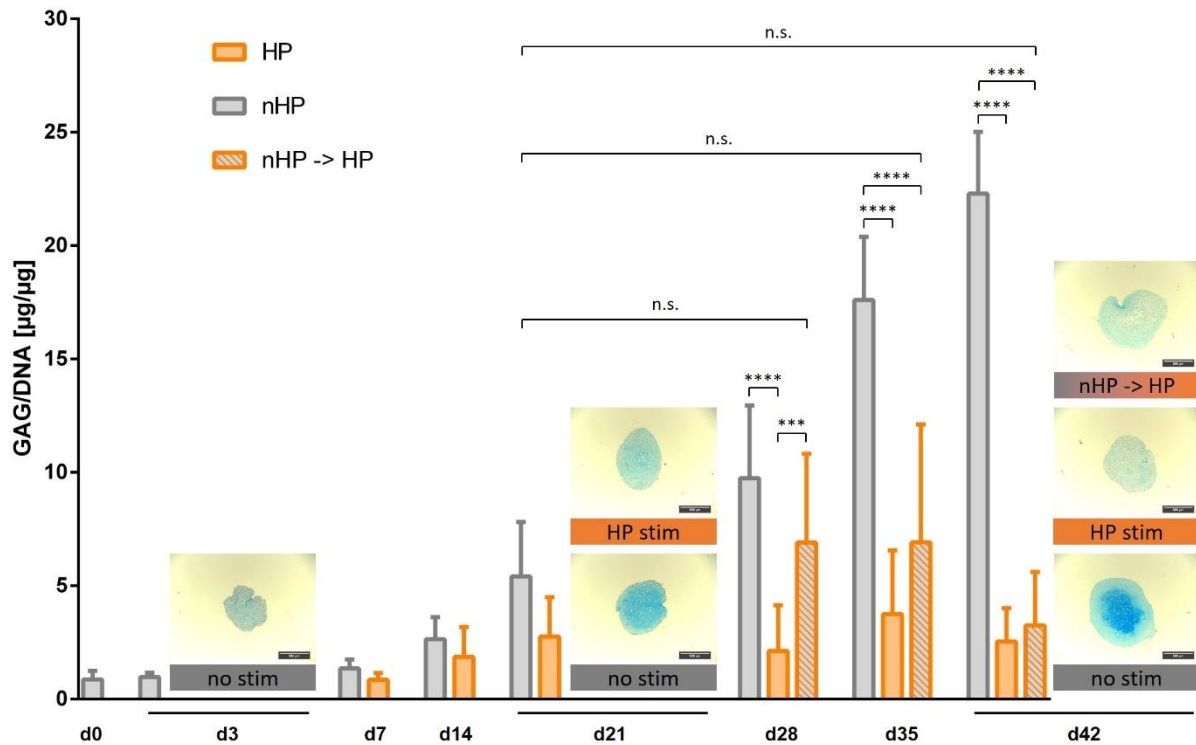


Fig. 42. Influence of hydrostatic pressure stimulation on quantitative glycosaminoglycan (GAG) to DNA amount. Static cultured pellets increased GAG to DNA ratio gradually over a 6 weeks culture period and expressed a 10-fold difference to continuously HP-stimulated pellets and a 7-fold difference to switched stimulated pellets on day 42, respectively. On day 21, continuously stimulated pellets showed a reduction of produced GAG compared to unstimulated pellets. Switched stimulated pellets that were cultured under static conditions for 21 days and then experienced hydrostatic loading for another 21 days marginally increased GAG/DNA ratio on day 28 and day 35 but had a GAG to DNA ratio on day 42 similar to pellets cultured continuously with HP for 42 days. Representative examples of Alcian blue stained pellets next to the respective bars qualitatively underline the results from the quantitative GAG to DNA ratio. Data from 3 individual donors, 4 replicates per donor; **p < 0.01, ****p < 0.0001

3.4 HP stimulation decreases viability of pellets over time

Besides the inhibitory and degenerative effect on cartilage formation, especially on GAGs (Fig. S4B), pellets subjected to HP stimulation displayed a reduced amount of DNA (Fig. S4C). DNA amount was highest on day 0 but decreased over one week to stabilize and remain on the same level for the rest of the experiment for static cultured pellets. In contrast, DNA amount of continuously stimulated pellets gradually decreased from day 7 to less than 50% of the starting value on day 42. Similarly, DNA of switched stimulated pellets dropped progressively from day 28 and reached their lowest value on day 42. Furthermore, to increase validity of short-term DNA data, viability of pellets was checked after one day of stimulation as well as one week of stimulation (Fig. S4D). One day of HP stimulation did not show any adverse effect on stimulated pellets. Similarly, one week of stimulation did not have a significant effect on the pellets either, which is in accordance with DNA data of day 7 (Fig. S4C).

3.5 RT-qPCR

3.5.1 Hydrostatic pressure (HP) decreases collagen type II to I ratio

Transcription levels of cartilage-specific genes were tracked using RT-qPCR. The ratio of collagen type II to collagen type I mRNA levels (COL2/COL1), commonly used as a cartilage differentiation

index[561], was significantly lower only in stimulated pellets after 21 days of culture, whereas no significant difference between static and any HP-stimulated group could be detected on day 42 (**Fig. 43**). Investigating the levels of collagen type II and collagen type I mRNA separately revealed that collagen type I mRNA expression is stronger influenced by HP stimulation than collagen type II. Cartilage-specific collagen type II expression was comparable between static and stimulated groups on day 21, as well as on day 42 for all groups. Collagen type I levels of the stimulated groups were significantly upregulated on day 21 but showed no difference compared to other groups on day 42. In contrast to histological stainings, expression of aggrecan, a proteoglycan and major structural component of articular cartilage, was significantly upregulated on day 21 in stimulated pellets but was equally expressed on day 42 in all groups. Similar to aggrecan, collagen type X, which is an early marker for hypertrophic chondrocyte, was significantly upregulated on day 21 but was not impacted in both HP-stimulated groups on day 42 compared to control.

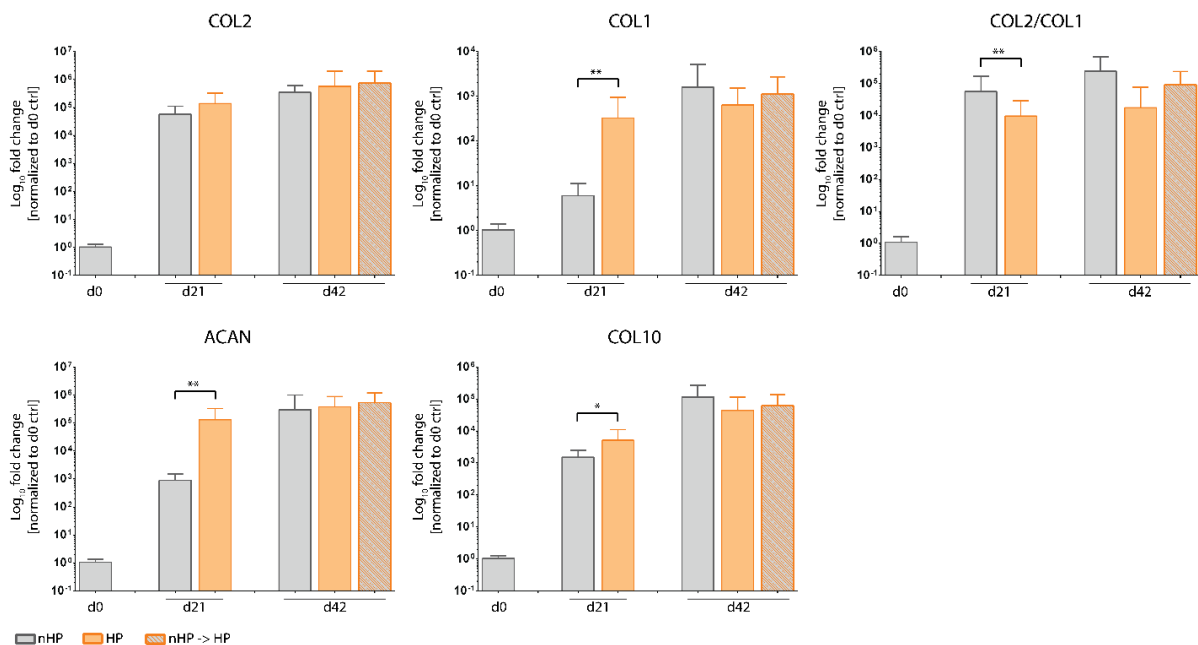


Fig. 43. Influence of hydrostatic pressure (HP) stimulation on gene expression of extracellular matrix proteins. The cartilage differentiation index, a ratio of collagen type II to collagen type I (Col2/Col1), was significantly downregulated on day 21 for HP-stimulated compared to static cultured pellets but showed no difference on day 42. Collagen type II of both stimulated groups was expressed at levels equal to the control group on day 21 as well as on day 42. Expression of collagen type I, aggrecan and collagen type X was significantly upregulated in HP-stimulated groups on day 21 but was equally expressed on day 42 for all groups. Data from 3 individual donors, 5 replicates per donor; *p < 0.05, **p < 0.01

3.5.2 HP stimulation upregulates expression of transcription factors SOX9 and RUNX2

Expression of SOX9, a crucial transcription factor for chondrocytes, was significantly upregulated after HP stimulation compared to control on day 21 but equally expressed in all groups on day 42 (**Fig. 8**). Similarly, RUNX2, a key osteoblastic transcription factor, was significantly upregulated in stimulated pellets on day 21 but equally expressed among all groups on day 42.

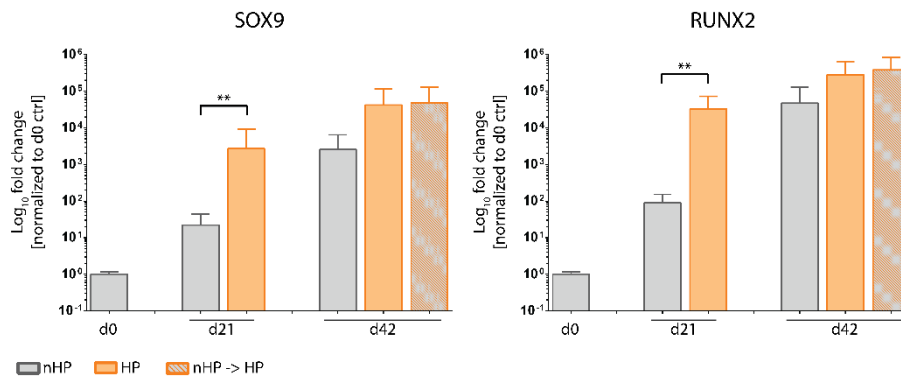


Fig. 44. Influence of hydrostatic pressure (HP) stimulation on gene expression of transcription factors. Both investigated transcription factors SOX9 and RUNX2 were significantly upregulated in HP-stimulated pellet cultures compared to static pellet cultures on day 21. Although not significantly different, hydrostatic stimulated pellets had higher levels of SOX9 as well as RUNX2 on day 42. Data from 3 individual donors, 5 replicates per donor; ** $p < 0.01$

3.5.3 HP-stimulated pellet cultures show augmented expression of matrix metalloproteinases (MMPs)

After observing a loss of GAGs and collagen type II in HP-treated pellets (**Fig. 40**), the expression of matrix metalloproteinases – essential in cartilage remodeling and osteoarthritis – was investigated. MMP3 (e.g. known to degrade cartilage proteoglycans), MMP9 (e.g. known to degrade different types of collagen) and MMP13 (e.g. known to cleave collagen type II) are described as the main mediators of cartilage matrix degradation in overstimulated and/or osteoarthritic cartilage[562], [563]. On day 21, the expression of all three MMPs was significantly upregulated following HP stimulation in comparison to unstimulated control pellets (**Fig. 45**). On day 42, expression levels for MMP3 and MMP9 were not significantly different between stimulated and static cultured pellets. Only MMP13 expression was enhanced for both HP-stimulated pellet groups compared to static controls, being significantly upregulated in HP-stimulated pellets from day 3 on. No difference was observed between the two HP stimulation regimes.

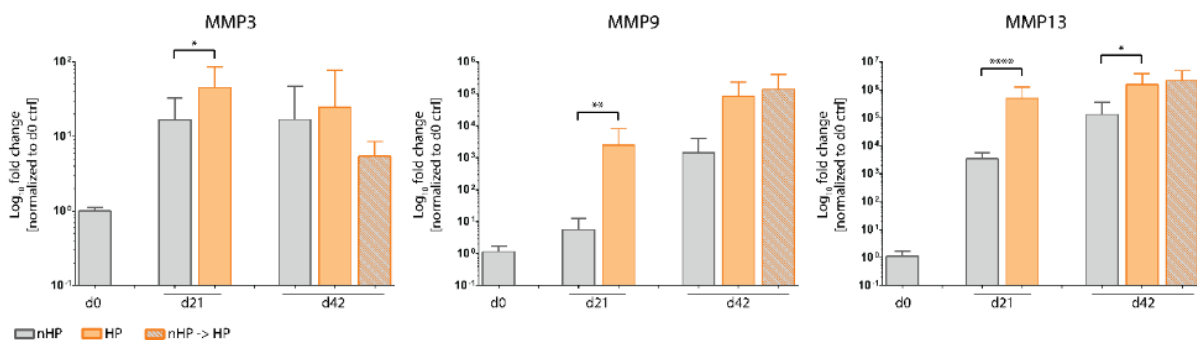


Fig. 45. Hydrostatic pressure (HP) stimulation increases gene expression of matrix metalloproteinases proteins. Gene expression of all investigated MMPs (MMP3, MMP9 and MMP13) was significantly upregulated in hydrostatic stimulated pellets on day 21. MMP9 and MMP13 had higher expression in both HP-stimulated groups on day 42 with MMP13 being significantly different to the continuously stimulated group. Data from 3 individual donors, 5 replicates per donor; * $p < 0.05$, ** $p < 0.01$, **** $p < 0.0001$

3.5.4 Upregulation of OA-associated pro-inflammatory cytokines by HP stimulation

In order to investigate the effect of HP stimulation on the expression of inflammation-related cytokines, three different pro-inflammatory cytokines which are generally upregulated in OA – IL-1 β , IL-6 and TNF- α – have been investigated (**Fig. 46**). On day 21, HP-stimulated pellets demonstrated increased expression levels of all three cytokines compared to static controls, with IL-1 β and TNF- α being significantly different ($p < 0.0001$). On day 42, a difference between all three pellet conditions could be observed and showed a trend towards elevated levels in HP-stimulated groups compared to static control pellets for all 3 investigated cytokines. Interestingly, expression of IL-1 β and IL-6 in control pellets was lower on day 21 than on day 0.

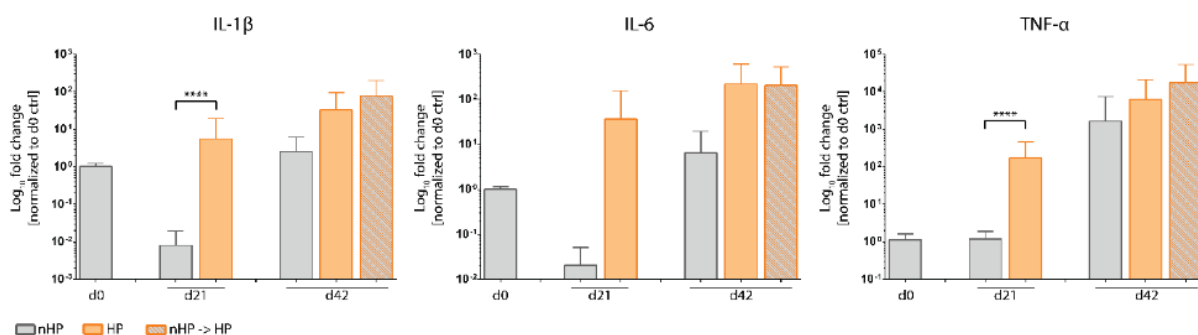


Fig. 46. Hydrostatic pressure (HP)-stimulated pellet cultures show increased gene expression levels of inflammatory cytokines. In comparison to the static group, HP-stimulated pellet cultures showed increased gene expression of the pro-inflammatory cytokines IL-1 β , IL-6 and TNF- α on day 21. On day 42, in both HP-stimulated groups IL-1 β , IL-6 and TNF- α expression was upregulated compared to unstimulated pellets. IL-6 was equally highly expressed in both HP-stimulated groups. Compared to day 0, unstimulated pellets harvested on day 21 had reduced IL-1 β and IL-6 gene expression, though TNF- α was similarly expressed. Data from 3 individual donors, 5 replicates per donor; **** $p < 0.0001$

3.6 Western Blot

Subsequently to gene expression analysis, prominent signaling targets of upregulated inflammatory cytokines – ERK1/2 and p38 MAPK – were investigated on the protein level in the switched stimulated pellet group (nHP \rightarrow HP) compared to unstimulated static pellets. Analysis of immunoblots of proteins related to OA (**Fig. 47A**) showed that, starting with day 21, stimulated pellets showed higher ERK1/2 activation compared to unstimulated static pellet cultures (**Fig. 47B**). This trend continued over time and reached its maximum on day 35 but declined at the end of the stimulation period (day 42 of pellet culture). In contrast, p38 MAPK did not follow such a pattern with comparable early activation levels of stimulated and static pellets (**Fig. 47C**). This was also the case for ribosomal protein S6 (**Fig. 47D**), which is involved in the regulation of cell size and cell proliferation. Furthermore, Akt, a major component in the canonical mTOR pathway and downstream target of inflammatory cytokines, showed an activation profile similar to ERK1/2. Compared to unstimulated pellets, HP-stimulated pellets exhibited a higher level of activation for Akt at each time point over the entire experimental period (**Fig. 47E**). To investigate another possible trigger of OA, β -Catenin was investigated. Compared to unstimulated pellets on day 21, stimulated pellets showed an increased expression pattern towards the

end of the stimulation period, whilst the expression of unstimulated pellets gradually decreased (**Fig. 47F**).

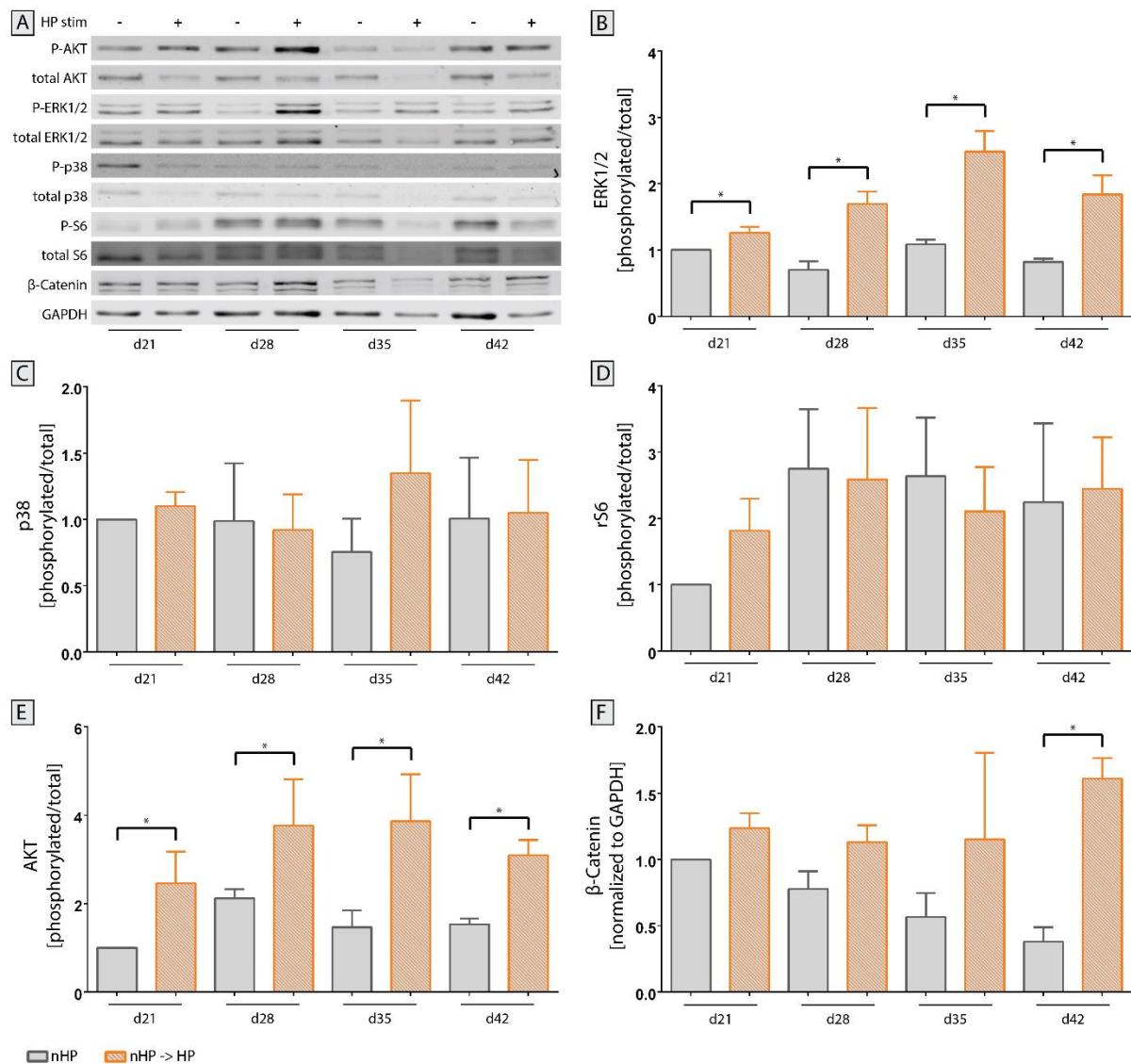


Fig. 47. Activation of crucial signaling pathways in osteoarthritis after hydrostatic pressure (HP) stimulation. **(A)** Representative immunoblots from the same gel were cropped to show specific bands for phosphorylated and total protein of Akt, ERK1/2, p38, ribosomal protein S6 as well as β -Catenin using GAPDH as housekeeping protein. Full-length blots are presented in **Fig. S5**. Pellets of unstimulated and HP-stimulated groups were harvested once every week for the last 21 days of the experiment and protein was isolated. Both **(B)** ERK1/2 and **(E)** Akt showed a statistically significant increase in activation in HP-stimulated pellets compared to static controls at all timepoints. **(C)** Protein expression of p38 did not significantly change over time. **(D)** Ribosomal protein S6, a downstream target of ERK1/2 and mTOR, did not exhibit an enhanced activation at any sampling timepoint. **(F)** Expression of β -Catenin increased towards the end of the stimulation period for stimulated pellets whilst it declined for unstimulated pellets. Mean + SEM; data from 2 individual donors, 6 replicates for each donor; * $p < 0.05$

4 Discussion

Osteoarthritis (OA) represents a burden for a growing number of people across the globe, especially due to the increased prevalence in risk factors leading to OA, such as obesity and a sedentary lifestyle [564]. Despite intensive research over the past 20 years, a detailed understanding of the triggers and mechanisms leading to initiation and progression of this degenerative joint disease is still incomplete

[565]. Historically, OA was described as a simple “wear-and-tear” type disease but is now accepted to be a more complex disease in which inflammation processes play a critical role [539]. In recently published studies, elevated ROS levels due to oxidative stress are associated with formation and progression of cartilage degradation as seen in OA [566]–[568].

In the presented study, the application of hydrostatic pressure (HP) via a custom-made bioreactor system (**Fig. 37**) led to generation of acellular ROS. Via a series of EPR measurements we could demonstrate that superoxide ($O_2^{\cdot-}$) is initially generated, which subsequently reacts to produce other ROS (**Fig. 39**) including hydrogen peroxide (H_2O_2) and hydroxyl radicals ($\cdot OH$). Notably, the increased HP leads to generation of elevated levels of acellular ROS. Interestingly, elevated levels of HP have also been described in OA-affected joints [569], [570]. In knee joints, these elevated intra-articular fluid pressure levels are attributed to effusions which occur in over 80% of patients [571], [572]. Another cause for elevated intra-articular fluid pressure is body weight, a well-known OA risk factor. In this regard, Felson *et al.* describe that gaining 10 pounds body weight results in approximately 30 pounds more load on the knee during walking [573]. In general, excessive joint loadings, either a single acute impact event or repetitive cumulative contact stresses, are regarded as main contributor in the pathogenesis of OA [574], [575]. Via *in vitro* studies using bioreactor systems [576]–[578] to mimic joint loading it could be demonstrated that excessive mechanical stimulation of articular cartilage initiates the production of ROS and reactive nitrogen species. This oxidative stress is then the primary trigger for the characteristic inflammation process associated with OA.

Additionally, EPR measurements indicated that free iron is a critical component of acellular ROS formation after HP stimulation. Notably, elevated synovial iron levels have been indicated in patients with degenerative joint diseases such as rheumatoid arthritis and OA [579], [580]. The origin of iron is suggested to be blood which enters the joint due to trauma or secretion from inflamed areas of synovial membranes [579]. Joint bleeding leads to iron release from haemoglobin which induces an inflammatory environment mediated by cytokines and hydroxyl radical formation [581], [582]. Non-protein-bound iron has been investigated as a trigger but also as a marker for degenerative joint diseases [583]. In this regard, Kawai *et al.* [584] showed that IL-1-treated rats developed arthritis which was accompanied by statistically higher free iron levels in synovial fluid compared to saline-treated controls.

There is consensus that elevated levels of reactive oxygen and nitrogen species directly damage chondrocytes, for example by lipid peroxidation [585] or DNA damage [586] and lead to disturbed collagen type II and GAG synthesis as well as to enhanced expression of matrix metalloproteinase (MMP) [587]–[589]. Moreover, ROS, especially hydrogen peroxide, are described to fragment link proteins and to inhibit association of proteoglycan monomers with other ECM components (e.g. hyaluronic acid) [590], [591]. The above described dual effect could also be seen in the presented study. HP stimulation, and thereby generated ROS, led to a reduction of already formed GAG and collagen type II (**Fig. 41**) as well as to an inhibition of the formation of these cartilage-specific ECM proteins in

chondrogenic MSC pellets (**Fig. 40**). The degradative effects occurred despite the culture media containing potent chondrogenic growth factors TGF- β 3 and BMP6. We could clearly indicate that the HP stimulation significantly upregulated the expression of all three investigated MMPs 3, 9 and 13 (**Fig. 45**). This was further accompanied by a severe loss in cartilage matrix proteins in chondrogenically pre-differentiated pellets over time. One limitation of this study is that it is still to be investigated if the formation of cartilage matrix was hindered directly by disturbing essential chondrogenic signaling pathways, by the expression of matrix-degrading MMPs or as a result of both effects. Another factor that most likely additionally affected the reduced GAG content of the stimulated pellets is the induction of apoptosis due to the HP-induced oxidative stress. HP-treated pellets showed significantly lower amounts of DNA which can be directly correlated to reduced cell numbers. Despite the possible induction of apoptosis, no direct effects on cell viability could be detected (**Fig. S4**). Hence, more specific experiments need to be executed in future studies to address these questions and decipher the detailed mechanisms.

In contrast to collagen type II and GAG downregulation, collagen type I expression was upregulated, which could be seen in RT-qPCR (**Fig. 43**) as well as in the histological analyses (**Fig. 40, Fig. 41**). The upregulation of collagen type I additionally contributed to a decrease in collagen type II to collagen type I ratio, which has been used as a differentiation marker for healthy cartilage cells [561], [581], [592]. Remarkably, the exposition to ROS in the experimental set-up was not accompanied by collagen type III expression (data not shown), as it has been described for injured regions of articular cartilage by Hosseininia *et al.* [593], comparable to wound healing and scar tissue formation in skin or tendon [594], [595].

Gene expression analysis in our study further included the OA-associated cytokines IL-1 β , TNF- α and IL-6. It is well reported that upregulation of cytokine expression can be linked to increased ROS levels and can play an important role in the pathogenesis of OA. For instance, Davies *et al.* demonstrated that IL-1 β mediates ROS-induced DNA damage in osteoarthritic cartilage [596]. Interestingly, IL-1 β and IL-6 expression in control pellets on day 21 was reduced compared to day 0 levels (**Fig. 46**), which might have been caused by mechanical stress during the pelleting procedure. Furthermore, the catabolic effect of these interleukins on articular cartilage has been associated with activation of different signaling pathways including MAPK/ERK and PI3K/Akt. Different studies reported the ERK pathway as a negative regulator of chondrogenesis. For instance, Wang *et al.* showed that IL-1 β enhances MMP3 and MMP13 expression but inhibits collagen type II and aggrecan via simultaneous MAPK/ERK pathway activation [597]. In this regard, Mio *et al.* have shown that ERK pathway activation leads to suppression of SOX9 expression in hydrostatic pressure-treated chondrocytes [598]. Mechanical loading-induced ERK1/2 phosphorylation leads to a decrease in proteoglycan synthesis in cartilage explant cultures [599].

Different signaling pathways including ERK1/2 and Akt have been investigated in unstimulated static cultures compared to pellets pre-differentiated into the chondrogenic lineage for 21 days in which OA-like conditions have then been induced (nHP→HP, **Fig. 47**). In accordance with literature [600], upregulation of OA-associated gene and protein expression in the presented study could be associated with increased ERK1/2 activation. Similar to MAPK/ERK, also the PI3K/Akt signaling pathway was activated via HP stimulation treatment. The activation of the PI3K/Akt pathway can result in diverse regulations due to its broad range of target proteins such as mTOR, NF-κB, GSK-3β, and p53 [601]. Nevertheless, PI3K/Akt has been reported to be involved in OA regulation and progression since its overactivation leads to inflammation and apoptosis of chondrocytes [602], [603]. Activation of Akt and thereby induced apoptosis could be linked to the observed reduced pellet size and DNA content in HP-stimulated group compared to unstimulated samples (**Fig. 40, Fig. 41, Fig. S4**). Interestingly, Lopez-Armada *et al.* [604] have proposed that apoptosis can lead to increased ROS production which might facilitate chondrocyte death.

Besides Akt and ERK1/2, other targets including p38 MAPK and β-Catenin were activated but less pronounced; activation of Akt and ERK1/2 was up to 4-fold higher, whereas the activation of p38 MAPK and β-Catenin was only 1.5-fold higher relative to unstimulated controls on day 21. In this regard Cheleschi *et al.* [605] could show that cyclic HP can lower the β-Catenin expression in OA chondrocytes which might therefore be the key modulator for the restored expression of miRNAs dysregulated in OA leading to significant reduction of proteases including MMP13. It is likely that the influence of the described bioreactor system on these signaling pathways, previously demonstrated to be involved in OA initiation and progression [606], [607], can be statistically verified through repetition of the experiment.

Unlike other signaling molecules, ribosomal S6 protein did not appear to be activated by HP stimulation. This is in contrast to other studies which showed that the severity of OA could be reduced in preclinical and animal models [608] by both pharmacological and genetic deletion of mTOR.

This study mainly describes the effects of the observed acellular ROS formation due to HP treatment on ASC chondrogenic pellets but did not investigate the direct effects of mechanical deformation on the cellular integrity. In literature, HP treatment is described to lead to ultrastructural and cytoskeletal changes of 2D cultured OA-chondrocytes [547], [549]. Future studies are needed to elucidate if the applied HP similarly leads to changes of the cytoskeleton of individual cells cultured in pellet cultures.

5 Conclusion/Outlook

In summary, a custom-made hydrostatic pressure bioreactor system capable of generating acellular ROS was utilized to generate an *in vitro* model for OA that produced comparable biological effects known for initiation and progression of the degenerative joint disease. In future studies, the created system will be used to test antioxidant properties of numerous drugs proposed as potential OA treatments [609], such as aucubin [553] or curcumin [610]. Another possible application may pursue the involvement of

free iron and oxygen stress related signaling pathways present in OA in order to elucidate possible novel targets for future therapeutic approaches.

6 Acknowledgments

Financial support by the Austrian Research Agency FFG (COIN Project DiseaseTissue, #845443 and Bridge Project CartiScaff, #842455), the City of Vienna Projects; Tissue Engineering International (MA23, #14-06), and the Competence Team signalTissue (MA23, #18-08) is gratefully acknowledged. The authors would like to thank Jon Bernhard for native language review. Further, we would like to thank Andrey Kozlov for the fruitful discussions about the detection of reactive oxygen species using electron paramagnetic resonance measurements.

7 Competing Interests

The authors declare no competing interests.

8 Supplemental Information

8.1 Supplemental Figures

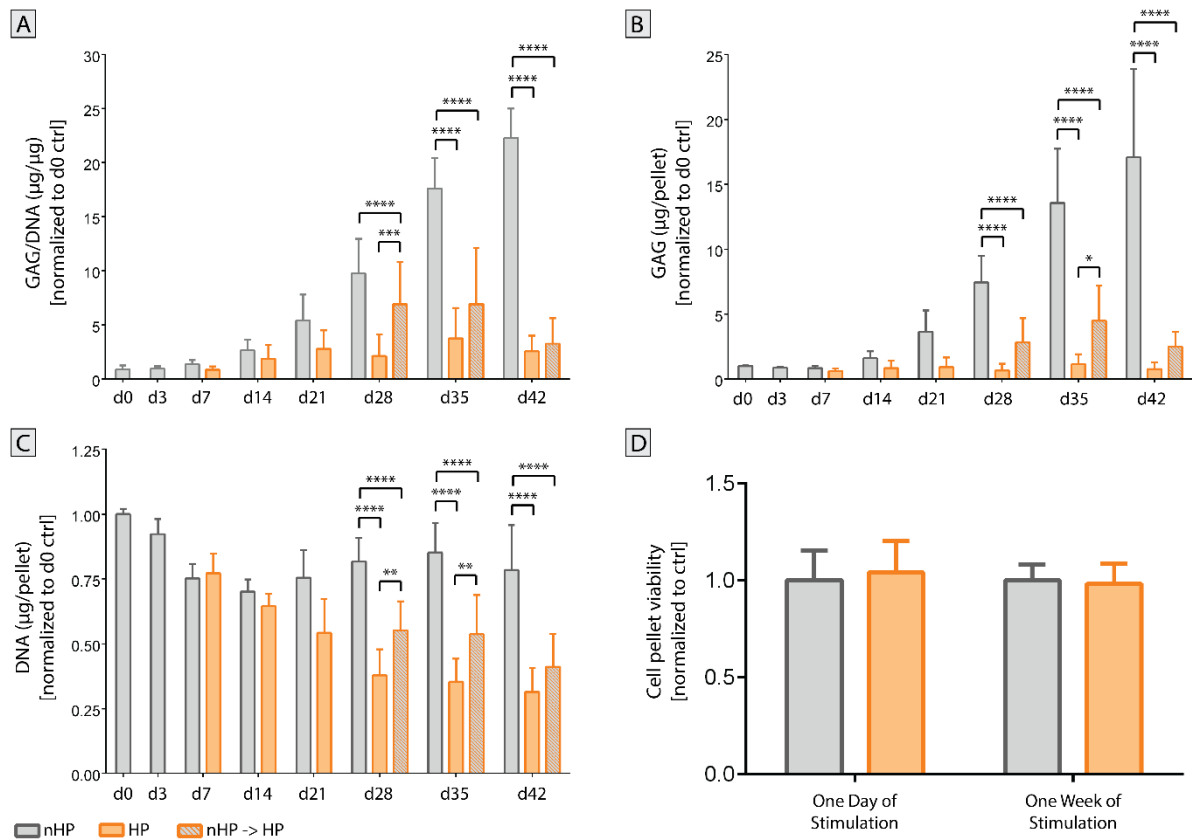


Fig. S4. Influence of hydrostatic pressure (HP) stimulation on viability of cells. **(A)** One day of stimulation did not adversely affect stimulated cells. Similarly, one week of stimulation did not have a significant effect on the pellets either. **(B)** GAG to DNA ratio gradually increased over the 6 weeks period for the static cultured pellets and expressed a 10-fold difference compared to continuously HP-stimulated pellets, as well as a 7-fold difference to switched stimulated pellets on the last day of the experiment. **(C)** Complementary to the GAG/DNA ratio, the amount of GAG did increase for the static cultured pellets but stayed on the same level for the continuously HP-stimulated pellets over the course of the experiment. Pellets that were stimulated after day 21 till the end of the experiment expressed the least amount of GAG on day 42. **(D)** Amount of DNA in unstimulated pellets was highest on day 0, decreased for one week but stabilized on day 7 for the rest of the experiment. In contrast, DNA content of continuously HP-stimulated pellets did gradually decrease over time with the lowest DNA value on day 42. Similarly, DNA amount of switched stimulated pellets dropped progressively from values similar to static control to values comparable to continuously HP-stimulated pellets at the end of the experiment. (A) Data from 2 individual donors, 10 replicates per donor (B,C,D) Data from 3 individual donors, 4 replicates per donor, ** $p < 0.05$, *** $p < 0.001$, **** $p < 0.0001$

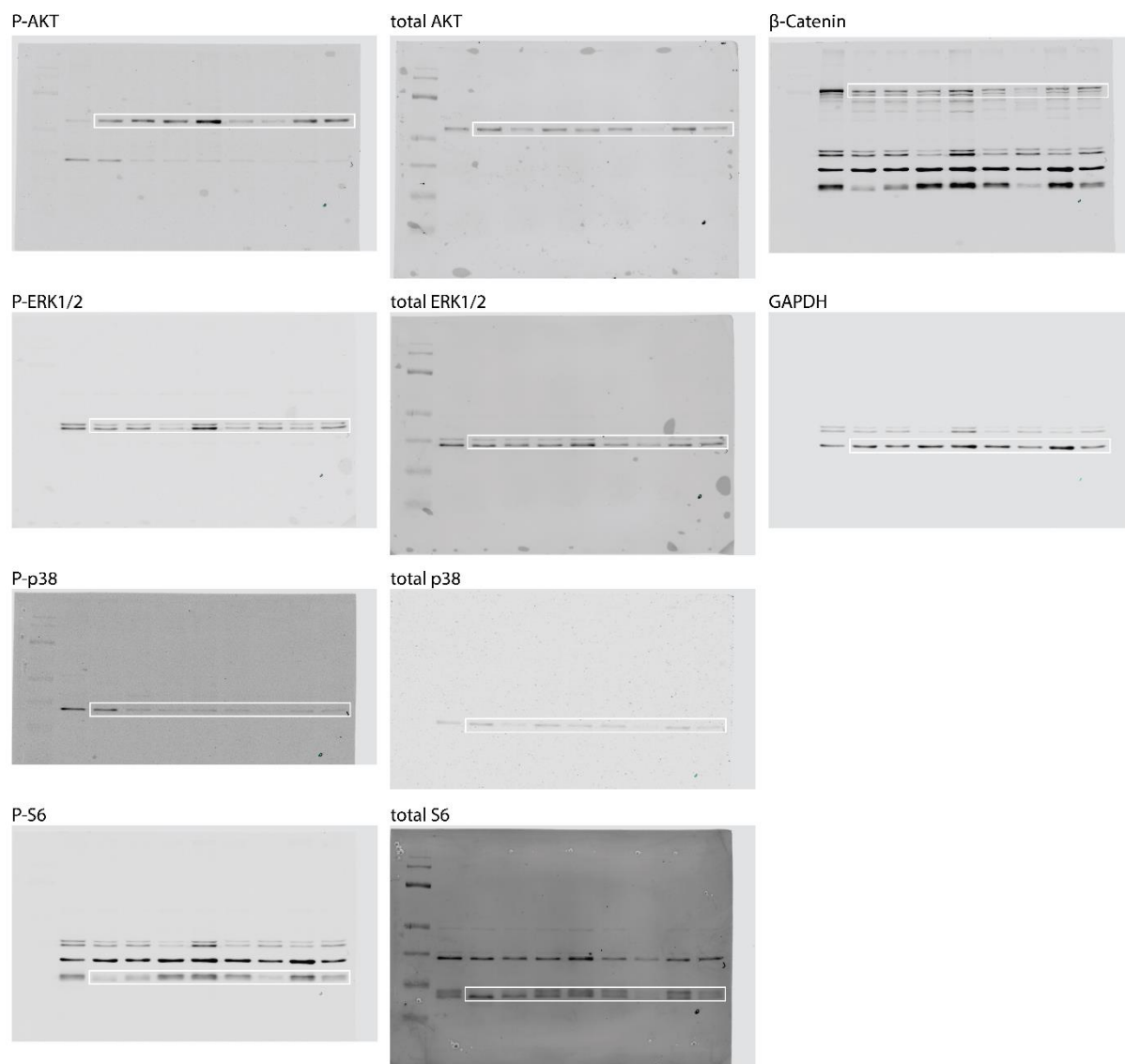


Fig. S5. Full-length blots of P-Akt, total AKT, phospho-p44/42 MAPK (phospho-Erk1/2), total p44/42 MAPK (total ERK1/2), phospho-p38 MAPK, total p38 MAPK, phospho-S6 ribosomal protein, total S6 ribosomal protein, β-Catenin, and GAPDH. Areas marked with a white rectangle were used for **Fig. 47A**.

REFERENCES

- [1] S. Bevan, "Economic impact of musculoskeletal disorders (MSDs) on work in Europe.," *Best Pract. Res. Clin. Rheumatol.*, vol. 29, no. 3, pp. 356–73, Jun. 2015.
- [2] *United States Bone and Joint Initiative: The Burden of Musculoskeletal Diseases in the United States (BMUS)*, 3rd ed. Rosemont: United States Bone and Joint Initiative, 2014.
- [3] J. DeVoe, "The unsustainable US health care system: a blueprint for change.," *Ann. Fam. Med.*, vol. 6, no. 3, pp. 263–6, 2008.
- [4] R. Langer and J. P. Vacanti, "Tissue engineering.," *Science*, vol. 260, no. 5110, pp. 920–6, May 1993.
- [5] D. L. Butler, S. A. Goldstein, and F. Guilak, "Functional tissue engineering: the role of biomechanics.," *J. Biomech. Eng.*, vol. 122, no. 6, pp. 570–5, Dec. 2000.
- [6] A. J. Salgado *et al.*, "Tissue engineering and regenerative medicine: past, present, and future.," *Int. Rev. Neurobiol.*, vol. 108, pp. 1–33, 2013.
- [7] R. S. Tuan, "Regenerative medicine in 2012: the coming of age of musculoskeletal tissue engineering.," *Nat. Rev. Rheumatol.*, vol. 9, no. 2, pp. 74–6, Feb. 2013.
- [8] B. R. Olsen, A. M. Reginato, and W. Wang, "Bone development.," *Annu. Rev. Cell Dev. Biol.*, vol. 16, no. 1, pp. 191–220, Nov. 2000.
- [9] M. M. Stevens, "Biomaterials for bone tissue engineering," *Mater. Today*, vol. 11, no. 5, pp. 18–25, May 2008.
- [10] A. J. Sophia Fox, A. Bedi, and S. a Rodeo, "The basic science of articular cartilage: structure, composition, and function.," *Sports Health*, vol. 1, no. 6, pp. 461–8, Nov. 2009.
- [11] I.-R. Chang and A. Martin, *Anatomy, Cartilage*. StatPearls Publishing, 2019.
- [12] A. M. Bhosale and J. B. Richardson, "Articular cartilage: structure, injuries and review of management.," *Br. Med. Bull.*, vol. 87, no. 1, pp. 77–95, Aug. 2008.
- [13] B. N. Loy *et al.*, "A Biomechanical and Structural Comparison of Articular Cartilage and Subchondral Bone of the Glenoid and Humeral Head.," *Orthop. J. Sport. Med.*, vol. 6, no. 7, p. 2325967118785854, Jul. 2018.
- [14] P. G., "Challenges In Cartilage Tissue Engineering.," *J. Tissue Sci. Eng.*, vol. 03, no. 05, pp. 1–2, Dec. 2013.
- [15] S. Chen, P. Fu, H. Wu, and M. Pei, "Meniscus, articular cartilage and nucleus pulposus: a comparative review of cartilage-like tissues in anatomy, development and function.," *Cell Tissue Res.*, vol. 370, no. 1, pp. 53–70, Oct. 2017.
- [16] J. L. Forman, E. del Pozo de Dios, C. A. Dalmases, and R. W. Kent, "The contribution of the perichondrium to the structural mechanical behavior of the costal-cartilage.," *J. Biomech. Eng.*, vol. 132, no. 9, p. 094501, Sep. 2010.
- [17] S. Fowler, R. Roush, and J. Wise, *Concepts of biology*. OpenStax College, 2013.
- [18] Y. Krishnan and A. J. Grodzinsky, "Cartilage diseases.," *Matrix Biol.*, vol. 71–72, pp. 51–69, Oct. 2018.
- [19] V. C. Mow, A. Ratcliffe, and A. Robin Poole, "Cartilage and diarthrodial joints as paradigms for hierarchical materials and structures.," *Biomaterials*, vol. 13, no. 2, pp. 67–97, Jan. 1992.
- [20] J. C. Y. Hu and K. A. Athanasiou, "Structure and Function of Articular Cartilage," in *Handbook of Histology Methods for Bone and Cartilage*, Y. H. An and K. L. Martin, Eds. Totowa, NJ: Humana Press, 2003, pp. 73–95.
- [21] E. J.-M. A. Thonar, K. Masuda, D. H. Manicourt, and K. E. Kuettner, "Structure and Function of Normal Human Adult Articular Cartilage.," in *Osteoarthritis*, Berlin, Heidelberg: Springer Berlin Heidelberg, 1999, pp. 1–19.
- [22] R. Honner and R. C. Thompson, "The nutritional pathways of articular cartilage. An autoradiographic study in rabbits using ³⁵S injected intravenously.," *J. Bone Joint Surg. Am.*, vol. 53, no. 4, pp. 742–8, Jun. 1971.
- [23] B. Fermor, S. E. Christensen, I. Youn, J. M. Cernanec, C. M. Davies, and J. B. Weinberg, "Oxygen, nitric oxide and articular cartilage.," *Eur. Cell. Mater.*, vol. 13, pp. 56–65; discussion 65, Apr. 2007.
- [24] B. Fermor, A. Gurumurthy, and B. O. Diekman, "Hypoxia, RONS and energy metabolism in articular cartilage.," *Osteoarthritis Cartilage*, vol. 18, no. 9, pp. 1167–73, Sep. 2010.
- [25] M. Stefanovic-Racic, J. Stadler, H. I. Georgescu, and C. H. Evans, "Nitric oxide and energy production in articular chondrocytes.," *J. Cell. Physiol.*, vol. 159, no. 2, pp. 274–80, May 1994.
- [26] F. Tushan, G. P. Rodnan, M. Altman, and E. D. Robin, "Anaerobic glycolysis and lactate dehydrogenase (LDH) isoenzymes in articular cartilage.," *J. Lab. Clin. Med.*, vol. 73, no. 4, pp. 649–56, Apr. 1969.
- [27] E. B. Hunziker, M. Michel, and D. Studer, "Ultrastructure of adult human articular cartilage matrix after cryotechnical processing.," *Microsc. Res. Tech.*, vol. 37, no. 4, pp. 271–84, May 1997.
- [28] G. D. Jay and K. A. Waller, "The biology of lubricin: near frictionless joint motion.," *Matrix Biol.*, vol. 39, pp. 17–24, Oct. 2014.
- [29] P. S. Egli, E. B. Hunziker, and R. K. Schenk, "Quantitation of structural features characterizing weight- and less-weight-bearing regions in articular cartilage: a stereological analysis of medial femoral condyles in young adult rabbits.," *Anat. Rec.*, vol. 222, no. 3, pp. 217–27, Nov. 1988.
- [30] H. Muir, P. Bullough, and A. Maroudas, "The distribution of collagen in human articular cartilage with some of its physiological implications.," *J. Bone Joint Surg. Br.*, vol. 52, no. 3, pp. 554–63, Aug. 1970.
- [31] M. Venn and A. Maroudas, "Chemical composition and swelling of normal and osteoarthrotic femoral head cartilage. I. Chemical composition.," *Ann. Rheum. Dis.*, vol. 36, no. 2, pp. 121–9, Apr. 1977.

- [32] R. A. Stockwell, "The interrelationship of cell density and cartilage thickness in mammalian articular cartilage.," *J. Anat.*, vol. 109, no. Pt 3, pp. 411–21, Sep. 1971.
- [33] E. L. Radin and R. M. Rose, "Role of subchondral bone in the initiation and progression of cartilage damage.," *Clin. Orthop. Relat. Res.*, no. 213, pp. 34–40, Dec. 1986.
- [34] M. Brittberg, "Cartilage repair: on cartilaginous tissue engineering with the emphasis on chondrocyte transplantation," Göteborgs universitet/University of Gothenburg, 1996.
- [35] V. C. Mow and C. C. Wang, "Some bioengineering considerations for tissue engineering of articular cartilage.," *Clin. Orthop. Relat. Res.*, no. 367 Suppl, pp. S204-23, Oct. 1999.
- [36] C. A. Poole, M. H. Flint, and B. W. Beaumont, "Chondrons in cartilage: Ultrastructural analysis of the pericellular microenvironment in adult human articular cartilages," *J. Orthop. Res.*, vol. 5, no. 4, pp. 509–522, Jan. 1987.
- [37] M. M. Knight, D. A. Lee, and D. L. Bader, "The influence of elaborated pericellular matrix on the deformation of isolated articular chondrocytes cultured in agarose," *Biochim. Biophys. Acta - Mol. Cell Res.*, vol. 1405, no. 1–3, pp. 67–77, Oct. 1998.
- [38] C. A. Poole, S. Ayad, and J. R. Schofield, "Chondrons from articular cartilage: I. Immunolocalization of type VI collagen in the pericellular capsule of isolated canine tibial chondrons.," *J. Cell Sci.*, vol. 90 (Pt 4), pp. 635–43, Aug. 1988.
- [39] E. B. Hunziker, W. Herrmann, and R. K. Schenk, "Ruthenium hexammine trichloride (RHT)-mediated interaction between plasmalemmal components and pericellular matrix proteoglycans is responsible for the preservation of chondrocytic plasma membranes in situ during cartilage fixation.," *J. Histochem. Cytochem.*, vol. 31, no. 6, pp. 717–27, Jun. 1983.
- [40] I. Youn, J. B. Choi, L. Cao, L. A. Setton, and F. Guilak, "Zonal variations in the three-dimensional morphology of the chondron measured in situ using confocal microscopy.," *Osteoarthr. Cartil.*, vol. 14, no. 9, pp. 889–97, Sep. 2006.
- [41] R. K. Korhonen, P. Julkunen, W. Wilson, and W. Herzog, "Importance of collagen orientation and depth-dependent fixed charge densities of cartilage on mechanical behavior of chondrocytes.," *J. Biomech. Eng.*, vol. 130, no. 2, p. 021003, Apr. 2008.
- [42] J. B. Choi *et al.*, "Zonal changes in the three-dimensional morphology of the chondron under compression: the relationship among cellular, pericellular, and extracellular deformation in articular cartilage.," *J. Biomech.*, vol. 40, no. 12, pp. 2596–603, Jan. 2007.
- [43] R. S. Tuan and F. H. Chen, "Cartilage," in *Stem Cell and Gene-Based Therapy*, London: Springer London, 2006, pp. 179–193.
- [44] D. R. Eyre, "Collagen: molecular diversity in the body's protein scaffold.," *Science*, vol. 207, no. 4437, pp. 1315–22, Mar. 1980.
- [45] L. A. Setton, V. C. Mow, and D. S. Howell, "Mechanical behavior of articular cartilage in shear is altered by transection of the anterior cruciate ligament.," *J. Orthop. Res.*, vol. 13, no. 4, pp. 473–82, Jul. 1995.
- [46] G. N. Smith and K. D. Brandt, "Hypothesis: can type IX collagen 'glue' together intersecting type II fibers in articular cartilage matrix? A proposed mechanism.," *J. Rheumatol.*, vol. 19, no. 1, pp. 14–7, Jan. 1992.
- [47] O. Pullig, G. Weseloh, and B. Swoboda, "Expression of type VI collagen in normal and osteoarthritic human cartilage.," *Osteoarthr. Cartil.*, vol. 7, no. 2, pp. 191–202, Mar. 1999.
- [48] A. Maroudas, "Physicochemical properties of cartilage in the light of ion exchange theory.," *Biophys. J.*, vol. 8, no. 5, pp. 575–95, May 1968.
- [49] B. Caterson and J. Melrose, "Keratan sulfate, a complex glycosaminoglycan with unique functional capability.," *Glycobiology*, vol. 28, no. 4, pp. 182–206, Apr. 2018.
- [50] M. T. Bayliss, D. Osborne, S. Woodhouse, and C. Davidson, "Sulfation of chondroitin sulfate in human articular cartilage. The effect of age, topographical position, and zone of cartilage on tissue composition.," *J. Biol. Chem.*, vol. 274, no. 22, pp. 15892–900, May 1999.
- [51] T. E. Hardingham, "The role of link-protein in the structure of cartilage proteoglycan aggregates.," *Biochem. J.*, vol. 177, no. 1, pp. 237–47, Jan. 1979.
- [52] T. I. Morales, "Chondrocyte moves: clever strategies?," *Osteoarthr. Cartil.*, vol. 15, no. 8, pp. 861–71, Aug. 2007.
- [53] M. Pilar Fernandez *et al.*, "The structure of anchorin CII, a collagen binding protein isolated from chondrocyte membrane.," *J. Biol. Chem.*, vol. 263, no. 12, pp. 5921–5, Apr. 1988.
- [54] J. A. Martin and J. A. Buckwalter, "Effects of fibronectin on articular cartilage chondrocyte proteoglycan synthesis and response to insulin-like growth factor-I.," *J. Orthop. Res.*, vol. 16, no. 6, pp. 752–7, Nov. 1998.
- [55] E. Hedbom *et al.*, "Cartilage matrix proteins. An acidic oligomeric protein (COMP) detected only in cartilage.," *J. Biol. Chem.*, vol. 267, no. 9, pp. 6132–6, Mar. 1992.
- [56] D. Heinegård, "Proteoglycans and more--from molecules to biology.," *Int. J. Exp. Pathol.*, vol. 90, no. 6, pp. 575–86, 2009.
- [57] E. J. Mackie and S. Ramsey, "Expression of tenascin in joint-associated tissues during development and postnatal growth.," *J. Anat.*, vol. 188 (Pt 1), pp. 157–65, Feb. 1996.
- [58] C. B. Knudson and B. P. Toole, "Changes in the pericellular matrix during differentiation of limb bud mesoderm.," *Dev. Biol.*, vol. 112, no. 2, pp. 308–18, Dec. 1985.

- [59] W. Dessau, H. von der Mark, K. von der Mark, and S. Fischer, "Changes in the patterns of collagens and fibronectin during limb-bud chondrogenesis.," *J. Embryol. Exp. Morphol.*, vol. 57, pp. 51–60, Jun. 1980.
- [60] R. A. Kosher, W. M. Kulyk, and S. W. Gay, "Collagen gene expression during limb cartilage differentiation.," *J. Cell Biol.*, vol. 102, no. 4, pp. 1151–6, Apr. 1986.
- [61] W. M. Kulyk, C. N. Coelho, and R. A. Kosher, "Type IX collagen gene expression during limb cartilage differentiation.," *Matrix*, vol. 11, no. 4, pp. 282–8, Aug. 1991.
- [62] F. Mallein-Gerin, R. A. Kosher, W. B. Upholt, and M. L. Tanzer, "Temporal and spatial analysis of cartilage proteoglycan core protein gene expression during limb development by in situ hybridization.," *Dev. Biol.*, vol. 126, no. 2, pp. 337–45, Apr. 1988.
- [63] N. S. Stirpe and P. F. Goetinck, "Gene regulation during cartilage differentiation: temporal and spatial expression of link protein and cartilage matrix protein in the developing limb.," *Development*, vol. 107, no. 1, pp. 23–33, Sep. 1989.
- [64] F. M. Craig, G. Bentley, and C. W. Archer, "The spatial and temporal pattern of collagens I and II and keratan sulphate in the developing chick metatarsophalangeal joint.," *Development*, vol. 99, no. 3, pp. 383–91, Mar. 1987.
- [65] P. H. Francis-West, J. Parish, K. Lee, and C. W. Archer, "BMP/GDF-signalling interactions during synovial joint development.," *Cell Tissue Res.*, vol. 296, no. 1, pp. 111–9, Apr. 1999.
- [66] P. Dy *et al.*, "Synovial joint morphogenesis requires the chondrogenic action of Sox5 and Sox6 in growth plate and articular cartilage.," *Dev. Biol.*, vol. 341, no. 2, pp. 346–59, May 2010.
- [67] X. Guo, T. F. Day, X. Jiang, L. Garrett-Beal, L. Topol, and Y. Yang, "Wnt/beta-catenin signaling is sufficient and necessary for synovial joint formation.," *Genes Dev.*, vol. 18, no. 19, pp. 2404–17, Oct. 2004.
- [68] E. Koyama *et al.*, "A distinct cohort of progenitor cells participates in synovial joint and articular cartilage formation during mouse limb skeletogenesis.," *Dev. Biol.*, vol. 316, no. 1, pp. 62–73, Apr. 2008.
- [69] P. H. Francis-West *et al.*, "Mechanisms of GDF-5 action during skeletal development.," *Development*, vol. 126, no. 6, pp. 1305–15, Mar. 1999.
- [70] E. E. Storm and D. M. Kingsley, "GDF5 coordinates bone and joint formation during digit development.," *Dev. Biol.*, vol. 209, no. 1, pp. 11–27, May 1999.
- [71] L. J. Brunet, J. A. McMahon, A. P. McMahon, and R. M. Harland, "Noggin, cartilage morphogenesis, and joint formation in the mammalian skeleton.," *Science*, vol. 280, no. 5368, pp. 1455–7, May 1998.
- [72] Y. Shwartz, S. Viukov, S. Krief, and E. Zelzer, "Joint Development Involves a Continuous Influx of Gdf5-Positive Cells," *Cell Rep.*, vol. 15, no. 12, pp. 2577–2587, Jun. 2016.
- [73] A. J. Hayes, S. MacPherson, H. Morrison, G. Dowthwaite, and C. W. Archer, "The development of articular cartilage: evidence for an appositional growth mechanism.," *Anat. Embryol. (Berl.)*, vol. 203, no. 6, pp. 469–79, Jun. 2001.
- [74] E. Kozhemyakina *et al.*, "Identification of a Prg4-expressing articular cartilage progenitor cell population in mice.," *Arthritis Rheumatol. (Hoboken, N.J.)*, vol. 67, no. 5, pp. 1261–73, May 2015.
- [75] R. S. Decker *et al.*, "Cell origin, volume and arrangement are drivers of articular cartilage formation, morphogenesis and response to injury in mouse limbs.," *Dev. Biol.*, vol. 426, no. 1, pp. 56–68, Jun. 2017.
- [76] F. Cervantes-Diaz, P. Contreras, and S. Marcellini, "Evolutionary origin of endochondral ossification: the transdifferentiation hypothesis.," *Dev. Genes Evol.*, vol. 227, no. 2, pp. 121–127, Mar. 2017.
- [77] K. J. Noonan, E. B. Hunziker, J. Nessler, and J. A. Buckwalter, "Changes in cell, matrix compartment, and fibrillar collagen volumes between growth-plate zones.," *J. Orthop. Res.*, vol. 16, no. 4, pp. 500–8, Jul. 1998.
- [78] M. F. Carlevaro, S. Cermelli, R. Cancedda, and F. Descalzi Cancedda, "Vascular endothelial growth factor (VEGF) in cartilage neovascularization and chondrocyte differentiation: auto-paracrine role during endochondral bone formation.," *J. Cell Sci.*, vol. 113 (Pt 1, pp. 59–69, Jan. 2000.
- [79] Y.-Q. Yang, Y.-Y. Tan, R. Wong, A. Wenden, L.-K. Zhang, and A. B. M. Rabie, "The role of vascular endothelial growth factor in ossification.," *Int. J. Oral Sci.*, vol. 4, no. 2, pp. 64–8, Jun. 2012.
- [80] N. Ortega, D. J. Behonick, and Z. Werb, "Matrix remodeling during endochondral ossification.," *Trends Cell Biol.*, vol. 14, no. 2, pp. 86–93, Feb. 2004.
- [81] P. Aghajanian and S. Mohan, "The art of building bone: emerging role of chondrocyte-to-osteoblast transdifferentiation in endochondral ossification.," *Bone Res.*, vol. 6, no. 1, p. 19, Dec. 2018.
- [82] L. E. Jansen, N. P. Birch, J. D. Schiffman, A. J. Crosby, and S. R. Peyton, "Mechanics of intact bone marrow.," *J. Mech. Behav. Biomed. Mater.*, vol. 50, pp. 299–307, Oct. 2015.
- [83] R. S. Decker, E. Koyama, and M. Pacifici, "Genesis and morphogenesis of limb synovial joints and articular cartilage.," *Matrix Biol.*, vol. 39, pp. 5–10, Oct. 2014.
- [84] E. M. Thompson, A. Matsiko, E. Farrell, D. J. Kelly, and F. J. O'Brien, "Recapitulating endochondral ossification: a promising route to in vivo bone regeneration.," *J. Tissue Eng. Regen. Med.*, vol. 9, no. 8, pp. 889–902, Aug. 2015.
- [85] C. B. Carballo, Y. Nakagawa, I. Sekiya, and S. A. Rodeo, "Basic Science of Articular Cartilage.," *Clin. Sports Med.*, vol. 36, no. 3, pp. 413–425, Jul. 2017.
- [86] R. Huggenberger and M. Detmar, "The cutaneous vascular system in chronic skin inflammation.," *J. Investig. dermatology. Symp. Proc.*, vol. 15, no. 1, pp. 24–32, Dec. 2011.
- [87] G. C. Terry, F. Flandry, J. W. Van Manen, and L. A. Norwood, "Isolated chondral fractures of the knee.," *Clin. Orthop. Relat. Res.*, no. 234, pp. 170–7, Sep. 1988.

- [88] W. G. Clancy, D. A. Nelson, B. Reider, and R. G. Narechania, "Anterior cruciate ligament reconstruction using one-third of the patellar ligament, augmented by extra-articular tendon transfers.," *J. Bone Joint Surg. Am.*, vol. 64, no. 3, pp. 352–9, Mar. 1982.
- [89] J. S. Gilley, M. I. Gelman, D. M. Edson, and R. W. Metcalf, "Chondral fractures of the knee. Arthrographic, arthroscopic, and clinical manifestations.," *Radiology*, vol. 138, no. 1, pp. 51–4, Jan. 1981.
- [90] E. B. Hunziker, "Articular cartilage repair: are the intrinsic biological constraints undermining this process insuperable?," *Osteoarthr. Cartil.*, vol. 7, no. 1, pp. 15–28, Jan. 1999.
- [91] F. R. Convery, W. H. Akeson, and G. H. Keown, "The repair of large osteochondral defects. An experimental study in horses.," *Clin. Orthop. Relat. Res.*, vol. 82, pp. 253–62, 1972.
- [92] A. Mobasheri, C. Csaki, A. L. Clutterbuck, M. Rahmzadeh, and M. Shakibaei, "Mesenchymal stem cells in connective tissue engineering and regenerative medicine: applications in cartilage repair and osteoarthritis therapy.," *Histol. Histopathol.*, vol. 24, no. 3, pp. 347–66, 2009.
- [93] B. Johnstone and J. U. Yoo, "Autologous mesenchymal progenitor cells in articular cartilage repair.," *Clin. Orthop. Relat. Res.*, no. 367 Suppl, pp. S156-62, Oct. 1999.
- [94] J. A. Buckwalter, "Articular cartilage: injuries and potential for healing.," *J. Orthop. Sports Phys. Ther.*, vol. 28, no. 4, pp. 192–202, Oct. 1998.
- [95] V. C. Mow, A. Ratcliffe, M. P. Rosenwasser, and J. A. Buckwalter, "Experimental studies on repair of large osteochondral defects at a high weight bearing area of the knee joint: a tissue engineering study.," *J. Biomech. Eng.*, vol. 113, no. 2, pp. 198–207, May 1991.
- [96] M. Lotz and R. F. Loeser, "Effects of aging on articular cartilage homeostasis.," *Bone*, vol. 51, no. 2, pp. 241–8, Aug. 2012.
- [97] N. Arden and M. C. Nevitt, "Osteoarthritis: epidemiology.," *Best Pract. Res. Clin. Rheumatol.*, vol. 20, no. 1, pp. 3–25, Feb. 2006.
- [98] G. Verbruggen *et al.*, "Influence of aging on the synthesis and morphology of the aggrecans synthesized by differentiated human articular chondrocytes.," *Osteoarthr. Cartil.*, vol. 8, no. 3, pp. 170–9, May 2000.
- [99] Cahill, "Osteochondritis Dissecans of the Knee: Treatment of Juvenile and Adult Forms.," *J. Am. Acad. Orthop. Surg.*, vol. 3, no. 4, pp. 237–247, Jul. 1995.
- [100] K. Pridie, H. Z-k, and G. Gordon-Strachan, "A method of resurfacing osteoarthritis knee joints." 01-Jan-1959.
- [101] J. R. Steadman, W. G. Rodkey, S. B. Singleton, and K. K. Briggs, "Microfracture technique for full-thickness chondral defects: Technique and clinical results.," *Oper. Tech. Orthop.*, vol. 7, no. 4, pp. 300–304, Oct. 1997.
- [102] J. R. Steadman, W. G. Rodkey, and J. J. Rodrigo, "Microfracture: surgical technique and rehabilitation to treat chondral defects.," *Clin. Orthop. Relat. Res.*, no. 391 Suppl, pp. S362-9, Oct. 2001.
- [103] J. R. Steadman, B. S. Miller, S. G. Karas, T. F. Schlegel, K. K. Briggs, and R. J. Hawkins, "The microfracture technique in the treatment of full-thickness chondral lesions of the knee in National Football League players.," *J. Knee Surg.*, vol. 16, no. 2, pp. 83–6, Apr. 2003.
- [104] L. Hangody and P. Füles, "Autologous osteochondral mosaicplasty for the treatment of full-thickness defects of weight-bearing joints: ten years of experimental and clinical experience.," *J. Bone Joint Surg. Am.*, vol. 85-A Suppl, pp. 25–32, 2003.
- [105] L. Bartha, A. Vajda, Z. Duska, H. Rahmeh, and L. Hangody, "Autologous osteochondral mosaicplasty grafting.," *J. Orthop. Sports Phys. Ther.*, vol. 36, no. 10, pp. 739–50, Oct. 2006.
- [106] M. F. Erol and O. Karakoyun, "A new point of view for mosaicplasty in the treatment of focal cartilage defects of knee joint: honeycomb pattern.," *Springerplus*, vol. 5, no. 1, p. 1170, 2016.
- [107] C. Englert, K. B. McGowan, T. J. Klein, A. Giurea, B. L. Schumacher, and R. L. Sah, "Inhibition of integrative cartilage repair by proteoglycan 4 in synovial fluid.," *Arthritis Rheum.*, vol. 52, no. 4, pp. 1091–9, Apr. 2005.
- [108] P. M. Peterson L, Menche D, Grande D, "Chondrocyte transplantation – an experimental model in rabbits," in *Trans Orthop Res Soc*, 1984, p. 218.
- [109] W. Bartlett *et al.*, "Autologous chondrocyte implantation versus matrix-induced autologous chondrocyte implantation for osteochondral defects of the knee: a prospective, randomised study.," *J. Bone Joint Surg. Br.*, vol. 87, no. 5, pp. 640–5, May 2005.
- [110] F. Zeifang, D. Oberle, C. Nierhoff, W. Richter, B. Moradi, and H. Schmitt, "Autologous chondrocyte implantation using the original periosteum-cover technique versus matrix-associated autologous chondrocyte implantation: a randomized clinical trial.," *Am. J. Sports Med.*, vol. 38, no. 5, pp. 924–33, May 2010.
- [111] C. M. Hettrich, D. Crawford, and S. A. Rodeo, "Cartilage repair: third-generation cell-based technologies--basic science, surgical techniques, clinical outcomes.," *Sports Med. Arthrosc.*, vol. 16, no. 4, pp. 230–5, Dec. 2008.
- [112] J. E. J. Bekkers *et al.*, "One-stage focal cartilage defect treatment with bone marrow mononuclear cells and chondrocytes leads to better macroscopic cartilage regeneration compared to microfracture in goats.," *Osteoarthr. Cartil.*, vol. 21, no. 7, pp. 950–6, Jul. 2013.
- [113] G. N. Homminga, S. K. Bulstra, P. S. Bouwmeester, and A. J. van der Linden, "Perichondral grafting for cartilage lesions of the knee.," *J. Bone Joint Surg. Br.*, vol. 72, no. 6, pp. 1003–7, Nov. 1990.
- [114] H. Alfredson and R. Lorentzon, "Autologous periosteum transplantation for the treatment of full thickness patellar cartilage defects.," *Ortop. Traumatol. Rehabil.*, vol. 3, no. 2, pp. 216–23, Apr. 2001.

- [115] W. Schultz and D. Göbel, "Articular cartilage regeneration of the knee joint after proximal tibial valgus osteotomy: a prospective study of different intra- and extra-articular operative techniques.," *Knee Surg. Sports Traumatol. Arthrosc.*, vol. 7, no. 1, pp. 29–36, Jan. 1999.
- [116] M. Tatebe, R. Nakamura, H. Kagami, K. Okada, and M. Ueda, "Differentiation of transplanted mesenchymal stem cells in a large osteochondral defect in rabbit.," *Cytotherapy*, vol. 7, no. 6, pp. 520–30, 2005.
- [117] M. B. Aydelotte, R. R. Greenhill, and K. E. Kuettner, "Differences between sub-populations of cultured bovine articular chondrocytes. II. Proteoglycan metabolism.," *Connect. Tissue Res.*, vol. 18, no. 3, pp. 223–34, 1988.
- [118] M. B. Aydelotte and K. E. Kuettner, "Differences between sub-populations of cultured bovine articular chondrocytes. I. Morphology and cartilage matrix production.," *Connect. Tissue Res.*, vol. 18, no. 3, pp. 205–22, 1988.
- [119] D. A. Lee, T. Noguchi, M. M. Knight, L. O'Donnell, G. Bentley, and D. L. Bader, "Response of chondrocyte subpopulations cultured within unloaded and loaded agarose.," *J. Orthop. Res.*, vol. 16, no. 6, pp. 726–33, Nov. 1998.
- [120] S. Moskalewski, A. Hyc, and A. Osiecka-Iwan, "Immune response by host after allogeneic chondrocyte transplant to the cartilage.," *Microsc. Res. Tech.*, vol. 58, no. 1, pp. 3–13, Jul. 2002.
- [121] T. Niemietz, G. Zass, S. Hagmann, S. Diederichs, T. Gotterbarm, and W. Richter, "Xenogeneic transplantation of articular chondrocytes into full-thickness articular cartilage defects in minipigs: fate of cells and the role of macrophages.," *Cell Tissue Res.*, vol. 358, no. 3, pp. 749–61, Dec. 2014.
- [122] B. Arzi *et al.*, "Cartilage immunoprivilege depends on donor source and lesion location.," *Acta Biomater.*, vol. 23, pp. 72–81, Sep. 2015.
- [123] R. O. C. Oreffo, C. Cooper, C. Mason, and M. Clements, "Mesenchymal stem cells: lineage, plasticity, and skeletal therapeutic potential.," *Stem Cell Rev.*, vol. 1, no. 2, pp. 169–78, 2005.
- [124] F. Gao *et al.*, "Mesenchymal stem cells and immunomodulation: current status and future prospects.," *Cell Death Dis.*, vol. 7, no. 1, p. e2062, Jan. 2016.
- [125] P. Ganguly, J. J. El-Jawhari, P. V. Giannoudis, A. N. Burska, F. Ponchel, and E. A. Jones, "Age-related Changes in Bone Marrow Mesenchymal Stromal Cells: A Potential Impact on Osteoporosis and Osteoarthritis Development.," *Cell Transplant.*, vol. 26, no. 9, pp. 1520–1529, Sep. 2017.
- [126] Y.-H. K. Yang, "Aging of mesenchymal stem cells: Implication in regenerative medicine.," *Regen. Ther.*, vol. 9, pp. 120–122, Dec. 2018.
- [127] J. M. Murphy, K. Dixon, S. Beck, D. Fabian, A. Feldman, and F. Barry, "Reduced chondrogenic and adipogenic activity of mesenchymal stem cells from patients with advanced osteoarthritis.," *Arthritis Rheum.*, vol. 46, no. 3, pp. 704–13, Mar. 2002.
- [128] V. Dudics *et al.*, "Chondrogenic potential of mesenchymal stem cells from patients with rheumatoid arthritis and osteoarthritis: measurements in a microculture system.," *Cells. Tissues. Organs*, vol. 189, no. 5, pp. 307–16, 2009.
- [129] A. Scharstuhl, B. Schewe, K. Benz, C. Gaissmaier, H.-J. Bühring, and R. Stoop, "Chondrogenic potential of human adult mesenchymal stem cells is independent of age or osteoarthritis etiology.," *Stem Cells*, vol. 25, no. 12, pp. 3244–51, Dec. 2007.
- [130] A. Banfi, G. Bianchi, R. Notaro, L. Luzzatto, R. Cancedda, and R. Quarto, "Replicative aging and gene expression in long-term cultures of human bone marrow stromal cells.," *Tissue Eng.*, vol. 8, no. 6, pp. 901–10, Dec. 2002.
- [131] M. A. Baxter, R. F. Wynn, S. N. Jowitt, J. E. Wraith, L. J. Fairbairn, and I. Bellantuono, "Study of telomere length reveals rapid aging of human marrow stromal cells following in vitro expansion.," *Stem Cells*, vol. 22, no. 5, pp. 675–82, Sep. 2004.
- [132] S. P. Bruder, N. Jaiswal, and S. E. Haynesworth, "Growth kinetics, self-renewal, and the osteogenic potential of purified human mesenchymal stem cells during extensive subcultivation and following cryopreservation.," *J. Cell. Biochem.*, vol. 64, no. 2, pp. 278–94, Feb. 1997.
- [133] V. Vacanti, E. Kong, G. Suzuki, K. Sato, J. M. Canty, and T. Lee, "Phenotypic changes of adult porcine mesenchymal stem cells induced by prolonged passaging in culture.," *J. Cell. Physiol.*, vol. 205, no. 2, pp. 194–201, Nov. 2005.
- [134] E. J. Koay, G. M. B. Hoben, and K. A. Athanasiou, "Tissue engineering with chondrogenically differentiated human embryonic stem cells.," *Stem Cells*, vol. 25, no. 9, pp. 2183–90, Sep. 2007.
- [135] E. J. Koay and K. A. Athanasiou, "Development of serum-free, chemically defined conditions for human embryonic stem cell-derived fibrochondrogenesis.," *Tissue Eng. Part A*, vol. 15, no. 8, pp. 2249–57, Aug. 2009.
- [136] E. J. Koay and K. A. Athanasiou, "Hypoxic chondrogenic differentiation of human embryonic stem cells enhances cartilage protein synthesis and biomechanical functionality.," *Osteoarthr. Cartil.*, vol. 16, no. 12, pp. 1450–6, Dec. 2008.
- [137] K. Hug, "Sources of human embryos for stem cell research: ethical problems and their possible solutions.," *Medicina (Kaunas)*, vol. 41, no. 12, pp. 1002–10, 2005.
- [138] I. Gutierrez-Aranda *et al.*, "Human induced pluripotent stem cells develop teratoma more efficiently and faster than human embryonic stem cells regardless the site of injection.," *Stem Cells*, vol. 28, no. 9, pp. 1568–70, Sep. 2010.
- [139] J. Gorecka *et al.*, "The potential and limitations of induced pluripotent stem cells to achieve wound healing.," *Stem Cell Res. Ther.*, vol. 10, no. 1, p. 87, Mar. 2019.
- [140] K. Takahashi *et al.*, "Induction of pluripotent stem cells from adult human fibroblasts by defined factors.," *Cell*, vol. 131, no. 5, pp. 861–72, Nov. 2007.
- [141] J. Yu *et al.*, "Induced pluripotent stem cell lines derived from human somatic cells.," *Science*, vol. 318, no. 5858, pp.

- 1917–20, Dec. 2007.
- [142] T. Wang, H. Zhao, Q. Zhang, C. Xu, and C. Liu, “Generation of transgene-free induced pluripotent stem cells with non-viral methods.,” *Chinese Med. Sci. J. = Chung-kuo i hsueh k'o hsueh tsa chih*, vol. 28, no. 1, pp. 50–4, Mar. 2013.
- [143] X.-Y. Deng *et al.*, “Non-viral methods for generating integration-free, induced pluripotent stem cells.,” *Curr. Stem Cell Res. Ther.*, vol. 10, no. 2, pp. 153–8, 2015.
- [144] R. Castro-Viñuelas *et al.*, “Induced pluripotent stem cells for cartilage repair: current status and future perspectives.,” *Eur. Cell. Mater.*, vol. 36, pp. 96–109, Sep. 2018.
- [145] F. Soldner *et al.*, “Parkinson’s Disease Patient-Derived Induced Pluripotent Stem Cells Free of Viral Reprogramming Factors,” *Cell*, vol. 136, no. 5, pp. 964–977, Mar. 2009.
- [146] L. C. Davies, E. J. Blain, S. J. Gilbert, B. Caterson, and V. C. Duance, “The potential of IGF-1 and TGFbeta1 for promoting ‘adult’ articular cartilage repair: an in vitro study.,” *Tissue Eng. Part A*, vol. 14, no. 7, pp. 1251–61, Jul. 2008.
- [147] L. Longobardi *et al.*, “Effect of IGF-I in the chondrogenesis of bone marrow mesenchymal stem cells in the presence or absence of TGF-beta signaling.,” *J. Bone Miner. Res.*, vol. 21, no. 4, pp. 626–36, Apr. 2006.
- [148] K. J. Ekenstedt, W. E. Sonntag, R. F. Loeser, B. R. Lindgren, and C. S. Carlson, “Effects of chronic growth hormone and insulin-like growth factor 1 deficiency on osteoarthritis severity in rat knee joints.,” *Arthritis Rheum.*, vol. 54, no. 12, pp. 3850–8, Dec. 2006.
- [149] L. A. Fortier, H. O. Mohammed, G. Lust, and A. J. Nixon, “Insulin-like growth factor-I enhances cell-based repair of articular cartilage.,” *J. Bone Joint Surg. Br.*, vol. 84, no. 2, pp. 276–88, Mar. 2002.
- [150] F.-Y. Wei, J. K. Lee, L. Wei, F. Qu, and J.-Z. Zhang, “Correlation of insulin-like growth factor 1 and osteoarthritic cartilage degradation: a spontaneous osteoarthritis in guinea-pig.,” *Eur. Rev. Med. Pharmacol. Sci.*, vol. 21, no. 20, pp. 4493–4500, Oct. 2017.
- [151] T. Vincent, M. Hermansson, M. Bolton, R. Wait, and J. Saklatvala, “Basic FGF mediates an immediate response of articular cartilage to mechanical injury.,” *Proc. Natl. Acad. Sci. U. S. A.*, vol. 99, no. 12, pp. 8259–64, Jun. 2002.
- [152] H.-J. Im *et al.*, “Basic fibroblast growth factor accelerates matrix degradation via a neuro-endocrine pathway in human adult articular chondrocytes.,” *J. Cell. Physiol.*, vol. 215, no. 2, pp. 452–63, May 2008.
- [153] T. Fujisato, T. Sajiki, Q. Liu, and Y. Ikada, “Effect of basic fibroblast growth factor on cartilage regeneration in chondrocyte-seeded collagen sponge scaffold.,” *Biomaterials*, vol. 17, no. 2, pp. 155–62, Jan. 1996.
- [154] H.-J. Im *et al.*, “Basic fibroblast growth factor stimulates matrix metalloproteinase-13 via the molecular cross-talk between the mitogen-activated protein kinases and protein kinase Cdelta pathways in human adult articular chondrocytes.,” *J. Biol. Chem.*, vol. 282, no. 15, pp. 11110–21, Apr. 2007.
- [155] M. B. Ellman, H. S. An, P. Muddasani, and H.-J. Im, “Biological impact of the fibroblast growth factor family on articular cartilage and intervertebral disc homeostasis.,” *Gene*, vol. 420, no. 1, pp. 82–9, Aug. 2008.
- [156] K. K. Middleton, V. Barro, B. Muller, S. Terada, and F. H. Fu, “Evaluation of the effects of platelet-rich plasma (PRP) therapy involved in the healing of sports-related soft tissue injuries.,” *Iowa Orthop. J.*, vol. 32, pp. 150–63, 2012.
- [157] L. Casati, F. Celotti, P. Negri-Cesi, M. C. Sacchi, P. Castano, and A. Colciago, “Platelet derived growth factor (PDGF) contained in Platelet Rich Plasma (PRP) stimulates migration of osteoblasts by reorganizing actin cytoskeleton.,” *Cell Adh. Migr.*, vol. 8, no. 6, pp. 595–602, 2014.
- [158] Y. Mishima and M. Lotz, “Chemotaxis of human articular chondrocytes and mesenchymal stem cells.,” *J. Orthop. Res.*, vol. 26, no. 10, pp. 1407–12, Oct. 2008.
- [159] P. Liu, Y. Ying, and R. G. Anderson, “Platelet-derived growth factor activates mitogen-activated protein kinase in isolated caveolae.,” *Proc. Natl. Acad. Sci. U. S. A.*, vol. 94, no. 25, pp. 13666–70, Dec. 1997.
- [160] G.-Z. Zhao *et al.*, “Effects of platelet-derived growth factor on chondrocyte proliferation, migration and apoptosis via regulation of GIT1 expression.,” *Mol. Med. Rep.*, vol. 14, no. 1, pp. 897–903, Jul. 2016.
- [161] L. Weiser, M. Bhargava, E. Attia, and P. A. Torzilli, “Effect of serum and platelet-derived growth factor on chondrocytes grown in collagen gels.,” *Tissue Eng.*, vol. 5, no. 6, pp. 533–44, Dec. 1999.
- [162] C. A. Pangborn and K. A. Athanasiou, “Effects of growth factors on meniscal fibrochondrocytes.,” *Tissue Eng.*, vol. 11, no. 7–8, pp. 1141–8, Jul. 2005.
- [163] K. Stewart, M. Pabbruwe, S. Dickinson, T. Sims, A. P. Hollander, and J. B. Chaudhuri, “The effect of growth factor treatment on meniscal chondrocyte proliferation and differentiation on polyglycolic acid scaffolds.,” *Tissue Eng.*, vol. 13, no. 2, pp. 271–80, Feb. 2007.
- [164] M. Y. Wu and C. S. Hill, “Tgf-beta superfamily signaling in embryonic development and homeostasis.,” *Dev. Cell*, vol. 16, no. 3, pp. 329–43, Mar. 2009.
- [165] Ł. A. Poniatowski, P. Wojdasiewicz, R. Gasik, and D. Szukiewicz, “Transforming growth factor Beta family: insight into the role of growth factors in regulation of fracture healing biology and potential clinical applications.,” *Mediators Inflamm.*, vol. 2015, p. 137823, 2015.
- [166] J. Yang *et al.*, “Bone morphogenetic proteins: Relationship between molecular structure and their osteogenic activity,” *Food Sci. Hum. Wellness*, vol. 3, no. 3–4, pp. 127–135, Sep. 2014.
- [167] P. A. Guerne, A. Sublet, and M. Lotz, “Growth factor responsiveness of human articular chondrocytes: distinct profiles in primary chondrocytes, subcultured chondrocytes, and fibroblasts.,” *J. Cell. Physiol.*, vol. 158, no. 3, pp. 476–84, Mar. 1994.

- [168] E. Grimaud, D. Heymann, and F. Rédini, "Recent advances in TGF-beta effects on chondrocyte metabolism. Potential therapeutic roles of TGF-beta in cartilage disorders.," *Cytokine Growth Factor Rev.*, vol. 13, no. 3, pp. 241–57, Jun. 2002.
- [169] T. Blunk *et al.*, "Differential effects of growth factors on tissue-engineered cartilage.," *Tissue Eng.*, vol. 8, no. 1, pp. 73–84, Feb. 2002.
- [170] B. D. Elder and K. a Athanasiou, "Systematic assessment of growth factor treatment on biochemical and biomechanical properties of engineered articular cartilage constructs.," *Osteoarthr. Cartil.*, vol. 17, no. 1, pp. 114–23, Jan. 2009.
- [171] E. N. Blaney Davidson, P. M. van der Kraan, and W. B. van den Berg, "TGF-beta and osteoarthritis.," *Osteoarthr. Cartil.*, vol. 15, no. 6, pp. 597–604, Jun. 2007.
- [172] Q. O. Tang *et al.*, "TGF-beta3: A potential biological therapy for enhancing chondrogenesis.," *Expert Opin. Biol. Ther.*, vol. 9, no. 6, pp. 689–701, Jun. 2009.
- [173] S. D. Thorpe, C. T. Buckley, T. Vinardell, F. J. O'Brien, V. A. Campbell, and D. J. Kelly, "The response of bone marrow-derived mesenchymal stem cells to dynamic compression following TGF-beta3 induced chondrogenic differentiation.," *Ann. Biomed. Eng.*, vol. 38, no. 9, pp. 2896–909, Sep. 2010.
- [174] L. Danisovic, I. Varga, R. Zamborsky, and D. Böhmer, "The tissue engineering of articular cartilage: cells, scaffolds and stimulating factors.," *Exp. Biol. Med. (Maywood)*, vol. 237, no. 1, pp. 10–7, Jan. 2012.
- [175] S. Chubinskaya, D. Segalite, D. Pikovsky, A. A. Hakimiyani, and D. C. Rueger, "Effects induced by BMPs in cultures of human articular chondrocytes: comparative studies.," *Growth Factors*, vol. 26, no. 5, pp. 275–83, Oct. 2008.
- [176] D. M. Erickson *et al.*, "Recombinant bone morphogenetic protein (BMP)-2 regulates costochondral growth plate chondrocytes and induces expression of BMP-2 and BMP-4 in a cell maturation-dependent manner.," *J. Orthop. Res.*, vol. 15, no. 3, pp. 371–80, May 1997.
- [177] T. Gründer *et al.*, "Bone morphogenetic protein (BMP)-2 enhances the expression of type II collagen and aggrecan in chondrocytes embedded in alginate beads.," *Osteoarthr. Cartil.*, vol. 12, no. 7, pp. 559–67, Jul. 2004.
- [178] D. Ollitrault *et al.*, "BMP-2, hypoxia, and COL1A1/HtrA1 siRNAs favor neo-cartilage hyaline matrix formation in chondrocytes.," *Tissue Eng. Part C. Methods*, vol. 21, no. 2, pp. 133–47, Feb. 2015.
- [179] N. D. Miljkovic, G. M. Cooper, and K. G. Marra, "Chondrogenesis, bone morphogenetic protein-4 and mesenchymal stem cells.," *Osteoarthr. Cartil.*, vol. 16, no. 10, pp. 1121–30, Oct. 2008.
- [180] A. Steinert *et al.*, "Chondrogenic differentiation of mesenchymal progenitor cells encapsulated in ultrahigh-viscosity alginate.," *J. Orthop. Res.*, vol. 21, no. 6, pp. 1090–7, Nov. 2003.
- [181] K. Bobacz, R. Gruber, A. Soleiman, L. Erlacher, J. S. Smolen, and W. B. Graninger, "Expression of bone morphogenetic protein 6 in healthy and osteoarthritic human articular chondrocytes and stimulation of matrix synthesis in vitro.," *Arthritis Rheum.*, vol. 48, no. 9, pp. 2501–8, Sep. 2003.
- [182] B. O. Diekman, B. T. Estes, and F. Guilak, "The effects of BMP6 overexpression on adipose stem cell chondrogenesis: Interactions with dexamethasone and exogenous growth factors.," *J. Biomed. Mater. Res. A*, vol. 93, no. 3, pp. 994–1003, Jun. 2010.
- [183] M. Pecina, M. Jelic, S. Martinovic, M. Haspl, and S. Vukicevic, "Articular cartilage repair: the role of bone morphogenetic proteins.," *Int. Orthop.*, vol. 26, no. 3, pp. 131–6, Jun. 2002.
- [184] M. Mattioli-Belmonte *et al.*, "N,N-dicarboxymethyl chitosan as delivery agent for bone morphogenetic protein in the repair of articular cartilage.," *Med. Biol. Eng. Comput.*, vol. 37, no. 1, pp. 130–4, Jan. 1999.
- [185] S. Chubinskaya, M. Hurtig, and D. C. Rueger, "OP-1/BMP-7 in cartilage repair.," *Int. Orthop.*, vol. 31, no. 6, pp. 773–81, Dec. 2007.
- [186] C. Vinatier *et al.*, "Cartilage tissue engineering: towards a biomaterial-assisted mesenchymal stem cell therapy.," *Curr. Stem Cell Res. Ther.*, vol. 4, no. 4, pp. 318–29, Dec. 2009.
- [187] K. Huang *et al.*, "Cartilage Tissue Regeneration: The Roles of Cells, Stimulating Factors and Scaffolds.," *Curr. Stem Cell Res. Ther.*, vol. 13, no. 7, pp. 547–567, Aug. 2018.
- [188] L. Zhang, J. Hu, and K. A. Athanasiou, "The role of tissue engineering in articular cartilage repair and regeneration.," *Crit. Rev. Biomed. Eng.*, vol. 37, no. 1–2, pp. 1–57, 2009.
- [189] A. Getgood, R. Brooks, L. Fortier, and N. Rushton, "Articular cartilage tissue engineering: today's research, tomorrow's practice?," *J. Bone Joint Surg. Br.*, vol. 91, no. 5, pp. 565–76, May 2009.
- [190] S. Chattopadhyay and R. T. Raines, "Review collagen-based biomaterials for wound healing.," *Biopolymers*, vol. 101, no. 8, pp. 821–33, Aug. 2014.
- [191] A. K. Lynn, I. V. Yannas, and W. Bonfield, "Antigenicity and immunogenicity of collagen.," *J. Biomed. Mater. Res. B. Appl. Biomater.*, vol. 71, no. 2, pp. 343–54, Nov. 2004.
- [192] T. Kimura, N. Yasui, S. Ohsawa, and K. Ono, "Chondrocytes embedded in collagen gels maintain cartilage phenotype during long-term cultures.," *Clin. Orthop. Relat. Res.*, no. 186, pp. 231–9, Jun. 1984.
- [193] M.-H. Zheng *et al.*, "Matrix-induced autologous chondrocyte implantation (MACI): biological and histological assessment.," *Tissue Eng.*, vol. 13, no. 4, pp. 737–46, Apr. 2007.
- [194] R. Dorotka, U. Bindreiter, K. Macfelda, U. Windberger, and S. Nehrer, "Marrow stimulation and chondrocyte transplantation using a collagen matrix for cartilage repair.," *Osteoarthr. Cartil.*, vol. 13, no. 8, pp. 655–64, Aug. 2005.

- [195] L. Zheng *et al.*, “Chondrogenic differentiation of mesenchymal stem cells induced by collagen-based hydrogel: an in vivo study.,” *J. Biomed. Mater. Res. A*, vol. 93, no. 2, pp. 783–92, May 2010.
- [196] S. Nehrer *et al.*, “Canine chondrocytes seeded in type I and type II collagen implants investigated in vitro.,” *J. Biomed. Mater. Res.*, vol. 38, no. 2, pp. 95–104, 1997.
- [197] C. R. Lee, H. A. Breinan, S. Nehrer, and M. Spector, “Articular cartilage chondrocytes in type I and type II collagen-GAG matrices exhibit contractile behavior in vitro.,” *Tissue Eng.*, vol. 6, no. 5, pp. 555–65, Oct. 2000.
- [198] C. L. Murphy and A. Sambanis, “Effect of oxygen tension and alginate encapsulation on restoration of the differentiated phenotype of passaged chondrocytes.,” *Tissue Eng.*, vol. 7, no. 6, pp. 791–803, Dec. 2001.
- [199] H. J. Häuselmann *et al.*, “Phenotypic stability of bovine articular chondrocytes after long-term culture in alginate beads.,” *J. Cell Sci.*, vol. 107 (Pt 1, pp. 17–27, Jan. 1994.
- [200] G. Birdi, R. H. Bridson, A. M. Smith, S. P. M. Bohari, and L. M. Grover, “Modification of alginate degradation properties using orthosilicic acid.,” *J. Mech. Behav. Biomed. Mater.*, vol. 6, pp. 181–7, Feb. 2012.
- [201] K. Y. Lee and D. J. Mooney, “Alginate: properties and biomedical applications.,” *Prog. Polym. Sci.*, vol. 37, no. 1, pp. 106–126, Jan. 2012.
- [202] D. R. Diduch, L. C. M. Jordan, C. M. Mierisch, and G. Balian, “Marrow stromal cells embedded in alginate for repair of osteochondral defects.,” *Arthroscopy*, vol. 16, no. 6, pp. 571–7, Sep. 2000.
- [203] P. D. Benya and J. D. Shaffer, “Dedifferentiated chondrocytes reexpress the differentiated collagen phenotype when cultured in agarose gels.,” *Cell*, vol. 30, no. 1, pp. 215–24, Aug. 1982.
- [204] D. B. Saris, N. Mukherjee, L. J. Berglund, F. M. Schultz, K. N. An, and S. W. O’Driscoll, “Dynamic pressure transmission through agarose gels.,” *Tissue Eng.*, vol. 6, no. 5, pp. 531–7, Oct. 2000.
- [205] S. H. Elder, S. A. Goldstein, J. H. Kimura, L. J. Soslowsky, and D. M. Spengler, “Chondrocyte differentiation is modulated by frequency and duration of cyclic compressive loading.,” *Ann. Biomed. Eng.*, vol. 29, no. 6, pp. 476–82, Jun. 2001.
- [206] R. L. Mauck *et al.*, “Functional tissue engineering of articular cartilage through dynamic loading of chondrocyte-seeded agarose gels.,” *J. Biomech. Eng.*, vol. 122, no. 3, pp. 252–60, Jun. 2000.
- [207] P. E. Donnelly, T. Chen, A. Finch, C. Brial, S. A. Maher, and P. A. Torzilli, “Photocrosslinked tyramine-substituted hyaluronate hydrogels with tunable mechanical properties improve immediate tissue-hydrogel interfacial strength in articular cartilage.,” *J. Biomater. Sci. Polym. Ed.*, vol. 28, no. 6, pp. 582–600, Apr. 2017.
- [208] T. Wang, J. H. Lai, and F. Yang, “Effects of Hydrogel Stiffness and Extracellular Compositions on Modulating Cartilage Regeneration by Mixed Populations of Stem Cells and Chondrocytes In Vivo.,” *Tissue Eng. Part A*, vol. 22, no. 23–24, pp. 1348–1356, 2016.
- [209] W. S. Toh, T. C. Lim, M. Kurisawa, and M. Spector, “Modulation of mesenchymal stem cell chondrogenesis in a tunable hyaluronic acid hydrogel microenvironment.,” *Biomaterials*, vol. 33, no. 15, pp. 3835–45, May 2012.
- [210] M. J. Kujawa and A. I. Caplan, “Hyaluronic acid bonded to cell-culture surfaces stimulates chondrogenesis in stage 24 limb mesenchyme cell cultures.,” *Dev. Biol.*, vol. 114, no. 2, pp. 504–18, Apr. 1986.
- [211] B. Grigolo *et al.*, “Evidence for redifferentiation of human chondrocytes grown on a hyaluronan-based biomaterial (HYAff 11): molecular, immunohistochemical and ultrastructural analysis.,” *Biomaterials*, vol. 23, no. 4, pp. 1187–95, Feb. 2002.
- [212] R. B. Jakobsen, A. Shahdadfar, F. P. Reinholt, and J. E. Brinckmann, “Chondrogenesis in a hyaluronic acid scaffold: Comparison between chondrocytes and MSC from bone marrow and adipose tissue.,” *Knee Surgery, Sport. Traumatol. Arthrosc.*, vol. 18, no. 10, pp. 1407–1416, Oct. 2010.
- [213] B. Grigolo *et al.*, “Osteoarthritis treated with mesenchymal stem cells on hyaluronan-based scaffold in rabbit.,” *Tissue Eng. Part C. Methods*, vol. 15, no. 4, pp. 647–58, Dec. 2009.
- [214] S.-H. Lee and H. Shin, “Matrices and scaffolds for delivery of bioactive molecules in bone and cartilage tissue engineering.,” *Adv. Drug Deliv. Rev.*, vol. 59, no. 4–5, pp. 339–59, May 2007.
- [215] H. J. Chung and T. G. Park, “Surface engineered and drug releasing pre-fabricated scaffolds for tissue engineering.,” *Adv. Drug Deliv. Rev.*, vol. 59, no. 4–5, pp. 249–62, May 2007.
- [216] P. Gentile, V. Chiono, I. Carmagnola, and P. V. Hatton, “An overview of poly(lactic-co-glycolic) acid (PLGA)-based biomaterials for bone tissue engineering.,” *Int. J. Mol. Sci.*, vol. 15, no. 3, pp. 3640–59, Feb. 2014.
- [217] D. A. Grande, C. Halberstadt, G. Naughton, R. Schwartz, and R. Manji, “Evaluation of matrix scaffolds for tissue engineering of articular cartilage grafts.,” *J. Biomed. Mater. Res.*, vol. 34, no. 2, pp. 211–20, Feb. 1997.
- [218] J. C. Middleton and A. J. Tipton, “Synthetic biodegradable polymers as orthopedic devices.,” *Biomaterials*, vol. 21, no. 23, pp. 2335–46, Dec. 2000.
- [219] S. L. Ishaug-Riley, L. E. Okun, G. Prado, M. A. Applegate, and A. Ratcliffe, “Human articular chondrocyte adhesion and proliferation on synthetic biodegradable polymer films.,” *Biomaterials*, vol. 20, no. 23–24, pp. 2245–56, Dec. 1999.
- [220] N. K. Lee, H. J. Oh, C. M. Hong, H. Suh, and S. H. Hong, “Comparison of the synthetic biodegradable polymers, polylactide (PLA), and polylactic-co-glycolic acid (PLGA) as scaffolds for artificial cartilage.,” *Biotechnol. Bioprocess Eng.*, vol. 14, no. 2, pp. 180–186, Apr. 2009.
- [221] A. T. Mehlhorn *et al.*, “Chondrogenesis of adipose-derived adult stem cells in a poly-lactide-co-glycolide scaffold.,” *Tissue Eng. Part A*, vol. 15, no. 5, pp. 1159–67, May 2009.

- [222] S.-C. Wu, J.-K. Chang, C.-K. Wang, G.-J. Wang, and M.-L. Ho, "Enhancement of chondrogenesis of human adipose derived stem cells in a hyaluronan-enriched microenvironment," *Biomaterials*, vol. 31, no. 4, pp. 631–640, Feb. 2010.
- [223] Y. Wei, H. Hu, H. Wang, Y. Wu, L. Deng, and J. Qi, "Cartilage regeneration of adipose-derived stem cells in a hybrid scaffold from fibrin-modified PLGA.," *Cell Transplant.*, vol. 18, no. 2, pp. 159–70, 2009.
- [224] Q. Huang, J. C. H. Goh, D. W. Hutmacher, and E. H. Lee, "In vivo mesenchymal cell recruitment by a scaffold loaded with transforming growth factor beta1 and the potential for in situ chondrogenesis.," *Tissue Eng.*, vol. 8, no. 3, pp. 469–82, Jul. 2002.
- [225] G. A. Ameer, T. A. Mahmood, and R. Langer, "A biodegradable composite scaffold for cell transplantation.," *J. Orthop. Res.*, vol. 20, no. 1, pp. 16–9, Jan. 2002.
- [226] B. Li, J. Yang, L. Ma, F. Li, Z. Tu, and C. Gao, "Fabrication of poly(lactide-co-glycolide) scaffold filled with fibrin gel, mesenchymal stem cells, and poly(ethylene oxide)-b-poly(L-lysine)/TGF- β 1 plasmid DNA complexes for cartilage restoration in vivo.," *J. Biomed. Mater. Res. A*, vol. 101, no. 11, pp. 3097–108, Nov. 2013.
- [227] C. V. Gemmiti and R. E. Guldberg, "Fluid flow increases type II collagen deposition and tensile mechanical properties in bioreactor-grown tissue-engineered cartilage.," *Tissue Eng.*, vol. 12, no. 3, pp. 469–79, Mar. 2006.
- [228] N. Yusoff, N. A. Abu Osman, and B. Pinguan-Murphy, "Design and validation of a bi-axial loading bioreactor for mechanical stimulation of engineered cartilage.," *Med. Eng. Phys.*, vol. 33, no. 6, pp. 782–8, Jul. 2011.
- [229] M. Sun, D. Lv, C. Zhang, and L. Zhu, "Culturing functional cartilage tissue under a novel bionic mechanical condition.," *Med. Hypotheses*, vol. 75, no. 6, pp. 657–9, Dec. 2010.
- [230] M. Jin, E. H. Frank, T. M. Quinn, E. B. Hunziker, and A. J. Grodzinsky, "Tissue shear deformation stimulates proteoglycan and protein biosynthesis in bovine cartilage explants.," *Arch. Biochem. Biophys.*, vol. 395, no. 1, pp. 41–8, Nov. 2001.
- [231] E. H. Frank, M. Jin, A. M. Loening, M. E. Levenston, and A. J. Grodzinsky, "A versatile shear and compression apparatus for mechanical stimulation of tissue culture explants.," *J. Biomech.*, vol. 33, no. 11, pp. 1523–7, Nov. 2000.
- [232] M. J. Stoddart, L. Ettinger, and H. J. Häuselmann, "Enhanced matrix synthesis in de novo, scaffold free cartilage-like tissue subjected to compression and shear.," *Biotechnol. Bioeng.*, vol. 95, no. 6, pp. 1043–51, Dec. 2006.
- [233] A.-M. Freyria, D. Cortial, M.-C. Ronzière, S. Guerret, and D. Herbage, "Influence of medium composition, static and stirred conditions on the proliferation of and matrix protein expression of bovine articular chondrocytes cultured in a 3-D collagen scaffold.," *Biomaterials*, vol. 25, no. 4, pp. 687–97, Feb. 2004.
- [234] G. Zhu *et al.*, "Comparing effects of perfusion and hydrostatic pressure on gene profiles of human chondrocyte.," *J. Biotechnol.*, vol. 210, pp. 59–65, Sep. 2015.
- [235] R. L. Smith *et al.*, "Effects of fluid-induced shear on articular chondrocyte morphology and metabolism in vitro.," *J. Orthop. Res.*, vol. 13, no. 6, pp. 824–31, Nov. 1995.
- [236] R. Lane Smith *et al.*, "Effects of shear stress on articular chondrocyte metabolism.," *Biorheology*, vol. 37, no. 1–2, pp. 95–107, 2000.
- [237] M. S. Lee, M. C. D. Trindade, T. Ikenoue, D. J. Schurman, S. B. Goodman, and R. L. Smith, "Effects of shear stress on nitric oxide and matrix protein gene expression in human osteoarthritic chondrocytes in vitro.," *J. Orthop. Res.*, vol. 20, no. 3, pp. 556–61, May 2002.
- [238] R. L. Mauck, C. T. Hung, and G. A. Ateshian, "Modeling of neutral solute transport in a dynamically loaded porous permeable gel: implications for articular cartilage biosynthesis and tissue engineering.," *J. Biomech. Eng.*, vol. 125, no. 5, pp. 602–14, Oct. 2003.
- [239] Y. J. Kim, R. L. Y. Sah, A. J. Grodzinsky, A. H. K. Plaas, and J. D. Sandy, "Mechanical Regulation of Cartilage Biosynthetic Behavior: Physical Stimuli," *Arch. Biochem. Biophys.*, vol. 311, no. 1, pp. 1–12, May 1994.
- [240] P. A. Torzilli *et al.*, "Characterization of cartilage metabolic response to static and dynamic stress using a mechanical explant test system.," *J. Biomech.*, vol. 30, no. 1, pp. 1–9, Jan. 1997.
- [241] S. Nebelung *et al.*, "Simultaneous anabolic and catabolic responses of human chondrocytes seeded in collagen hydrogels to long-term continuous dynamic compression.," *Ann. Anat.*, vol. 194, no. 4, pp. 351–8, Jul. 2012.
- [242] J. D. Kisiday, M. Jin, M. A. DiMicco, B. Kurz, and A. J. Grodzinsky, "Effects of dynamic compressive loading on chondrocyte biosynthesis in self-assembling peptide scaffolds.," *J. Biomech.*, vol. 37, no. 5, pp. 595–604, May 2004.
- [243] Y. Jung *et al.*, "Cartilaginous tissue formation using a mechano-active scaffold and dynamic compressive stimulation.," *J. Biomater. Sci. Polym. Ed.*, vol. 19, no. 1, pp. 61–74, Jan. 2008.
- [244] J. A. Kornblatt and M. J. Kornblatt, "The effects of osmotic and hydrostatic pressures on macromolecular systems.," *Biochim. Biophys. Acta*, vol. 1595, no. 1–2, pp. 30–47, Mar. 2002.
- [245] B. D. Elder and K. a Athanasiou, "Hydrostatic pressure in articular cartilage tissue engineering: from chondrocytes to tissue regeneration.," *Tissue Eng. Part B. Rev.*, vol. 15, no. 1, pp. 43–53, Mar. 2009.
- [246] E. M. Darling and K. A. Athanasiou, "Articular cartilage bioreactors and bioprocesses.," *Tissue Eng.*, vol. 9, no. 1, pp. 9–26, Feb. 2003.
- [247] W. A. Hodge, R. S. Fijan, K. L. Carlson, R. G. Burgess, W. H. Harris, and R. W. Mann, "Contact pressures in the human hip joint measured in vivo.," *Proc. Natl. Acad. Sci. U. S. A.*, vol. 83, no. 9, pp. 2879–83, May 1986.
- [248] A. C. Hall, E. R. Horwitz, and R. J. Wilkins, "The cellular physiology of articular cartilage.," *Exp. Physiol.*, vol. 81, no. 3, pp. 535–45, May 1996.

- [249] J. J. Parkkinen, M. J. Lammi, A. Pelttari, H. J. Helminen, M. Tammi, and I. Virtanen, "Altered Golgi apparatus in hydrostatically loaded articular cartilage chondrocytes.," *Ann. Rheum. Dis.*, vol. 52, no. 3, pp. 192–8, Mar. 1993.
- [250] M. J. Lammi *et al.*, "Expression of reduced amounts of structurally altered aggrecan in articular cartilage chondrocytes exposed to high hydrostatic pressure.," *Biochem. J.*, vol. 304 (Pt 3, pp. 723–30, Dec. 1994.
- [251] K. Takahashi *et al.*, "Hydrostatic pressure induces expression of interleukin 6 and tumour necrosis factor alpha mRNAs in a chondrocyte-like cell line.," *Ann. Rheum. Dis.*, vol. 57, no. 4, pp. 231–6, Apr. 1998.
- [252] R. L. Smith *et al.*, "Time-dependent effects of intermittent hydrostatic pressure on articular chondrocyte type II collagen and aggrecan mRNA expression.," *J. Rehabil. Res. Dev.*, vol. 37, no. 2, pp. 153–61, 2000.
- [253] J. C. Hu and K. A. Athanasiou, "The effects of intermittent hydrostatic pressure on self-assembled articular cartilage constructs.," *Tissue Eng.*, vol. 12, no. 5, pp. 1337–44, May 2006.
- [254] N. J. Gunja, R. K. Uthamanthil, and K. A. Athanasiou, "Effects of TGF-beta1 and hydrostatic pressure on meniscus cell-seeded scaffolds.," *Biomaterials*, vol. 30, no. 4, pp. 565–73, Feb. 2009.
- [255] S. Park, C. T. Hung, and G. A. Ateshian, "Mechanical response of bovine articular cartilage under dynamic unconfined compression loading at physiological stress levels.," *Osteoarthr. Cartil.*, vol. 12, no. 1, pp. 65–73, Jan. 2004.
- [256] C. C.-B. Wang, J.-M. Deng, G. A. Ateshian, and C. T. Hung, "An automated approach for direct measurement of two-dimensional strain distributions within articular cartilage under unconfined compression.," *J. Biomech. Eng.*, vol. 124, no. 5, pp. 557–67, Oct. 2002.
- [257] A. K. Williamson, A. C. Chen, K. Masuda, E. J.-M. A. Thonar, and R. L. Sah, "Tensile mechanical properties of bovine articular cartilage: variations with growth and relationships to collagen network components.," *J. Orthop. Res.*, vol. 21, no. 5, pp. 872–80, Sep. 2003.
- [258] G. E. Kempson, M. A. Freeman, and S. A. Swanson, "Tensile properties of articular cartilage.," *Nature*, vol. 220, no. 5172, pp. 1127–8, Dec. 1968.
- [259] M. A. Soltz and G. A. Ateshian, "A Conewise Linear Elasticity mixture model for the analysis of tension-compression nonlinearity in articular cartilage.," *J. Biomech. Eng.*, vol. 122, no. 6, pp. 576–86, Dec. 2000.
- [260] S. Park and G. A. Ateshian, "Dynamic response of immature bovine articular cartilage in tension and compression, and nonlinear viscoelastic modeling of the tensile response.," *J. Biomech. Eng.*, vol. 128, no. 4, pp. 623–30, Aug. 2006.
- [261] E. Y. Salinas, J. C. Hu, and K. A. Athanasiou, "A Guide for Using Mechanical Stimulation to Enhance Tissue-Engineered Articular Cartilage Properties," *Tissue Eng. Part B Rev.*, vol. 24, no. 5, p. ten.TEB.2018.0006, 2018.
- [262] J. K. Lee *et al.*, "Tension stimulation drives tissue formation in scaffold-free systems.," *Nat. Mater.*, vol. 16, no. 8, pp. 864–873, Aug. 2017.
- [263] R. F. MacBarb, N. K. Paschos, R. Abeug, E. A. Makris, J. C. Hu, and K. A. Athanasiou, "Passive strain-induced matrix synthesis and organization in shape-specific, cartilaginous neotissues.," *Tissue Eng. Part A*, vol. 20, no. 23–24, pp. 3290–302, Dec. 2014.
- [264] T.-A. N. Kelly *et al.*, "Tissue-engineered articular cartilage exhibits tension-compression nonlinearity reminiscent of the native cartilage.," *J. Biomech.*, vol. 46, no. 11, pp. 1784–91, Jul. 2013.
- [265] K. Athanasiou, D. J. Responde, W. E. Brown, and J. C. Hu, "Harnessing Biomechanics to Develop Cartilage Regeneration Strategies.," *J. Biomech. Eng.*, Oct. 2014.
- [266] J. A. Bishop, A. A. Palanca, M. J. Bellino, and D. W. Lowenberg, "Assessment of compromised fracture healing.," *J. Am. Acad. Orthop. Surg.*, vol. 20, no. 5, pp. 273–82, May 2012.
- [267] M. A. Flierl *et al.*, "Outcomes and complication rates of different bone grafting modalities in long bone fracture nonunions: a retrospective cohort study in 182 patients.," *J. Orthop. Surg. Res.*, vol. 8, no. 1, p. 33, Sep. 2013.
- [268] F. H. Albee, "Evolution of bone graft surgery," *Am. J. Surg.*, vol. 63, no. 3, pp. 421–436, Mar. 1944.
- [269] C. T. Laurencin, A. M. Ambrosio, M. D. Borden, and J. A. Cooper, "Tissue engineering: orthopedic applications.," *Annu. Rev. Biomed. Eng.*, vol. 1, no. 1, pp. 19–46, Aug. 1999.
- [270] A. J. Salgado, O. P. Coutinho, and R. L. Reis, "Bone tissue engineering: state of the art and future trends.," *Macromol. Biosci.*, vol. 4, no. 8, pp. 743–65, Aug. 2004.
- [271] A. R. Amini, C. T. Laurencin, and S. P. Nukavarapu, "Bone tissue engineering: recent advances and challenges.," *Crit. Rev. Biomed. Eng.*, vol. 40, no. 5, pp. 363–408, 2012.
- [272] P. Bianco, F. D. Cancedda, M. Riminucci, and R. Cancedda, "Bone formation via cartilage models: the 'borderline' chondrocyte.," *Matrix Biol.*, vol. 17, no. 3, pp. 185–92, Jul. 1998.
- [273] L. C. Gerstenfeld, D. M. Cullinane, G. L. Barnes, D. T. Graves, and T. A. Einhorn, "Fracture healing as a post-natal developmental process: molecular, spatial, and temporal aspects of its regulation.," *J. Cell. Biochem.*, vol. 88, no. 5, pp. 873–84, Apr. 2003.
- [274] T. A. Einhorn, "The cell and molecular biology of fracture healing.," *Clin. Orthop. Relat. Res.*, no. 355 Suppl, pp. S7-21, Oct. 1998.
- [275] M. B. Goldring, K. Tsuchimochi, and K. Ijiri, "The control of chondrogenesis.," *J. Cell. Biochem.*, vol. 97, no. 1, pp. 33–44, Jan. 2006.
- [276] S. C. Dennis, C. J. Berkland, L. F. Bonewald, and M. S. Detamore, "Endochondral ossification for enhancing bone regeneration: converging native extracellular matrix biomaterials and developmental engineering in vivo.," *Tissue*

- Eng. Part B. Rev.*, vol. 21, no. 3, pp. 247–66, Jun. 2015.
- [277] E. Farrell *et al.*, “In-vivo generation of bone via endochondral ossification by in-vitro chondrogenic priming of adult human and rat mesenchymal stem cells,” *BMC Musculoskelet. Disord.*, vol. 12, no. 1, p. 31, Jan. 2011.
- [278] E. Farrell *et al.*, “Chondrogenic priming of human bone marrow stromal cells: a better route to bone repair?,” *Tissue Eng. Part C. Methods*, vol. 15, no. 2, pp. 285–95, Jun. 2009.
- [279] J. van der Stok *et al.*, “Chondrogenically differentiated mesenchymal stromal cell pellets stimulate endochondral bone regeneration in critical-sized bone defects,” *Eur. Cell. Mater.*, vol. 27, pp. 137–48; discussion 148, Feb. 2014.
- [280] N. Harada *et al.*, “Bone regeneration in a massive rat femur defect through endochondral ossification achieved with chondrogenically differentiated MSCs in a degradable scaffold,” *Biomaterials*, vol. 35, no. 27, pp. 7800–10, Sep. 2014.
- [281] K. Bardsley, A. Kwarciak, C. Freeman, I. Brook, P. Hatton, and A. Crawford, “Repair of bone defects in vivo using tissue engineered hypertrophic cartilage grafts produced from nasal chondrocytes,” *Biomaterials*, vol. 112, pp. 313–323, Jan. 2017.
- [282] C. Scotti *et al.*, “Recapitulation of endochondral bone formation using human adult mesenchymal stem cells as a paradigm for developmental engineering,” *Proc. Natl. Acad. Sci. U. S. A.*, vol. 107, no. 16, pp. 7251–6, Apr. 2010.
- [283] E. M. Thompson, A. Matsiko, D. J. Kelly, J. P. Gleeson, and F. J. O’Brien, “An Endochondral Ossification-Based Approach to Bone Repair: Chondrogenically Primed Mesenchymal Stem Cell-Laden Scaffolds Support Greater Repair of Critical-Sized Cranial Defects Than Osteogenically Stimulated Constructs In Vivo,” *Tissue Eng. Part A*, vol. 22, no. 5–6, pp. 556–67, Mar. 2016.
- [284] K. Pelttari *et al.*, “Premature induction of hypertrophy during in vitro chondrogenesis of human mesenchymal stem cells correlates with calcification and vascular invasion after ectopic transplantation in SCID mice,” *Arthritis Rheum.*, vol. 54, no. 10, pp. 3254–66, Oct. 2006.
- [285] E. J. Sheehy, T. Mesallati, L. Kelly, T. Vinardell, C. T. Buckley, and D. J. Kelly, “Tissue Engineering Whole Bones Through Endochondral Ossification: Regenerating the Distal Phalanx,” *Biores. Open Access*, vol. 4, no. 1, pp. 229–41, Dec. 2015.
- [286] D. J. Hak *et al.*, “Delayed union and nonunions: epidemiology, clinical issues, and financial aspects,” *Injury*, vol. 45 Suppl 2, pp. S3–7, Jun. 2014.
- [287] G. Pachón-Peña *et al.*, “Stromal stem cells from adipose tissue and bone marrow of age-matched female donors display distinct immunophenotypic profiles,” *J. Cell. Physiol.*, vol. 226, no. 3, pp. 843–51, Mar. 2011.
- [288] J. M. Gimble and F. Guilak, “Adipose-derived adult stem cells: isolation, characterization, and differentiation potential,” *Cytotherapy*, vol. 5, no. 5, pp. 362–9, Jan. 2003.
- [289] R. Osinga *et al.*, “Generation of a Bone Organ by Human Adipose-Derived Stromal Cells Through Endochondral Ossification,” *Stem Cells Transl. Med.*, vol. 5, no. 8, pp. 1090–7, Aug. 2016.
- [290] J. M. Jukes, S. K. Both, A. Leusink, L. M. T. Sterk, C. A. van Blitterswijk, and J. de Boer, “Endochondral bone tissue engineering using embryonic stem cells,” *Proc. Natl. Acad. Sci. U. S. A.*, vol. 105, no. 19, pp. 6840–5, May 2008.
- [291] M. B. Mueller and R. S. Tuan, “Functional characterization of hypertrophy in chondrogenesis of human mesenchymal stem cells,” *Arthritis Rheum.*, vol. 58, no. 5, pp. 1377–88, May 2008.
- [292] W. L. Grayson *et al.*, “Effects of initial seeding density and fluid perfusion rate on formation of tissue-engineered bone,” *Tissue Eng. Part A*, vol. 14, no. 11, pp. 1809–20, Nov. 2008.
- [293] W. L. Grayson *et al.*, “Engineering anatomically shaped human bone grafts,” *Proc. Natl. Acad. Sci. U. S. A.*, vol. 107, no. 8, pp. 3299–304, Feb. 2010.
- [294] I. Marcos-Campos, D. Marolt, P. Petridis, S. Bhumiratana, D. Schmidt, and G. Vunjak-Novakovic, “Bone scaffold architecture modulates the development of mineralized bone matrix by human embryonic stem cells,” *Biomaterials*, vol. 33, no. 33, pp. 8329–42, Nov. 2012.
- [295] P. Bourin *et al.*, “Stromal cells from the adipose tissue-derived stromal vascular fraction and culture expanded adipose tissue-derived stromal/stem cells: a joint statement of the International Federation for Adipose Therapeutics and Science (IFATS) and the International So,” *Cytotherapy*, vol. 15, no. 6, pp. 641–8, Jun. 2013.
- [296] M. Fröhlich, W. L. Grayson, D. Marolt, J. M. Gimble, N. Kregar-Velikonja, and G. Vunjak-Novakovic, “Bone grafts engineered from human adipose-derived stem cells in perfusion bioreactor culture,” *Tissue Eng. Part A*, vol. 16, no. 1, pp. 179–89, Jan. 2010.
- [297] O. B. Betz *et al.*, “The repair of critical-sized bone defects using expedited, autologous BMP-2 gene-activated fat implants,” *Tissue Eng. Part A*, vol. 16, no. 3, pp. 1093–101, Mar. 2010.
- [298] T. Aigner, K. R. Gresk-otter, J. C. Fairbank, K. von der Mark, and J. P. Urban, “Variation with age in the pattern of type X collagen expression in normal and scoliotic human intervertebral discs,” *Calcif. Tissue Int.*, vol. 63, no. 3, pp. 263–8, Sep. 1998.
- [299] K. Donath, “Die Trenn-Dünnschliff-Technik zur Herstellung histologischer Präparate von nicht schneidbaren Geweben und Materialien,” in *Der Präparator*, 34th ed., 1988, pp. 197–206.
- [300] L. Jenö and L. Géza, “A simple differential staining method for semi-thin sections of ossifying cartilage and bone tissues embedded in epoxy resin,” *Mikroskopie*, vol. 31, no. 1–2, pp. 1–4, Apr. 1975.
- [301] H. Chen *et al.*, “Runx2 regulates endochondral ossification through control of chondrocyte proliferation and differentiation,” *J. Bone Miner. Res.*, vol. 29, no. 12, pp. 2653–65, Dec. 2014.

- [302] G. Karsenty, "Role of Cbfa1 in osteoblast differentiation and function.," *Semin. Cell Dev. Biol.*, vol. 11, no. 5, pp. 343–6, Oct. 2000.
- [303] L. C. C. Gerstenfeld and F. D. D. Shapiro, "Expression of bone-specific genes by hypertrophic chondrocytes: implication of the complex functions of the hypertrophic chondrocyte during endochondral bone development.," *J. Cell. Biochem.*, vol. 62, no. 1, pp. 1–9, Jul. 1996.
- [304] A. C. Wu, L. J. Raggatt, K. A. Alexander, and A. R. Pettit, "Unraveling macrophage contributions to bone repair.," *Bonekey Rep.*, vol. 2, p. 373, Jun. 2013.
- [305] S. Bhumiratana *et al.*, "Tissue-engineered autologous grafts for facial bone reconstruction," *Sci. Transl. Med.*, vol. 8, no. 343, pp. 343ra83-343ra83, Jun. 2016.
- [306] C. Scotti *et al.*, "Engineering of a functional bone organ through endochondral ossification.," *Proc. Natl. Acad. Sci. U. S. A.*, vol. 110, no. 10, pp. 3997–4002, Mar. 2013.
- [307] A. Boccaccio and C. Pappalettere, "Mechanobiology of Fracture Healing: Basic Principles and Applications in Orthodontics and Orthopaedics," in *Theoretical Biomechanics*, InTech, 2011.
- [308] A. Houben *et al.*, "β-catenin activity in late hypertrophic chondrocytes locally orchestrates osteoblastogenesis and osteoclastogenesis.," *Development*, vol. 143, no. 20, pp. 3826–3838, Oct. 2016.
- [309] G. M. Cunniffe *et al.*, "Porous decellularized tissue engineered hypertrophic cartilage as a scaffold for large bone defect healing.," *Acta Biomater.*, vol. 23, pp. 82–90, Sep. 2015.
- [310] P. E. Bourguine, C. Scotti, S. Pigeot, L. A. Tchang, A. Todorov, and I. Martin, "Osteoinductivity of engineered cartilaginous templates devitalized by inducible apoptosis.," *Proc. Natl. Acad. Sci. U. S. A.*, vol. 111, no. 49, pp. 17426–31, Dec. 2014.
- [311] H. P. Gerber, T. H. Vu, A. M. Ryan, J. Kowalski, Z. Werb, and N. Ferrara, "VEGF couples hypertrophic cartilage remodeling, ossification and angiogenesis during endochondral bone formation.," *Nat. Med.*, vol. 5, no. 6, pp. 623–8, Jun. 1999.
- [312] L. Yang, K. Y. Tsang, H. C. Tang, D. Chan, and K. S. E. Cheah, "Hypertrophic chondrocytes can become osteoblasts and osteocytes in endochondral bone formation.," *Proc. Natl. Acad. Sci. U. S. A.*, vol. 111, no. 33, pp. 12097–102, Aug. 2014.
- [313] X. Zhou, K. von der Mark, S. Henry, W. Norton, H. Adams, and B. de Crombrugge, "Chondrocytes transdifferentiate into osteoblasts in endochondral bone during development, postnatal growth and fracture healing in mice.," *PLoS Genet.*, vol. 10, no. 12, p. e1004820, Dec. 2014.
- [314] C. S. Bahney *et al.*, "Stem cell-derived endochondral cartilage stimulates bone healing by tissue transformation.," *J. Bone Miner. Res.*, vol. 29, no. 5, pp. 1269–82, May 2014.
- [315] L. J. Raggatt *et al.*, "Fracture healing via periosteal callus formation requires macrophages for both initiation and progression of early endochondral ossification.," *Am. J. Pathol.*, vol. 184, no. 12, pp. 3192–204, Dec. 2014.
- [316] C. Schlundt *et al.*, "Macrophages in bone fracture healing: Their essential role in endochondral ossification.," *Bone*, vol. 106, pp. 78–89, Jan. 2018.
- [317] C.-N. Lin, C.-J. Wang, Y.-J. Chao, M.-D. Lai, and Y.-S. Shan, "The significance of the co-existence of osteopontin and tumor-associated macrophages in gastric cancer progression.," *BMC Cancer*, vol. 15, no. 1, p. 128, Mar. 2015.
- [318] C. K. F. Chan *et al.*, "Endochondral ossification is required for haematopoietic stem-cell niche formation.," *Nature*, vol. 457, no. 7228, pp. 490–4, Jan. 2009.
- [319] M. Serafini *et al.*, "Establishment of bone marrow and hematopoietic niches in vivo by reversion of chondrocyte differentiation of human bone marrow stromal cells.," *Stem Cell Res.*, vol. 12, no. 3, pp. 659–72, May 2014.
- [320] L. Polo-Corrales, M. Latorre-Esteves, and J. E. Ramirez-Vick, "Scaffold design for bone regeneration.," *J. Nanosci. Nanotechnol.*, vol. 14, no. 1, pp. 15–56, Jan. 2014.
- [321] D. J. Lee *et al.*, "Decellularized bone matrix grafts for calvaria regeneration.," *J. Tissue Eng.*, vol. 7, p. 2041731416680306, Jan. 2016.
- [322] M. Bottlang and F. Feist, "Biomechanics of far cortical locking.," *J. Orthop. Trauma*, vol. 25 Suppl 1, pp. S21-8, Feb. 2011.
- [323] M. Bottlang *et al.*, "Far cortical locking can improve healing of fractures stabilized with locking plates.," *J. Bone Joint Surg. Am.*, vol. 92, no. 7, pp. 1652–60, Jul. 2010.
- [324] V. Viateau, D. Logeart-Avramoglou, G. Guillemain, and H. Petite, "Animal Models for Bone Tissue Engineering Purposes," in *Sourcebook of Models for Biomedical Research*, Totowa, NJ: Humana Press, 2008, pp. 725–736.
- [325] Y. Li, S.-K. Chen, L. Li, L. Qin, X.-L. Wang, and Y.-X. Lai, "Bone defect animal models for testing efficacy of bone substitute biomaterials.," *J. Orthop. Transl.*, vol. 3, no. 3, pp. 95–104, Jul. 2015.
- [326] P. Lenas, M. Moos, and F. P. Luyten, "Developmental engineering: a new paradigm for the design and manufacturing of cell-based products. Part I: from three-dimensional cell growth to biomimetics of in vivo development.," *Tissue Eng. Part B Rev.*, vol. 15, no. 4, pp. 381–94, Dec. 2009.
- [327] J. Bernhard *et al.*, "Tissue-engineered hypertrophic chondrocyte grafts enhanced long bone repair.," *Biomaterials*, vol. 139, pp. 202–212, Sep. 2017.
- [328] I. Martin, D. Wendt, and M. Heberer, "The role of bioreactors in tissue engineering.," *Trends Biotechnol.*, vol. 22, no. 2, pp. 80–6, Feb. 2004.

- [329] J. Rauh, F. Milan, K.-P. Günther, and M. Stiehler, "Bioreactor systems for bone tissue engineering.," *Tissue Eng. Part B. Rev.*, vol. 17, no. 4, pp. 263–80, Aug. 2011.
- [330] N. Salehi-Nik *et al.*, "Engineering parameters in bioreactor's design: a critical aspect in tissue engineering.," *Biomed Res. Int.*, vol. 2013, p. 762132, 2013.
- [331] G. N. Bancroft, V. I. Sikavitsas, and A. G. Mikos, "Design of a flow perfusion bioreactor system for bone tissue-engineering applications.," *Tissue Eng.*, vol. 9, no. 3, pp. 549–54, Jun. 2003.
- [332] V. I. Sikavitsas, G. N. Bancroft, H. L. Holtorf, J. A. Jansen, and A. G. Mikos, "Mineralized matrix deposition by marrow stromal osteoblasts in 3D perfusion culture increases with increasing fluid shear forces.," *Proc. Natl. Acad. Sci. U. S. A.*, vol. 100, no. 25, pp. 14683–8, Dec. 2003.
- [333] G. N. Bancroft *et al.*, "Fluid flow increases mineralized matrix deposition in 3D perfusion culture of marrow stromal osteoblasts in a dose-dependent manner.," *Proc. Natl. Acad. Sci. U. S. A.*, vol. 99, no. 20, pp. 12600–5, Oct. 2002.
- [334] S. H. Cartmell, B. D. Porter, A. J. García, and R. E. Guldberg, "Effects of medium perfusion rate on cell-seeded three-dimensional bone constructs in vitro.," *Tissue Eng.*, vol. 9, no. 6, pp. 1197–203, Dec. 2003.
- [335] Y. Wang, T. Uemura, J. Dong, H. Kojima, J. Tanaka, and T. Tateishi, "Application of perfusion culture system improves in vitro and in vivo osteogenesis of bone marrow-derived osteoblastic cells in porous ceramic materials.," *Tissue Eng.*, vol. 9, no. 6, pp. 1205–14, Dec. 2003.
- [336] M. L. Alves da Silva *et al.*, "Chondrogenic differentiation of human bone marrow mesenchymal stem cells in chitosan-based scaffolds using a flow-perfusion bioreactor.," *J. Tissue Eng. Regen. Med.*, vol. 5, no. 9, pp. 722–32, Oct. 2011.
- [337] A. Gonçalves, P. Costa, M. T. Rodrigues, I. R. Dias, R. L. Reis, and M. E. Gomes, "Effect of flow perfusion conditions in the chondrogenic differentiation of bone marrow stromal cells cultured onto starch based biodegradable scaffolds.," *Acta Biomater.*, vol. 7, no. 4, pp. 1644–52, Apr. 2011.
- [338] N. Mahmoudifar and P. M. Doran, "Chondrogenic differentiation of human adipose-derived stem cells in polyglycolic acid mesh scaffolds under dynamic culture conditions.," *Biomaterials*, vol. 31, no. 14, pp. 3858–67, May 2010.
- [339] L. M. Kock, J. Malda, W. J. A. Dhert, K. Ito, and D. Gawlitta, "Flow-perfusion interferes with chondrogenic and hypertrophic matrix production by mesenchymal stem cells.," *J. Biomech.*, vol. 47, no. 9, pp. 2122–9, Jun. 2014.
- [340] N. C. Nowlan, P. Murphy, and P. J. Prendergast, "A dynamic pattern of mechanical stimulation promotes ossification in avian embryonic long bones.," *J. Biomech.*, vol. 41, no. 2, pp. 249–58, Jan. 2008.
- [341] H. Inoue *et al.*, "Effect of mechanical stress on the hypertrophic differentiation related gene expression in cultured chondrocytes.," *Osteoarthr. Cartil.*, vol. 21, pp. S212–S213, Apr. 2013.
- [342] W. L. Grayson, D. Marolt, S. Bhumiratana, M. Fröhlich, X. E. Guo, and G. Vunjak-Novakovic, "Optimizing the medium perfusion rate in bone tissue engineering bioreactors.," *Biotechnol. Bioeng.*, vol. 108, no. 5, pp. 1159–70, May 2011.
- [343] K. von der Mark *et al.*, "Type X collagen synthesis in human osteoarthritic cartilage. Indication of chondrocyte hypertrophy.," *Arthritis Rheum.*, vol. 35, no. 7, pp. 806–11, Jul. 1992.
- [344] B. Johnstone, T. M. Hering, A. I. Caplan, V. M. Goldberg, and J. U. Yoo, "In vitro chondrogenesis of bone marrow-derived mesenchymal progenitor cells.," *Exp. Cell Res.*, vol. 238, no. 1, pp. 265–72, Jan. 1998.
- [345] M. B. Albro *et al.*, "Heterogeneous engineered cartilage growth results from gradients of media-supplemented active TGF- β and is ameliorated by the alternative supplementation of latent TGF- β .," *Biomaterials*, vol. 77, pp. 173–185, Jan. 2016.
- [346] D. R. Carter and M. Wong, "Modelling cartilage mechanobiology.," *Philos. Trans. R. Soc. Lond. B. Biol. Sci.*, vol. 358, no. 1437, pp. 1461–71, Sep. 2003.
- [347] S. S. Stevens, G. S. Beaupré, and D. R. Carter, "Computer model of endochondral growth and ossification in long bones: biological and mechanobiological influences.," *J. Orthop. Res.*, vol. 17, no. 5, pp. 646–53, Sep. 1999.
- [348] S. Chen, P. Fu, R. Cong, H. Wu, and M. Pei, "Strategies to minimize hypertrophy in cartilage engineering and regeneration.," *Genes Dis.*, vol. 2, no. 1, pp. 76–95, Mar. 2015.
- [349] M. J. Duer, T. Frisčić, R. C. Murray, D. G. Reid, and E. R. Wise, "The mineral phase of calcified cartilage: its molecular structure and interface with the organic matrix.," *Biophys. J.*, vol. 96, no. 8, pp. 3372–8, Apr. 2009.
- [350] C. Rey, K. Beshah, R. Griffin, and M. J. Glimcher, "Structural studies of the mineral phase of calcifying cartilage.," *J. Bone Miner. Res.*, vol. 6, no. 5, pp. 515–25, May 1991.
- [351] L. C. Gerstenfeld and W. J. Landis, "Gene expression and extracellular matrix ultrastructure of a mineralizing chondrocyte cell culture system.," *J. Cell Biol.*, vol. 112, no. 3, pp. 501–13, Feb. 1991.
- [352] J. Li and S. Dong, "The Signaling Pathways Involved in Chondrocyte Differentiation and Hypertrophic Differentiation.," *Stem Cells Int.*, vol. 2016, p. 2470351, 2016.
- [353] D. Studer, C. Millan, E. Öztürk, K. Maniura-Weber, and M. Zenobi-Wong, "Molecular and biophysical mechanisms regulating hypertrophic differentiation in chondrocytes and mesenchymal stem cells.," *Eur. Cell. Mater.*, vol. 24, pp. 118–35; discussion 135, Jul. 2012.
- [354] E. Kozhemyakina, A. B. Lassar, and E. Zelzer, "A pathway to bone: signaling molecules and transcription factors involved in chondrocyte development and maturation.," *Development*, vol. 142, no. 5, pp. 817–31, Mar. 2015.
- [355] A. Vortkamp, K. Lee, B. Lanske, G. V Segre, H. M. Kronenberg, and C. J. Tabin, "Regulation of rate of cartilage differentiation by Indian hedgehog and PTH-related protein.," *Science*, vol. 273, no. 5275, pp. 613–22, Aug. 1996.

- [356] T. Kobayashi *et al.*, “Indian hedgehog stimulates periarticular chondrocyte differentiation to regulate growth plate length independently of PTHrP.,” *J. Clin. Invest.*, vol. 115, no. 7, pp. 1734–42, Jul. 2005.
- [357] J. C. H. Leijten *et al.*, “Gremlin 1, frizzled-related protein, and Dkk-1 are key regulators of human articular cartilage homeostasis.,” *Arthritis Rheum.*, vol. 64, no. 10, pp. 3302–12, Oct. 2012.
- [358] P. Abdel-Sayed and D. P. Pioletti, “Strategies for improving the repair of focal cartilage defects.,” *Nanomedicine (Lond.)*, vol. 10, no. 18, pp. 2893–905, Sep. 2015.
- [359] E. Kon *et al.*, “Second-generation autologous chondrocyte implantation: results in patients older than 40 years.,” *Am. J. Sports Med.*, vol. 39, no. 8, pp. 1668–75, Aug. 2011.
- [360] G. Filardo *et al.*, “Second-generation arthroscopic autologous chondrocyte implantation for the treatment of degenerative cartilage lesions.,” *Knee Surg. Sports Traumatol. Arthrosc.*, vol. 20, no. 9, pp. 1704–13, Sep. 2012.
- [361] S. Marlovits *et al.*, “Clinical and radiological outcomes 5 years after matrix-induced autologous chondrocyte implantation in patients with symptomatic, traumatic chondral defects.,” *Am. J. Sports Med.*, vol. 40, no. 10, pp. 2273–80, Oct. 2012.
- [362] G. Filardo, E. Kon, L. Andriolo, B. Di Matteo, F. Balboni, and M. Marcacci, “Clinical profiling in cartilage regeneration: prognostic factors for midterm results of matrix-assisted autologous chondrocyte transplantation.,” *Am. J. Sports Med.*, vol. 42, no. 4, pp. 898–905, Apr. 2014.
- [363] H. B. Schuette, M. J. Kraeutler, and E. C. McCarty, “Matrix-Assisted Autologous Chondrocyte Transplantation in the Knee: A Systematic Review of Mid- to Long-Term Clinical Outcomes.,” *Orthop. J. Sport. Med.*, vol. 5, no. 6, p. 2325967117709250, Jun. 2017.
- [364] J. D. Wylie, M. K. Hartley, A. L. Kapron, S. K. Aoki, and T. G. Maak, “Failures and Reoperations After Matrix-Assisted Cartilage Repair of the Knee: A Systematic Review.,” *Arthroscopy*, vol. 32, no. 2, pp. 386–92, Feb. 2016.
- [365] A. C. DiBartola *et al.*, “Correlation between histological outcome and surgical cartilage repair technique in the knee: A meta-analysis.,” *Knee*, vol. 23, no. 3, pp. 344–9, Jun. 2016.
- [366] M.-H. Zheng *et al.*, “Matrix-induced autologous chondrocyte implantation (MACI): biological and histological assessment.,” *Tissue Eng.*, vol. 13, no. 4, pp. 737–46, Apr. 2007.
- [367] D. Enea, S. Cecconi, A. Busilacchi, S. Manzotti, R. Gesuita, and A. Gigante, “Matrix-induced autologous chondrocyte implantation (MACI) in the knee.,” *Knee Surg. Sports Traumatol. Arthrosc.*, vol. 20, no. 5, pp. 862–9, May 2012.
- [368] Z. Zhang *et al.*, “Matrix-induced autologous chondrocyte implantation for the treatment of chondral defects of the knees in Chinese patients.,” *Drug Des. Devel. Ther.*, vol. 8, pp. 2439–48, Dec. 2014.
- [369] F. Taraballi, G. Bauza, P. McCulloch, J. Harris, and E. Tasciotti, “Concise Review: Biomimetic Functionalization of Biomaterials to Stimulate the Endogenous Healing Process of Cartilage and Bone Tissue.,” *Stem Cells Transl. Med.*, vol. 6, no. 12, pp. 2186–2196, Dec. 2017.
- [370] D. Mittelstaedt, Y. Xia, A. Shmelyov, N. Casciani, and A. Bidthanapally, “Quantitative determination of morphological and territorial structures of articular cartilage from both perpendicular and parallel sections by polarized light microscopy.,” *Connect. Tissue Res.*, vol. 52, no. 6, pp. 512–22, Dec. 2011.
- [371] S. Nuernberger, N. Cyran, C. Albrecht, H. Redl, V. Vécsei, and S. Marlovits, “The influence of scaffold architecture on chondrocyte distribution and behavior in matrix-associated chondrocyte transplantation grafts.,” *Biomaterials*, vol. 32, no. 4, pp. 1032–40, Feb. 2011.
- [372] A. R. Armiento, M. J. Stoddart, M. Alini, and D. Eglin, “Biomaterials for articular cartilage tissue engineering: Learning from biology.,” *Acta Biomater.*, vol. 65, pp. 1–20, Jan. 2018.
- [373] G. D. Nicodemus and S. J. Bryant, “Cell encapsulation in biodegradable hydrogels for tissue engineering applications.,” *Tissue Eng. Part B. Rev.*, vol. 14, no. 2, pp. 149–65, Jun. 2008.
- [374] K. Fléreau *et al.*, “Toward the development of biomimetic injectable and macroporous biohydrogels for regenerative medicine.,” *Adv. Colloid Interface Sci.*, vol. 247, pp. 589–609, Sep. 2017.
- [375] C. O. Kean, R. J. Brown, and J. Chapman, “The role of biomaterials in the treatment of meniscal tears.,” *PeerJ*, vol. 5, p. e4076, Nov. 2017.
- [376] S. Nehrer *et al.*, “Matrix collagen type and pore size influence behaviour of seeded canine chondrocytes.,” *Biomaterials*, vol. 18, no. 11, pp. 769–76, Jun. 1997.
- [377] A. Gigante, C. Bevilacqua, M. Cappella, S. Manzotti, and F. Greco, “Engineered articular cartilage: influence of the scaffold on cell phenotype and proliferation.,” *J. Mater. Sci. Mater. Med.*, vol. 14, no. 8, pp. 713–6, Aug. 2003.
- [378] H. Lu, T. Hoshiba, N. Kawazoe, I. Koda, M. Song, and G. Chen, “Cultured cell-derived extracellular matrix scaffolds for tissue engineering.,” *Biomaterials*, vol. 32, no. 36, pp. 9658–66, Dec. 2011.
- [379] W. Zhang *et al.*, “Cell-Derived Extracellular Matrix: Basic Characteristics and Current Applications in Orthopedic Tissue Engineering.,” *Tissue Eng. Part B. Rev.*, vol. 22, no. 3, pp. 193–207, Jun. 2016.
- [380] Y. Yang, H. Lin, H. Shen, B. Wang, G. Lei, and R. S. Tuan, “Mesenchymal stem cell-derived extracellular matrix enhances chondrogenic phenotype of and cartilage formation by encapsulated chondrocytes in vitro and in vivo.,” *Acta Biomater.*, vol. 69, pp. 71–82, Mar. 2018.
- [381] Z. Huang, O. Godkin, and G. Schulze-Tanzil, “The Challenge in Using Mesenchymal Stromal Cells for Recellularization of Decellularized Cartilage.,” *Stem Cell Rev.*, vol. 13, no. 1, pp. 50–67, Feb. 2017.
- [382] E. Kheir, T. Stapleton, D. Shaw, Z. Jin, J. Fisher, and E. Ingham, “Development and characterization of an acellular porcine cartilage bone matrix for use in tissue engineering.,” *J. Biomed. Mater. Res. A*, vol. 99, no. 2, pp. 283–94,

- Nov. 2011.
- [383] K. Gelse *et al.*, “Transplantation of Chemically Processed Decellularized Meniscal Allografts,” *Cartilage*, vol. 8, no. 2, pp. 180–190, Apr. 2017.
- [384] L. Utomo *et al.*, “Preparation and characterization of a decellularized cartilage scaffold for ear cartilage reconstruction,” *Biomed. Mater.*, vol. 10, no. 1, p. 015010, Jan. 2015.
- [385] A. C. Lendrum, D. S. Fraser, W. Slidders, and R. Henderson, “Studies on the character and staining of fibrin.,” *J. Clin. Pathol.*, vol. 15, no. 5, pp. 401–13, Sep. 1962.
- [386] Y. J. Kim, R. L. Y. Sah, J.-Y. Y. Doong, and A. J. Grodzinsky, “Fluorometric assay of DNA in cartilage explants using Hoechst 33258.,” *Anal. Biochem.*, vol. 174, no. 1, pp. 168–76, Oct. 1988.
- [387] R. W. Farndale, D. J. Buttle, and A. J. Barrett, “Improved quantitation and discrimination of sulphated glycosaminoglycans by use of dimethylmethylene blue.,” *Biochim. Biophys. Acta*, vol. 883, no. 2, pp. 173–7, Sep. 1986.
- [388] L. Knezevic *et al.*, “Engineering Blood and Lymphatic Microvascular Networks in Fibrin Matrices.,” *Front. Bioeng. Biotechnol.*, vol. 5, p. 25, Apr. 2017.
- [389] T. Hennig *et al.*, “Reduced chondrogenic potential of adipose tissue derived stromal cells correlates with an altered TGFbeta receptor and BMP profile and is overcome by BMP-6.,” *J. Cell. Physiol.*, vol. 211, no. 3, pp. 682–91, Jun. 2007.
- [390] G. C. Schüller *et al.*, “An in vivo mouse model for human cartilage regeneration.,” *J. Tissue Eng. Regen. Med.*, vol. 2, no. 4, pp. 202–9, Jun. 2008.
- [391] M. B. Albro *et al.*, “Accumulation of exogenous activated TGF-β in the superficial zone of articular cartilage.,” *Biophys. J.*, vol. 104, no. 8, pp. 1794–804, Apr. 2013.
- [392] C. Schneider *et al.*, “Systematic Comparison of Protocols for the Preparation of Human Articular Cartilage for Use as Scaffold Material in Cartilage Tissue Engineering.,” *Tissue Eng. Part C. Methods*, vol. 22, no. 12, pp. 1095–1107, Dec. 2016.
- [393] P. M. Crapo, T. W. Gilbert, and S. F. Badylak, “An overview of tissue and whole organ decellularization processes.,” *Biomaterials*, vol. 32, no. 12, pp. 3233–43, Apr. 2011.
- [394] X. Dong *et al.*, “RGD-modified acellular bovine pericardium as a bioprosthetic scaffold for tissue engineering.,” *J. Mater. Sci. Mater. Med.*, vol. 20, no. 11, pp. 2327–36, Nov. 2009.
- [395] E. M. Darling and K. A. Athanasiou, “Rapid phenotypic changes in passaged articular chondrocyte subpopulations.,” *J. Orthop. Res.*, vol. 23, no. 2, pp. 425–32, Mar. 2005.
- [396] L. E. Kokai, K. Marra, and J. P. Rubin, “Adipose stem cells: biology and clinical applications for tissue repair and regeneration.,” *Transl. Res.*, vol. 163, no. 4, pp. 399–408, Apr. 2014.
- [397] F. Zarei and H. Daraee, “Recent Progresses in Breast Reconstruction: Stem Cells, Biomaterials, and Growth Factors.,” *Drug Res. (Stuttg.)*, vol. 68, no. 6, pp. 311–316, Jun. 2018.
- [398] Y.-G. Koh, Y.-J. Choi, S.-K. Kwon, Y.-S. Kim, and J.-E. Yeo, “Clinical results and second-look arthroscopic findings after treatment with adipose-derived stem cells for knee osteoarthritis.,” *Knee Surg. Sports Traumatol. Arthrosc.*, vol. 23, no. 5, pp. 1308–16, May 2015.
- [399] C. H. Jo *et al.*, “Intra-articular injection of mesenchymal stem cells for the treatment of osteoarthritis of the knee: a proof-of-concept clinical trial.,” *Stem Cells*, vol. 32, no. 5, pp. 1254–66, May 2014.
- [400] H. Bansal *et al.*, “Intra-articular injection in the knee of adipose derived stromal cells (stromal vascular fraction) and platelet rich plasma for osteoarthritis.,” *J. Transl. Med.*, vol. 15, no. 1, p. 141, Dec. 2017.
- [401] E. Oberbauer, C. Steffenhagen, C. Wurzer, C. Gabriel, H. Redl, and S. Wolbank, “Enzymatic and non-enzymatic isolation systems for adipose tissue-derived cells: current state of the art.,” *Cell Regen. (London, England)*, vol. 4, no. 1, p. 7, Jan. 2015.
- [402] I. Roato *et al.*, “Adipose Derived-Mesenchymal Stem Cells Viability and Differentiating Features for Orthopaedic Reparative Applications: Banking of Adipose Tissue.,” *Stem Cells Int.*, vol. 2016, p. 4968724, Nov. 2016.
- [403] F. Hildner, C. Albrecht, C. Gabriel, H. Redl, and M. van Griensven, “State of the art and future perspectives of articular cartilage regeneration: a focus on adipose-derived stem cells and platelet-derived products.,” *J. Tissue Eng. Regen. Med.*, vol. 5, no. 4, pp. e36-51, Apr. 2011.
- [404] F. Veronesi, M. Maglio, M. Tschon, N. N. Aldini, and M. Fini, “Adipose-derived mesenchymal stem cells for cartilage tissue engineering: state-of-the-art in in vivo studies.,” *J. Biomed. Mater. Res. A*, vol. 102, no. 7, pp. 2448–66, Jul. 2014.
- [405] A. Bielli, M. G. Scioli, P. Gentile, V. Cervelli, and A. Orlandi, “Adipose-derived stem cells in cartilage regeneration: current perspectives.,” *Regen. Med.*, vol. 11, no. 7, pp. 693–703, Oct. 2016.
- [406] Q. Sun *et al.*, “Combined use of adipose derived stem cells and TGF-β3 microspheres promotes articular cartilage regeneration in vivo.,” *Biotech. Histochem.*, vol. 93, no. 3, pp. 168–176, Apr. 2018.
- [407] M. M. Pleumeekers, L. Nimeskern, J. L. M. Koevoet, M. Karperien, K. S. Stok, and G. J. V. M. van Osch, “Trophic effects of adipose-tissue-derived and bone-marrow-derived mesenchymal stem cells enhance cartilage generation by chondrocytes in co-culture.,” *PLoS One*, vol. 13, no. 2, p. e0190744, Feb. 2018.
- [408] E. Amann, P. Wolff, E. Breel, M. van Griensven, and E. R. Balmayor, “Hyaluronic acid facilitates chondrogenesis and matrix deposition of human adipose derived mesenchymal stem cells and human chondrocytes co-cultures.,” *Acta*

- Biomater.*, vol. 52, pp. 130–144, Apr. 2017.
- [409] L. Bian, D. Y. Zhai, R. L. Mauck, and J. A. Burdick, “Coculture of human mesenchymal stem cells and articular chondrocytes reduces hypertrophy and enhances functional properties of engineered cartilage.,” *Tissue Eng. Part A*, vol. 17, no. 7–8, pp. 1137–45, Apr. 2011.
- [410] C. Acharya *et al.*, “Enhanced chondrocyte proliferation and mesenchymal stromal cells chondrogenesis in coculture pellets mediate improved cartilage formation.,” *J. Cell. Physiol.*, vol. 227, no. 1, pp. 88–97, Jan. 2012.
- [411] S. Lopa, A. Colombini, V. Sansone, F. W. B. Preis, and M. Moretti, “Influence on chondrogenesis of human osteoarthritic chondrocytes in co-culture with donor-matched mesenchymal stem cells from infrapatellar fat pad and subcutaneous adipose tissue.,” *Int. J. Immunopathol. Pharmacol.*, vol. 26, no. 1 Suppl, pp. 23–31, Jan. 2013.
- [412] M. A. Sabatino *et al.*, “Cartilage graft engineering by co-culturing primary human articular chondrocytes with human bone marrow stromal cells.,” *J. Tissue Eng. Regen. Med.*, vol. 9, no. 12, pp. 1394–403, Dec. 2012.
- [413] N.-C. Cheng, B. T. Estes, T.-H. Young, and F. Guilak, “Genipin-crosslinked cartilage-derived matrix as a scaffold for human adipose-derived stem cell chondrogenesis.,” *Tissue Eng. Part A*, vol. 19, no. 3–4, pp. 484–96, Feb. 2013.
- [414] S. R. Caliarì and B. A. C. Harley, “Collagen-GAG scaffold biophysical properties bias MSC lineage choice in the presence of mixed soluble signals.,” *Tissue Eng. Part A*, vol. 20, no. 17–18, pp. 2463–72, Sep. 2014.
- [415] H. V. Almeida *et al.*, “Controlled release of transforming growth factor- β 3 from cartilage-extra-cellular-matrix-derived scaffolds to promote chondrogenesis of human-joint-tissue-derived stem cells.,” *Acta Biomater.*, vol. 10, no. 10, pp. 4400–9, Oct. 2014.
- [416] C. R. Rowland, L. A. Colucci, and F. Guilak, “Fabrication of anatomically-shaped cartilage constructs using decellularized cartilage-derived matrix scaffolds.,” *Biomaterials*, vol. 91, pp. 57–72, Jun. 2016.
- [417] D. O. Visscher *et al.*, “Cartilage Tissue Engineering: Preventing Tissue Scaffold Contraction Using a 3D-Printed Polymeric Cage.,” *Tissue Eng. Part C Methods*, vol. 22, no. 6, pp. 573–84, Jun. 2016.
- [418] B. D. Idowu, M. M. Knight, D. L. Bader, and D. A. Lee, “Confocal analysis of cytoskeletal organisation within isolated chondrocyte sub-populations cultured in agarose.,” *Histochem. J.*, vol. 32, no. 3, pp. 165–74, Mar. 2000.
- [419] J. Parreno, S. Raju, P. Wu, and R. A. Kandel, “MRTF-A signaling regulates the acquisition of the contractile phenotype in dedifferentiated chondrocytes.,” *Matrix Biol.*, vol. 62, pp. 3–14, Oct. 2017.
- [420] J. Parreno, M. Nabavi Niaki, K. Andrejevic, A. Jiang, P. Wu, and R. A. Kandel, “Interplay between cytoskeletal polymerization and the chondrogenic phenotype in chondrocytes passaged in monolayer culture.,” *J. Anat.*, vol. 230, no. 2, pp. 234–248, Feb. 2017.
- [421] S. Grad, D. Eglin, M. Alini, and M. J. Stoddart, “Physical stimulation of chondrogenic cells in vitro: a review.,” *Clin. Orthop. Relat. Res.*, vol. 469, no. 10, pp. 2764–72, Oct. 2011.
- [422] C. Correia *et al.*, “Dynamic culturing of cartilage tissue: the significance of hydrostatic pressure.,” *Tissue Eng. Part A*, vol. 18, no. 19–20, pp. 1979–91, Oct. 2012.
- [423] J. A. Panadero, S. Lanceros-Mendez, and J. L. G. Ribelles, “Differentiation of mesenchymal stem cells for cartilage tissue engineering: Individual and synergetic effects of three-dimensional environment and mechanical loading.,” *Acta Biomater.*, vol. 33, pp. 1–12, Mar. 2016.
- [424] N. Fahy, M. Alini, and M. J. Stoddart, “Mechanical stimulation of mesenchymal stem cells: Implications for cartilage tissue engineering.,” *J. Orthop. Res.*, vol. 36, no. 1, pp. 52–63, Aug. 2018.
- [425] N. Elmali, R. Tandoğan, M. Demirel, M. Bozkurt, and T. Beyzadeoglu, “Cartilage repair strategies in the knee: A survey of Turkish surgeons.,” *Acta Orthop. Traumatol. Turc.*, vol. 50, no. 5, pp. 533–538, Oct. 2016.
- [426] A. He *et al.*, “Cell yield, chondrogenic potential, and regenerated cartilage type of chondrocytes derived from ear, nasoseptal, and costal cartilage.,” *J. Tissue Eng. Regen. Med.*, vol. 12, no. 4, pp. 1123–1132, Apr. 2018.
- [427] M. Mumme *et al.*, “Nasal chondrocyte-based engineered autologous cartilage tissue for repair of articular cartilage defects: an observational first-in-human trial.,” *Lancet (London, England)*, vol. 388, no. 10055, pp. 1985–1994, Oct. 2016.
- [428] L.-H. Chiu *et al.*, “Differential effect of ECM molecules on re-expression of cartilaginous markers in near quiescent human chondrocytes.,” *J. Cell. Physiol.*, vol. 226, no. 8, pp. 1981–8, Aug. 2011.
- [429] L. L. Y. Chiu, R. Giardini-Rosa, J. F. Weber, S. L. Cushing, and S. D. Waldman, “Comparisons of Auricular Cartilage Tissues from Different Species.,” *Ann. Otol. Rhinol. Laryngol.*, vol. 126, no. 12, pp. 819–828, Dec. 2017.
- [430] U. Galili, D. C. LaTemple, A. W. Walgenbach, and K. R. Stone, “Porcine and bovine cartilage transplants in cynomolgus monkey: II. Changes in anti-Gal response during chronic rejection.,” *Transplantation*, vol. 63, no. 5, pp. 646–51, Mar. 1997.
- [431] K. R. Stone, G. Ayala, J. Goldstein, R. Hurst, A. Walgenbach, and U. Galili, “Porcine cartilage transplants in the cynomolgus monkey. III. Transplantation of alpha-galactosidase-treated porcine cartilage.,” *Transplantation*, vol. 65, no. 12, pp. 1577–83, Jun. 1998.
- [432] S.-Y. Choi, H.-J. Jeong, H.-G. Lim, S.-S. Park, S.-H. Kim, and Y. J. Kim, “Elimination of alpha-gal xenoreactive epitope: alpha-galactosidase treatment of porcine heart valves.,” *J. Heart Valve Dis.*, vol. 21, no. 3, pp. 387–97, May 2012.
- [433] J. Nam *et al.*, “Changes of the Structural and Biomechanical Properties of the Bovine Pericardium after the Removal of α -Gal Epitopes by Decellularization and α -Galactosidase Treatment.,” *Korean J. Thorac. Cardiovasc. Surg.*, vol. 45, no. 6, pp. 380–9, Dec. 2012.

- [434] W. Feng, D. Li, J. Zang, and L. Fu, "Biomechanical comparison of xenogeneic bone material treated with different methods.," *Xenotransplantation*, vol. 24, no. 6, p. e12343, Nov. 2017.
- [435] A. Sogal and A. J. Tofe, "Risk assessment of bovine spongiform encephalopathy transmission through bone graft material derived from bovine bone used for dental applications.," *J. Periodontol.*, vol. 70, no. 9, pp. 1053–63, Sep. 1999.
- [436] B. Wenz, B. Oesch, and M. Horst, "Analysis of the risk of transmitting bovine spongiform encephalopathy through bone grafts derived from bovine bone.," *Biomaterials*, vol. 22, no. 12, pp. 1599–606, Jun. 2001.
- [437] J. D. Harris, R. A. Siston, X. Pan, and D. C. Flanigan, "Autologous Chondrocyte Implantation," *J. Bone Jt. Surgery-American Vol.*, vol. 92, no. 12, pp. 2220–2233, Sep. 2010.
- [438] E. Kon *et al.*, "Second-Generation Autologous Chondrocyte Implantation," *Am. J. Sports Med.*, vol. 39, no. 8, pp. 1668–1676, Aug. 2011.
- [439] G. Knutsen *et al.*, "A Randomized Trial Comparing Autologous Chondrocyte Implantation with Microfracture<sbid="1140484">Findings at Five Years</sbid>," *J. Bone Jt. Surg.*, vol. 89, no. 10, p. 2105, Oct. 2007.
- [440] A. G. McNickle, M. T. Provencher, and B. J. Cole, "Overview of Existing Cartilage Repair Technology," *Sports Med. Arthrosc.*, vol. 16, no. 4, pp. 196–201, Dec. 2008.
- [441] E. Kon, M. Delcogliano, G. Filardo, C. Montaperto, and M. Marcacci, "Second Generation Issues in Cartilage Repair," *Sports Med. Arthrosc.*, vol. 16, no. 4, pp. 221–229, Dec. 2008.
- [442] B. Mollon, R. Kandel, J. Chahal, and J. Theodoropoulos, "The clinical status of cartilage tissue regeneration in humans.," *Osteoarthr. Cartil.*, vol. 21, no. 12, pp. 1824–33, Dec. 2013.
- [443] K. L. Spiller, S. A. Maher, and A. M. Lowman, "Hydrogels for the Repair of Articular Cartilage Defects," *Tissue Eng. Part B Rev.*, vol. 17, no. 4, pp. 281–299, 2011.
- [444] F. T. Moutos and F. Guilak, "Composite scaffolds for cartilage tissue engineering.," *Biorheology*, vol. 45, no. 3–4, pp. 501–12, 2008.
- [445] R. Castro-Viñuelas *et al.*, "Induced pluripotent stem cells for cartilage repair: current status and future perspectives," *Eur. Cells Mater.*, vol. 36, pp. 96–109, Sep. 2018.
- [446] V. Savkovic, H. Li, J.-K. Seon, M. Hacker, S. Franz, and J.-C. Simon, "Mesenchymal stem cells in cartilage regeneration.," *Curr. Stem Cell Res. Ther.*, vol. 9, no. 6, pp. 469–88, 2014.
- [447] M. Lo Monaco *et al.*, "Stem Cells for Cartilage Repair: Preclinical Studies and Insights in Translational Animal Models and Outcome Measures.," *Stem Cells Int.*, vol. 2018, p. 9079538, 2018.
- [448] C. Gaut and K. Sugaya, "Critical review on the physical and mechanical factors involved in tissue engineering of cartilage.," *Regen. Med.*, vol. 10, no. 5, pp. 665–79, 2015.
- [449] V. Rai, M. F. Dilisio, N. E. Dietz, and D. K. Agrawal, "Recent strategies in cartilage repair: A systemic review of the scaffold development and tissue engineering.," *J. Biomed. Mater. Res. A*, vol. 105, no. 8, pp. 2343–2354, Aug. 2017.
- [450] C. Scotti *et al.*, "Cartilage Repair in the Inflamed Joint: Considerations for Biological Augmentation Toward Tissue Regeneration.," *Tissue Eng. Part B Rev.*, vol. 22, no. 2, pp. 149–59, Apr. 2016.
- [451] A. J. Sophia Fox, A. Bedi, and S. A. Rodeo, "The basic science of articular cartilage: structure, composition, and function.," *Sports Health*, vol. 1, no. 6, pp. 461–8, Nov. 2009.
- [452] A. R. Poole, T. Kojima, T. Yasuda, F. Mwale, M. Kobayashi, and S. Laverty, "Composition and structure of articular cartilage: a template for tissue repair.," *Clin. Orthop. Relat. Res.*, no. 391 Suppl, pp. S26-33, Oct. 2001.
- [453] P. Abdel-Sayed and D. P. Pioletti, "Strategies for improving the repair of focal cartilage defects," *Nanomedicine*, vol. 10, no. 18, pp. 2893–2905, Sep. 2015.
- [454] S. Nuernberger, N. Cyran, C. Albrecht, H. Redl, V. Vécsei, and S. Marlovits, "The influence of scaffold architecture on chondrocyte distribution and behavior in matrix-associated chondrocyte transplantation grafts," *Biomaterials*, vol. 32, no. 4, pp. 1032–1040, Feb. 2011.
- [455] K.-X. A. Lee, H. Y. Ng, L.-J. Wei, and Y.-F. Shen, "3D functional scaffolds for cartilage tissue engineering," *Funct. 3D Tissue Eng. Scaffolds*, pp. 391–421, Jan. 2018.
- [456] X. Zhang, W. Zhang, and M. Yang, "Application of Hydrogels in Cartilage Tissue Engineering," *Curr. Stem Cell Res. Ther.*, vol. 13, no. 7, pp. 497–516, Aug. 2018.
- [457] W. Zhang *et al.*, "Cell-Derived Extracellular Matrix: Basic Characteristics and Current Applications in Orthopedic Tissue Engineering.," *Tissue Eng. Part B Rev.*, vol. 22, no. 3, pp. 193–207, 2016.
- [458] E. A. Kiyotake, E. C. Beck, and M. S. Detamore, "Cartilage extracellular matrix as a biomaterial for cartilage regeneration," *Ann. N. Y. Acad. Sci.*, vol. 1383, no. 1, pp. 139–159, Nov. 2016.
- [459] F. Taraballi, G. Bauza, P. McCulloch, J. Harris, and E. Tasciotti, "Concise Review: Biomimetic Functionalization of Biomaterials to Stimulate the Endogenous Healing Process of Cartilage and Bone Tissue," *Stem Cells Transl. Med.*, vol. 6, no. 12, pp. 2186–2196, Dec. 2017.
- [460] X. Ma *et al.*, "Repair of osteochondral defects by mosaicplasty and allogeneic BMSCs transplantation.," *Int. J. Clin. Exp. Med.*, vol. 8, no. 4, pp. 6053–9, 2015.
- [461] F. A. Monibi and J. L. Cook, "Tissue-Derived Extracellular Matrix Bioscaffolds: Emerging Applications in Cartilage and Meniscus Repair.," *Tissue Eng. Part B Rev.*, vol. 23, no. 4, pp. 386–398, 2017.
- [462] S. Schwarz *et al.*, "Decellularized cartilage matrix as a novel biomatrix for cartilage tissue-engineering applications.,"

- Tissue Eng. Part A*, vol. 18, no. 21–22, pp. 2195–209, Nov. 2012.
- [463] L. Utomo *et al.*, “Preparation and characterization of a decellularized cartilage scaffold for ear cartilage reconstruction,” *Biomed. Mater.*, vol. 10, no. 1, p. 015010, Jan. 2015.
- [464] C. Schneider *et al.*, “Systematic Comparison of Protocols for the Preparation of Human Articular Cartilage for Use as Scaffold Material in Cartilage Tissue Engineering,” *Tissue Eng. Part C. Methods*, vol. 22, no. 12, pp. 1095–1107, 2016.
- [465] K. Gelse *et al.*, “Transplantation of Chemically Processed Decellularized Meniscal Allografts,” *Cartilage*, vol. 8, no. 2, pp. 180–190, Apr. 2017.
- [466] L. Luo, R. Eswaramoorthy, K. J. Mulhall, and D. J. Kelly, “Decellularization of porcine articular cartilage explants and their subsequent repopulation with human chondroprogenitor cells,” *J. Mech. Behav. Biomed. Mater.*, vol. 55, pp. 21–31, Mar. 2016.
- [467] S. Nürnberger *et al.*, “Repopulation of an auricular cartilage scaffold, AuriScaff, perforated with an enzyme combination,” *Acta Biomater.*, vol. 86, pp. 207–222, Mar. 2019.
- [468] C. J. O’Conor, N. Case, and F. Guilak, “Mechanical regulation of chondrogenesis,” *Stem Cell Res. Ther.*, vol. 4, no. 4, p. 61, Jul. 2013.
- [469] C.-H. Chen, C.-Y. Kuo, and J.-P. Chen, “Effect of Cyclic Dynamic Compressive Loading on Chondrocytes and Adipose-Derived Stem Cells Co-Cultured in Highly Elastic Cryogel Scaffolds,” *Int. J. Mol. Sci.*, vol. 19, no. 2, Jan. 2018.
- [470] S. Wolbank *et al.*, “Dose-dependent immunomodulatory effect of human stem cells from amniotic membrane: a comparison with human mesenchymal stem cells from adipose tissue,” *Tissue Eng.*, vol. 13, no. 6, pp. 1173–83, Jun. 2007.
- [471] Z. Li, L. Kupcsik, S.-J. Yao, M. Alini, and M. J. Stoddart, “Chondrogenesis of human bone marrow mesenchymal stem cells in fibrin-polyurethane composites,” *Tissue Eng. Part A*, vol. 15, no. 7, pp. 1729–37, Jul. 2009.
- [472] A. Cochis *et al.*, “Bioreactor mechanically guided 3D mesenchymal stem cell chondrogenesis using a biocompatible novel thermo-reversible methylcellulose-based hydrogel,” *Sci. Rep.*, vol. 7, no. October 2016, pp. 1–12, 2017.
- [473] O. F. W. Gardner *et al.*, “Asymmetrical seeding of MSCs into fibrin-poly(ester-urethane) scaffolds and its effect on mechanically induced chondrogenesis,” *J. Tissue Eng. Regen. Med.*, vol. 11, no. 10, pp. 2912–2921, Oct. 2017.
- [474] F. M. Hilz *et al.*, “Influence of extremely low frequency, low energy electromagnetic fields and combined mechanical stimulation on chondrocytes in 3-D constructs for cartilage tissue engineering,” *Bioelectromagnetics*, vol. 35, no. 2, pp. 116–128, 2014.
- [475] M. Petrou *et al.*, “Mesenchymal stem cell chondrogenesis: Composite growth factor-bioreactor synergism for human stem cell chondrogenesis,” *Regen. Med.*, vol. 8, no. 2, pp. 157–170, 2013.
- [476] O. Schätti *et al.*, “A combination of shear and dynamic compression leads to mechanically induced chondrogenesis of human mesenchymal stem cells,” *Eur. Cell. Mater.*, vol. 22, pp. 214–225, 2011.
- [477] R. M. Frank *et al.*, “Reoperation Rates After Cartilage Restoration Procedures in the Knee: Analysis of a Large US Commercial Database,” *Am. J. Orthop.*, vol. 47, no. 6, Jun. 2018.
- [478] T. M. Simon and D. W. Jackson, “Articular Cartilage,” *Sports Med. Arthrosc.*, vol. 26, no. 1, pp. 31–39, Mar. 2018.
- [479] S. Grad, D. Eglin, M. Alini, and M. J. Stoddart, “Physical Stimulation of Chondrogenic Cells In Vitro: A Review,” *Clin. Orthop. Relat. Res.*, vol. 469, no. 10, pp. 2764–2772, Oct. 2011.
- [480] J. Sanchez-Adams, H. A. Leddy, A. L. McNulty, C. J. O’Conor, and F. Guilak, “The mechanobiology of articular cartilage: bearing the burden of osteoarthritis,” *Curr. Rheumatol. Rep.*, vol. 16, no. 10, p. 451, Oct. 2014.
- [481] L. Kupcsik, M. J. Stoddart, Z. Li, L. M. Benneker, and M. Alini, “Improving Chondrogenesis: Potential and Limitations of SOX9 Gene Transfer and Mechanical Stimulation for Cartilage Tissue Engineering,” *Tissue Eng. Part A*, vol. 16, no. 6, pp. 1845–1855, 2010.
- [482] R. Ossendorff *et al.*, “Autologous Chondrocyte Implantation in Osteoarthritic Surroundings: TNF α and Its Inhibition by Adalimumab in a Knee-Specific Bioreactor,” *Am. J. Sports Med.*, vol. 46, no. 2, pp. 431–440, 2018.
- [483] V. Ronfard and Y. Barrandon, “Migration of keratinocytes through tunnels of digested fibrin,” *Proc. Natl. Acad. Sci. U. S. A.*, vol. 98, no. 8, pp. 4504–9, Apr. 2001.
- [484] E. M. Darling and K. A. Athanasiou, “Rapid phenotypic changes in passaged articular chondrocyte subpopulations,” *J. Orthop. Res.*, vol. 23, no. 2, pp. 425–432, Mar. 2005.
- [485] C. R. Fellows, C. Matta, R. Zakany, I. M. Khan, and A. Mobasheri, “Adipose, Bone Marrow and Synovial Joint-Derived Mesenchymal Stem Cells for Cartilage Repair,” *Front. Genet.*, vol. 7, p. 213, Dec. 2016.
- [486] J. I. Huang, N. Kazmi, M. M. Durbhakula, T. M. Hering, J. U. Yoo, and B. Johnstone, “Chondrogenic potential of progenitor cells derived from human bone marrow and adipose tissue: a patient-matched comparison,” *J. Orthop. Res.*, vol. 23, no. 6, pp. 1383–9, Nov. 2005.
- [487] Y. Sakaguchi, I. Sekiya, K. Yagishita, and T. Muneta, “Comparison of human stem cells derived from various mesenchymal tissues: superiority of synovium as a cell source,” *Arthritis Rheum.*, vol. 52, no. 8, pp. 2521–9, Aug. 2005.
- [488] H. Afizah, Z. Yang, J. H. P. Hui, H.-W. Ouyang, and E.-H. Lee, “A Comparison Between the Chondrogenic Potential of Human Bone Marrow Stem Cells (BMSCs) and Adipose-Derived Stem Cells (ADSCs) Taken from the Same Donors,” *Tissue Eng.*, vol. 13, no. 4, pp. 659–666, Apr. 2007.

- [489] M. C. Ronzière, E. Perrier, F. Mallein-Gerin, and A.-M. Freyria, "Chondrogenic potential of bone marrow- and adipose tissue-derived adult human mesenchymal stem cells.," *Biomed. Mater. Eng.*, vol. 20, no. 3, pp. 145–58, 2010.
- [490] X. Li *et al.*, "Bone Marrow- and Adipose Tissue-Derived Mesenchymal Stem Cells: Characterization, Differentiation, and Applications in Cartilage Tissue Engineering," *Crit. Rev. Eukaryot. Gene Expr.*, vol. 28, no. 4, pp. 285–310, 2018.
- [491] D. Noël *et al.*, "Cell specific differences between human adipose-derived and mesenchymal-stromal cells despite similar differentiation potentials.," *Exp. Cell Res.*, vol. 314, no. 7, pp. 1575–84, Apr. 2008.
- [492] F. Veronesi, M. Maglio, M. Tschon, N. N. Aldini, and M. Fini, "Adipose-derived mesenchymal stem cells for cartilage tissue engineering: State-of-The-Art in in vivo studies," *J. Biomed. Mater. Res. Part A*, vol. 102, no. 7, pp. 2448–2466, Jul. 2014.
- [493] H. Kang *et al.*, "In vivo cartilage repair using adipose-derived stem cell-loaded decellularized cartilage ECM scaffolds," *J. Tissue Eng. Regen. Med.*, vol. 8, no. 6, pp. 442–453, Jun. 2014.
- [494] L. Wu, X. Cai, S. Zhang, M. Karperien, and Y. Lin, "Regeneration of articular cartilage by adipose tissue derived mesenchymal stem cells: Perspectives from stem cell biology and molecular medicine," *J. Cell. Physiol.*, vol. 228, no. 5, pp. 938–944, May 2013.
- [495] D. NESIC, R. WHITESIDE, M. BRITTBURG, D. WENDT, I. MARTIN, and P. MAINILVARLET, "Cartilage tissue engineering for degenerative joint disease☆," *Adv. Drug Deliv. Rev.*, vol. 58, no. 2, pp. 300–322, May 2006.
- [496] B. Khozoe, P. Mafī, R. Mafī, and W. S. Khan, "Mechanical Stimulation Protocols of Human Derived Cells in Articular Cartilage Tissue Engineering - A Systematic Review.," *Curr. Stem Cell Res. Ther.*, vol. 12, no. 3, pp. 260–270, Feb. 2017.
- [497] E. Y. Salinas, J. C. Hu, and K. Athanasiou, "A Guide for Using Mechanical Stimulation to Enhance Tissue-Engineered Articular Cartilage Properties.," *Tissue Eng. Part B Rev.*, vol. 24, no. 5, pp. 345–358, 2018.
- [498] I. Martin, M. Jakob, D. Schäfer, W. Dick, G. Spagnoli, and M. Heberer, "Quantitative analysis of gene expression in human articular cartilage from normal and osteoarthritic joints.," *Osteoarthr. Cartil.*, vol. 9, no. 2, pp. 112–8, Feb. 2001.
- [499] C. Albrecht, B. Tichy, L. Zak, S. Aldrian, S. Nürnberger, and S. Marlovits, "Influence of cell differentiation and IL-1 β expression on clinical outcomes after matrix-associated chondrocyte transplantation," *Am. J. Sports Med.*, vol. 42, no. 1, pp. 59–69, 2014.
- [500] A. Barlič, M. Drobnič, E. Maličev, and N. Kregar-Velikonja, "Quantitative analysis of gene expression in human articular chondrocytes assigned for autologous implantation," *J. Orthop. Res.*, vol. 26, no. 6, pp. 847–853, Jun. 2008.
- [501] C. G. Jeong and S. J. Hollister, "A comparison of the influence of material on in vitro cartilage tissue engineering with PCL, PGS, and POC 3D scaffold architecture seeded with chondrocytes," *Biomaterials*, vol. 31, no. 15, pp. 4304–4312, May 2010.
- [502] J.-P. Stromps, N. E. Paul, B. Rath, M. Nourbakhsh, J. Bernhagen, and N. Pallua, "Chondrogenic Differentiation of Human Adipose-Derived Stem Cells: A New Path in Articular Cartilage Defect Management?," *Biomed Res. Int.*, vol. 2014, pp. 1–7, 2014.
- [503] S. Finlay, B. B. Seedhom, D. O. Carey, A. J. Bulpitt, D. E. Treanor, and J. Kirkham, "In Vitro Engineering of High Modulus Cartilage-Like Constructs.," *Tissue Eng. Part C. Methods*, vol. 22, no. 4, pp. 382–97, Apr. 2016.
- [504] E. G. Lima *et al.*, "The beneficial effect of delayed compressive loading on tissue-engineered cartilage constructs cultured with TGF- β 3," *Osteoarthr. Cartil.*, vol. 15, no. 9, pp. 1025–1033, Sep. 2007.
- [505] D. E. Anderson and B. Johnstone, "Dynamic Mechanical Compression of Chondrocytes for Tissue Engineering: A Critical Review," *Front. Bioeng. Biotechnol.*, vol. 5, p. 76, Dec. 2017.
- [506] Z. Li, L. Kupesik, S. J. Yao, M. Alini, and M. J. Stoddart, "Mechanical load modulates chondrogenesis of human mesenchymal stem cells through the TGF- β pathway," *J. Cell. Mol. Med.*, vol. 14, no. 6 A, pp. 1338–1346, 2010.
- [507] S. Nebelung *et al.*, "Simultaneous anabolic and catabolic responses of human chondrocytes seeded in collagen hydrogels to long-term continuous dynamic compression," *Ann. Anat. - Anat. Anzeiger*, vol. 194, no. 4, pp. 351–358, Jul. 2012.
- [508] P.-Y. Wang, H.-H. Chow, W.-B. Tsai, and H.-W. Fang, "Modulation of Gene Expression of Rabbit Chondrocytes by Dynamic Compression in Polyurethane Scaffolds with Collagen Gel Encapsulation," *J. Biomater. Appl.*, vol. 23, no. 4, pp. 347–366, Jan. 2009.
- [509] D. W. Taylor *et al.*, "Collagen Type XII and Versican Are Present in the Early Stages of Cartilage Tissue Formation by Both Redifferentating Passaged and Primary Chondrocytes," *Tissue Eng. Part A*, vol. 21, no. 3–4, pp. 683–693, Feb. 2015.
- [510] K. Choocheep *et al.*, "Versican facilitates chondrocyte differentiation and regulates joint morphogenesis.," *J. Biol. Chem.*, vol. 285, no. 27, pp. 21114–25, Jul. 2010.
- [511] K. Kimata *et al.*, "A large chondroitin sulfate proteoglycan (PG-M) synthesized before chondrogenesis in the limb bud of chick embryo.," *J. Biol. Chem.*, vol. 261, no. 29, 1986.
- [512] K. Miyanishi *et al.*, "Effects of Hydrostatic Pressure and Transforming Growth Factor- β 3 on Adult Human Mesenchymal Stem Cell Chondrogenesis In Vitro," *Tissue Eng.*, vol. 12, no. 6, pp. 1419–1428, Jun. 2006.
- [513] P. M. van der Kraan, "Differential Role of Transforming Growth Factor-beta in an Osteoarthritic or a Healthy Joint.," *J. bone Metab.*, vol. 25, no. 2, pp. 65–72, May 2018.
- [514] M. B. Albro *et al.*, "Dynamic mechanical compression of devitalized articular cartilage does not activate latent TGF-

- β,” *J. Biomech.*, vol. 46, no. 8, pp. 1433–1439, May 2013.
- [515] R. Serra and C. Chang, “TGF-beta signaling in human skeletal and patterning disorders,” *Birth Defects Res. C. Embryo Today*, vol. 69, no. 4, pp. 333–51, Nov. 2003.
- [516] P. M. van der Kraan, E. N. Blaney Davidson, A. Blom, and W. B. van den Berg, “TGF-beta signaling in chondrocyte terminal differentiation and osteoarthritis,” *Osteoarthr. Cartil.*, vol. 17, no. 12, pp. 1539–1545, Dec. 2009.
- [517] T.-F. Li, R. J. O’Keefe, and D. Chen, “TGF-beta signaling in chondrocytes,” *Front. Biosci.*, vol. 10, pp. 681–8, Jan. 2005.
- [518] Ł. A. Poniatowski, P. Wojdasiewicz, R. Gasik, and D. Szukiewicz, “Transforming Growth Factor Beta Family: Insight into the Role of Growth Factors in Regulation of Fracture Healing Biology and Potential Clinical Applications,” *Mediators Inflamm.*, vol. 2015, pp. 1–17, 2015.
- [519] K. W. Finsson, Y. Chi, G. Bou-Gharios, A. Leask, and A. Philip, “TGF-b signaling in cartilage homeostasis and osteoarthritis,” *Front. Biosci. (Schol. Ed.)*, vol. 4, pp. 251–68, Jan. 2012.
- [520] W. Wang, D. Rigueur, and K. M. Lyons, “TGFβ signaling in cartilage development and maintenance,” *Birth Defects Res. C. Embryo Today*, vol. 102, no. 1, pp. 37–51, Mar. 2014.
- [521] J. J. Song *et al.*, “Connective tissue growth factor (CTGF) acts as a downstream mediator of TGF-β1 to induce mesenchymal cell condensation,” *J. Cell. Physiol.*, vol. 210, no. 2, pp. 398–410, Feb. 2007.
- [522] R. Tuli *et al.*, “Transforming Growth Factor-β-mediated Chondrogenesis of Human Mesenchymal Progenitor Cells Involves N-cadherin and Mitogen-activated Protein Kinase and Wnt Signaling Cross-talk,” *J. Biol. Chem.*, vol. 278, no. 42, pp. 41227–41236, Oct. 2003.
- [523] F. Barry, R. E. Boynton, B. Liu, and J. M. Murphy, “Chondrogenic Differentiation of Mesenchymal Stem Cells from Bone Marrow: Differentiation-Dependent Gene Expression of Matrix Components,” *Exp. Cell Res.*, vol. 268, no. 2, pp. 189–200, Aug. 2001.
- [524] A. S. Patil, R. B. Sable, and R. M. Kothari, “An update on transforming growth factor-β (TGF-β): sources, types, functions and clinical applicability for cartilage/bone healing,” *J. Cell. Physiol.*, vol. 226, no. 12, pp. 3094–103, Dec. 2011.
- [525] M. B. Mueller *et al.*, “Hypertrophy in Mesenchymal Stem Cell Chondrogenesis: Effect of TGF-β Isoforms and Chondrogenic Conditioning,” *Cells Tissues Organs*, vol. 192, no. 3, pp. 158–166, 2010.
- [526] N. Shintani, K. A. Siebenrock, and E. B. Hunziker, “TGF-β1 Enhances the BMP-2-Induced Chondrogenesis of Bovine Synovial Explants and Arrests Downstream Differentiation at an Early Stage of Hypertrophy,” *PLoS One*, vol. 8, no. 1, p. e53086, Jan. 2013.
- [527] L. S. Baptista *et al.*, “Bioengineered Cartilage in a Scaffold-Free Method by Human Cartilage-Derived Progenitor Cells: A Comparison With Human Adipose-Derived Mesenchymal Stromal Cells,” *Artif. Organs*, vol. 37, no. 12, pp. 1068–1075, Dec. 2013.
- [528] M. Mardani, S. Roshankhah, B. Hashemibeni, M. Salahshoor, E. Naghsh, and E. Esfandiari, “Induction of chondrogenic differentiation of human adipose-derived stem cells by low frequency electric field,” *Adv. Biomed. Res.*, vol. 5, p. 97, 2016.
- [529] M. B. Albro *et al.*, “Shearing of synovial fluid activates latent TGF-β,” *Osteoarthr. Cartil.*, vol. 20, no. 11, pp. 1374–1382, Nov. 2012.
- [530] O. F. W. Gardner, N. Fahy, M. Alini, and M. J. Stoddart, “Joint mimicking mechanical load activates TGFβ1 in fibrin-poly(ester-urethane) scaffolds seeded with mesenchymal stem cells,” *J. Tissue Eng. Regen. Med.*, vol. 11, no. 9, pp. 2663–2666, Sep. 2017.
- [531] J. Ahamed, N. Burg, K. Yoshinaga, C. A. Janczak, D. B. Rifkin, and B. S. Coller, “In vitro and in vivo evidence for shear-induced activation of latent transforming growth factor- 1,” *Blood*, vol. 112, no. 9, pp. 3650–3660, Nov. 2008.
- [532] Q. Bian *et al.*, “Mechanosignaling activation of TGFβ maintains intervertebral disc homeostasis,” *Bone Res.*, vol. 5, p. 17008, Mar. 2017.
- [533] M. N. Helder, M. Knippenberg, J. Klein-Nulend, and P. I. J. M. Wuisman, “Stem Cells from Adipose Tissue Allow Challenging New Concepts for Regenerative Medicine,” *Tissue Eng.*, vol. 13, no. 8, pp. 1799–1808, Aug. 2007.
- [534] W. J. Jurgens, R. J. Kroeze, R. A. Bank, M. J. P. F. Ritt, and M. N. Helder, “Rapid attachment of adipose stromal cells on resorbable polymeric scaffolds facilitates the one-step surgical procedure for cartilage and bone tissue engineering purposes,” *J. Orthop. Res.*, vol. 29, no. 6, pp. 853–860, Jun. 2011.
- [535] B. Weber *et al.*, “Injectable living marrow stromal cell-based autologous tissue engineered heart valves: first experiences with a one-step intervention in primates,” *Eur. Heart J.*, vol. 32, no. 22, pp. 2830–2840, Nov. 2011.
- [536] J. R. Choi, K. W. Yong, and J. Y. Choi, “Effects of mechanical loading on human mesenchymal stem cells for cartilage tissue engineering,” *J. Cell. Physiol.*, vol. 233, no. 3, pp. 1913–1928, Mar. 2018.
- [537] C. G. Helmick *et al.*, “Estimates of the prevalence of arthritis and other rheumatic conditions in the United States. Part I,” *Arthritis Rheum.*, vol. 58, no. 1, pp. 15–25, Jan. 2008.
- [538] R. C. Lawrence *et al.*, “Estimates of the prevalence of arthritis and other rheumatic conditions in the United States. Part II,” *Arthritis Rheum.*, vol. 58, no. 1, pp. 26–35, Jan. 2008.
- [539] F. Berenbaum, “Osteoarthritis as an inflammatory disease (osteoarthritis is not osteoarthrosis!),” *Osteoarthr. Cartil.*, vol. 21, no. 1, pp. 16–21, Jan. 2013.
- [540] G. P. Dobson *et al.*, “Defining the osteoarthritis patient: back to the future,” *Osteoarthr. Cartil.*, vol. 26, no. 8, pp.

- 1003–1007, 2018.
- [541] R. Liu-Bryan and R. Terkeltaub, “Emerging regulators of the inflammatory process in osteoarthritis,” *Nat. Rev. Rheumatol.*, vol. 11, no. 1, pp. 35–44, 2015.
- [542] S. J. Kim *et al.*, “Therapeutic effects of neuropeptide substance P coupled with self-assembled peptide nanofibers on the progression of osteoarthritis in a rat model,” *Biomaterials*, vol. 74, pp. 119–30, Jan. 2016.
- [543] G. Smith, S. L. Myers, K. D. Brandt, E. A. Mickler, and M. E. Albrecht, “Effect of intraarticular hyaluronan injection on vertical ground reaction force and progression of osteoarthritis after anterior cruciate ligament transection,” *J. Rheumatol.*, vol. 32, no. 2, pp. 325–34, Feb. 2005.
- [544] C. I. Johnson, D. J. Argyle, and D. N. Clements, “In vitro models for the study of osteoarthritis,” *Vet. J.*, vol. 209, pp. 40–9, Mar. 2016.
- [545] J. F. Weber and S. D. Waldman, “Calcium signaling as a novel method to optimize the biosynthetic response of chondrocytes to dynamic mechanical loading,” *Biomech. Model. Mechanobiol.*, vol. 13, no. 6, pp. 1387–1397, 2014.
- [546] K. Scherer, M. Schünke, R. Sellckau, J. Hassenpflug, and B. Kurz, “The influence of oxygen and hydrostatic pressure on articular chondrocytes and adherent bone marrow cells in vitro,” *Biorheology*, vol. 41, no. 3–4, pp. 323–33, 2004.
- [547] A. Fioravanti, E. Moretti, G. Scapigliati, R. Cervone, M. Galeazzi, and G. Collodel, “Morphological, immunocytochemical and biochemical studies in human osteoarthritic chondrocytes exposed to IL-1b and cyclical hydrostatic pressure,” *Clin. Exp. Rheumatol.*, vol. 25, no. 5, pp. 690–5, 2007.
- [548] M. M. Knight, T. Toyoda, D. A. Lee, and D. L. Bader, “Mechanical compression and hydrostatic pressure induce reversible changes in actin cytoskeletal organisation in chondrocytes in agarose,” *J. Biomech.*, vol. 39, no. 8, pp. 1547–1551, 2006.
- [549] N. A. Pascarelli, G. Collodel, E. Moretti, S. Chelleschi, and A. Fioravanti, “Changes in ultrastructure and cytoskeletal aspects of human normal and osteoarthritic chondrocytes exposed to interleukin-1 β and cyclical hydrostatic pressure,” *Int. J. Mol. Sci.*, vol. 16, no. 11, pp. 26019–26034, 2015.
- [550] Y. Henrotin, B. Kurz, and T. Aigner, “Oxygen and reactive oxygen species in cartilage degradation: Friends or foes?,” *Osteoarthr. Cartil.*, vol. 13, no. 8, pp. 643–654, 2005.
- [551] C. Ziskoven, M. Jäger, C. Zilkens, W. Bloch, K. Brixius, and R. Krauspe, “Oxidative stress in secondary osteoarthritis: from cartilage destruction to clinical presentation?,” *Orthop. Rev. (Pavia)*, vol. 2, no. 2, p. e23, 2010.
- [552] I. M. Khan, S. J. Gilbert, B. Caterson, L. J. Sandell, and C. W. Archer, “Oxidative stress induces expression of osteoarthritis markers procollagen IIA and 3B3(-) in adult bovine articular cartilage,” *Osteoarthr. Cartil.*, vol. 16, no. 6, pp. 698–707, 2008.
- [553] I.-C. Young *et al.*, “Protective effects of aucubin on osteoarthritic chondrocyte model induced by hydrogen peroxide and mechanical stimulus,” *BMC Complement. Altern. Med.*, vol. 17, no. 1, p. 91, 2017.
- [554] S. D’Adamo, S. Cetrullo, S. Guidotti, R. M. Borzi, and F. Flamigni, “Hydroxytyrosol modulates the levels of microRNA-9 and its target sirtuin-1 thereby counteracting oxidative stress-induced chondrocyte death,” *Osteoarthr. Cartil.*, vol. 25, no. 4, pp. 600–610, 2017.
- [555] S. Chelleschi *et al.*, “Could oxidative stress regulate the expression of microRNA-146a and microRNA-34a in human osteoarthritic chondrocyte cultures?,” *Int. J. Mol. Sci.*, vol. 18, no. 12, 2017.
- [556] A. Facchini, I. Stanic, S. Cetrullo, R. M. Borzi, G. Filardo, and F. Flamigni, “Sulforaphane protects human chondrocytes against cell death induced by various stimuli,” *J. Cell. Physiol.*, vol. 226, no. 7, pp. 1771–1779, 2011.
- [557] T. S. Hiran, P. J. Moulton, and J. T. Hancock, “Detection of superoxide and NADPH oxidase in porcine articular chondrocytes,” *Free Radic. Biol. Med.*, vol. 23, no. 5, pp. 736–43, 1997.
- [558] E. A. Regan, R. P. Bowler, and J. D. Crapo, “Joint fluid antioxidants are decreased in osteoarthritic joints compared to joints with macroscopically intact cartilage and subacute injury,” *Osteoarthr. Cartil.*, vol. 16, no. 4, pp. 515–521, 2008.
- [559] E. Regan *et al.*, “Extracellular superoxide dismutase and oxidant damage in osteoarthritis,” *Arthritis Rheum.*, vol. 52, no. 11, pp. 3479–3491, 2009.
- [560] A. Banerjee *et al.*, “Cellular and Site-Specific Mitochondrial Characterization of Vital Human Amniotic Membrane,” *Cell Transplant.*, vol. 27, no. 1, pp. 3–11, Jan. 2018.
- [561] I. Martin, M. Jakob, D. Schäfer, W. Dick, G. Spagnoli, and M. Heberer, “Quantitative analysis of gene expression in human articular cartilage from normal and osteoarthritic joints,” *Osteoarthr. Cartil.*, vol. 9, no. 2, pp. 112–118, Feb. 2001.
- [562] L. Troeberg and H. Nagase, “Proteases involved in cartilage matrix degradation in osteoarthritis,” *Biochim. Biophys. Acta*, vol. 1824, no. 1, pp. 133–45, Jan. 2012.
- [563] M. B. Goldring, “The role of the chondrocyte in osteoarthritis,” *Arthritis Rheum.*, vol. 43, no. 9, pp. 1916–26, Sep. 2000.
- [564] C. Palazzo, C. Nguyen, M.-M. Lefevre-Colau, F. Rannou, and S. Poiraudou, “Risk factors and burden of osteoarthritis,” *Ann. Phys. Rehabil. Med.*, vol. 59, no. 3, pp. 134–8, Jun. 2016.
- [565] H. Fang and F. Beier, “Mouse models of osteoarthritis: modelling risk factors and assessing outcomes,” *Nat. Rev. Rheumatol.*, vol. 10, no. 7, pp. 413–421, 2014.
- [566] J. P. Pelletier *et al.*, “Selective inhibition of inducible nitric oxide synthase reduces progression of experimental osteoarthritis in vivo: possible link with the reduction in chondrocyte apoptosis and caspase 3 level,” *Arthritis Rheum.*,

- vol. 43, no. 6, pp. 1290–9, Jun. 2000.
- [567] J.-M. Mongkhon, M. Thach, Q. Shi, J. C. Fernandes, H. Fahmi, and M. Benderdour, “Sorbitol-modified hyaluronic acid reduces oxidative stress, apoptosis and mediators of inflammation and catabolism in human osteoarthritic chondrocytes,” *Inflamm. Res.*, vol. 63, no. 8, pp. 691–701, Aug. 2014.
- [568] S. J. Kim *et al.*, “Therapeutic effects of neuropeptide substance P coupled with self-assembled peptide nanofibers on the progression of osteoarthritis in a rat model,” *Biomaterials*, vol. 74, no. March, pp. 119–30, Jan. 2016.
- [569] N. J. Goddard and P. T. Gosling, “Intra-articular fluid pressure and pain in osteoarthritis of the hip,” *J. Bone Joint Surg. Br.*, vol. 70, no. 1, pp. 52–5, Jan. 1988.
- [570] S. Jawed, K. Gaffney, and D. R. Blake, “Intra-articular pressure profile of the knee joint in a spectrum of inflammatory arthropathies,” *Ann. Rheum. Dis.*, vol. 56, no. 11, pp. 686–9, Nov. 1997.
- [571] D. S. Meredith, E. Losina, G. Neumann, H. Yoshioka, P. K. Lang, and J. N. Katz, “Empirical evaluation of the inter-relationship of articular elements involved in the pathoanatomy of knee osteoarthritis using magnetic resonance imaging,” *BMC Musculoskelet. Disord.*, vol. 10, p. 133, Oct. 2009.
- [572] S. Krasnokutsky *et al.*, “Quantitative magnetic resonance imaging evidence of synovial proliferation is associated with radiographic severity of knee osteoarthritis,” *Arthritis Rheum.*, vol. 63, no. 10, pp. 2983–91, Oct. 2011.
- [573] D. T. Felson, “Weight and osteoarthritis,” *J. Rheumatol. Suppl.*, vol. 43, pp. 7–9, Feb. 1995.
- [574] J. A. Buckwalter, D. D. Anderson, T. D. Brown, Y. Tochigi, and J. A. Martin, “The Roles of Mechanical Stresses in the Pathogenesis of Osteoarthritis: Implications for Treatment of Joint Injuries,” *Cartilage*, vol. 4, no. 4, pp. 286–294, 2013.
- [575] M. Koike *et al.*, “Mechanical overloading causes mitochondrial superoxide and SOD2 imbalance in chondrocytes resulting in cartilage degeneration,” *Sci. Rep.*, vol. 5, no. March, p. 11722, 2015.
- [576] F. Zhu, P. Wang, N. H. Lee, M. B. Goldring, and K. Konstantopoulos, “Prolonged Application of High Fluid Shear to Chondrocytes Recapitulates Gene Expression Profiles Associated with Osteoarthritis,” *PLoS One*, vol. 5, no. 12, 2010.
- [577] P. Ramakrishnan *et al.*, “Oxidant conditioning protects cartilage from mechanically induced damage,” *J. Orthop. Res.*, vol. 28, no. 7, pp. 914–20, Jul. 2010.
- [578] I.-C. Young *et al.*, “Protective effects of aucubin on osteoarthritic chondrocyte model induced by hydrogen peroxide and mechanical stimulus,” *BMC Complement. Altern. Med.*, vol. 17, no. 1, p. 91, Feb. 2017.
- [579] K. D. Muirden and G. B. Senator, “Iron in the synovial membrane in rheumatoid arthritis and other joint diseases,” *Ann. Rheum. Dis.*, vol. 27, no. 1, pp. 38–48, Jan. 1968.
- [580] M. Yazar, S. Sarban, A. Kocyigit, and U. E. Isikan, “Synovial fluid and plasma selenium, copper, zinc, and iron concentrations in patients with rheumatoid arthritis and osteoarthritis,” *Biol. Trace Elem. Res.*, vol. 106, no. 2, pp. 123–32, Aug. 2005.
- [581] M. J. J. Hooiveld, G. Roosendaal, H. M. van den Berg, J. W. J. Bijlsma, and F. P. J. G. Lafeber, “Haemoglobin-derived iron-dependent hydroxyl radical formation in blood-induced joint damage: an in vitro study,” *Rheumatology (Oxford)*, vol. 42, no. 6, pp. 784–90, Jun. 2003.
- [582] D. Melchiorre, M. Manetti, and M. Matucci-Cerinic, “Pathophysiology of Hemophilic Arthropathy,” *J. Clin. Med.*, vol. 6, no. 7, p. 63, Jun. 2017.
- [583] a J. Dabbagh, C. W. Trenam, C. J. Morris, and D. R. Blake, “Iron in joint inflammation,” *Ann. Rheum. Dis.*, vol. 52, no. 1, pp. 67–73, Jan. 1993.
- [584] Y. Kawai, E. Kubota, and E. Okabe, “Reactive oxygen species participation in experimentally induced arthritis of the temporomandibular joint in rats,” *J. Dent. Res.*, vol. 79, no. 7, pp. 1489–1495, 2000.
- [585] M. L. Tiku, R. Shah, and G. T. Allison, “Evidence linking chondrocyte lipid peroxidation to cartilage matrix protein degradation. Possible role in cartilage aging and the pathogenesis of osteoarthritis,” *J. Biol. Chem.*, vol. 275, no. 26, pp. 20069–76, Jun. 2000.
- [586] F. J. Blanco, R. L. Ochs, H. Schwarz, and M. Lotz, “Chondrocyte apoptosis induced by nitric oxide,” *Am. J. Pathol.*, vol. 146, no. 1, pp. 75–85, Jan. 1995.
- [587] G. A. Murrell, D. Jang, and R. J. Williams, “Nitric oxide activates metalloprotease enzymes in articular cartilage,” *Biochem. Biophys. Res. Commun.*, vol. 206, no. 1, pp. 15–21, Jan. 1995.
- [588] R. F. Loeser, C. S. Carlson, M. Del Carlo, and A. Cole, “Detection of nitrotyrosine in aging and osteoarthritic cartilage: Correlation of oxidative damage with the presence of interleukin-1beta and with chondrocyte resistance to insulin-like growth factor 1,” *Arthritis Rheum.*, vol. 46, no. 9, pp. 2349–57, Sep. 2002.
- [589] M. Del Carlo, D. Schwartz, E. A. Erickson, and R. F. Loeser, “Endogenous production of reactive oxygen species is required for stimulation of human articular chondrocyte matrix metalloproteinase production by fibronectin fragments,” *Free Radic. Biol. Med.*, vol. 42, no. 9, pp. 1350–8, May 2007.
- [590] C. R. Roberts, P. J. Roughley, and J. S. Mort, “Degradation of human proteoglycan aggregate induced by hydrogen peroxide. Protein fragmentation, amino acid modification and hyaluronic acid cleavage,” *Biochem. J.*, vol. 259, no. 3, pp. 805–11, May 1989.
- [591] H. Uchiyama, Y. Dobashi, K. Ohkouchi, and K. Nagasawa, “Chemical change involved in the oxidative reductive depolymerization of hyaluronic acid,” *J. Biol. Chem.*, vol. 265, no. 14, pp. 7753–9, May 1990.
- [592] S. Marlovits, M. Hombauer, M. Truppe, V. Vècsei, and W. Schlegel, “Changes in the ratio of type-I and type-II collagen expression during monolayer culture of human chondrocytes,” *J. Bone Joint Surg. Br.*, vol. 86, no. 2, pp.

- 286–95, Mar. 2004.
- [593] S. Hosseininia *et al.*, “Evidence for enhanced collagen type III deposition focally in the territorial matrix of osteoarthritic hip articular cartilage.,” *Osteoarthr. Cartil.*, vol. 24, no. 6, pp. 1029–35, 2016.
- [594] L. H. Linder, D. L. Sukin, R. T. Burks, and R. C. Haut, “Biomechanical and histological properties of the canine patellar tendon after removal of its medial third.,” *Am. J. Sports Med.*, vol. 22, no. 1, pp. 136–42, 1994.
- [595] M. J. Barnes, L. F. Morton, R. C. Bennett, A. J. Bailey, and T. J. Sims, “Presence of type III collagen in guinea-pig dermal scar.,” *Biochem. J.*, vol. 157, no. 1, pp. 263–6, Jul. 1976.
- [596] C. M. Davies, F. Guilak, J. B. Weinberg, and B. Fermor, “Reactive nitrogen and oxygen species in interleukin-1-mediated DNA damage associated with osteoarthritis.,” *Osteoarthr. Cartil.*, vol. 16, no. 5, pp. 624–30, May 2008.
- [597] X. Wang, F. Li, C. Fan, C. Wang, and H. Ruan, “Effects and relationship of ERK1 and ERK2 in interleukin-1 β -induced alterations in MMP3, MMP13, type II collagen and aggrecan expression in human chondrocytes.,” *Int. J. Mol. Med.*, vol. 27, no. 4, pp. 583–9, Apr. 2011.
- [598] K. Mio, J. Kirkham, and W. A. Bonass, “Possible role of extracellular signal-regulated kinase pathway in regulation of Sox9 mRNA expression in chondrocytes under hydrostatic pressure.,” *J. Biosci. Bioeng.*, vol. 104, no. 6, pp. 506–9, Dec. 2007.
- [599] J. A. Ryan, E. A. Eisner, G. DuRaine, Z. You, and A. H. Reddi, “Mechanical compression of articular cartilage induces chondrocyte proliferation and inhibits proteoglycan synthesis by activation of the ERK pathway: implications for tissue engineering and regenerative medicine.,” *J. Tissue Eng. Regen. Med.*, vol. 3, no. 2, pp. 107–16, Feb. 2009.
- [600] D. S. He, X. J. Hu, Y. Q. Yan, and H. Liu, “Underlying mechanism of Sirt1 on apoptosis and extracellular matrix degradation of osteoarthritis chondrocytes,” *Mol. Med. Rep.*, vol. 16, no. 1, pp. 845–850, 2017.
- [601] J. Chen, R. Crawford, and Y. Xiao, “Vertical inhibition of the PI3K/Akt/mTOR pathway for the treatment of osteoarthritis.,” *J. Cell. Biochem.*, vol. 114, no. 2, pp. 245–9, Feb. 2013.
- [602] Y. Lou *et al.*, “Paeonol Inhibits IL-1 β -Induced Inflammation via PI3K/Akt/NF- κ B Pathways: In Vivo and Vitro Studies.,” *Inflammation*, vol. 40, no. 5, pp. 1698–1706, Oct. 2017.
- [603] T. Pan *et al.*, “Geniposide Suppresses Interleukin-1 β -Induced Inflammation and Apoptosis in Rat Chondrocytes via the PI3K/Akt/NF- κ B Signaling Pathway.,” *Inflammation*, vol. 41, no. 2, pp. 390–399, Mar. 2018.
- [604] M. J. López-Armada *et al.*, “Cytokines, tumor necrosis factor-alpha and interleukin-1beta, differentially regulate apoptosis in osteoarthritis cultured human chondrocytes.,” *Osteoarthr. Cartil.*, vol. 14, no. 7, pp. 660–9, Jul. 2006.
- [605] S. Cheleschi *et al.*, “Hydrostatic pressure regulates MicroRNA expression levels in osteoarthritic chondrocyte cultures via the Wnt/ β -catenin pathway,” *Int. J. Mol. Sci.*, vol. 18, no. 1, 2017.
- [606] B. C. Sondergaard, N. Schultz, S. H. Madsen, A. C. Bay-Jensen, M. Kassem, and M. A. Karsdal, “MAPKs are essential upstream signaling pathways in proteolytic cartilage degradation - divergence in pathways leading to aggrecanase and MMP-mediated articular cartilage degradation,” *Osteoarthr. Cartil.*, vol. 18, no. 3, pp. 279–288, 2010.
- [607] Y. Zhou, T. Wang, J. L. Hamilton, and D. Chen, “Wnt/ β -catenin Signaling in Osteoarthritis and in Other Forms of Arthritis,” *Curr. Rheumatol. Rep.*, vol. 19, no. 9, 2017.
- [608] B. Pal, H. Endisha, Y. Zhang, and M. Kapoor, “mTOR: A Potential Therapeutic Target in Osteoarthritis?,” *Drugs R D*, vol. 15, no. 1, pp. 27–36, 2015.
- [609] Y. . Henrotin and B. . Kurz, “Antioxidant to treat osteoarthritis: dream or reality?,” *Curr. Drug Targets*, vol. 8, no. 2, pp. 347–57, Feb. 2007.
- [610] K.-Y. Chin, “The spice for joint inflammation: anti-inflammatory role of curcumin in treating osteoarthritis.,” *Drug Des. Devel. Ther.*, vol. 10, pp. 3029–3042, 2016.

LIST OF ABBREVIATIONS

μCT	Micro-computed Tomography
AA	Ascorbic Acid
AC	Articular Cartilage
ACAN	Aggrecan
ACI	Autologous Chondrocyte Implantation
Akt or PKB	Protein Kinase B
ALPL	Alkaline Phosphatase
ANOVA	Analysis of Variance
ASC	Adipose-derived Stromal/Stem Cell
AZAN	Azocarmine and Aniline Blue
B2M	β2-Microglobulin
bAC	Bovine Articular Chondrocyte
bFGF or FGF2	Basic Fibroblast Growth Factor or Fibroblast Growth Factor 2
BM	Bone Marrow
BM-MSC	Bone Marrow Mesenchymal Stem Cell
BMP	Bone Morphogenetic Proteins
BMSC	Bone Marrow-derived Stem Cell
CNP	C-type Natriuretic Peptide
COL10A1	Collagen Type X
COL1A1	Collagen Type I
COL2A1	Collagen Type II
COMP	Cartilage Oligomeric Matrix Protein
COO ⁻	Carboxyl
CS	Chondroitin Sulfate
CZ	Calcified Zone
DCB	Decellularized Bone
Dcx	Doublecortin
DEX	Dexamethasone
DKK1	Dickkopf-related Protein 1
DL	Dynamic Loading
DM	Differentiation Medium
DMEM	Dulbecco's Modified Eagle Medium
DMMB	Dimethyl Methylene Blue
DMSO	Dimethyl Sulfoxide
DNA	Deoxyribonucleic Acid
DTPA	Diethylenetriaminepentaacetic Acid
DZ	Deep Zone
ECM	Extra Cellular Matrix
EDTA	Ethylenediaminetetraacetic Acid
EGF	Epidermal Growth Factor
ELISA	Enzyme-linked Immunosorbent Assay
EPR	EPR measurement
ERK	Extracellular Signal-regulated Kinase
ESC	Embryonic Stem Cell
FBS	Fetal Bovine Serum

FGF	Fibroblast Growth Factor
FGFR	Fibroblast Growth Factor Receptor
FS	Free Swelling
FT	Fibrous Tissue
FOXA	Forkhead Box A
FRA2	FOS-related Antigen 2
GAG	Glycosaminoglycan
GAPDH	Glyceraldehyde 3-Phosphate Dehydrogenase
GDP	Gross Domestic Product
GF	Growth factors
H ₂ O ₂	Hydrogen peroxide
HA	Hyaluronic Acid or Hyaluronan
hAC	Human Articular Chondrocyte
HDAC4	Histone Deacetylase 4
HEPES	4-(2-Hydroxyethyl)-1-Piperazineethanesulfonic Acid
HIF1 α	Hypoxia-inducible Transcription Factor 1 α
HO*	Hydroxyl Radical
HOX	Homeobox Transcription Factor
HP	Hydrostatic Pressure
IBMX	Isobutylmethylxanthin
IBSP	Integrin Binding Sialoprotein or Bone Sialoprotein
IGF	Insulin-like Growth Factor
IHH	Indian Hedgehog Protein
IL-1 β	Interleukin 1 β
IL-6	Interleukin 6
iPSC	Induced Pluripotent Stem Cell
ITM	Interterritorial Matrix
ITS	Insulin, Transferrin and Sodium Selenite
KS	Keratan Sulfate
MACI	Matrix-assisted Autologous Chondrocyte Implantation
MAPK	Mitogen-activated Protein Kinase
Matn1	Matrilin 1
MEF2	Mosin Enhancer Factor 2
MMP	Matrix Metalloproteinase or Matrix Metallopeptidase
MMP13	Matrix Metallopeptidase 13
MMP3	Matrix Metallopeptidase 3
MMP9	Matrix Metallopeptidase 9
MSB	Martius Scarlet Blue
MSC	Mesenchymal Stem Cell
MSD	Musculoskeletal Disorder
MTT	Methylthiazolyldiphenyl-tetrazolium bromide
MZ	Middle Zone
NB	Newly-deposited Bone
NEAA	Nonessential Amino Acid
NKX3-2	NK3 homeobox 2
NMRI	Naval Medical Research Institute
NPR2	Natriuretic Peptide Receptor

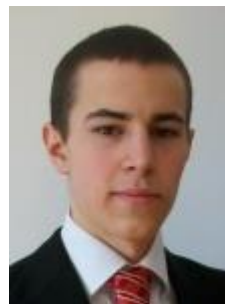
OA	Osteoarthritis
OAT	Osteochondral Autograft Transfer
OCA	Osteochondral Allograft Transfer
OCD	Osteochondritis Dissecans
OCN	Osteocalcin
OPN	Osteopontin
P/S	Penicillin/Streptomycin
PBS	Phosphate-buffered Saline
PCL	Polycaprolactone
PDGF	Platelet-derived Growth Factor
PDMS	Polydimethylsiloxane
PEG	Polyethylene Glycol
PGA	Polyglycolic Acid
PI3K	Phosphoinositide 3-Kinase
PLA	Poly-lactic Acid
PM	Pericellular Matrix
PMSF	Phenyl-Methyl-Sulfonyl Fluoride
POC	Primary Ossification Center
POM	Polyoxymethylene
PRP	Platelet-rich Plasma
PTCH	Patched
PTHrP	Parathyroid-hormone Related Protein
RA	Rheumatoid Arthritis
RANKL	RANK-Ligand
RNU	Rowett Nude
ROS	Reactive Oxygen Species
RT-qPCR	Quantitative Reverse Transcription Polymerase Chain Reaction
RUNX2	Runt Related Transcription Factor 2
SD	Standard Deviation
SDS	Sodium Dodecyl Sulfate
SEM	Scanning Electron Microscope
SHH	Sonic Hedgehog
SO ₄ ²⁻	Sulfate
SOC	Secondary Ossification Center
SOD	Superoxide Dismutase
SOP	Standard Operating Procedure
SOX9	SRY (Sex Determining Region Y)-Box 9
STAT	Signal Transducer and Activator of Transcription 1
SZ	Superficial Zone
TBS	Tris-buffered Saline
TE	Tissue Engineering
TEM	Transmission Electron Microscope
TERM	Tissue Engineering and Regenerative Medicine
Tgfr2	TGFβ type II receptor
TGF-β	Transforming Growth Factor β
TM	Territorial Matrix
TNF-α	Tumor Necrosis Factor α

TRPV4	Transient Receptor Potential Vanilloid 4
VCAN	Versican
VEGF	Vascular Endothelial Growth Factor
Wnt	Drosophila segment polarity gene wingless and vertebrate homolog integrated int-1
ZFP521	Zinc-finger Protein 52

CURRICULUM VITAE



Europass Curriculum Vitae



Personal information

First name(s) / Surname(s) **Bernhard Rieder**
Address Krummgasse 14/1, 1030 Vienna (Austria)
Mobile +43 680 1461037
E-mail(s) rieder.bernhard@gmx.net
Nationality Austrian
Date of birth 01/06/1988
Gender Male

Desired employment / Occupational field **Scientific Researcher**

Work experience

Dates 03/11/2017 – 30/04/2019
Occupation or position held Junior Researcher
Main activities and responsibilities Development of hydrostatic bioreactors for chondrogenic tissue engineering
Name and address of employer Trauma Care Consult
Gonzagagasse 11/25, 1010 Vienna (Austria)
Type of business or sector Research & Development

Dates 04/11/2013 – 31/10/2017
Occupation or position held Junior Researcher
Main activities and responsibilities Development of bioreactors in the Vienna project "Tissue Engineering International"
Name and address of employer FH Technikum Wien (University of Applied Sciences)
Institute for Biochemical Engineering
Mariahilfer Straße 37-39, 1060 Vienna (Austria)
Type of business or sector Research & Development, Education

Dates 01/01/2013 – 31/8/2013
Occupation or position held Master student
Main activities and responsibilities Investigation of the influence of pH on human nasal chondrocytes within EU project BIO-COMET

Name and address of employer	University Hospital Basel Institute for Surgical Research and Hospital Management Tissue Engineering Group ZLF, Hebelstrasse 20, 4031 Basel (Switzerland)
Type of business or sector	Research & Development
Dates	01/07/2010 – 31/10/2012
Occupation or position held	Part-time laboratory assistant
Main activities and responsibilities	Design of a bioreactor system for the stimulation of various cells with hydrostatic pressure
Name and address of employer	FH Technikum Wien (University of Applied Sciences) Höchstädtplatz 5, 1200 Vienna (Austria)
Type of business or sector	Research & Development, Education
Dates	01/07/2006 – 01/08/2006
Occupation or position held	Motor mechanic
Main activities and responsibilities	Activities of a trainee
Name and address of employer	Michael Madner Hirschmillerstraße 16, 2115 Ernstbrunn (Austria)
Type of business or sector	Wholesale and Retail Trade; Repair of Motor Vehicles and Motorcycles
Dates	01/07/2005 – 01/08/2005
Occupation or position held	Motor mechanic
Main activities and responsibilities	Activities of a trainee
Name and address of employer	Georg Einsiedl 81, 2031 Eggendorf im Thale (Austria)
Type of business or sector	Wholesale and Retail Trade; Repair of Motor Vehicles and Motorcycles
Dates	01/07/2004 – 01/08/2004
Occupation or position held	Motor mechanic
Main activities and responsibilities	Activities of a trainee
Name and address of employer	Michael Madner Hirschmillerstraße 16, 2115 Ernstbrunn (Austria)
Type of business or sector	Wholesale and Retail Trade; Repair of Motor Vehicles and Motorcycles
Education and training	
Dates	31/03/2014 –
Title of qualification awarded	Doctoral programme in Natural Sciences Technical Chemistry, PhD
Principal subjects / occupational skills covered	Biochemistry and Molecular Cell Biology, Regenerative Medicine, Bioinformatics, Biotechnology and Bioprocess Development, Biomaterials
Name and type of organisation providing education and training	TU Wien Getreidemarkt 9, 1060 Wien (Austria)
Dates	05/09/2011 – 24/9/2013
Title of qualification awarded	Master of Science in Engineering, MSc
Principal subjects / occupational skills covered	Biochemistry and Cell Biology, Regenerative Medicine, Bioinformatics, Cell and Tissue Engineering, Business and Law, Biotechnology

Name and type of organisation providing education and training | FH Technikum Wien (University of Applied Sciences)
Höchstädtplatz 5, 1200 Wien (Austria)

Dates | 08/09/2008 – 21/06/2011

Title of qualification awarded | Bachelor of Science in Engineering, BSc

Principal subjects / occupational skills covered | Molecular Genetics, Immunology, Bioinformatics, Pharmacokinetics and Toxicology, Cell Culture Techniques and Laboratory

Name and type of organisation providing education and training | FH Technikum Wien (University of Applied Sciences)
Höchstädtplatz 5, 1200 Wien (Austria)

Dates | 09/09/2002 - 29/06/2007

Title of qualification awarded | Engineer of Mechatronics, High school diploma

Principal subjects / occupational skills covered | Process Measuring and Control Technology, Electronics and Digital Technology, Mechanics and Automation, Process Control, Construction Design

Name and type of organisation providing education and training | HTL Rennweg (Secondary College of Engineering)
Rennweg 89b, 1030 Wien (Austria)

Publications

2018

Rieder B, Weihs AM, Weidinger A, Szwarc D, Nürnberger S, Redl H, Rünzler D, Huber-Gries C, Teuschl AH. *Hydrostatic pressure-generated reactive oxygen species induce osteoarthritic conditions in cartilage pellet cultures*. Sci Rep. 2018 Nov 19;8(1):17010. doi: 10.1038/s41598-018-34718-8.

Nürnberger S, Schneider C, van Osch GVM, Keibl C, Rieder B, Monforte X, Teuschl A, Mühleder S, Holnthoner W, Barbara S, Gahleitner C, Redl H, Wolbank S. *Repopulation of an auricular cartilage scaffold, AuriScaff, perforated with an enzyme combination*. Acta Biomater. 2018 Dec 24. pii: S1742-7061(18)30760-8. doi: 10.1016/j.actbio.2018.12.035.

Bernhard JC, Hulphers E, Rieder B, Ferguson J, Rünzler D, Nau T, Redl H, Vunjak-Novakovic G. *Perfusion Enhances Hypertrophic Chondrocyte Matrix Deposition, But Not the Bone Formation*. Tissue Eng Part A. 2018 Jun;24(11-12):1022-1033. doi: 10.1089/ten.TEA.2017.0356. Epub 2018 Mar 2.

2017

Bernhard J, Ferguson J, Rieder B, Heimel P, Nau T, Tangl S, Redl H, Vunjak-Novakovic G. *Tissue-engineered hypertrophic chondrocyte grafts enhanced long bone repair*. Biomaterials. 2017 Sep;139:202-212. doi: 10.1016/j.biomaterials.2017.05.045. Epub 2017 May 31.

Personal skills and competences

Mother tongue(s)

German

Other language(s)

Self-assessment
European level (*)

English

Understanding				Speaking				Writing	
Listening		Reading		Spoken interaction		Spoken production			
C2	Proficient user	C2	Proficient user	C1	Proficient user	B2	Independent user	C1	Proficient user

(*) [Common European Framework of Reference \(CEF\) level](#)

Social skills and competences	Good ability to communicate with different parties gained through my work with collaboration partners as well as outside the workplace while renovating a flat and building various other structures. In this case I also learnt to be patient, but make my standpoint clear when it is necessary. Logically, successfully completing bigger projects is hardly possible alone, so working with friends and colleagues improved my team spirit and turned me into a team player. Although I prefer team work I can work independently and am able to deal with setbacks, if unexpected things happen.
Organisational skills and competences	Besides working in well stocked lab, various projects made it necessary to be self-sustain when organize special material used for construction, starting with simple screws and ending up with special devices. Furthermore, I had to arrange meetings and make sure that everything was ready when due. I think this improved my project management skills and gave me a sense of organisation.
Technical skills and competences	My technical skills also became better because I practiced many tasks which I had never done before only by reading the instruction or user manual. Adopting new technical skills was always easy for me, sometimes just observing someone while working made me able to imitate the task instantly. That is why I prefer the technical part of a project and why I chose a technical high school in the first place.
Computer skills and competences	Good command of Microsoft Office™ tools (Word™, Excel™ and PowerPoint™) gained through several years of writing laboratory reports and preparing presentation for university and scientific meetings. Furthermore, I have experience in computer languages like C, C#, and PHP.
Artistic skills and competences	My artistic strengths are not in art or music, although I have played the piano for several years. I rather love to design and construct various structures and devices. For example, over the years I have built and completed a fence and several walls at my family home and I am the go-to person for my peers when things need fixing.
Other skills and competences	My favourite skill is my determination to finish every possible task that I start. So far, I have never given up, neither a challenge in sport nor an exercise in school. This might be a reason why people lay trust in me and willingly agreed to finance bigger projects. Another important skill that convinced them is how I finish my task. My priority is to do things well, not just quickly, to avoid major mistakes.
Driving licence(s)	C, C1, B, B1, BE